Autophagy as a therapeutic target to enhance chemotherapy in oral squamous cell carcinoma

By

Aisling Anderson

A dissertation submitted to the university of Dublin in candidature for the degree of Doctor in Philosophy

School of Dental Science

Trinity College

Dublin

September 2022

Declaration

I declare that this thesis has not been submitted as an exercise for a degree at this or any other university and it is entirely my own work.

I agree to deposit this thesis in the University's open access institutional repository or allow the Library to do so on my behalf, subject to Irish Copyright Legislation and Trinity College Library conditions of use and acknowledgement.

I consent to the examiner retaining a copy of the thesis beyond the examining period, should they so wish (EU GDPR May 2018).

Aisling Anderson

2021

Acknowledgements

I would like to start by expressing my sincerest gratitude to my supervisor, Dr. Jeff O'Sullivan. I can't tell you enough how grateful I am that you took me on as a PhD student four years ago. I really appreciate the opportunity you've given me to develop as a researcher and I know that I'm a much more focused and dedicated scientist to the one I was when I started. Thank you for putting up with me and not losing your reason when it took me almost four years to write a small literature review! Between all the science related panics, you've been really supportive as a friend, whether it was giving me the time I needed to deal with my depression or showing me trailers for Star Wars when I was upset over a breakup. You've been an amazing supervisor and you've made the last four years a lot less stressful than they could have been. Thank you.

Thank you to all the staff of TBSI and the Dublin Dental hospital. I would especially like to thank Barry Moran in the flow cytometry facility and Gavin McManus in the microscopy facility for their help setting up experiments and for all the troubleshooting. I'd like to say a huge thanks to Liam and Noel for everything they've done for the lab and for me over the last four years. Thank you to Glynis, Audrey and Brian in the prep room for all the help during lab demonstrating and poster printing. Thanks, also, to Des and Dave in the delivery bay.

Thank you to the past and present members of the O'Sullivan and Davey labs: Ola, Isabel, Nicoletta, Gavin, Sahar, Darren, Ryan, Olga, Yong Jing and Jer. You've all been incredibly helpful to me when I needed advice and have provided endless entertainment in the lab (especially the sing-a-longs with Darren and Gav!) Ola and Isabel, I'm so glad you joined the lab! Our little family has been amazing and I'm going to miss our little lab gossip sessions!

Natalie, Laura and Nikki, you girls were the best people to meet when I started in TBSI and you still are fantastic friends. I really appreciate the

laughs and all the scientific and non-scientific advice you've given me over the years.

Thank you to all the past and present members of the reading room(s). Nidhi, thank you for all the chats and comfort when I needed it. Karen, thanks for being such an hilarious person and for being the kindest human, I owe you several drinks for the TMRM! Thanks to the members of the Covfefe gang for all the coffee and giggles: Ji, Livia, Dan, Katie and James. James, you've been my rock during this. You've been endlessly supportive on my worst days, and you've made me laugh until my face hurt on my better days. I'll never be able to thank you enough simply for being your lovely self and not letting me get too upset over failed experiments.

I also want to say a special thanks to everyone who started their PhD journey at the same time as me: Katie, Jess, Peter, Emma and Louise. You're all amazing and it's been great to go through all this by your side. I especially need to thank Katie for really being the kindest person I've ever met. You've been consistently upbeat and sweet for the last four years and you've always helped me with my stupid science questions even when you've been busy and stressed. You're a great scientist and an even better friend. I owe you countless espresso martinis!

I want to thank Kasia, and all the girls at Flow Fitness for all the laughs and much-needed stress relief over the last 9 months. You've all helped me to clear my head and take my mind off my thesis and I really appreciate all the support you've all been giving me.

Thanks to Molly and Mandy for always being the most amazing friends anyone could ask for. You've both always been there for me and you've helped me get out of my research bubble when I've been getting too caught up in it!

Last, but certainly not least, I'd like to thank my family. Mom, Dad, Clíona and Stephen, I'm sure you're thrilled that this PhD is over. I can't thank you all enough for everything you've done for me. I'm so lucky to have the best family. You've let me cry on your shoulders over failed

experiments and missed deadlines and you've been there to celebrate the little victories. I know it must have been hard for you to watch me repeatedly lose faith in myself so thank you for consistently telling me when I was being stupid and for getting me to the finish line. I love you guys so much.

Summary

Oral cancer is the 15th most common cancer worldwide and oral squamous cell carcinoma accounts for 90% of oral cancer cases. Current therapeutic interventions for OSCC include surgical intervention with radiation therapy and chemotherapy used as an adjuvant therapy to shrink the tumour prior to surgery. Chemotherapeutic intervention is often avoided due to the potential for chemo-resistance to develop, which has a high prevalence in OSCC. This study focuses on the optimisation of chemotherapeutic interventions to reduce the likelihood of resistance and the improve the patients' quality of life after treatment.

The most frequently used chemotherapeutics in OSCC are Cisplatin, Carboplatin, 5-fluorouracil and docetaxel. Despite the use of these drugs in most OSCC chemotherapeutic research, their IC_{50} values are not well documented making comparisons between studies difficult. This thesis presents IC_{50} values for the four previously mentioned chemotherapeutics after 24, 48, 72, 96 and 120h in Ca9-22, SCC4, TR146 and DOK cell lines.

Metabolic stress from chemotherapeutics is known to activate autophagy, a cell survival mechanism, and mediate acquired resistance to these compounds. There has been a lot of discussion as to whether the current methods of measuring autophagic changes are reliable or not. This research presented in this thesis demonstrates that by combining western blotting of LC3B and P62 with acridine orange staining, a clear understanding of drug-induced modulations to autophagy can be obtained. The induction of autophagy by chemotherapeutic intervention

was verified in the OSCC cell lines Ca9-22, SCC4 and TR146 and the dysplastic cell line, DOK. Inhibition of cisplatin-mediated autophagy by chloroquine in TR146 cells resulted in decrease in cisplatin's IC_{50} from 7.80 μM to 0.07 μM while co-treatment in DOK cells reduced the IC_{50} of cisplatin from 13.00 μM to 1.35 μM. Co-treatment in Ca9-22 cells had no impact on the IC_{50} of cisplatin.

Treatment of OSCC cells with cisplatin and/or chloroquine had differential impacts on cellular respiration, determined using Seahorse Real-Time cell metabolic analysis and mitochondrial membrane potential, analysed by flow cytometry using TMRM. Ca9-22 cells demonstrated a decrease in basal respiration in response to co-treatment with a corresponding decrease in mitochondrial membrane potential during treatment with chloroquine while TR146 cells underwent a decrease in both the maximum and spare respiratory capacity in response to chloroquine treatment without any fluctuations in mitochondrial membrane potential. The pre-malignant DOK cell line had increased basal respiration in response to cisplatin treatment while the maximum respiration increased in response to co-treatment and the spare respiratory capacity increased in response to chloroquine treatment. Chloroquine treatment also resulted in an increased mitochondrial membrane potential in DOK cells.

The tumour-supressing gene, *P53*, is associated with susceptibility to cancer and mutations in this gene (found in ~50% of oral cancers) are linked with the development of resistance to chemotherapy. By knocking down *P53* in TR146 cells, it was shown that $P53^-$ have a decreased rate of

basal respiration as determined by Seahorse Real-Time cell metabolic analysis.

The data presented in this thesis verify the hypothesis that inhibition of autophagy can prevent cell survival mechanisms and increase the efficacy of chemotherapeutic intervention in discrete OSCC cell lines.

Table of Contents

Abbreviations

2DG	2-deoxy-D-glucose
3MA	3-Methyladenine
5-FU	5-fluorouracil
AKT	Protein kinase B
AMBRA1	Activating molecule in BECN1-regulated autophagy protein
AMPK	AMP-activated protein kinase
AnA	Antimycin A
APAF-1	Apoptotic protease activating factor 1
Atg	Autophagy-related protein
ATP	Adenosine triphosphate
BAX	Bcl-2-associated X protein
BSA	Bovine serum albumin
CBDCA	Carboplatin
CCND-1	Cyclin D1 gene
CD147	Cluster of differentiation 147
CPt	Cisplatin
CQ	Chloroquine
DAPK	Damage-associated protein kinase
dH_2O	Deionised H_2O
DMEM	Dulbecco modified Eagle's medium
DMPK	Myotonic dystrophy protein kinase
DNA	Deoxyribonucleic acid
DRAM	Damage-regulated autophagy modulator
ECAR	Extracellular acidification rate
EGFR	Epidermal growth factor receptor
EMA	European medicines agency
EMT	Epithelial to mesenchymal transformation
ER	Endoplasmic reticulum
ERK	Extracellular signal-regulated kinase

FACS	Fluorescence-activated cell sorting
FBS	Foetal bovine serum
FCCP	Carbonyl cyanide 4-(trifluoromethoxy)phenylhydrazone
FDA	Food and drug administration
FDG	2-18F-2-D-deoxyglucose
FIP200	FAK family kinase-interacting protein of 200 kDa
FSC	Forward scatter
GFP	Green fluorescent protein
GßL	G-protein ß subunit-like
GSK3ß	Glycogen synthase kinase 3ß
GTP	Guanosine triphosphate
HCC	Hepatocellular carcinoma
HCQ	Hydroxychloroquine
HIF-1	Hypoxia inducible factor 1
HKII	Hexokinase II
HNSCC	Head and neck squamous cell carcinoma
HPV	Human papilloma virus
HRP	Horse radish peroxidase
IC_{50}	Half maximal inhibitory concentration
IGF	Insulin-like growth factor
IL-1	Interleukin-1
IMM	Mitochondrial inner membrane
LC3	Microtubule-associated protein light chain 3
LDH	Lactate dehydrogenase
MAPK	Mitogen-activated protein kinase
MCT	Monocarboxylate transporter
MEM	Minimum essential media
MPTP	Mitochondrial permeability transition pore
mtDNA	Mitochondrial DNA
mtETC	Mitochondrial electron transport chain
MTG	MitoTracker green
mTOR	Mammalian target of rapamycin

mTORC	mTOR complex
mTP53	Mutant P53
NAD	Nicotinamide adenosine dinucleotide
NADH	Reduced NAD
NADPH	Nicotinamide adenosine dinucleotide phosphate, reduced
$O^{\cdot-}$	Singlet oxygen
OCR	Oxygen consumption rate
OSCC	Oral squamous cell carcinoma
P53	Tumour suppressor protein 53
PAGE	Polyacrylamide gel electrophoresis
PBS	Phosphate buffered saline
PCD	Programmed cell death
PE	Phosphatidylethanolamine
PET	Positron emission tomography
PFKP	Phosphofructokinase-platelet
PI	Propidium iodide
PI3K	Phosphatidylinositol-3 kinase
PI3P	Phosphatidylinositol-3-phosphate
PKD	Protein kinase D
PKM2	Pyruvate kinase M2
PRAS40	Proline rich AKT1 substrate 1
PS	Phosphatidylserine
PTEN	Phosphate and tensin homolog
PUMA	P53 upregulated modulator of apoptosis
PVDF	Polyvinylidene difluoride
QOL	Quality of life
Rb	Retinoblastoma gene
RFP	Red Fluorescent protein
RNA	Ribonucleic acid
ROS	Reactive oxygen species
SCC	Squamous cell carcinoma
SDS	Sodium dodecyl sulphate

SEM	Standard error of the mean
SNARE	Soluble N-ethylmaleimide-sensitive factor attachment protein receptor
SSC	Side scatter
TBS	Tris-buffered saline
TBST	Tris-buffered saline with tween
TGF	Transforming growth factor
TMRM	Tetramethylrhodamine methyl ester
TSC1/2	Tumour sclerosis 1/2
TXT	Docetaxel
ULK1	Unc-51 like autophagy activating kinase 1
VEGF	Vascular endothelial growth factor
$\Delta\Psi m$	Mitochondrial membrane potential

Chapter 1

General Introduction

1.1 General Introduction

Autophagy is a cellular process that allows for the recycling of components of dying or damaged cells and is utilised as a cell survival mechanism during stress conditions such as starvation and hypoxia. Macroautophagy (commonly called autophagy) has been a major field of study since Yoshinori Ohsumi's ground-breaking research into its mechanisms using *Saccharomyces cerevisiae*, which earned him the Nobel Prize in 2016. As far back as the discovery of the lysosome by Christian de Duve in 1955, autophagy has been implicated in myriad physiological and pathological processes including neurodegeneration, inflammation, autoimmunity and cancer[1]. Autophagy has been referred to as a double-edged sword with regards to cancer research as it can both protect against the cellular damage that leads to cancer and can be exploited to protect cancer cells and drive tumour progression[2]. During chemotherapeutic intervention of cancers, autophagy can act to assist tumour cells in evading death thus leading to an acquired resistance to chemotherapy. Despite the abundance of research into autophagy's role in the development of chemoresistance, there is limited data linked to tumours of the oral cavity, which have a high rate of recurrence and resistance to chemotherapy. This study aims to identify the interactions between therapeutic agents and autophagy in oral squamous cell carcinoma cell lines to identify the possible mechanisms whereby autophagy influences therapeutic efficacy.

1.2 Oral Cancer

Oral cancer has been identified as the 16th most common cancer worldwide in 2018[3] with a 5 year survival rate estimated to be ~40%. According to the National Cancer Registry of Ireland, 386 new cases of oral and pharyngeal cancer present themselves each year. Throughout Europe and the rest of the world, oral cancer continues to be a major concern and has varying rates of incidence in different populations, with the highest rate of prevalence in Melanesia and the lowest in Western Africa. Oral squamous cell carcinoma (OSCC) is derived from the stratified squamous epithelial layer of the oral mucosa. It is the most common form of oral cancer, accounting for about 90% of oral cancers[4, 5].

Due to the nature of oral tumours, they are often initially asymptomatic and frequently result in early migration to distant organs, rendering these cancers difficult to diagnose within the right time frame for treatment to be effective. As stated previously, the most common form of oral cancer is OSCC, so called through its formation via the squamous cells that comprise most of the epidermis. OSCCs are most commonly detected on the lateral border of the tongue and the floor of the mouth[6], however, other common sites include the lip, the buccal mucosa and the gingiva.

1.2.1 Risk Factors

There are many causal factors of OSCC, including alcohol and tobacco smoke, which are heavily linked to its manifestation. OSCC is more prevalent in men, however a previously recorded 6:1 male:female ratio

has been reduced to 2:1, which is thought to be linked to increasing levels of alcohol consumption and smoking amongst women. Similarly, increasing age has been a large risk factor for OSCC with almost 50% of cases occurring among the over 65s, however, the disease is becoming more and more prevalent in younger patients. There is a high prevalence of the human papilloma virus (HPV) among patients, indicating its causal role in the disease[7], however the majority of HPV associated SCCs are localised to the oropharyngeal region[8]. Other lifestyle factors associated with OSCC include betel nut chewing, tobacco chewing, non-vegetarian diet and poor oral hygiene[9].

1.2.2 Presentation

OSCC often initially manifests as ulceration with erythroplakic or leukoplakic changes in the surrounding tissue. Erythroplakia (Figure 1.1) presents as a red plaque while leukoplakia (Figure 1.2) manifests as a white plaque. OSCC can also present as a granular ulcer with fissuring, a mixed white and red lesion (speckled leukoplakia,) a lump, a non-healing extraction socket or a lesion fixed to deeper tissues. These symptoms are often accompanied by enlargement of cervical lymph nodes; however, this is predominantly associated with oropharyngeal cancers. SCCs undergo a dysplastic, precancerous stage recognised as nuclear hyperplasia, hyperchromatism and increased nuclear/cytoplasmic ratio[10]. Due to unsought professional help, difficult diagnosis and fast progression, approximately two thirds of OSCCs are diagnosed at stages III or IV[11] (stages indicating a larger tumour with lymph node invasion that may have spread to other parts of the body.)

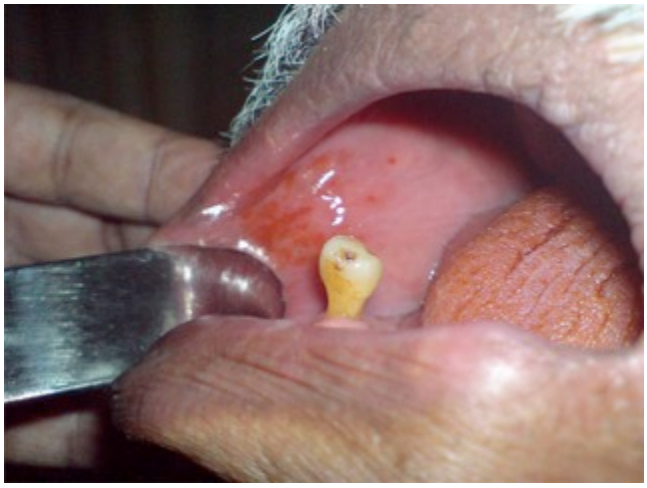

Figure 1.1: Erythroplakia of buccal mucosa. Erythroplakia manifests as a red patch on the epithelium. Taken from Shukla, 2014[12].

Figure 1.2: Leukoplakia on the floor of the mouth. Leukoplakia manifests as a white plaque on the epithelium. Taken from Van Der Waal, 2014[13]

1.2.3 Treatment of OSCC

Cancer treatment is dependent on the stage the tumour is diagnosed at. For head and neck cancers diagnosed at stages I and II (cancers that have not yet spread into surrounding tissues) the common treatment plan involves surgical interventions, radiotherapy or chemotherapy. Cancers diagnosed at stages III and IV (cancers that have invaded surrounding tissues or that have metastasised) are usually treated by surgery with radiotherapy and/or chemotherapy often being used as adjuvant therapies[14]. These treatments are all associated with complications such as disfigurement, osteoradionecrosis and xerostomia, which can have long term or permanent effects on the patients' quality of life (QOL).

Surgery often involves the removal of large amounts of facial tissues resulting in scarring or disfigurement. Removal of lymph nodes from the neck is associated with adverse effects on essential functions such as eating, drinking and speech[15].

Radiotherapy also has side effects, causing complications such as salivary gland hypofunction, xerostomia (dry mouth), osteoradionecrosis, dental caries, and damage of the oral mucosa and its vasculature. Studies have been carried out into improved methods of radiotherapy showing that altered fraction radiotherapy provides an improvement in overall survival of patients[16], however, very few studies have provided an insight into whether these refined techniques improve the QOL for these individuals.

Chemotherapy is rarely used as a primary therapy for OSCC, however it is frequently recommended as an adjuvant therapy and has been shown to prolong survival alongside surgery or radiotherapy[17]. Although chemotherapy is associated with reduced negative effects, cells develop a high risk of increasing levels of resistance with relapse of treatment-resistant cancers common[18]. Overcoming this acquired resistance would make chemotherapy a much more desirable and effective form of treatment for OSCC patients.

1.3 Cancer Metabolism

Cancer cells express specific traits that were outlined by Hanahan and Weinberg in 2000[19]. The six hallmarks described include sustained proliferative signalling, evasion of growth suppressors, activation of invasion and metastasis, replicative immortality, induction of angiogenesis and resistance to cell death. In 2011, these six hallmarks were revised with four additional properties; evasion of immune destruction, the reprogramming of energy metabolism, genomic instability and inflammation[20, 21]. In order to support their incessant proliferation, cancer cells consume vast amounts of glucose and utilise the glycolytic pathway to produce lactate[22]. As these cells produce a limited amount of pyruvate there is little activity of the Krebs cycle and low levels of oxidative phosphorylation. The metabolic reprogramming of cancer cells is essential for the generation of NADPH needed for the excessive production of lipids, nucleosides and amino acids required for tumorigenesis[23].

1.3.1 The Warburg effect

The key characteristic of the Warburg effect is the production of lactate from glycolysis in the presence of oxygen. In normal cells, this type of glycolysis only occurs in the absence of oxygen and is known as anaerobic glycolysis, however, during the Warburg effect this is known as 'aerobic glycolysis'. Positron emission tomography (PET) exploits the Warburg effect as a diagnostic tool by replacing one hydroxyl group in glucose with radioactive fluorine-18 to create 2-18F-2-D-deoxyglucose (FDG) which is injected into the bloodstream and is rapidly metabolised by tumour cells allowing for clear imaging of highly glycolytic tumour cells. The Warburg effect has a variety of beneficial roles in tumour development and survival including ATP synthesis, biosynthesis, immune system evasion, survival in the tumour microenvironment and cell signalling.

Tumour cells undergo continuous proliferation and require increased quantities of ATP to provide sufficient energy for this process. Studies have shown that increased ATP demand results in an increase in aerobic glycolysis[24] which indicates a role for the Warburg effect in maintaining the energy supply for cancer cells. ATP production by aerobic glycolysis per unit of glucose, is actually lower compared to that of mitochondrial respiration[25]. Due to the excessive rate of glucose metabolism to lactate by aerobic glycolysis, the flux through this pathway is 10-100 times faster than mitochondrial oxidation of glucose. The result is a similar amount of ATP synthesis regardless of the type of glucose metabolism[26].

Due to the excessive proliferation undergone by cancer cells, there is a huge demand for biosynthetic components. One of these components is carbon, which is required for the generation of proteins, lipids and nucleotides and can be generated from the increased rate of glycolysis seen during the Warburg effect[27]. Further to this, the increased rate of glucose metabolism results in the increased production of reducing equivalents such as NADPH which are essential during lipid biosynthesis[28]. It is important to note, however, that for excessive glucose metabolism to result in increased NADPH production, no lactate can be produced, and the Warburg effect cannot be involved as these metabolic pathways are exclusive of one another.

It has been shown that increased Warburg metabolism is linked to immune system evasion. Cascone *et al*. have shown that tumour cells undergoing the Warburg effect can inhibit T-cell killing and transport to the tumour microenvironment, resulting in resistance to adoptive T-cell therapy[29]. Furthermore, loss of the tumour suppressor phosphate and tensin homolog (PTEN) has been shown to result in the significant increase of glycolysis in tumour cells while having no effect on oxidative phosphorylation[30]. Loss of signalling by PTEN, has also been shown to promote resistance to immunotherapy via the inhibition of T-cell killing and trafficking[31].

The high level of lactate produced by the Warburg effect is an important part of the tumour microenvironment. By increasing the acidity of the surrounding area lactate can contribute to immune evasion. Lactate can also activate the hypoxia inducible factor-1 (HIF-1), vascular endothelial

growth factor (VEGF), transforming growth factor beta (TGFB) and interleukin-1 (IL-1)[32]. The lactate produced during aerobic glycolysis is transported out of cells by the monocarboxylate transporter (MCT). This creates an acidic pH within the tumour microenvironment. It has been shown that the acidic environment caused by lactate transport can assist immune system evasion by promoting the monocyte differentiation into tumour-associated dendritic cells. Gottfried *et al*. showed that this differentiation was prevented by blocking MCTs[33]. Similar research has shown that inhibition of MCT4 inhibits tumour growth and MCT1 inhibition decreases angiogenesis via inhibition of HIF-1 in vivo[34, 35.] It is clear that the influence of lactate on the tumour microenvironment is essential for tumour growth and survival.

The Warburg effect also has downstream effects on cell signalling. Two of the most studied signalling areas are that of reactive oxygen species (ROS) and the modulation of chromatin state. In cells undergoing normal aerobic glycolysis, pyruvate is converted to Acetyl-CoA which then enters the Krebs cycle. Acetyl-CoA is a known substrate for histone acetylation which has been shown to be regulated by glucose flux[36]. Histone acetylation is essential for alteration of chromatin structure which is a key regulator for many cellular functions including DNA repair and gene transcription. The increase in glycolytic flux by the Warburg effect may result in a decreased level of oxidative phosphorylation within cells and increase the mitochondrial redox potential due to the increasing availability of NADPH[37]. Reduction of oxidative phosphorylation can result in a decrease in ROS. Although excessive ROS production results in a wide range of cellular dysfunction,

a deficiency of ROS can have an equally negative impact on cellular function as ROS can act as signalling molecules. ROS signalling has been mostly associated with growth factor signalling, however ROS, as signalling molecules, have the potential to be involved in many more cellular pathways[38].

1.3.2 Mitochondria and oxidative phosphorylation

It is likely that tumours rely on glycolysis to prepare for the hypoxic conditions associated with tumour development, however, despite the high glycolytic flux in cancer cells, oxidative phosphorylation remains an essential component of cancer cell metabolism. Work by Tan *et al.* demonstrated the importance of mitochondria and the electron transport chain (mtETC) in cancer by injecting healthy mice with mtDNA null cancer cells, in which four out of five mtETC complexes lack mtDNA. Tumours formed in these mice at a delayed rate when compared to cancer cells with normal mtDNA and this delay was correlated to the recovery of the mtDNA by obtaining mtDNA from the host[39]. These experiments demonstrated that effective mtETC activity is essential for tumour progression.

The mtETC consists of five multi-subunit complexes which are imbedded within the inner mitochondrial membrane (MIM). These complexes are referred to as complexes I through V and can be separated into two functional groups; complexes I-IV, which are associated with electron transfer, and complex V, otherwise known as the F_0F_1-ATP Synthase, which is involved in the production of ATP[40, 41]. Oxidative phosphorylation is tightly regulated to maintain normal function of the

mitochondria. This system can be controlled from many points within the cell including expression regulation, post-translational modifications, the uncoupling of the ETC from complex V, second messenger systems, substrate availability and metabolite-binding. Flux control of oxidative phosphorylation is shared by all components of the system [42]. The mitochondrial membrane potential (ΔΨm) is involved in the control of the mitochondrial permeability transition pore (MPTP), a protein that alters the permeability of the mitochondrial membrane. Just as ΔΨm can control MPTP opening, MPTP opening can result in dissipation of the ΔΨm. The MPTP can be opened by calcium and can be further sensitised to calcium in the presence of ROS[43].

Recent work by Zhang *et al.* showed that MPTP opening can be exploited as an anti-cancer treatment by demonstrating that the activation of RPCK1 and PTEN and inactivation of PI3K (phosphatidylinositol-3 kinase) results in the dephosphorylation of GSK3β (glycogen synthase kinase 3 β) and MPTP opening leading to apoptosis[44]. Further to this, Solaini *et al.* have suggested that cancer cells may be utilising the dysfunction of MPTP opening to escape death[45].

It has been suggested that between 40 and 75% of ATP required by tumour cells is acquired by glycolysis while the remaining ATP is produced in the mitochondria[46]. Due to the excessive consumption of glucose by cancer cells, tumours are eventually required to look for an alternative fuel choice. HeLa cells in a glucose-based medium have been shown to metabolise about 80% of glucose via glycolysis to lactic acid while only 5% gets metabolised to substrates for the Krebs cycle[47],

however, in the absence of sugar, ATP levels are maintained. More recently, it has been shown in HeLa cells, that in the absence of glucose, tumour cells switch to glutaminolysis which allows these cells to produce ATP exclusively by oxidative phosphorylation and that this metabolic switch is due to structural changes in the mitochondria[48].

1.4 Tumour Associated Genes

There are several genes associated with either oncogenic (tumour promoting), or tumour supressing qualities. Oncogenes and proto-oncogenes are genes that encode growth factors (transforming growth factor; TGF), cell surface receptors (epidermal growth factor receptor; EGFR), intracellular signal transduction pathways (ras gene family), DNA binding proteins/ transcription factors (MYC, JUN), cell cycle proteins (cyclins and cyclin dependant kinases) and apoptosis inhibitors (bcl-2) whereas tumour suppressor genes are usually involved in maintenance of the cell cycle and DNA quality control and repair.

Some of the most common oncogenes are the EGFR gene family, CCND-1 and the RAS gene family. The EGFR gene family includes Her2 (human epidermal growth factor receptor 2) which is commonly associated with breast cancer. The overexpression of Her2 has been shown to be overexpressed in up to 30% of breast cancers and is associated with a more aggressive form of the disease[49]. Cyclin D1, encoded by the CCND-1 gene, is a promotor of cell proliferation and a key regulator of the cell cycle that is commonly overexpressed in many cancers such as breast, lung and bladder carcinomas, adenocarcinomas and mantle cell

lymphoma[50]. Mutations in CCND-1 have also been associated with oesophageal carcinoma[51].

The Ras gene family is comprised of three genes KRAS, NRAS and HRAS. Mutations in these genes have been long associated with tumour initiation and survival and are mutated in about 20% of oral cancer cases[52]. RAS proteins are members of a superfamily of small GTPases and act as cytoplasmic signal transducers in a diverse selection of cellular processes such as cell proliferation and apoptosis. It is therefore not surprising that gain-of-function mutations in RAS genes are found in almost 25% of human cancers[53].

Tumour supressing genes often undergo loss-of-function mutations in cancer. Examples of commonly mutated tumour supressing genes are the *P53* gene and the retinoblastoma gene (*Rb*). The *Rb* gene is a cell cycle regulator involved in DNA damage repair, maintenance of telomere length and regulation of chromosomal condensation and cohesion[54]. The majority of human cancers either have a mutation in the *Rb* gene or a mutation in the Rb signalling pathway resulting in the inactivation of the Rb protein[55] showing how integral this gene is in preventing tumorigenesis.

1.4.1 Tumour protein 53

The most widely studied tumour supressing gene is tumour suppressor protein 53. P53 is a transcription factor involved in cell cycle arrest, DNA repair and the apoptotic or senescent response to mutagenesis. P53 can regulate cellular metabolism by decreasing glycolytic flux and

promoting oxidative phosphorylation[56, 57]. By doing this, P53 can provide a mechanistic way of preventing the Warburg effect that contributes to tumorigenesis. For that reason, it is to be expected that mutations to the *P53* gene are found in about 50% of human cancers. *P53* can be activated by cellular events such as hypoxia, DNA damage, starvation, mitochondrial stress, heat/cold shock, protein misfolding, and activation of oncogenes[58].

Mutant *P53* (*mTP53*) regularly confers dominant negative effects over the wild type. As stated previously, P53 acts as a negative regulator of glycolysis and a positive regulator of oxidative phosphorylation in both tumour and normal cells. *MTP53*, however, works conversely by positively regulating glycolysis[59]. It was shown by Gualberto *et al.*, back in 1998 that *mTP53* can create polyploid genomes by disrupting the regulation of spindle checkpoints[60]. Genomic instability has since become one of the major hallmarks of cancer[20] and its link to *P53* mutations has become more established. *MTP53* can also promote cell migration and tumour invasion via direct or indirect interactions with P53-regulated genes such as *Rho* family genes, *IGF* (insulin-like growth factor) and *Cyclin G2*[61] .

Another common action of *mTP53* is resistance to apoptotic signalling. Normal *P53* induces apoptosis via BAX (Bcl-2-associated X protein), PUMA (*P53* upregulated modulator of apoptosis), NOXA and APAF-1 (apoptotic protease activating factor-1) and these pathways are often affected by *mTP53*[62]. *MTP53* is associated with increased resistance to apoptosis-inducing agents such as chemotherapeutics[63]. This *mTP53*-

associated resistance highlights the importance of screening patients for *P53* mutations prior to treatment.

1.5 Autophagy

Autophagy is a form of programmed cell death, classified as a type II cell death pathway. It is distinguished from apoptosis (type I cell death) and necrosis (type III cell death) by cell death occurring in the absence of chromatin condensation and the presence of autophagic vacuolisation of the cytoplasm. Despite being referred to as 'autophagic cell death' it would be more accurate to describe this process as cell death occurring with autophagy.

Autophagy is most commonly known as a cell survival mechanism, functioning by delivering cytosolic components to the lysosome for proteolytic degradation[64]. Through this process autophagy allows for the recycling of cellular components in extreme environments, such as starvation, prolonging the survival of the cell. Further discussion of autophagy within this thesis will be from the perspective of autophagy as a cell survival mechanism. Several studies have implicated a role for autophagy in both tumour suppression and tumorigenesis[65] both of which can occur as a result of over or under activation of the pathway.

Three types of autophagy have been identified: chaperone-mediated autophagy[66], microautophagy and macroautophagy. Macroautophagy (hereafter referred to as autophagy) is the process of degrading well-established proteins in a lysosome-dependant manner (Figure 1.3). One of the most common hallmarks of autophagy is the formation of double-membrane bound organelles called autophagosomes[65]. These

autophagosomes fuse with the lysosome to digest damaged organelles and other cytoplasmic material, which is released back to the cytoplasm by lysosomal proteases. The autophagic pathway has been linked to many cancers including oral cancer and as previously stated, is known as a "double edged sword" in cancer, as dysregulation of this pathway can be tumorigenic or tumour suppressing depending on the cancer and the type of dysregulation.

Autophagy is intrinsically linked with many other biological pathways including the mTOR pathway[67] which directly influences the activation or inhibition state of autophagy. mTOR inhibits the ULK1 complex, activation of which is required to initiation phagophore formation. Inhibition of mTOR, therefore, triggers the induction of autophagy thorough the failure of ULK1 activation. Autophagy is an integral part of basal cellular function for all cell types and is regulated in response to intracellular and extracellular cues such as starvation, hypoxia, amino acid depletion and endoplasmic reticulum (ER) stresses[68]. According to Shen and Codogno, there are three criteria for cell death to be classified as having occurred through autophagic mechanisms. These are: Cell death occurs without apoptosis, there is an increase in autophagic flux (not just autophagic markers) and suppression of autophagy via pharmacological inhibitors and by genetic approaches can rescue or prevent cell death[69]. There are five main stages in the autophagic pathway: induction, phagophore formation, autophagosome formation, lysosomal fusion and degradation (Figure 1.3).

Induction of autophagy begins with activation of the ULK1 (Unc-51 Like Autophagy Activating Kinase 1) complex, consisting of ULK1 (a serine/threonine protein kinase), Atg13 (autophagy-related protein 13), FIP200 (FAK Family Kinase-Interacting Protein Of 200 KDa) and Atg10[70]. Following induction, a phagophore or isolation membrane is formed. Studies show that this phagophore originates from the ER, although, it is still unclear if that is the only origin site[71] A second complex, the Phosphatidylinositol 3-kinase (PI3-K) complex, is also required for phagophore formation. The PI3-K complex consists of the class III PI3-K proteins hVps34 and hVps14, Atg14L, beclin1 and AMBRA1 (activating molecule in BECN1-regulated autophagy protein 1) and is required for the production of phosphatidylinositol 3-phosphate (PI3P), a phospholipid essential for phagophore assembly[72].

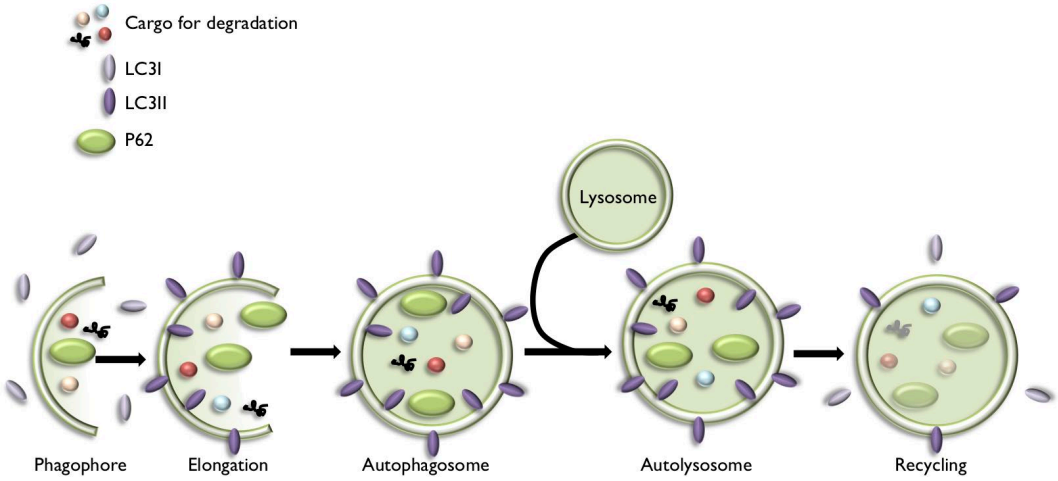

Figure 1.3: The autophagy pathway.

Autophagy begins with the formation of the phagophore which elongates to create the enclosed, double-membraned, autophagosome. The autophagosome then fuses with the lysosome to form the autolysosome which provides an acidic environment that allows nutrient recycling.

Two enzymatic pathways drive autophagosome formation, the Atg12 conjugation system (Figure 1.4A) and the LC3 conjugation system (Figure 1.4B). These pathways act as a cascade and conjugate Atg12 and microtubule-associated protein light chain 3 (LC3) to Atg5 and phosphatidylethanolamine (PE) respectively[73]. There are three different isoforms of LC3 in humans; LC3-A, LC3-B and LC3-C. LC3-B (henceforth referred to as LC3) is most studied isoform and is the only form accepted as a readout of autophagic flux. LC3 can exist in either the soluble form LC3-I or the functional form LC3-II with each form interacting with different Atg proteins. Both the LC3 and Atg12 conjugation systems involve Atg7, an E1 ubiquitin-activating enzyme involved in membrane fusion, however they have different E2, ubiquitin-conjugating enzymes (Atg10 and Atg3).

The autolysosome is formed through fusion of the lysosome with the autophagosome. Lysosomal fusion begins once extension of the phagophore has completed to form the enclosed autophagosome. Autophagosome maturation and lysosomal fusion require Rab proteins (small GTPases) and SNAREs (soluble N-ethylmaleimide-sensitive factor attachment protein receptors.) Rab7 has been identified as one of the key Rab proteins in autophagosome maturation where it was shown to guide cargo traffic along microtubules for use in lysosomal fusion [74]. VAMP7, a SNARE protein involved in the regulation of lysosome and matrix metalloprotease excretion, is another key protein in lysosomal fusion with the autophagosome to generate the autolysosome [75].

The discovery that Atg5$^{-/-}$ and Atg7$^{-/-}$ mice were healthy suggested the existence of an autophagic pathway independent of these proteins. Nishida *et al.* verified this in 2009 and identified ULK-1 and Beclin-1 as key mediators in this Atg5/Atg7 independent pathway [76]. It is still unclear what the exact mechanism is for this pathway.

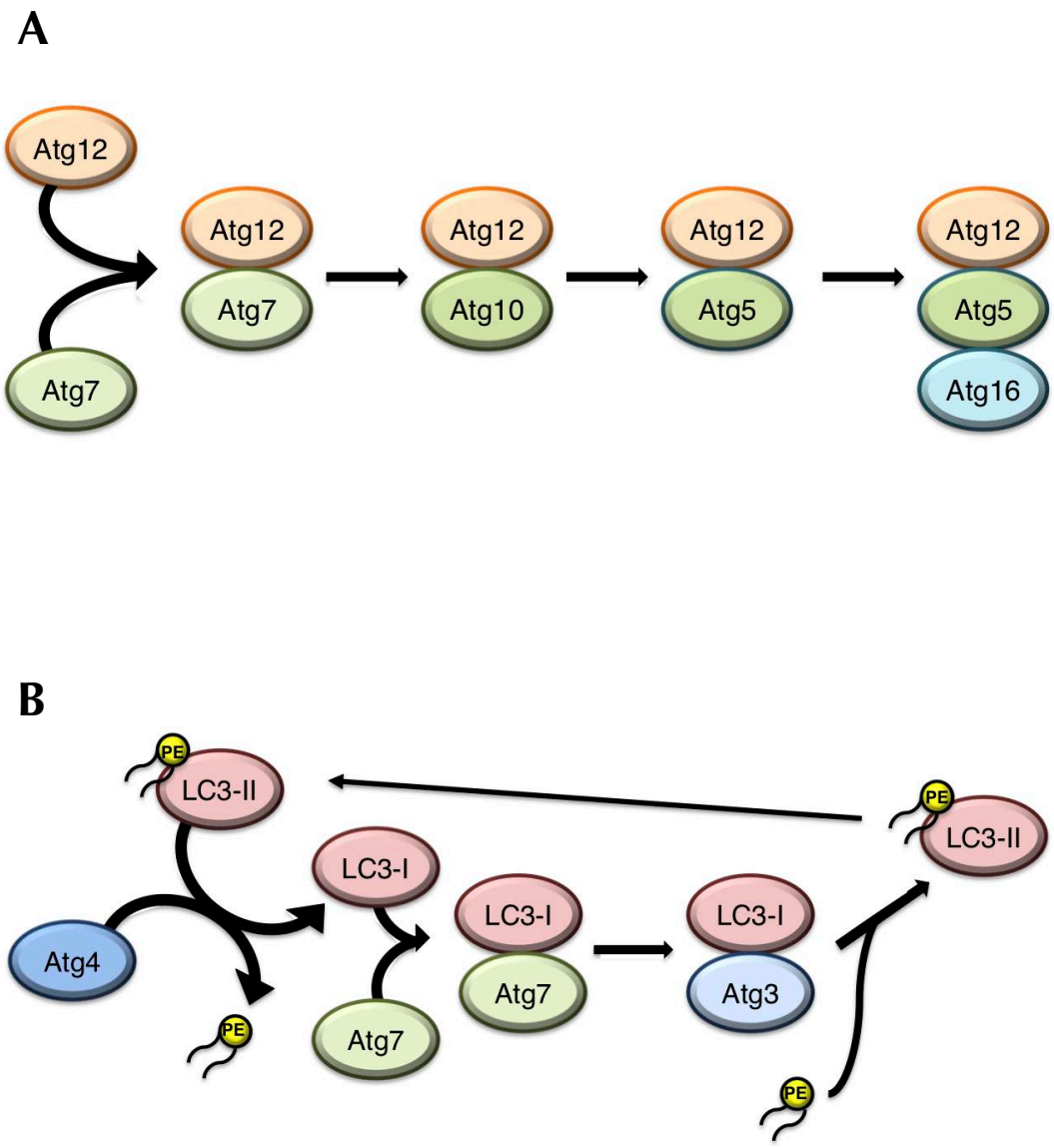

Figure 1.4: Atg12 (A) and LC3 (B) conjugation. These pathways conjugate Atg12 and LC3 to Atg5 and PE respectively and must take place to allow the formation of the autophagosome. Both conjugation systems involve Atg7, an E1 ubiquitin-activating enzyme involved in membrane fusion, however they have different E2, ubiquitin-conjugating enzymes (Atg10 and Atg3).

1.5.1 Regulation of autophagy

The process of autophagy is vital for cell survival as it promotes cellular senescence and cell surface antigen presentation, protects against genome instability, prevents necrosis, and provides an internal source of cellular energy. Autophagy involves the degradation of long-lived proteins which is essential as dysregulation can lead to cancer, infection, inflammatory diseases, autoimmunity, neurodegeneration and contributes to the aging process.

An extensively studied regulator of the autophagy pathway is the mammalian target of rapamycin complex (mTORC). In mammalian and other eukaryotic cells, autophagy is closely coupled to cell growth regulation by mTOR. One mTOR complex, mTORC1, is comprised of mTOR and raptor (a scaffold for mTOR-mediated phosphorylation of mTOR substrates), along with G-protein beta subunit-like (GβL) and proline rich AKT1 substrate 1 (PRAS40)[77]. Many of the pathways that drive the regulation of autophagy (Figure 1.5) involve mTORC1 including amino acid depletion and energy depletion, however, amino acid depletion can influence autophagy independently of mTOR[78], as can ER stress, and hypoxia stress.

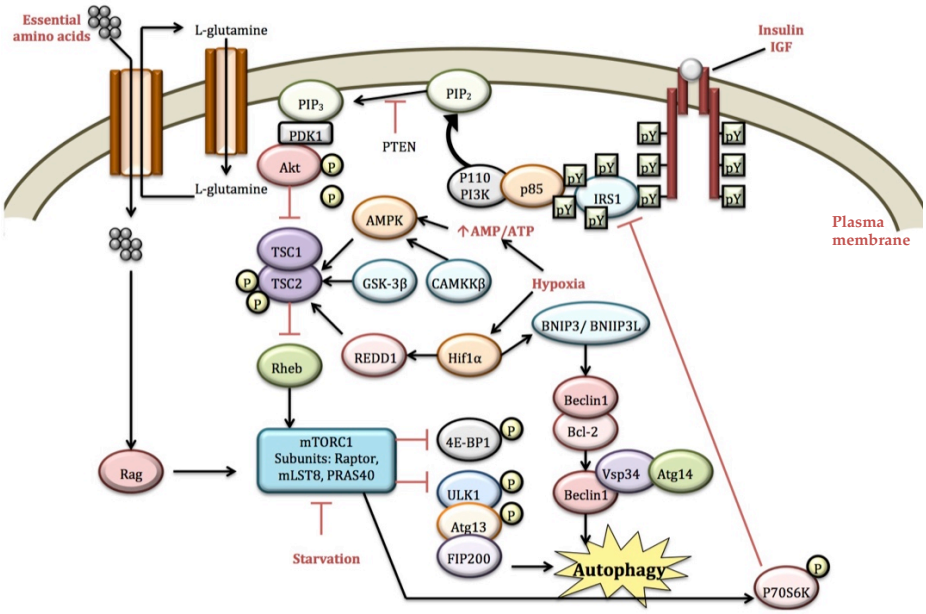

Figure 1.5: Signalling pathways leading to autophagy activation. Many pathways including the PI3K pathway can cause activation of autophagy. Autophagy is driven by the inhibition of mTORC1 which drives the ULK1 complex and initiates phagophore formation.

1.5.2 Selective and non-selective autophagy

Autophagy can be categorised as selective or non-selective. Although it was previously assumed that most autophagy is non-selective, accumulating research is indicating that autophagy is far more of a selective process than originally thought. Non-selective autophagy is a bulk degradation system that degrades any organelle or molecule in the vicinity of the autophagosome. Selective autophagy, on the other hand, includes the utilisation of adaptor proteins that interact with both LC3 and targeted organelles/molecules [79]. Over the last ten years, many cellular components have been identified as cargo for selective autophagy including mitochondria (mitophagy), peroxisomes (pexophagy), lipid droplets (lipophagy), endoplasmic reticulum (reticulophagy) and ribosomes (ribophagy)[80]. The most studied adaptor proteins are P62/SQSTM1 and NBR1 (neighbour of BRCA1 gene 1).

When p62 was originally cloned, its ability to form aggregates was noted landing it with the name sequestosome 1 (SQSTM1). P62 co-aggregates with ubiquitinated substrates such as misfolded proteins [81]. These ubiquitinated substrates are then linked to the autophagosome through p62's LC3-interacting region (LIR). P62 has been shown to bind directly to LC3A, LC3B and the GABARAP and GABARAP-like proteins through a 22-amino acid sequence located between P62's N-terminus and the UBA domain [82]. P62 can be degraded by the proteasome [83] and through endosomal-related autophagy [84] but is primarily degraded by selective autophagy and measuring its relative level has become a common method for determining the autophagic flux [85].

NBR1 has not been studied as extensively as P62. Although NBR1 is less researched, the gene displays a wider evolutionary distribution to P62. P62 is not found in plants and fungi whereas NBR1 is found in plants, fungi and metazoans. The difficulty with NBR1 research lies within the fact that the gene is lost within many model organisms including drosophila and *C. elegans* [79]. NBR1 contains an N-terminal PB1 domain, an LIR and a C-terminal UBA domain. It has many functions within the body. It binds directly to titin (a sarcomeric protein kinase) and p62 within the sarcomere of skeletal muscle [86]. NBR1 also interacts with Spred2 (to down-regulate fibroblast growth factor signalling. This allows for lysosomal degradation of activated receptors [87]. Loss of NBR1 has been shown to alter levels of p62 and increased osteoblastogenesis [88]. In this way, both p62 and NBR1 are involved in bone remodelling. NBR1 has been identified as a mediator of T-cell activation and has a role in the control of Th2 differentiation [89].

1.5.3 Autophagy in tumour suppression

Many tumour types display a depletion of autophagic proteins. The loss of beclin1 has been observed in human breast, ovarian and prostate cancers[90]. Similarly, deficiencies in the Atg5 gene in epithelial kidney cell lines and Beclin-1 (an autophagy promoting protein) in mammary cell lines have been shown to promote tumorigenesis[91]. Autophagy's role in damage mitigation allows for maintenance of general cellular health. When autophagy fails, damage can occur and accumulate through DNA mutations and chromosomal instability[91]. Accumulation of damaged mitochondria, P62 and ubiquitin-containing protein aggregates were

found in the cells of autophagy defective mice and both protein aggregation and damaged mitochondria are strongly associated with ROS production[92]. It may follow that persistent protein and organelle damage and excessive oxidative stress results in rendering autophagy-defective cells more tumour-prone. Similarly, defects in autophagy can result in chromosomal instability, indicating that autophagy plays a strong protective role in preventing tumorigenesis[93].

Chronic non-apoptotic cell death associated with stress, such as necrosis, can evoke an inflammatory response. Defects in the autophagy pathway can result in impaired survival in stress leading to inflammation[94], which can alter the tumour microenvironment and aid tumour progression. Hepatocellular carcinoma (HCC) is a prime example of tumorigenesis resulting from persistent inflammation. Excessive exposure to viral infections or toxins such as alcohol can result in chronic cell death, leading to tissue damage and inflammation. Normal hepatocyte cell death results in the activation of Kupffer cells and the stimulation of proliferation to compensate for cell death, however, over-proliferation in the case of chronic cell death can result in tumorigenesis[95].

Beclin-1 is essential for the activation of class III PI3K. Beclin-1 is mono-allelically deleted in human breast, ovarian and prostate cancer. Beclin-1 can also inhibit tumorigenesis in nude mice, further demonstrating the tumour suppressing abilities of autophagy[96]. Dual inhibition of mTOR and Class IA PI3K, which drives Akt activity, has been shown to result in anti-leukemic activity[97] showing, once again, the tumour suppressing activities of autophagy.

1.5.4 Autophagy in tumour survival

In many cancer types, including OSCC, autophagy can drive tumorigenesis by protecting tumour cells from their nutrient and oxygen depleted environment. A recent study of 7 normal tissue samples, 41 leukoplakias and 120 OSCC samples has shown increasing levels of LC3II associated with increasing severity of leukoplakia and advancing OSCC stage. This increase in LC3II with progression of leukoplakia correlated with the lesion's tendency towards malignant transformation[98]. Patient studies have shown a strong association between the autophagy markers LC3B and P62 with poor prognosis in OSCC patients[99, 100].

Both activation and inhibition of GSK3β, an enzyme that strongly influences protein and glycogen synthesis, can result in oncogenic progression in a cell type-dependant manner. Inhibition of GSK3β can induce autophagy via pro-survival signals, which could potentially lead to oncogenesis and tumour survival[101], this is important in oral cancers, where GSK3β is often inactivated[102]. It has also been shown that activation of GSK3β in oral cancer cells can reverse the epithelial to mesenchymal transformation (EMT) that occurs during cancer by the up-regulation of E-cadherin. This complements the research done by Kühn and Römer, which demonstrated that up regulation of E-cadherin can stabilise β-Catenin, preventing its transcriptional activity that inhibits the initiation of autophagy[103]. These data imply a possible relationship between autophagy and EMT. Recent work by Chen *et al.* has identified

two glycolytic enzymes, phosphofructokinase-platelet (PFKP) and hexokinase II (HKII) that drive both autophagy and EMT[104, 105].

During the initial stages of tumour progression, insufficient vascularisation can limit the amount of oxygen and nutrient supplied to the cancer cells. Throughout this stage of a tumour, activation of AMPK and HIF-1 can stimulate autophagy to promote survival of these hypoxic cells. ATG16L1, an essential protein in autophagy, is expressed in malignant oral cancer cells and stroma but not in normal tissues implying that increased levels of autophagy occur in malignant tissues[106]. In this circumstance autophagy is likely serving as a protective factor for tumour cells, allowing their survival in this stressful environment.

Several other gene mutations within the autophagy pathway or within autophagy regulators have also indicated a role for autophagy as a survival mechanism for tumour cells. Gain of function mutations in the ATG12 gene causing an increase in autophagy have been associated with HNSCC[107]. Wei *et al.* demonstrated that the conditional knock out of the FIP200 protein prevents oncogene-driven mammary tumorigenesis, indicating autophagy's tumorigenic role[108]. It is possible, however, that FIP200 may drive tumorigenesis independently of autophagy. In mice, mosaic deletion of ATG5 or ATG7 in the liver results in benign tumours in the liver and none in the other tissues[109]. The formation of these tumours in the ATG deletion sites, highlights the role of autophagy as a tumour suppressor.

1.5.5 Autophagy in cancer treatment

Thanks to the outstanding work by Yoshinori Ohsumi throughout the 90's, which lead to a Nobel Prize in 2016, autophagy has become a key player in the study of many diseases including cancer. Over the last decade, autophagy and cancer have become intrinsically linked becoming known as a "double edged sword" that is involved in both tumour suppression and tumour progression.

Cancer cells often have a deficient apoptotic mechanism, which they exploit to allow for prolonged cell proliferation. It has been shown that increased autophagy inhibits apoptosis in head and neck squamous cell carcinoma (HNSCC) cells[110]. This research correlates with previous work showing that cancer cells can escape necrotic cell death by utilising autophagy as a survival mechanism, driving tumour propagation[94]. Conversely, autophagy can promote tumour suppression by removing damaged proteins and organelles and by preventing genome damage that can result in tumorigenesis. Many activators of autophagy are tumour suppressors such as Beclin-1, PTEN, TSC1/2, P53 and ceramide (Table 1.1). Interestingly, P53 can drive autophagy through both its activation and inactivation[111]. Chronic activation of autophagy can allow some cancer cells to go into a dormant phase, which they exit when desired metabolic conditions return allowing for tumour survival[112]

Protein	Expression	Effect on Autophagy	Effect on Tumorigenesis	Type of Cancer	Ref.
Akt	Up regulation	Inhibitor	Tumour promoter	OSCC	[113]
Akt	Inhibition	Promoter	Tumour promoter	OSCC	[114]
MTOR	Up regulation	Inhibitor	Tumour promoter	Large intestine adenocarcinoma, renal cell carcinoma	[115, 116]
mTOR	Inhibition	Promoter	Tumour suppressor*	Not Specified	[115, 117]
PTEN	Over-expression	Promoter	Tumour suppressor	Colon Cancer	[118]
PTEN	Deletion	Inhibiter	Tumour promoter	Breast, glioma, colorectal, gastric, endometrial, liver, haematological, lung, skin, prostate	[119, 120]
TSC2	Up regulation	Promoter	Tumour suppressor	Not Specified	[121]
PI3K	Up regulation	Inhibitor	Tumour promoter	Head and neck, thyroid, lung gastric, squamous cell, cervical, adenocarcinoma, breast, oesophageal adenocarcinoma	[122, 123]
PI3K	Down regulation	Promoter	Tumour suppressor	Neuroblastoma	[124]

Table 1.1: Proteins effecting autophagy and tumorigenesis.

*Most effective anti-tumour activity occurs in combination with inhibition of other components of the PI3K/Akt/mTOR pathway or chemotherapeutics.

1.6 Chemoresistance

One of the major factors impacting OSCC patients is late diagnosis, necessitating the treatment of advanced, late-stage tumours. Treatment of these types of tumours with chemotherapy tends to be less effective as significant transformation will have occurred within the DNA of the tumour cells allowing for lowered sensitivity to apoptosis-inducing factors[125]. For other cancers with similar late diagnosis, such as ovarian cancer, surgical removal of the tumour is the primary treatment followed by chemotherapy[126], however, due to the location of OSCCs, tumour removal frequently results in large amounts of facial tissue and bone being removed leaving severe facial disfiguration which is an extremely undesirable outcome and impacts greatly on the patients QOL. Chemoresistance is a common occurrence in OSCC. Cisplatin (CPt) is one of the most commonly used chemotherapy drugs in OSCC and is usually used in combination with other chemotherapeutics such as 5-fluorouracil (5-FU)[127]

CPt is one of the most widely used chemotherapeutic drugs. First synthesised in 1845 by Peyrone, cisplatin's antiproliferative properties weren't discovered until 1965 by Rosenburg who later went on to show its ability to cure solid tumours[128]. In 1978 cisplatin was first approved by the FDA (food and drug administration) and since then has become the first choice of chemotherapeutic intervention in many cancer types including ovarian, bladder, lung, ovarian, testicular and head and neck cancers[129]. CPt works by creating crosslinks in the purine bases of double stranded DNA. This crosslinking then induces DNA damage and

interferes with DNA repair mechanisms and subsequently induces apoptosis. As cancerous cells divide more rapidly than non-cancerous cells, CPt induces apoptosis more frequently and more rapidly in cancerous tissues.

There is evidence that *mTP53* is linked to the development of CPt resistance. Nrf2 (nuclear factor erythroid 2-related factor 2) is a transcription factor that is upregulated by *mTP53* and its activation is involved in cisplatin resistance in non-small lung cell cancer[130]. In colon carcinoma cells the loss of *P53* has been shown to increase the rate of resistance formation particularly when combined with DNA mismatch repair[131]. In OSCC it has been shown that tumours with *mTP53* or loss of *P53* confer a significantly lower response to CPt treatment when compared to patients with wild type *P53*[132], implicating its involvement in the high rate of chemoresistance development in OSCC.

1.6.1 Autophagy in chemoresistance

Autophagy initiation appears to play an important role in the mediation of resistance. Due to autophagy's role in allowing a cell to adapt to stress, treatment with chemotherapeutic agents can induce autophagy, thus promoting cell survival and lowering the efficacy of the chemotherapeutics. Inhibition of the PI3K/Akt pathway has been shown to enhance sensitivity of cells to CPt in ovarian cancer cell lines, implying that by preventing initiation of the survival system, cells were more sensitive to apoptosis[133]. A limited amount of research has gone into the use of autophagy inhibitors to re-sensitise tumour cells to chemotherapeutics, however, chloroquine (CQ), the broad spectrum

autophagy inhibitor and anti-malarial drug, has been investigated in clinical trials to test its use in conjunction with chemotherapy with some promise for enhanced efficacy of treatment[133]. CQ is an ideal autophagy inhibiting drug as it has already been approved by the European Medicines Agency (EMA) and the FDA for use in humans, however, due to its many actions on the cell other than autophagy it is important to identify more specific inhibitors of autophagy to ensure that the correct pathway is being targeted. A more recent experiment which examined the autophagy inhibitor 3-methyladenine (3MA) in conjunction with radiotherapy in oesophageal SCC cells *in vivo,* showed similarly promising outcomes for autophagy inhibition sensitising cells to apoptosis[134].

Tumours require autophagy to survive hypoxic and nutrient-depleted conditions. Because of this, autophagy is often found to be upregulated in tumour cells conferring these cells with a survival advantage when subjected to chemotherapy. Recent work by Ma *et al.* (2017)[135] has shown that resistance to CPt can be mediated by CD147, a plasma membrane protein involved in intracellular recognition of immunologic phenomena. This was shown to occur via the MAPK/ERK signalling pathway, a pathway that directly affects mTORC1 and the induction of autophagy. CD147 has also been shown to be overexpressed in CPt-resistant HNSCC cell lines[136].

1.7 Conclusion

The role of autophagy within cancers, particularly OSCC is still ambiguous and both over activation and under activation of autophagy can result in tumorigenesis. A common consensus among researchers is that autophagy restricts tumour initiation, but it can serve as a protective mechanism in established tumours. In more advanced tumours, where autophagy is up regulated to maintain cells in a stressful, nutrient and oxygen-starved environment, autophagy may also protect the tumour cells from chemotherapy. This survival mechanism is likely to result in the formation of resistance leading to further cellular alterations caused by the chemotherapeutic agents. Establishing the link between autophagy and resistance is essential so that more focused and specific treatment plans can be made for patients. If resistance biomarkers are uncovered, and treatment for OSCC is more targeted to the individual then the likelihood of resistance and tumour recurrence could be decreased.

1.8 Aims

This study aims to characterise and manipulate the mechanisms of cell death induced in OSCC cell lines (described in section 2.2) following treatment with known chemotherapeutics. It is understood that damaged and dying cells trigger autophagy. Autophagic survival may lead to an acquired resistance to chemotherapy by retaining components of the cell that have been affected by the chemotherapeutics and have adapted to withstand its toxic properties. By inhibiting the autophagic process during chemotherapy it may be possible to impede this survival mechanism and prevent resistance developing, thereby making the therapy more effective and less invasive to the patient. This investigation into the interplay between chemotherapy and autophagy will be explored though the following key objectives:

1. **Identification of a robust mechanism for measuring the autophagy modulations in OSCC**

   Staining of acidic vesicles using acridine orange and western blot analysis of LC3B an P62 will be used to understand the response of Ca9-22, SCC4, TR146 and DOK cells to both induction and inhibition of autophagy. These methods will be analysed for their robustness and reliability when monitoring autophagy modulation across distinct cell lines.

2. **To characterise of the impact of chemotherapeutic intervention on autophagy in OSCC cell lines**

   The OSCC cell lines Ca9-22, SCC4 and TR146 and the dysplastic, DOK, cell line will be treated with CPt, CBDCA, 5-FU and TXT to

investigate the impact of chemotherapeutic intervention on autophagy.

3. **Determine how modulating autophagy may influence the efficacy of a chemotherapy regime in OSCC cell lines**

   Autophagy will be inhibited in Ca9-22, TR146 and DOK cells in parallel to treatment with CPt to investigate whether autophagy inhibition has the potential to improve chemotherapeutic efficacy.

4. **Investigation into metabolic alterations during chemotherapeutic intervention in OSCC cell lines**

   Using flowcytometric analysis of TMRM and MitoTracker green alongside seahorse analysis, metabolic alterations to OSCC cells will be examined in response to CPt treatment in the presence or absence of autophagy inhibitors.

5. **Identification of *P53*'s role in cisplatin sensitivity in OSCC cell lines**

   P53 will be knocked down in TR146 cells using siRNA. By comparing $P53^{+}$ and $P53^{-}$ cells, the *P53*-mediated response to cell death and metabolic changes will be investigated by measuring the effect on cellular metabolic activity through using the alamar blue assay and Seahorse Real-Time cell metabolic analysis in conditions of CPt treatment in the presence or absence of autophagy inhibitors.

Chapter 2

Materials and Methods

2.1 General Methods

All chemicals were obtained from Merck (Ireland), unless otherwise stated.

2.1.1 Buffers and solutions

Aqueous solutions were prepared using water from a Millipore Direct-Q3 Water Purification System. All buffers and solutions were prepared at the appropriate pH using a Corning pH meter model 240. The pH meter was calibrated daily conforming to the manufacturer's guidance using standard buffer solutions of pH 4, 7 and 10. Weights of 1g or less were weighed using a Mettler four place fine balance while larger quantities were weighed on a Mettler two place balance.

Reagent	Product code	Solvent
3-Methyladenine	M9281	DMF
Chloroquine	C6626	dH_2O
DBeq	SML0031	DMSO
E64d	E8640	MeOH:H_2O (1:1)
PepstatinA	77170	EtOH
Cisplatin	P4394	dH_2O
Carboplatin	C2538	dH_2O
5-Fluorouracil	F6627	DMSO
Docetaxel	O1885	EtOH

Table 2.1. Reagents and their solvents

Annexin V binding buffer

10 mM Hepes/NaOH (pH 7.4), 140mM NaCl, 2.5 mM CaCl2

DNA gel electrophoresis loading buffer (2x Laemmli buffer)

4% (w/v) Sodium dodecyl sulphate (SDS), 10% (v/v) 2-mercaptoethanol, 20% (v/v) glycerol, 0.004% (w/v) bromophenol blue, 0.125 M Tris-HCl (pH 6.8).

Flow cytometry buffer

PBS, 20% culture media (cell specific, see section 2.2)

Krebs buffer

300 μM KCl, 14 mM NaCl, 2.5 mM Tris-HCl (pH 7.4), 200 μM MgCl2, 200 μM CaCl, 10 mM glucose.

Lysis buffer (RIPA)

50 mM Tris-HCl (pH8.0), 150 mM NaCL, 0.1% (v/v) Triton X-100, 0.5% (w/v) sodium deoxycholate, 0.1% (w/v) SDS, Protease Inhibitor Cocktail (1 tablet per 10 mL of buffer, Roche).

Western blotting running buffer

25 mM Tris-HCl (pH 8.3), 190 mM glycine, 0.1% (w/v) SDS.

Western blotting Anode I buffer

300 mM Tris (pH 10.4), 10% (v/v) methanol.

Western blotting Anode II buffer

25 mM Tris-HCl (pH 10.4), 10% (v/v) methanol.

Western blotting Cathode buffer

25 mM Tris-HCl (pH 9.4), 40 mM glycine.

Tris-buffered saline solution (TBS)

20 mM Tris-HCl (pH 7.5), 150 mM NaCl.

Tris-buffered saline with tween (TBST) buffer

20 mM Tris-HCl (pH 7.5), 150 mM NaCl, 0.1% (v/v) Tween 20.

Western blotting blocking solution

5% (w/v) non-fat dried milk solution in TBST.

2.1.2 Antibodies and Reagents

All reagents were obtained from Merck (Ireland) unless otherwise stated.

Name	Species	Final Dilution	Manufacturer
β-Actin	Mouse	1 : 10,000	Abcam
P62	Mouse	1 : 1,000	Abcam
LC3B	Rabbit	1 : 1,000	Cell Signalling
Parp	Rabbit	1 : 1,000	Abcam
P53	Mouse	1 : 1000	Abcam

Table 2.2: Primary Antibodies

Antibody Generated	Host Species	Final Dilution	Manufacturer
Mouse	Goat	1 : 10,000	Jackson Immunoresearch
Rabbit	Goat	1 : 5,000	Cell Signalling

Table 2.3: Horse radish peroxidase-conjugated secondary antibodies

2.1.3 Measurements of weight

Mass-based measurements in the range of 5 g to 200 g were obtained using a Mettler model B2002-S top-loading balance and weights of >5 g were obtained using a Mettler model College150 analytical balance.

2.1.4 Measurements of volume

Volumes in the range of 2 μL to 5 mL were measured and delivered using a set of standard Gilson Pipetman automatic pipettes. All pipettes were regularly calibrated according to the manufacturer's instructions.

2.1.5 Centrifugation

For cell culture, cells were centrifuged in a bench top Eppendorf Centrifuge 5910 R at room temperature. Cells being prepared for western blots were centrifuged in a bench top Eppendorf Centrifuge 5415 at 4^{o}C.

2.1.6 Spectrophotometry

Absorbance assays were performed in a Spectra MAX M3 plate reader using clear 96 well plates and SoftmaxPro 6.2.1 software. Fluorescent assays were performed in a Spectra Max GeminiXS plate reader using black 96 well plates and SoftmaxPro 5.4.1 software.

2.2 Cell Culture

Cells were cultured at 37^{o}C in a humidified environment at 5% CO_2 and 95% air in a Thermo Scientific™ Series 8000 direct-heat CO_2 incubator. All cell culture work was carried out in sterile conditions in an ESCO Airstream® Class II Type A2 Biological Safety Cabinet. Cell confluence was monitored using a Nikon Eclipse TS100 light microscope with 10X and 40X dry objectives and cells were passaged every 2-3 days, when 80-90% confluent.

Cells were passaged by washing the cells with pre-warmed phosphate buffered saline (PBS) followed by incubating the cells in trypsin-EDTA (0.5% trypsin, 0.02% EDTA) for 5 min at 37°C. Fresh, pre-warmed, medium was added to the cells to deactivate the trypsin and the suspended cells were centrifuged in a falcon tube (1200 rpm/5 min). The supernatant was discarded, and the cell pellet was resuspended in fresh, pre-warmed, medium, counted and cultured at a density of $4x10^6$ cells/T175 flask.

2.2.1 Characteristics of cell lines.

Three oral squamous cell carcinoma cell lines and one dysplastic oral cell line were used throughout this research. The characteristics and distinguishing features of these cell lines are described in table 2.3 below.

OSCC Cell line	Gender	Age	Cell type	P53 status
Ca9-22	Male	-	Gingival	P53 mutated
TR146	Female	67	Buccal	P53 normal
DOK	Male	57	Tongue Dysplastic keratinocyte	12bp deletion (with no known impact on functionality)
SCC-4	Male	55	Tongue	P53 mutated Overexpressed

Table 2.4: Characteristics of four oral cell lines used.

2.2.2 Culture of Ca9-22 cells

The Ca9-22 oral carcinoma cell line (Health Science Research Resources Bank, Osaka, Japan) was maintained in minimum essential media (MEM) with 10% (v/v) foetal bovine serum (FBS), Penicillin/Streptomycin (100U/mL penicillin, 0.1mg/mL streptomycin) and L-Glutamine (2mM)(Biosciences-Ltd). These cells were cultured as described in section 2.2.

2.2.3 Culture of TR146 cells

The TR146 oral carcinoma cell line (HPA Cultures, UK) was maintained in high glucose Dulbecco Modified Eagle's Medium (DMEM) with 10% (v/v) FBS and Penicillin/Streptomycin (100U/mL penicillin, 0.1mg/mL streptomycin) and cultured as described in section 2.2.

2.2.4 Culture of SCC4 cells

The SCC4 oral carcinoma cell line (HPA Cultures, UK) was maintained in high glucose DMEM with 10% (v/v) FBS and Penicillin/Streptomycin (100U/mL penicillin, 0.1mg/mL streptomycin) and cultured as described in section 2.2.

2.2.5 Culture of DOK cells

The DOK dysplastic oral cell line (HPA Cultures, UK)) was maintained in high glucose DMEM with 10% (v/v) FBS, Penicillin/Streptomycin (100U/mL penicillin, 0.1mg/mL streptomycin) and hydrocortisone (5 μg/mL) cultured as described in section 2.2.

2.2.6 Trypan blue exclusion

Cell viability was determined using the trypan blue exclusion assay. This assay works on the principle that the intact membranes of live cells will exclude the trypan blue dye. Dead cells with permeable membranes allow the dye entry to the cytosol resulting in blue staining. Cells were counted by a Luna II™ Automated Cell Counter set to appropriate cell size restrictions for specific cell lines.

2.3 Alamar Blue

Alamar Blue (Invitrogen) is a chemical reagent used to assess cell proliferation and cytotoxicity of drugs. The main component of Alamar Blue is resazurin, which is a blue, non-fluorescent, cell permeable compound. Reducing compounds released by living cells reduce resazurin to resorufin, which carries red fluorescence (Figure 2.1).

Cells were seeded in a clear 96 well plate (15,000/well) in serum-starved culture media (1% FBS) overnight. Cells were treated with the required drug for specific time points in full serum (10% FBS) culture media. Six hours before the end point, Alamar Blue was added (10% v/v). Absorbance was read on a Spectra MAX M3 plate reader at 570 nm and 600 nm

2.3.1 Determination of IC_{50} value

The half maximum inhibitory concentration (IC_{50}) is a measure of drug concentration used to determine relative potency between drugs with similar actions, it can also be used to determine a drugs potency between

different cell types. IC_{50} values are determined by plotting the log of a drug's concentration against the percentage inhibition (Figure 2.2).

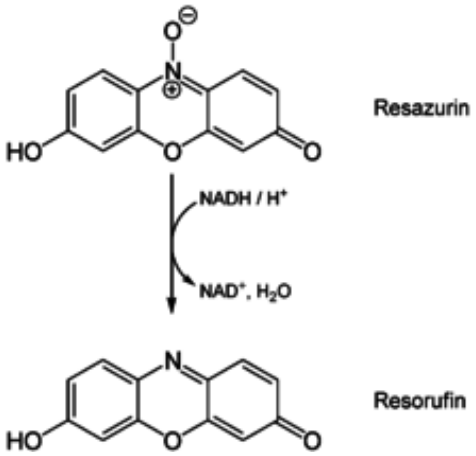

Figure 2.1: Alamar Blue works by using reducing compounds released by living cells to reduce resazurin to resorufin, which carries red fluorescence

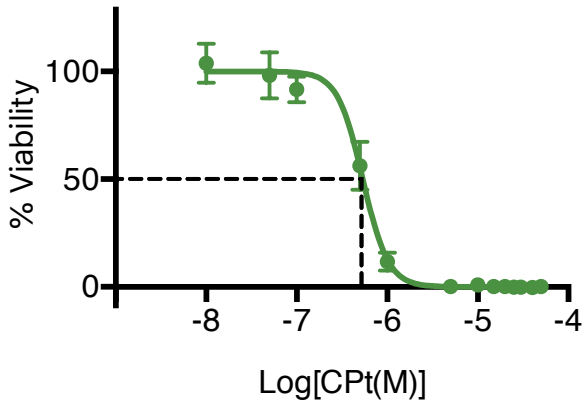

Figure 2.2: Example of IC_{50} curve showing the IC_{50} of Ca9-22 cells treated with Cisplatin for 120 h.

Cells were seeded in a clear 96 well plate in starved medium for 24 h and allowed to recover in full medium for a further 24 h before being treated with a range of concentrations of cisplatin for 120 h. Alamar Blue reagent was added 4 h before the end point and absorbance values were read at λ=570 nm and λ=600 nm Data shown n=3 ± SEM.

2.4 Fluorescent Microscopy

Live cells were viewed using a Leica SP8 confocal microscope and a 40x oil immersion objective. Several diode lasers of respective wavelengths provided excitation at 405 nm, 488 nm, 552 nm and 638 nm.

2.4.1 Analysis of acidic vesicle formation

Ca9-22 cells were cultured in 34mm four-compartment glass bottomed culture dishes at a density of 30,000 cells per compartment for 24 h. Cells were starved for 24 h in media containing 1% FBS followed by a 24 h incubation in media containing 10% FBS before being treated in the appropriate conditions for a further 24 h. Immediately before imaging, Acridine Orange was directly added to the media at a final concentration of 1 μg/mL.

An OPSL 488 nm laser provided excitation and emission was set at a range of 500 – 575 nm in the green channel and a range of 625 – 725 nm in the red channel. Cells were viewed at 1x and 3x zoom using a Leica SP8 scanning confocal microscope and Leica Application Suite X software.

2.5 Flow Cytometry

2.5.1 Analysis of cell cycle by propidium iodide

Propidium iodide (PI) is a fluorescent dye that intercalates with DNA. In non-permeabilised cells, PI will only enter cells with compromised plasma membranes, however, in permeabilised cells, PI can bind to all fragments of DNA and the resulting fluorescence correlates to the

amount of DNA and size of fragments within a cell population. By altering the conditions of PI staining, flow cytometry can be used to analyse both cell cycle and apoptotic stages in a cell population.

The distribution of cells within the cell cycle can be analysed by PI. PI intercalates with double stranded DNA resulting in levels of fluorescence, which correlate to the amount of DNA in a cell population. These varying amounts of DNA can be quantified in a flow cytometer.

Cells were treated for the required time before being trypsinised and centrifuged at 1200 rpm for 5 min. The cell pellet was washed with warm PBS, which was then removed, and the cells were resuspended in 2 mL of ice-cold EtOH and left to fix at 4°C for 30 min. Samples were pelleted at 1200 rpm for 5 min and the EtOH was removed. Cells were resuspended in 400 μL PBS containing ribonuclease A (500 μg/mL) and PI (150 μg/mL). The samples were incubated at 37 °C in darkness for 30 min. The PI was excited using a 488 nm laser in a FACS Canto flow cytometer and the resulting histograms were generated using FlowJo software (Treestar) (Figure 2.3).

2.5.2 Detection of apoptosis by Annexin V and PI

Cells undergoing programmed cell death (PCD) have characteristics associated with different types of cell death. Annexin V binds to phosphatidylserine (PS) which is located on the cytoplasmic leaflet of the plasma membrane. During early stages of apoptosis, PS translocates to the exoplasmic leaflet. PI can enter cells and bind to DNA when there is a compromised membrane, which occurs during both late-stage

apoptosis and necrosis. As necrotic cells undergo membrane disruption without the exposure of PS, the combination of Annexin V (bound to FITC) and PI allows us to determine different types of cell death occurring in different treatment conditions.

Cells were treated for the required time, then trypsinised and centrifuged at 1200 rpm for 5 min. The cell pellet was resuspended in 500 μL of ice-cold Annexin V binding buffer (BD Pharmingen) and centrifuged at 4°C for 5 min at 600 g. The supernatant was discarded, and the resulting pellet was resuspended in 100 μL Annexin V binding buffer, 5 μL PI (75 μM) and 5 μL FITCAnnexin V (BD Pharmingen; Cat No. 556419). The samples were incubated on ice for 15 min before adding 400 μL Annexin V binding buffer and transferring to FACS tubes for analysis. The Annexin V-FITC and PI were excited using a 488 nm laser in a BD Accuri C6 flow cytometer. Cells were gated as described in section 2.5.4.

2.5.3 Analysis of mitochondrial mass and polarisation state

Mitochondrial mass can change in response to changes in aerobic activity. The mitochondrial inner membrane (IMM) contains many folds (cristae) which allow for a greater surface area. Highly aerobic mitochondria, producing more ATP have more extensive cristae than those with a low aerobic activity. MitoTracker Green (MTG) labels the IMM independent of the mitochondrial membrane potential ($\Delta\Psi m$) to give a fluorescence that is proportional to the mitochondrial mass.

Mitochondria with healthy membranes need to maintain a difference in electrical potential across the inner and outer membranes in order to

maintain a stable electron transport chain, this is known as the mitochondrial membrane potential. Tetramethylrhodamine methyl ester (TMRM) accumulates in active mitochondria with intact ΔΨm. Cells with functioning mitochondria give a bright signal whereas in cells with a loss of ΔΨm , TMRM accumulation does not occur and the signal dissipates.

Cells were treated for the required time and were then trypsinised and centrifuged at 1200 rpm for 5 min and resuspended in 100 μL flow cytometry buffer containing MTG (100 μM) and TMRM (100 μM). Cells were then incubated at 37^{o}C for 30 min. Cells were then centrifuged at 1200 rpm for 5 min to wash off the staining solution and resuspended in 100 μL flow cytometry buffer. Samples were analysed immediately using a BD LSRFortessa cytometer. The MTG and TMRM were excited using lasers at 488nm and 561nm respectively. Cells were gated by side scatter area (SSC-A) vs FSC-A and doubled cells were further excluded based on forward scatter width (FSC-W) vs FCS-A (Figure 2.5).

2.5.4 Gating strategy

Single cells were gated based on their forward scatter height (FSC-H) vs forward scatter area (FSC-A) (Figure 2.4).

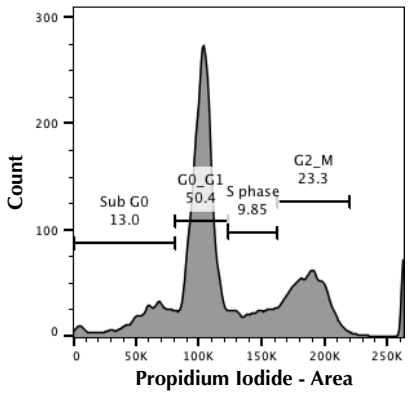

Figure 2.3: Example of typical distribution within the cell cycle in TR146 cells stained with PI.

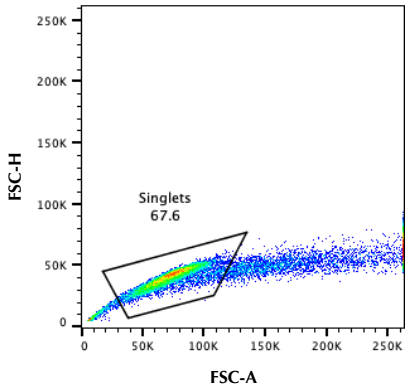

Figure 2.4: Gating of single cells in SCC4 cells.

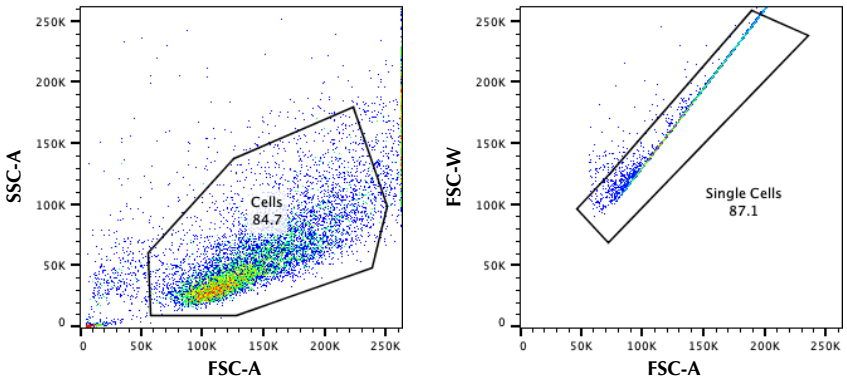

Figure 2.5: Gating strategy of single cells using the BD LSRFortessa in TR146 cells.

2.6 Protein Analysis

2.6.1 Preparation of cell lysates

Cells were seeded in T25 flasks at a density of $1x10^6$ and serum starved (1% FBS) overnight. Cells were then treated as required in full media for the desired length of time. Cells were then removed from the flasks using a cell scraper. Cells were pelleted at 1200 rpm for 5 min and resuspended in 200 μL of RIPA buffer. Cells in RIPA were maintained at constant agitation for 30 min at 4°C before sonicating using a MicroTip sonicator for 10s to degrade DNA. Lysates were then centrifuged at 3000rpm for 20 min at 4°C in a pre-cooled centrifuge. The supernatant was transferred to a clean tube and the pellet was discarded. 10 μL of each sample was taken for analysis of protein concentration. The samples were stored at -20°C until required.

2.6.2 Determination of protein content

Protein concentrations were estimated as per Bradford's method (1976), with modifications. A protein standard curve was made from serial dilutions of bovine serum albumin (BSA) ranging from 25 μg/mL to 2000 μg/mL. 10 μL of each standard or unknown was added in triplicate to a 96-well plate and 200 μL of Coomassie Plus Reagent (Figure 2.6). Samples were then incubated in the dark for 10 min at room temperature. Absorbance was read on a Spectra MAX M3 plate reader at 595 nm.

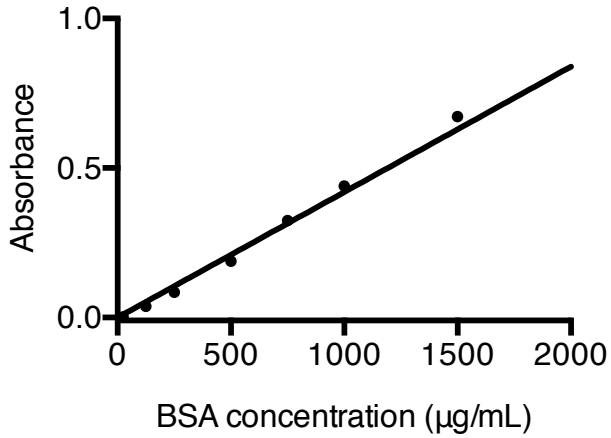

Figure 2.6. Example of protein standard curve using BSA as a protein standard.

2.6.3 SDS-polyacrylamide gel electrophoresis (SDS-PAGE)

20 μg of protein from each of the samples was added to equal volumes of 2x Laemmli buffer. The samples were heated at 65°C for 15 min.

The resolving gel was prepared at the appropriate % for target protein size as in Table 2.4 with the acrylamide polymerisation being initialised by the addition of TEMED followed by APS. This gel was left to set between the glass plates. To ensure a level boundary between the resolving gel and the stacking gel, the resolving gel was overlaid with a solution of water-saturated butan-1-ol. Once the resolving gel had set, the butanol was washed off with dH_2O. The stacking gel was prepared and poured on top of the resolving gel and the comb was inserted into the unset gel in order to form the loading wells. Once the stacking gel had polymerised, the wells were washed with dH_2O to remove any unset acrylamide. The gel cassettes were then placed into a vertical gel electrophoresis tank and immersed in running buffer.

10 – 20 μg of sample protein was loaded into each well along with Spectra multicolour broad range protein ladder (Thermo Scientific) as a marker of the progression of protein migration. The gels were then resolved at 120 V in an Atto gel box using a Biorad power pack until the protein markers were sufficiently separated.

2.6.4 Western blotting

The gel was removed from the electrophoresis tank and soaked in transfer buffer (cathode buffer). A semi-dry transfer technique was used to transfer the proteins from the gel to the PVDF membrane by

sandwiching the pre-soaked sheets of 3 mm filter paper at the anode, followed by the gel, the PVDF membrane (activated in methanol) and another pre-soaked sheet of 3 mm filter paper at the cathode (Figure 2.7). Proteins were electroblotted in a combination of Cathode and Anode buffers for 1 h at 10 V using a Trans-Blot module (Biorad).

Non-specific binding sites were blocked in 5% milk at room temperature for 1h. The membrane was washed in TBST before incubation with the primary antibody at a 1 in 1000 dilution in 5% milk overnight at 4°C. The membrane was then washed three times for 10 min in TBST and immediately placed into the secondary antibody (anti-mouse diluted at 1 in 10,000; anti-rabbit diluted at 1 in 5000) in 2% milk at room temperature and left to incubate for 1 hr. The membrane was then washed a further 3 times for 10 min.

Antibody-labelled proteins were visualized using Enhanced Chemiluminescent HRP substrate (Millipore). The two Enhanced Chemi-Luminsence reagents were mixed in a 1:1 ratio and then poured onto the membrane and incubated for ~2mins at RT. The signal generated by the HRP substrate was promptly detected using a Chemi-Luminescent gel documentation system (BioRad). The images generated were analysed using ImageLab software (BioRad) and densitometry was carried out relative to a β-Actin labelled control.

Reagents	Resolving			Stacking
	10%	12%	15%	5%
dH_20	4.0	3.3	2.3	2.1
30% Acrylamide mix	3.3	4.0	0.5	0.5
1.5M Tris (pH 8.8)	2.5	2.5	2.5	-
1M Tris (pH 6.8)	-	-	-	0.38
10% SDS	0.1	0.1	0.1	0.03
10% APS	0.1	0.1	0.1	0.03
TEMED	0.005	0.005	0.005	0.004

Table 2.4: Components of resolving and stacking gels used in SDS-PAGE given in mL reagent per gel.

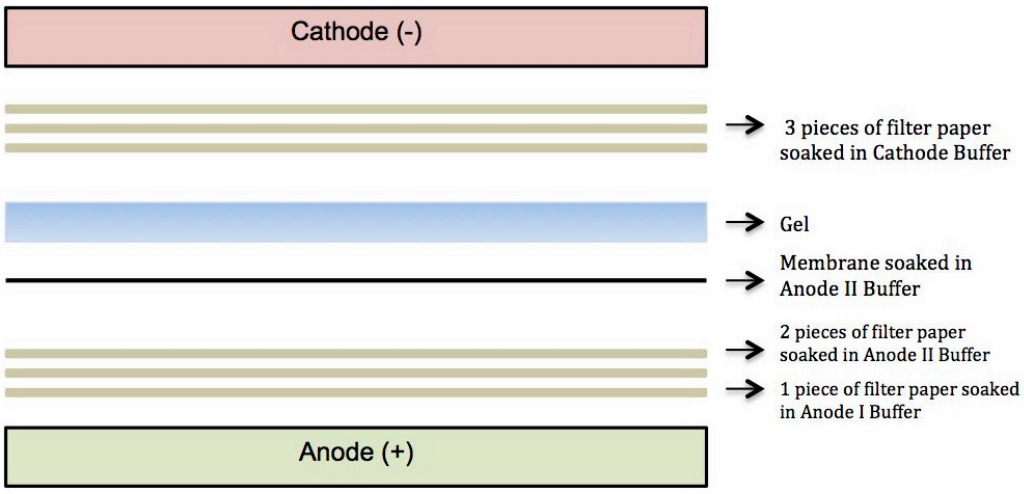

Figure 2.7: Semi-dry transfer apparatus set up.

2.7 Metabolic Analysis by Seahorse

A Seahorse XF-96 Extracellular Flux Analyzer (Agilent) was used for real-time analysis of the extracellular acidification rate (ECAR), as a measure of the glycolytic rate; and oxygen consumption rates (OCR), as an indicator of the rate of oxidative phosphorylation in OSCC cell lines under various conditions.

Cells were seeded in a 96 well seahorse plate at 20,000 cells per well and allowed to adhere before treating under various conditions for the required time. One day prior to analysis, the seahorse cartridge plate was hydrated with 200 μL sterile H_2O per well and placed in a non-CO_2 incubator at 37°C according to manufacturer's instructions.

One hour before analysis, the H_2O in the seahorse cartridge plate was replaced by 200 μL pre-warmed calibration buffer (Agilent) and left in a non-CO_2 incubator at 37°C. The seahorse cell plate was washed with 200 μL seahorse XF base medium per well before adding 180 μL of seahorse XF base medium per well supplemented with 1mM glucose and 2mM L-glutamine.

Inhibitors were added to the designated ports of the seahorse cartridge as per table 2.5 with inhibitor concentrations as follows; oligomycin (2 μM), carbonyl cyanide 4-(trifluoromethoxy)phenylhydrazone (FCCP, 0.5 μM), rotenone (100 nM) with antimycin A (4 μM) and 2-deoxy-D-glucose (2DG, 30mM). After calibration of the seahorse cartridge according to the manufacturer's instructions, the cell plate was put in the seahorse machine for analysis.

Using the traces produced for OCR (Figure 2.8) and ECAR (Figure 2.9), basal respiration, ATP-linked respiration, proton leak, maximal respiratory capacity, reserve capacity, non-mitochondrial respiration, basal glycolysis, glycolytic capacity, glycolytic reserve and non-glycolytic acidification were calculated using the differences between the points on the seahorse traces shown in Figures 2.8 and 2.9.

Port	Compound	Injecting Volume	Injecting Concentration	Final Concentration
A	Oligomycin	20 µL	20 µM	2 µM
B	FCCP	22 µL	5.05 µM	0.5 µM
C	Rotenone/ Antimycin A	20 µL	1.21 µM / 48.4 µM	0.1 µM / 4 µM
D	2-DG	20 µL	393 mM	30 mM

Table 2.5: Seahorse injection port layout and inhibitor concentrations.

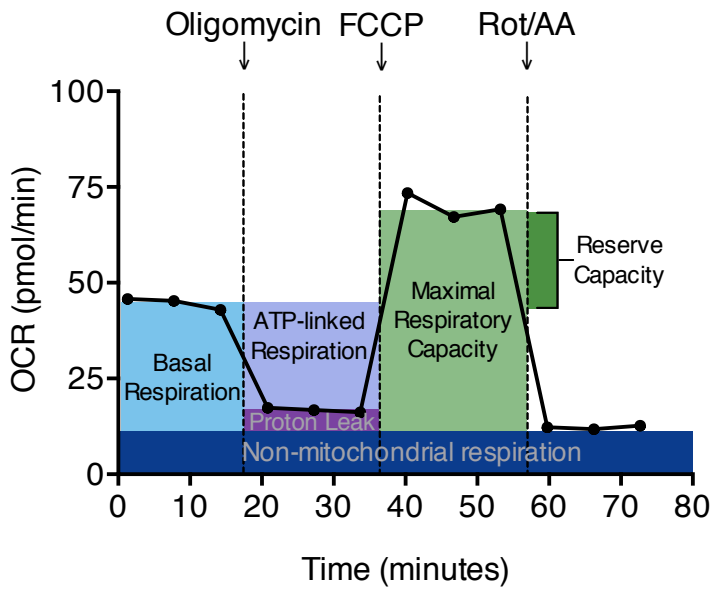

Figure 2.8. Representative seahorse trace for OCR in Ca9-22 cells. Basal respiration, ATP-linked respiration, proton leak, maximal respiratory capacity, reserve capacity and non-mitochondrial respiration can be calculated using the differences between the points shown on the seahorse trace.

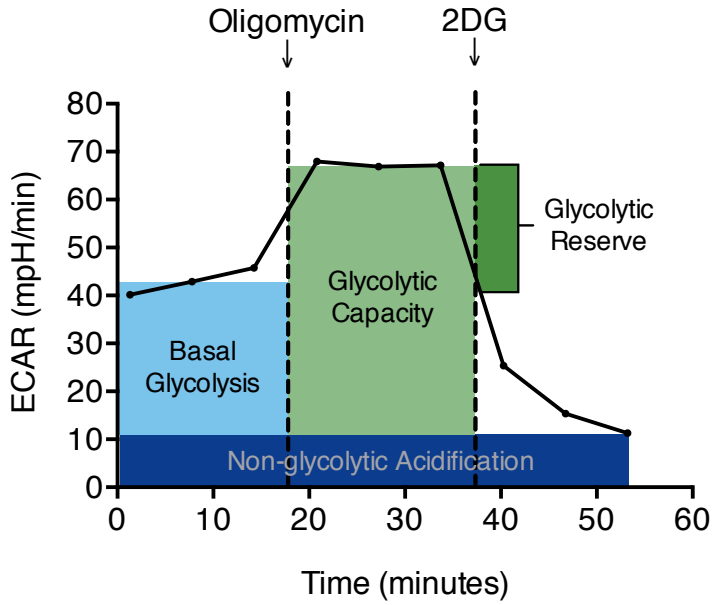

Figure 2.9. Representative seahorse trace for ECAR in Ca9-22 cells. Basal glycolysis, glycolytic capacity, glycolytic reserve, and non-glycolytic acidification can be calculated using the differences between the points shown on the seahorse trace.

2.8 Knockdown of *P53* using siRNA

The oligonucleotide sequences of small interfering RNAs (siRNAs) were designed for *P53* and pooled for optimum knockdown (see Table 2.6 below). Each siRNA is unwound into two single-stranded RNAs), the passenger strand and the guide strand. The passenger strand will be degraded while the guide strand will incorporated into the RNA-induced silencing complex in order to induce a transient knockdown of the P53 gene.

For transient transfection, the cells were seeded 2.5 x10^4 on a 96-well plate with serum starved medium (1% FBS). Following incubation overnight, targeting siRNA (20nm IBONI *P53*-siRNA pool) was transfected using RIBOXX-FECT transfection reagent (1% v/v) (MSC). Following overnight incubation, cells were treated as appropriate for the given experiment. Successful knockdown of *P53* was measured at protein level by western blotting 48 h post transfection.

***P53* siRNA (Gene ID 7157)**	
5′-3′ sequence (guide)	**5′-3′ sequence (passenger)**
UUAUUUCAUUAACCCUCACCCCC	GGGGGUGAGGGUUAAUGAAAUAA
ACAAUUGUAAUCCCAGCACCCCC	GGGGGUGCUGGGAUUACAAUUGU
ACUAACCCUUAACUGCAAGCCCCC	GGGGGCUUGCAGUUAAGGGUUAGU
Negative Control	
UUGUACUACACAAAAGUACCCCC	GGGGGUACUUUUGUGUAGUACAA

Table 2.6: Sequences for *P53* siRNA

2.9 Statistics

All data are represented as mean ± SEM unless stated otherwise. Statistical analysis was carried out on GraphPad Prism software (Version 6). Unpaired t-tests were performed to analyse samples of two different groups. One-way ANOVA followed by Dunnett's multiple comparison tests were used for samples with more than two groups. Two-way ANOVA followed by Dunnett's multiple comparison tests were used for samples containing more than two groups that were split into two variables. A p-value of 0.05 or less was taken to be statistically significant.

Chapter 3

Modulation of autophagy in immortalised OSCC cell lines

3.1 Introduction

Autophagy has been implicated as a therapeutic target in many cancer types, however research in this field has proven to be challenging due to the many disputes over the reliability of common methods for monitoring alterations to autophagic flux and identifying autophagy induction or inhibition.

3.1.1 Measuring autophagic flux

In 2008, Klionsky et al wrote a detailed review outlining all the complications and inconsistencies associated with the reporting of autophagy including the pros and cons of each experimental method[137]. It has been over twelve years since is publication and there are still no set guidelines as to what the acceptable experimental methods for monitoring autophagy modulation are.

There are two primary ways of monitoring autophagy: direct observation by steady-state methods; and monitoring autophagic flux by quantification of autophagosome formation and autolysosome degradation[85]. Measurement of autophagy using steady state methods is useful to determine whether autophagy induction has taken place but gives no information on whether there is any inhibition at later stages of the autophagic pathway. Some examples of steady state measurements are electron microscopy, western blotting for LC3II, fluorescence microscopy using GFP conjugated LC3, monitoring mTOR activity by western blotting of phosphr-S6-kinase and qRT-PCR of LC3 transcriptional regulation[137]. Acridine orange is one of many fluorescent

dyes that can be used to identify autophagic vesicles using fluorescence microscopy. It can easily cross cell membranes and due to its basic properties, it accumulates in acidic vesicles such as lysosomes and autolysosomes where it becomes protonated and trapped due to the ATP-dependent proton pumps on the membranes of these vesicles. At this low pH, acridine orange demonstrates a red fluorescence under UV light while the nuclear material fluoresces green due to acridine orange's ability to intercalate into nucleic acids. This dual fluorescence allows the observer to easily visualise changes in lysosome/autolysosome quantities within a cell or population of cells[138].

Measurements of autophagic flux are considered the gold standard and are highly recommended as they give a better understanding of autophagy as a dynamic process and give more detailed information as to what alterations are being made to the pathway under different treatment conditions. Some examples of flux measurements include the radioactive labelling of proteins to monitor their autophagic degradation, LC3-II turnover by western blotting, GFP-LC3 proteolysis, p62 western blotting, autophagy sequestration assays, tandem mRFP-GFP-LC3 fluorescence microscopy and tissue fractionation in combination with electron microscopy[137]. One of the major issues with measuring autophagy in cancer research is the lack of characterisation of basal autophagic flux within different cancer types and cell lines[139]. Due to the abundance of autophagic markers it can be difficult to determine the most suitable choice for a specific cell or autophagy type. The two most common markers are LC3B (in the forms LC3I and LC3II) and P62 (the most common adaptor protein). Combined measurement of LC3I

and LC3II can give a dynamic image of changes in autophagic flux as the cytosolic LC3I is converted to the membrane bound LC3II during autophagosome formation and then back to LC3I as the autophagosome breaks down. This method of autophagy measurement can be quite tricky as the antibodies used for LC3B staining often have a higher affinity for LC3II making LC3I either quite faint or non-detectible. Therefore , LC3I can be an unreliable measurement and it is more common to measure LC3II relative to a housekeeping protein such as ß-Actin[85]. Most measurements of autophagy proteins rely on proteins that are degraded along with the autophagic vesicles. Alongside LC3II, the next most common protein measured is P62. P62 is an autophagy substrate that delivers polyubiquitinated proteins to the autophagy machinery[140]. Some issues can arise when measuring P62 as a reporter of autophagic flux. Overexpressed P62 also has the tendency to self-aggregate, resulting in an apparent, yet inaccurate, reduction in autophagic activity[141]. During starvation (the most frequently used autophagy inducer in the lab), P62 transcription is activated. It has been shown that P62 can be reduced in the initial stages of starvation, however after prolonged starvation, P62 returns to basal levels[142]. Another limitation with P62 measurement is its role as an adaptor protein for selective autophagy. Other adaptor proteins exist for different forms of selective autophagy such as NBR1, NDP52, optineurin, and VCP[143]. Without knowing the correct adaptor protein required for the type of autophagy being detected, P62 may not give an accurate representation of autophagic flux alone.

As autophagy has been shown to be either increased or decreased depending on the cancer type and cell line, it is essential to have a better understanding of its dynamics in different tissue types and cell lines before focusing on it as a target for therapy.

3.1.2 Implications of modulating autophagy in cancer therapy

Autophagy has been implicated in many diseases but in cancer research its association with both tumorigenesis and tumour suppression is particularly interesting. Some studies suggest that tumour resistance to therapy could be linked to cell survival through autophagy, thus heightened autophagy may be a mechanism of resistance for cancer cells undergoing metabolic or therapeutic stress[144, 145]. A pro-death role of autophagy in response to high levels of stress and a complex crosstalk between autophagy and apoptotic cell death has also been reported[146]. Although a dual role of autophagy as a pro-survival and pro-death mechanism has been reported in several cancers, the role of autophagy in OSCC remains poorly understood. There has been much research conducted into the ability of cancer cells to exploit autophagy's protective mechanism to prolong tumour survival. Autophagy inhibitors, therefore, have generated particular interest to increase cancer cell sensitivity to chemo and radiotherapy. Cells which are deficient in their apoptotic abilities may use autophagy as a survival mechanism, implying a higher rate of basal autophagy would be present in cancer cells which naturally evade apoptotic cell death. It has been suggested that in these cells with increased autophagy the inhibition of autophagy would make these cells more susceptible to treatment by

chemotherapeutics. Recent work by Jia et al (2017) has shown the inhibition of autophagy by CQ exhibits anti-proliferative effects in two OSCC cell lines and prevents tumour growth *in vivo*[147]. Furthermore CQ has been used to re-sensitise refractory non-small-cell lung cancer cells to cisplatin after the acquisition of resistance[148]. It has been shown in the oral adenosquamous cell carcinoma cell line CAL27, that CQ can enhance chemotherapeutic sensitivity to CPt[149]. Research by Zhao et al. demonstrated that autophagy inhibition by CQ enhances the anti-tumour effect of CPt in hypopharyngeal xenograft tumours[150].

A clinical trial has recently (2017) begun using CQ in combination with the potential anti-cancer drug, metformin, in chondrosarcoma, glioma and intrahepatic cholangiocarcinoma[151] (results currently not available as of July 2021). Other autophagy inhibitors have also been explored as potential treatment options. Combining the autophagy inhibitor, 3MA, with the DNA damaging agent, camptothecin, resulted in a marked increase in cell death in human lung cancer cell lines[152]. In oesophageal cancer, 3MA was able to increase the effects of radiation therapy *in vitro* and *in vivo* by preventing radiation-induced autophagic survival[153]. In human glioma cell lines, 3MA has been shown to increase the effects of cisplatin-induced apoptosis[154].

Autophagy inhibition may have promising therapeutic potential but to fully appreciate its benefits as an anti-cancer drug or as an adjuvant therapy, autophagy must be characterised in a more detailed way across different cancer types and different cell types.

Several pharmacological modulators of autophagy are available for use in research. Among these inhibitors are ULK1 inhibitors such as Ulk-101 which prevents formation of the phagophore, class III PI3K inhibitors such as 3MA (figure 3.1 A) and the Vps34 inhibitor SAR405 which prevents formation of autophagosome, P97 inhibitors such as DBeq (figure 3.1 B) which prevent SNARE disassembly after membrane fusion, thus preventing complete lysosomal fusion with the autophagosome and lysosomal protease inhibitors such as E64d (figure 3.1 D) and pepstatinA. One of the most studied autophagy inhibitors is chloroquine (CQ) (figure 3.1 C). CQ is an anti-malarial and anti-rheumatoid drug that has been shown to raise the lysosomal pH and prevent lysosomal fusion with the autophagosome. These drugs target the autophagy pathway at different stages, shown in the schematic (figure 3.2).

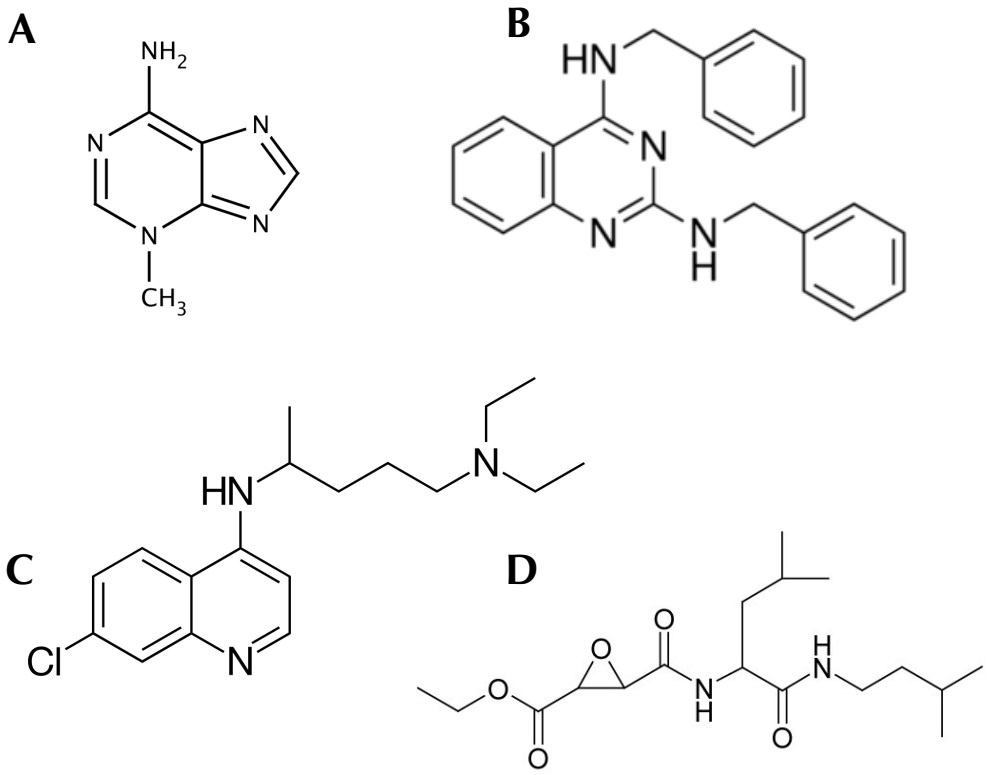

Figure 3.1. Structures of autophagy inhibitors.

Autophagy can be inhibited by several drugs such as the ones shown above. (A) 3-Methyladenine inhibits PI3 kinase. (B) DBeq inhibits ATPase P97 thus preventing closure of the phagophore. (C) CQ lowers the pH of the lysosome, preventing fusion with the autophagosome. (D) E64d works in conjunction with pepstatinA to inhibit lysosomal proteases, preventing lysosomal fusion with the autophagosome.

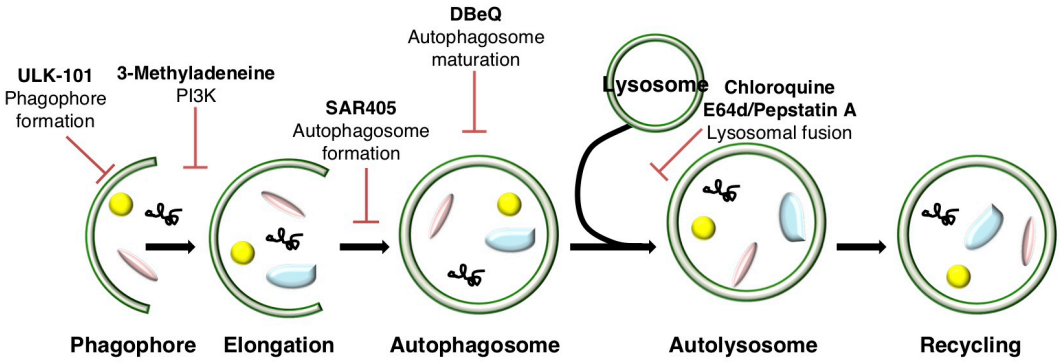

Figure 3.2. Autophagy inhibitors and their targets within the autophagy pathway.

Autophagy begins with the formation of the phagophore which elongates to form the double-membraned autophagosome. The autophagosome then fuses with the lysosome to form the autolysosome which has an acidic environment that allows for the breakdown of the cargo inside, leading to cellular recycling. This pathway can be inhibited at different stages. Phagophore formation can be inhibited by ULK-101. The PI3K inhibitor 3-Methyladenine prevents autophagosome formation while SAR405 inhibits autophagosome formation by inhibiting Vsp34. The P97 inhibitor DBeq prevents autophagosome maturation. CQ decreases the lysosomal pH, thus preventing fusion with the autophagosome. Lysosomal fusion can also be prevented by combing E64d (a cysteine protease inhibitor) with the aspartyl protease inhibitor pepstatinA.

3.2 Aims of Chapter

Despite the vast amount of autophagy research, there is still little consensus on the best method to measure autophagic flux and interpretation of experimental outputs vary from cell line to cell line even within the same tumour type. This study aims to characterise the basal levels of autophagy and its modulation in four OSCC cell lines; Ca9-22 cells are derived from gingival SCC, SCC4 cells are epithelial-like tongue SCC cells, TR146 cells originate from buccal SCC and DOK (dysplastic oral keratinocytes) are derived from a precancerous tongue lesion.

1. **To identify variations in autophagic protein expressions in distinct OSCC cell lines.**

   Levels of P62 and LC3II will be determined by western blotting under conditions of autophagy induction and inhibition in OSCC cell lines.

2. **To characterise the variation in acidic vesicle quantity during the modulation of autophagy in distinct OSCC cell lines.**

   Acridine orange staining followed by fluorescent microscopy analysis will be used to determine any changes to acidic vesicle quantity and size under conditions of autophagy induction and inhibition in OSCC cell lines. These acidic vesicles will include lysosomes and autolysosomes.

3. **To determine if modulation of autophagy leads to enhanced cell death in OSCC cell lines.**

   The occurrence of cell death by modulators of autophagy will be assessed by monitoring cellular metabolic activity using the Alamar Blue assay, quantification of PARP cleavage by western blotting and

cell cycle analysis using propidium iodide staining with flow cytometry to determine the quantity of cells proceeding through cell death pathways.

3.3 Results

3.3.1 Differences in autophagy protein expression during autophagy modulation within OSCC cell lines

Autophagy is a complex, multi-stage process. To fully interpret the effects of modulating this pathway quantification of P62 and LC3II by western blotting was used to examine the response of OSCC cells to induction and inhibition of the pathway at multiple stages. Cells were treated with starvation medium EBSS to determine the ability of these cell lines to undergo autophagy activation in response to external stimuli such as nutrient deprivation. Cells were also treated with four autophagy modulators reported to target different aspects of autophagy; two early-stage and two late-stage inhibitors.

Western blotting of Ca9-22 cells treated with EBSS (figure 3.3 A) shows a decrease in expression levels of both LC3II (figure 3.3 C) and p62 (figure 3.3B) when compared to vehicle treated cells. The notable decrease in p62 levels may indicate the expected activation of autophagy in response to nutrient deprivation. Treatment of Ca9-22 cells with autophagy inhibitors has no impact on P62 expression (figure 3.3 B) and treatment with the early-stage autophagy inhibitor, 3MA results in no change in LC3II (figure 3.3 C) expression compared to vehicle controls. In response to treatment with inhibitors of mid to late-stage autophagy, DBeq, CQ and E64d, there is a notable increase in LC3II (figure 3.3 C).

In SCC4 cells, western blotting of P62 and LC3II (figure 3.4. A) shows a decrease of P62 levels (figure 3.4 B) in response to treatment with EBSS.

Treatment with 3MA or E64d results in no change in LC3II expression (figure 3.4 C) whereas treatment with CQ results in an increase in LC3II expression. Again, there is no change in P62 expression levels in response to treatment with autophagy inhibitors, however in SCC4 cells there is a decrease in P62 response to treatment with EBSS (figure 3.4 B).

LC3II and P62 levels in TR146 cells (figure 3.5. A) show a similar response to autophagy modulation to those in SCC4 and Ca9-22 cells. Treatment with EBSS results in no change in P62 (figure 3.5 B) or LC3II (figure 3.5 C) levels. Treatment with autophagy inhibitors also results in no change in P62 expression (figure 3.5 B) relative to vehicle control. Treatment with early-stage inhibitors 3MA and DBeq results in no changes in LC3II expression (figure 3.5 C) compared to the vehicle controls and treatment with late-stage inhibitor CQ and E64d results in increased LC3II levels.

In DOK cells (figure 3.6.), treatment with EBSS results in a decrease in LC3II levels (figure 3.6 A and C) and an increase in P62 levels (figure 3.6. A and B). Treatment with 3MA shows no change in LC3II (figure 3.6 C and F) or P62 (figure 3.6 C and E), whereas treatment with CQ and E64d results in increased LC3II levels (figure 3.6 F), again without any notable changes to P62 (figure 3.6. B). It should be noted that the increase in LC3II expression levels in response to CQ was more discernible than with the other late-stage inhibitor E64d in all four cell lines.

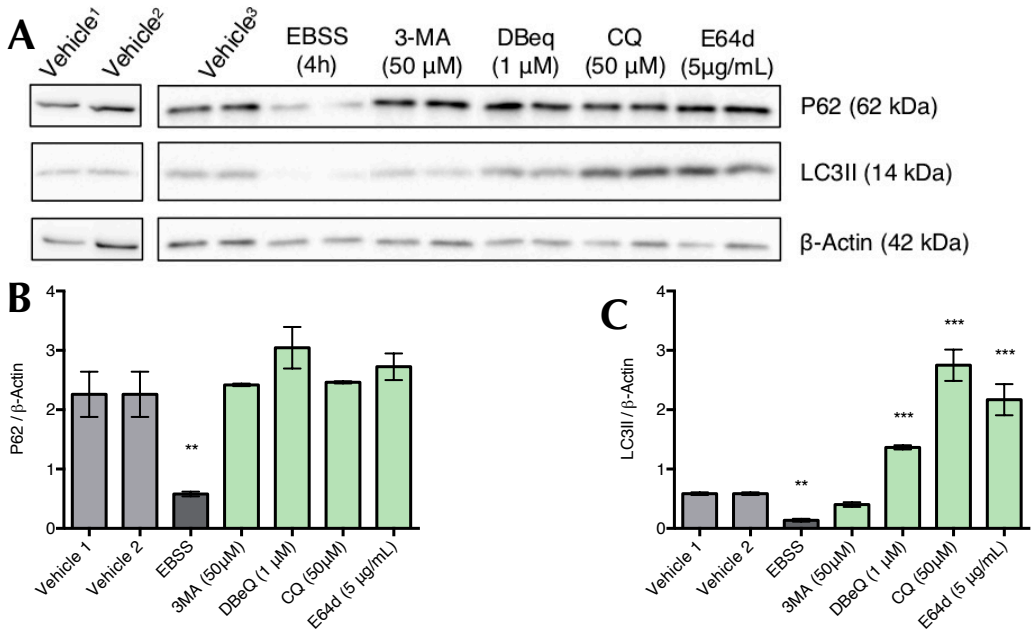

Figure 3.3. Treatment of Ca9-22 cells with inhibitors of late-stage autophagy results in increased expression of LC3II.

Blot shown is a representative blot demonstrating Ca9-22 cells treated with EBSS for 4 h or autophagy inhibitors 3MA (50 μM), DBeq (1 μM), CQ (50 μM) and E64d/pepstatinA (5 μg/mL) for 24 h at 37°C before being lysed in RIPA buffer. Lysates (10 µg) were resolved by SDS-PAGE on a 15% gel, followed by transfer onto PVDF membrane. The membranes were then probed with anti-P62, anti-LC3II and anti ß-actin antibodies and visualised using a gel documentation system (Biorad) and enhanced chemiluminescent HRP substrate (millipore). (A) Blot of EBSS and autophagy inhibitor treatment in Ca9-22 cells (all presented as n=2 where each lane represents a separate treatment occasion. (B) Densitometry of P62 expression after treatment with EBSS or autophagy inhibitors. (C) Densitometry of LC3II expression after treatment with EBSS or autophagy inhibitors. Experiments were repeated on three individual occasions to ensure reproducibility. Vehicle[1]: Ca9-22 cells treated for 24h with 1% EtOH (vehicle control for DBeq). Vehicle[2]: Ca9-22 cells treated for 24h with 1% DMSO/MeOH mixed at 1:1 ratio (vehicle control for E64d/pepstatinA). Vehicle[3]: Ca9-22 cells treated for 24h with deionised H_2O (vehicle control for 3MA and CQ). Sham[3], EBSS, 3MA, Dbeq, CQ and E64d. n=3 ± SEM. One-way ANOVA followed by Tukey's multiple comparisons test. ***p<0.001, **p<0.01.

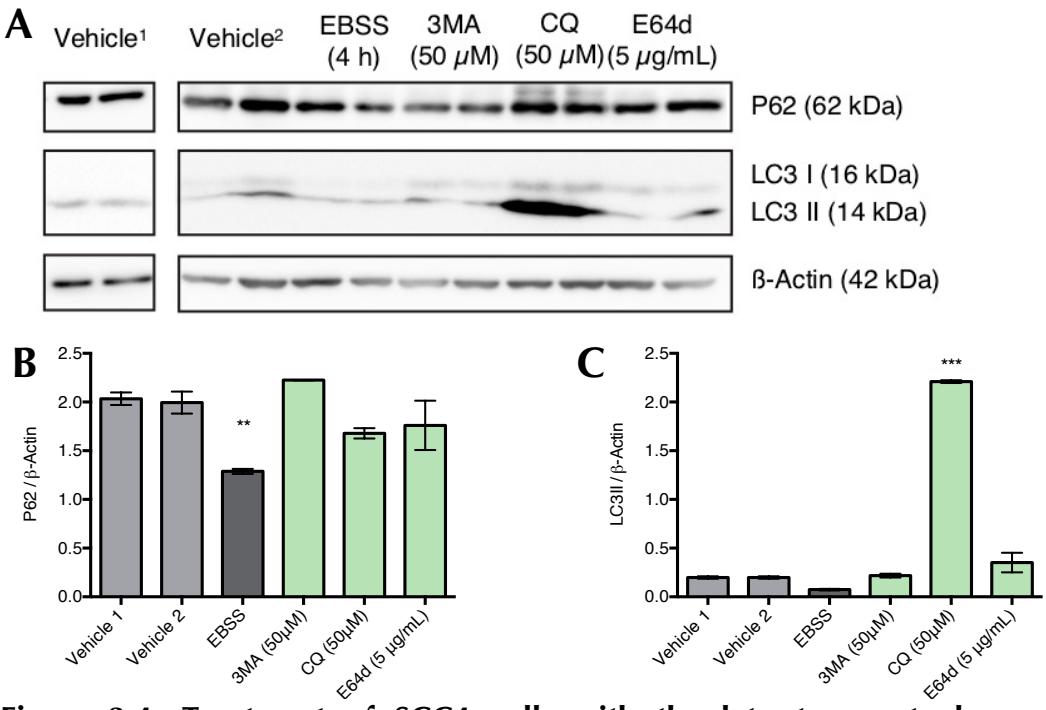

Figure 3.4. Treatment of SCC4 cells with the late-stage autophagy inhibitor CQ results in increased expression of LC3II.

SCC4 cells were treated with EBSS for 4 h or autophagy inhibitors 3MA (50 μM), CQ (50 μM) and E64d/pepstatinA (5 μg/mL) for 24 h at 37°C before being lysed in RIPA buffer. Lysates (20 μg) were resolved by SDS-PAGE on a 15% gel, followed by transfer onto PVDF membrane. The membranes were then probed with anti-P62, anti-LC3B and anti- ß-actin antibodies and visualised using a gel documentation system (Biorad) and enhanced chemiluminescent HRP substrate (millipore). (A) Blot of EBSS and autophagy inhibitor treatment in SCC4 cells (all treatment conditions presented as n=2 where each lane represents a separate treatment occasion.) (B) Densitometry of P62 expression after treatment with EBSS or autophagy inhibitors. (C) Densitometry of LC3II expression after treatment with EBSS or autophagy inhibitors. Blot shown is a representative blot from an experiment performed on three separate occasions. Vehicle¹: SCC4 cells treated for 24h with 1% DMSO/MeOH mixed at 1:1 ratio (vehicle control for E64d/pepstatinA). Vehicle²: SCC4 cells treated for 24h with deionised H_2O (vehicle control for 3MA and CQ). n=3 ± SEM. One-way ANOVA followed by Tukey's multiple comparisons test. ***p<0.001, **p<0.01.

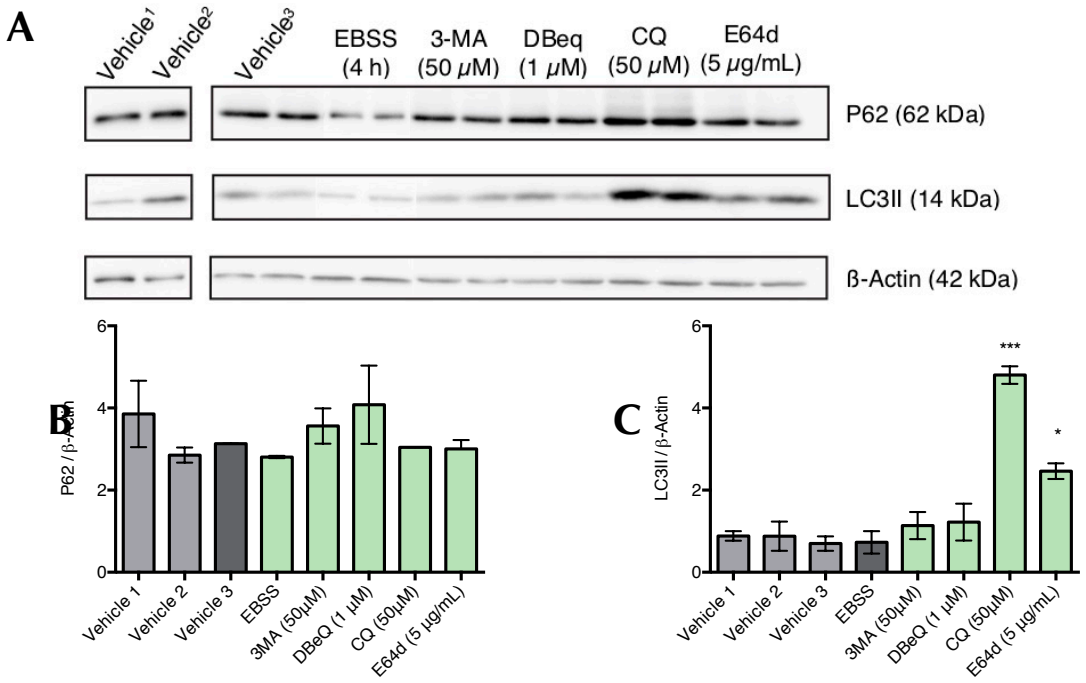

Figure 3.5. Treatment of TR146 cells with CQ and E64d results in an increased expression of LC3II.

TR146 cells were treated with EBSS for 4 h or autophagy inhibitors 3MA (50 μM), DBeq (1 μM), CQ (50 μM) and E64d/pepstatinA (5 μg/mL) for 24 h at 37^{o}C before being lysed in RIPA buffer. Lysates (20 μg) were resolved by SDS-PAGE on a 15% gel, followed by transfer onto PVDF membrane. The membranes were then probed with anti-P62, anti-LC3B and anti- ß-actin antibodies and visualised using a gel documentation system (Biorad) and enhanced chemiluminescent HRP substrate (millipore). (A) Blot of EBSS and autophagy inhibitor treatment in TR146 cells (all presented as n=2 where each column represents a separate treatment occasion.) (B) Densitometry of P62 expression after treatment with EBSS or autophagy inhibitors. (C) Densitometry of LC3II expression after treatment with EBSS or autophagy inhibitors. Blot shown is a representative blot from an experiment performed on three separate occasions. Vehicle^{1}: TR146 cells treated for 24h with 1% EtOH (vehicle control for DBeq). Vehicle^{2}: TR146 cells treated for 24h with 1% DMSO/MeOH mixed at 1:1 ratio (vehicle control for E64d/pepstatinA). Vehicle^{3}: TR146 cells treated for 24h with deionised H_2O (vehicle control for 3MA and CQ). Sham^{3}, EBSS, 3MA, DBeq, CQ and E64d n=3 ± SEM. One-way ANOVA followed by Tukey's multiple comparisons test. ***$p<0.001$, *$p<0.05$.

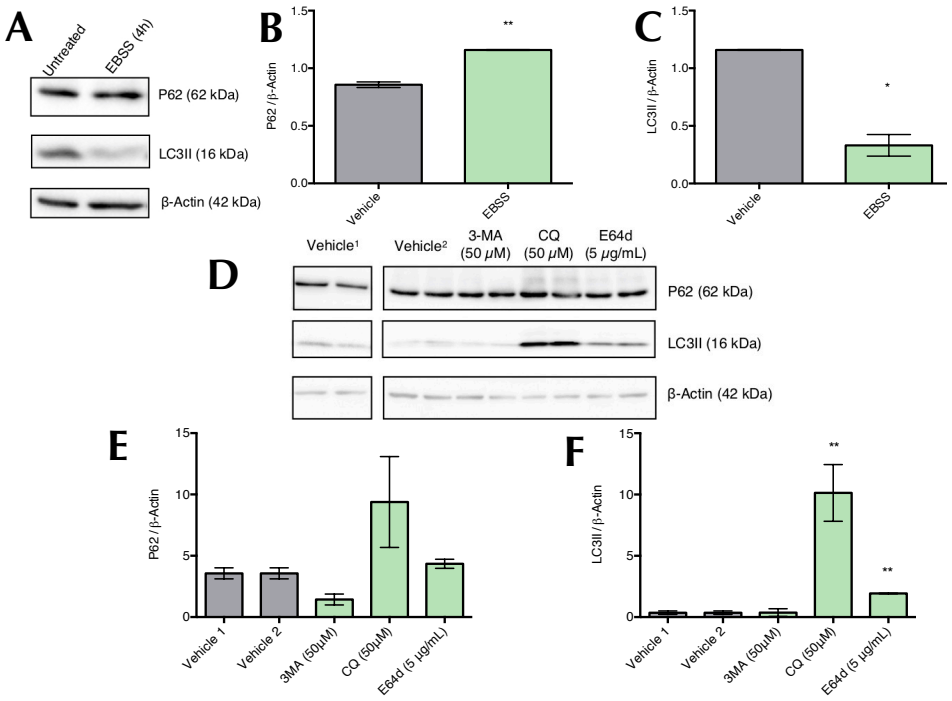

Figure 3.6. Inhibition of late-stage autophagy results in increased expression of LC3II in DOK cells.

DOK cells were treated with EBSS for 4 h or autophagy inhibitors 3MA (50 μM), CQ (50 μM) and E64d/pepstatinA (5 μg/mL) for 24 h at 37°C before being lysed in RIPA buffer. Lysates (10 μg) were resolved by SDS-PAGE on a 15% gel, followed by transfer onto PVDF membrane. The membranes were then probed with anti-P62, anti-LC3B and anti- ß-actin antibodies and visualised using a gel documentation system (Biorad) and enhanced chemiluminescent HRP substrate (millipore). (A) Blot of EBSS treatment in DOK cells. (B) Densitometry of P62 expression after treatment with EBSS. (C) Densitometry of LC3II expression after treatment with EBSS. (D) Blot of autophagy inhibitor treatment on DOK cells (all treatment conditions presented as n=2 where each column represents a separate treatment occasion.) (E) Densitometry of P62 expression after treatment with autophagy inhibitors. (F) Densitometry of LC3II expression after treatment with autophagy inhibitors. Blot shown is a representative blot from an experiment performed on three separate occasions. Vehicle[1]: DOK cells treated for 24h with 1% DMSO/MeOH mixed at 1:1 ratio (vehicle control for E64d/pepstatinA). Vehicle[2]: DOK cells treated for 24h with deionised H_2O (vehicle control for 3MA and CQ). n=3 ± SEM. One-way ANOVA followed by Tukey's multiple comparisons test. **p<0.01, *p<0.05.

3.3.2 Variations in acidic vesicle quantity during autophagy modulation in OSCC cell lines

Acridine orange stains acidic vesicles such as lysosomes and autolysosomes in red while nuclear and cytoplasmic material is stained in green. Although acridine orange is not a direct measurement of autophagy, it is a useful tool to analyse the alterations in acidic vesicle quantity and quality under conditions of autophagy modulation[155, 156].

Acridine Orange staining shows similar results in Ca9-22 (figure 3.7. A), SCC4 (figure 3.8. A), TR146 (figure 3.9. A) and DOK (figure 3.10. A) cells.

In Ca9-22 cells (figure 3.7.) treatment with the autophagy inducer EBSS or treatment with early-stage autophagy inhibitors 3MA or DBeq results in no significant changes to acidic vesicles compared to vehicle controls. In contrast, treatment with inhibitors of late-stage autophagy by CQ and E64d results in increased quantity of acidic vesicles (figure 3.7 B).

In SCC4 cells (figure 3.8.) treatment with 3MA or DBeq has no significant effect on acidic vesicle quantity. Treatment with EBSS, CQ or E64d results in an increase in acidic vesicles (figure 3.8 B).

In TR146 cells (figure 3.9.) 3MA has no impact on the quantity of acidic vesicles, however treatment with EBSS, CQ and E64d results in an increase in acidic vesicles (figure 3.9 B). In TR146 cells, acridine orange staining with CQ results in a yellow staining. This is due to CQ raising the lysosomal pH resulting in red fluorescence that changes to green as the pH is raised. At the time the images were captured, the dye is at an

intermediate stage where it is demonstrating both red and green fluorescence.

DOK cells (figure 3.10.) treatment with EBSS or early-stage autophagy inhibitor 3MA have no impact on acidic vesicles. Treatment of DOK cells with CQ shows an increase in acidic vesicles (figure 3.10 B) as seen in all OSCC cells.

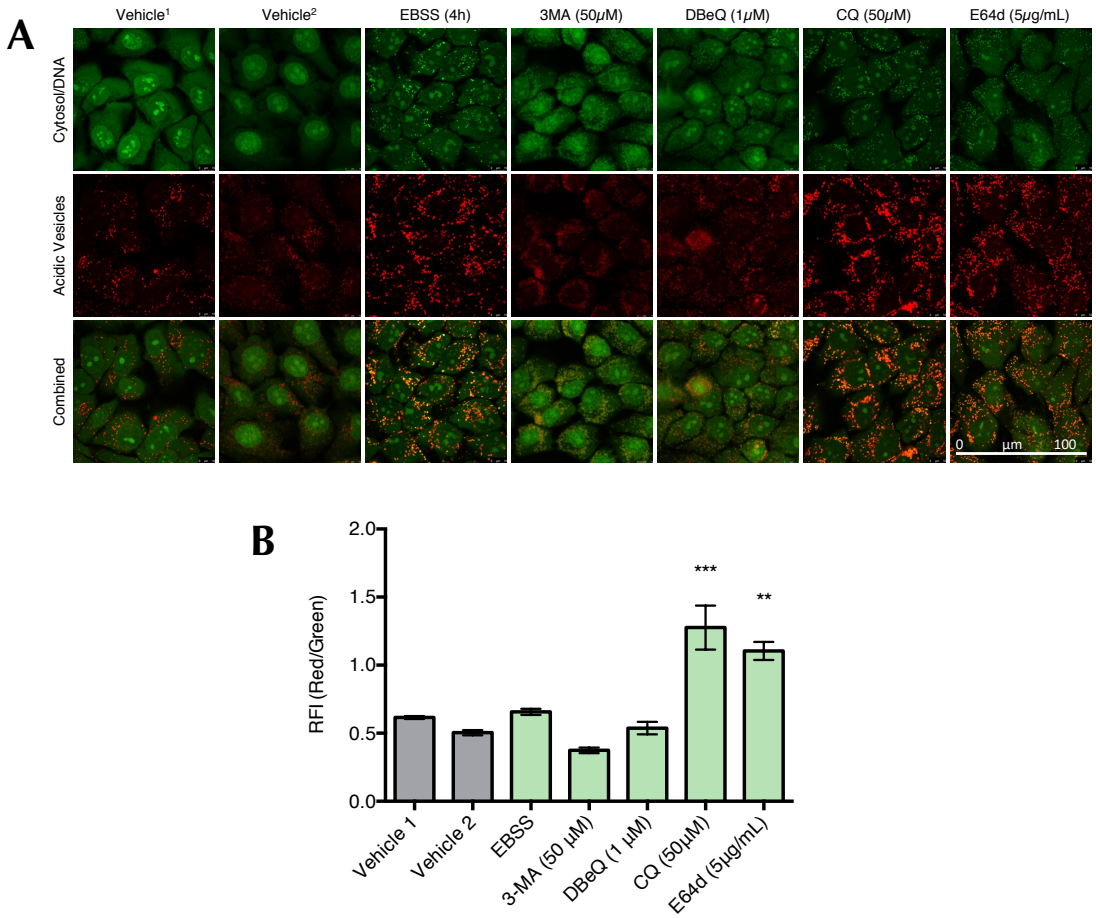

Figure 3.7. Effect of exposure to autophagy inhibitors and EBSS on acidic vesicle quantity in Ca9-22 cells.

Ca9-22 cells were treated with EBSS for 4 h or autophagy inhibitors 3MA (50 μM), DBeq (1 μM), CQ (50 μM) and E64d/pepstatinA (5 μg/mL) for 24 h. Acridine orange (1 μg/mL) was added 15 min before imaging. Acridine orange was excited by a 488 nm laser and emission was set at 500 – 575 nm and 625 – 725 nm. Cells were viewed using a Leica SP8 scanning confocal microscope. Vehicle[1]: Ca9-22 cells treated for 24h with 1% EtOH (vehicle control for DBeq). Vehicle[2]: Ca9-22 cells treated for 24h with 1% DMSO/MeOH mixed at 1:1 ratio (vehicle control for E64d/pepstatinA). Scale bar 100 μm. (A) Fluorescent microscopy of acridine orange staining in Ca9-22 cells. (B) Relative fluorescent intensity of red to green fluorescence; n=3 ± SEM. One-way ANOVA followed by Tukey's multiple comparisons test. ***p<0.001, **p<0.01. Image shown is a representative of an experiment performed on three separate occasions. For full page image without legend, see Appendix 1.

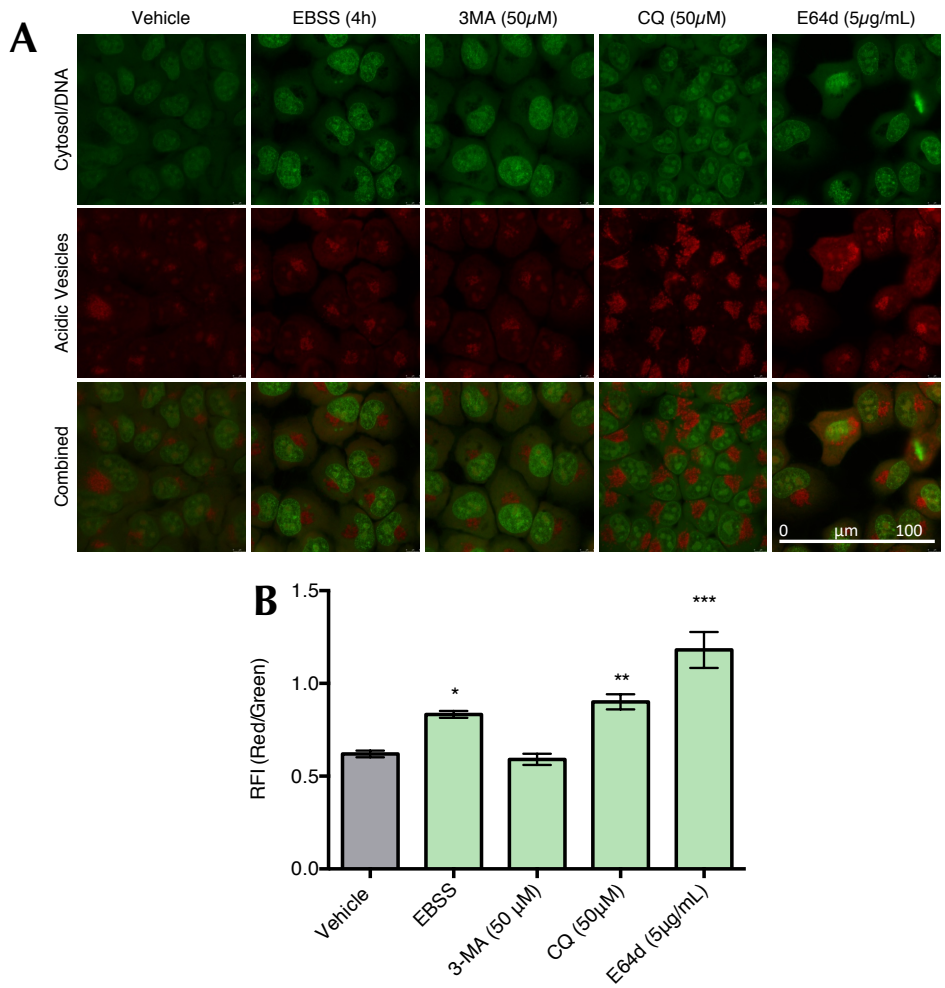

Figure 3.8. Effect of exposure to autophagy inhibitors and EBSS on acidic vesicle quantity on SCC4 cells.

SCC4 cells were treated with EBSS for 4 h or autophagy inhibitors 3MA (50 μM), CQ (50 μM) and E64d/pepstatinA (5 μg/mL) for 24 h. Acridine orange (1 μg/mL) was added 15 min before imaging. Acridine orange was excited by a 488 nm laser and emission was set at 500 – 575 nm and 625 – 725 nm. Cells were viewed using a Leica SP8 scanning confocal microscope. Vehicle: SCC4 cells treated for 24h with 1% DMSO/MeOH mixed at 1:1 ratio (vehicle control for E64d/pepstatinA). Scale bar 100 μm. (A) Fluorescent microscopy of acridine orange staining in SCC4 cells. (B) Relative fluorescent intensity of red to green fluorescence; n=3 ± SEM. One-way ANOVA followed by Tukey's multiple comparisons test. ***$p<0.001$, **$p<0.01$, *$p<0.05$. Image shown is a representative of an experiment performed on three separate occasions.
For full page image without legend, see Appendix 1.

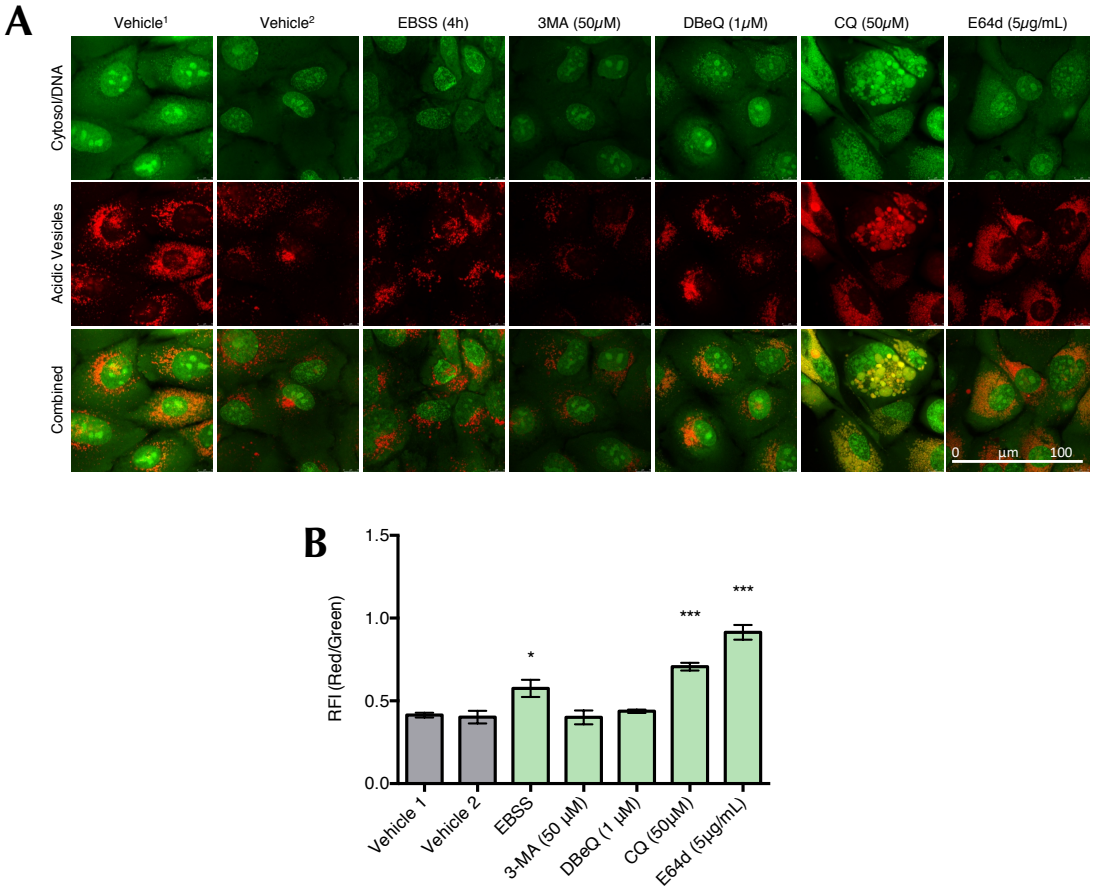

Figure 3.9. Effect of exposure to autophagy inhibitors and EBSS on acidic vesicle quantity in TR146 cells.

TR146 cells were treated with EBSS for 4 h or autophagy inhibitors 3MA (50 μM), DBeq (1 μM), CQ (50 μM) and E64d/pepstatinA (5 μg/mL) for 24 h. Acridine orange (1 μg/mL) was added 15 min before imaging. Acridine orange was excited by a 488 nm laser and emission was set at 500 – 575 nm and 625 – 725 nm. Cells were viewed using a Leica SP8 scanning confocal microscope. Vehicle[1]: TR146 cells treated for 24h with 1% EtOH (vehicle control for DBeq). Vehicle[2]: TR146 cells treated for 24h with 1% DMSO/MeOH mixed at 1:1 ratio (vehicle control for E64d/pepstatinA). Scale bar 100 μm. (A) Fluorescent microscopy of acridine orange staining in TR146 cells. (B) Relative fluorescent intensity of red to green fluorescence; n=3 ± SEM. One-way ANOVA followed by Tukey's multiple comparisons test. ***$p<0.001$, *$p<0.05$. Image shown is a representative of an experiment performed on three separate occasions. For full page image without legend, see Appendix 1.

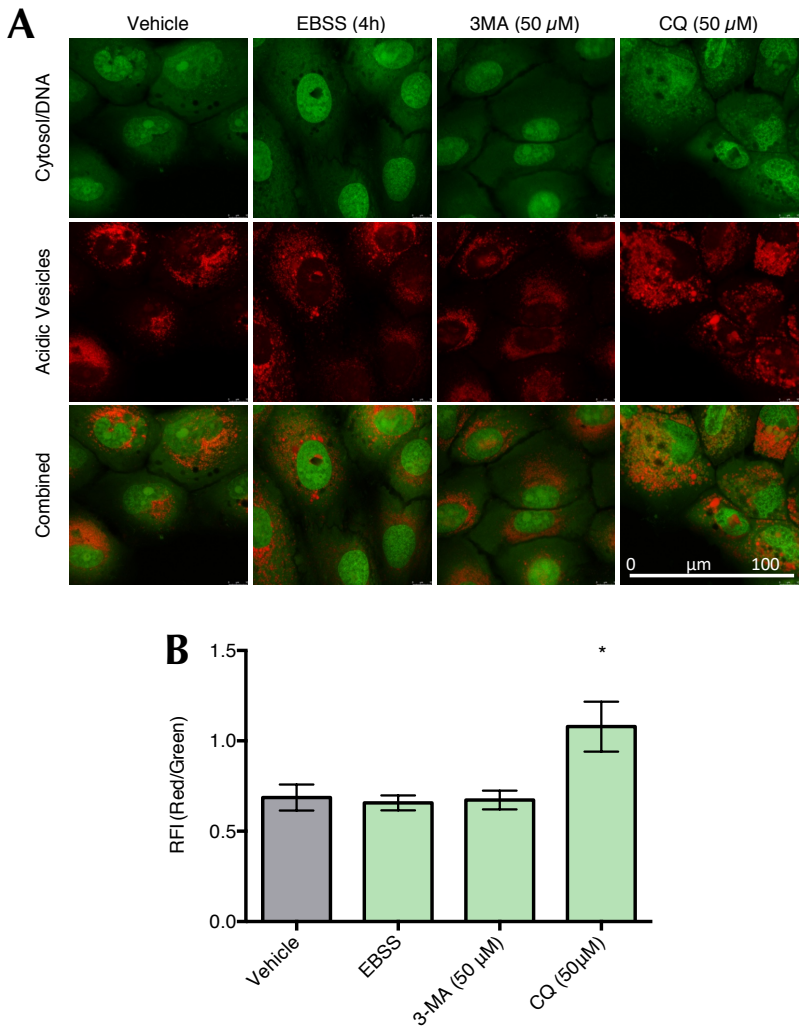

Figure 3.10. Effect of exposure to autophagy inhibitors and EBSS on acidic vesicle quantity in DOK cells.

DOK cells were treated with EBSS for 4 h or autophagy inhibitors 3MA (50 μM) or CQ (50 μM) for 24 h. Acridine orange (1 μg/mL) was added 15 min before imaging. Acridine orange was excited by a 488 nm laser and emission was set at 500 – 575 nm and 625 – 725 nm. Cells were viewed using a Leica SP8 scanning confocal microscope. Vehicle: DOK cells treated for 24h with deionised H_2O (vehicle control for 3MA and CQ). Scale bar 100 μm. (A) Fluorescent microscopy of acridine orange staining in DOK cells. (B) Relative fluorescent intensity of red to green fluorescence n=3 ± SEM. One-way ANOVA followed by Tukey's multiple comparisons test. *$p<0.05$. Image shown is a representative of an experiment performed on three separate occasions.
For full page image without legend, see Appendix 1.

3.3.3 Altered effects of autophagy modulation on cell cycle distribution between OSCC cell lines

Under conditions of stress, cell cycle alterations can occur. It is possible, therefore, that modulation of autophagy may induce stress-related cell cycle responses. Cell cycle alterations were measured through flow cytometric analysis of propidium iodide-stained DNA fragments.

Treatment of Ca9-22 cells with EBSS for 4 h results in a minimal effect on the cell cycle profile. No significant changes are observed in the percentage of cells in the Sub G_0, G_1 or G_2/M peaks compared to control cells. A very small but significant decrease of 1.83% in the percentage of cells in the S phase of the cell cycle (figure 3.11.). Treatment of Ca9-22 cells with autophagy inhibitors (figure 3.12.) results in a small increase in the percentage of cells in the sub-G_0 peak after treatment with 3MA (2.83% increase), DBeq (8.09% increase) or E64d (2.77% increase) which is accompanied by a 13.38%, 12.82% and 6.52% decrease respectively in cells in the S phase of the cell cycle. In cells treated with 3MA, there is also an 14.44% increase in cells in the G_0/G_1 phase. Treatment with CQ has no impact on the cell cycle in Ca9-22 cells after 24 h.

In a manner similar to Ca9-22 cells, treatment of SCC4 cells with EBSS for 4 h results in a minimal effect on the cell cycle profile (figure 3.13). No significant changes are observed in the percentage of cells in the sub-G_0, G_1 or G_2/M peaks compared to control cells. A very small but significant increase of 3.86% in the percentages of cells in the S phase is observed. Treatment with the late-stage inhibitors CQ and E64d decreases the number of cells in the G_2/M phase of the cell cycle by 11.55% and 9.28%

respectively. The decrease in the percentage of cells in the G_2/M peak is paralleled with small, although non-significant, increases in the sub-G_0 and G_1 peaks.

TR146 cells (figure 3.14.) treated with the late-stage inhibitor CQ show a 17.90% decrease in cells in the G_0/G_1 phase of the cell cycle with a correlating 7.98%, 3.57% and 5.67% increase in cells in the Sub G_0, S and G_2/M phases respectively. Treatment with 3MA has no effect on cell cycle distribution in TR146 cells after 24 h.

Treatment of DOK cells with the autophagy inducer EBSS has no effect on cell cycle distribution (figure 3.15.) In DOK cells treated with autophagy inhibitors (figure 3.16.) treatment with 3MA or CQ has no impact on cell cycle distribution, whereas treatment with E64d results in a 27.67% increase in cell in the G_0/G_1 phase and a correlating 7.31% and 11.57% decrease in cells in the S and G_2/M arrest phases respectively.

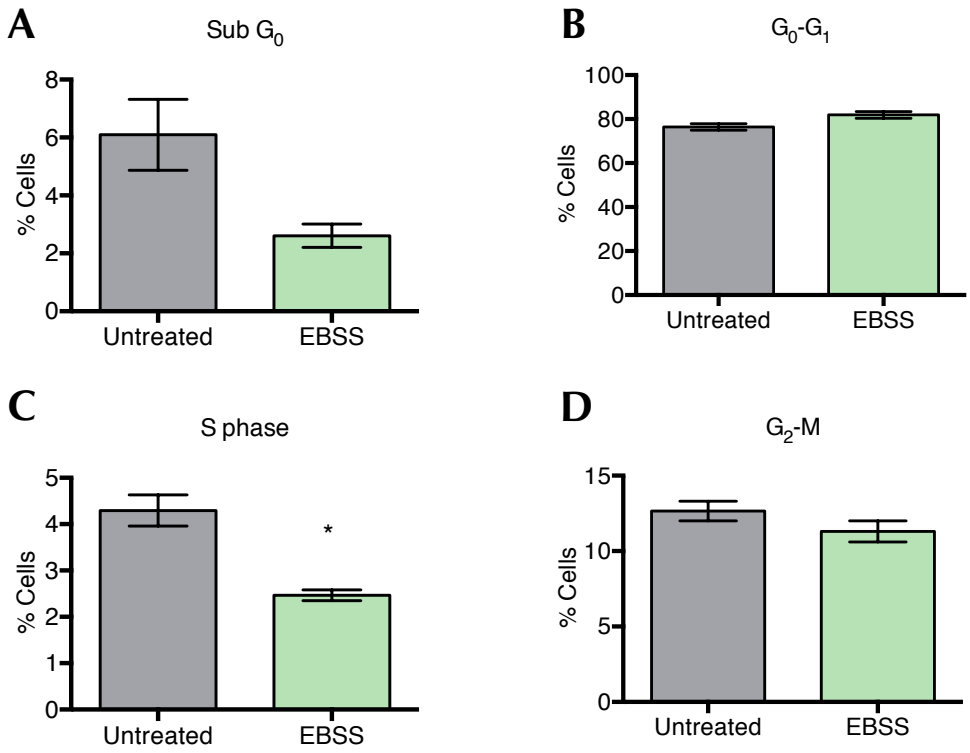

Figure 3.11. Treatment of Ca9-22 cells with EBSS results in a minimal effect on the cell cycle profile

Ca9-22 cells were starved for 24 h in 1% FBS and cultured for a further 24 h in full media (10% FBS), then treated for 4 h with EBSS. Whole cells were then fixed in 100% EtOH and resuspended in PBS containing RNase (500 μg/mL) and PI (150 μg/mL). Graph show percentage of cells in (A) Sub-G_0, (B) G_0/G_1, (C) S and (D) G_2/M phases of the cell cycle for each population of cells. Data shown n=3 ± SEM. Students t-test. *$p<0.05$.

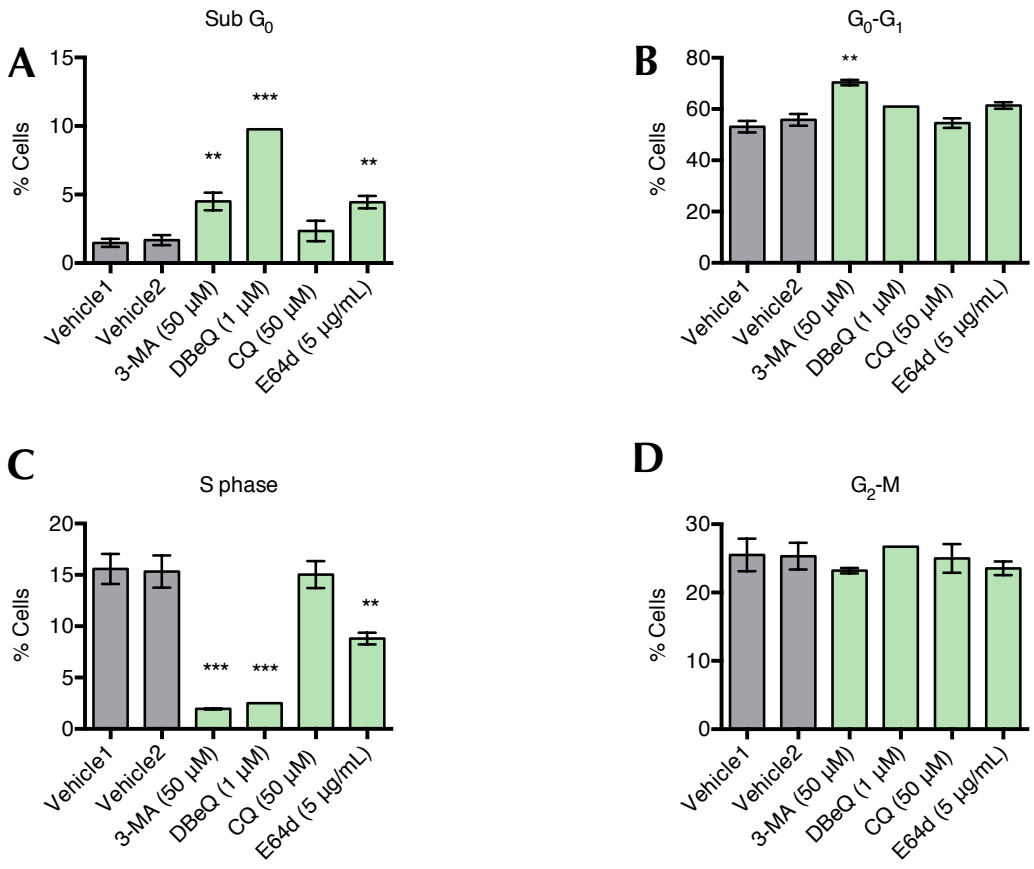

Figure 3.12. Effect of autophagy inhibitors on cell cycle profile of Ca9-22 cells

Ca9-22 cells were starved for 24 h in 1% FBS and cultured for a further 24 h in full media (10% FBS), then treated for 24 h with autophagy inhibitors 3MA (50 μM), DBeq (1 μM), CQ (50 μM) and E64d/pepstatinA (5 μg/mL). Whole cells were then fixed in 100% EtOH and resuspended in PBS containing RNase (500 μg/mL) and PI (150 μg/mL). Graphs show percentage of cells in (A) Sub-G0, (B) G_0/G_1, (C) S and (D) G_2/M phases of the cell cycle for each population of cells. Vehicle1: Ca9-22 cells treated for 24h with 1% EtOH (vehicle control for DBeq). Vehicle2: Ca9-22 cells treated for 24h with 1% DMSO/MeOH mixed at 1:1 ratio (vehicle control for E64d/pepstatinA). Data shown n=3 ± SEM. One-way ANOVA followed by Dunnett's multiple comparisons test compared to vehicle control. **p<0.01, ***p<0.001.

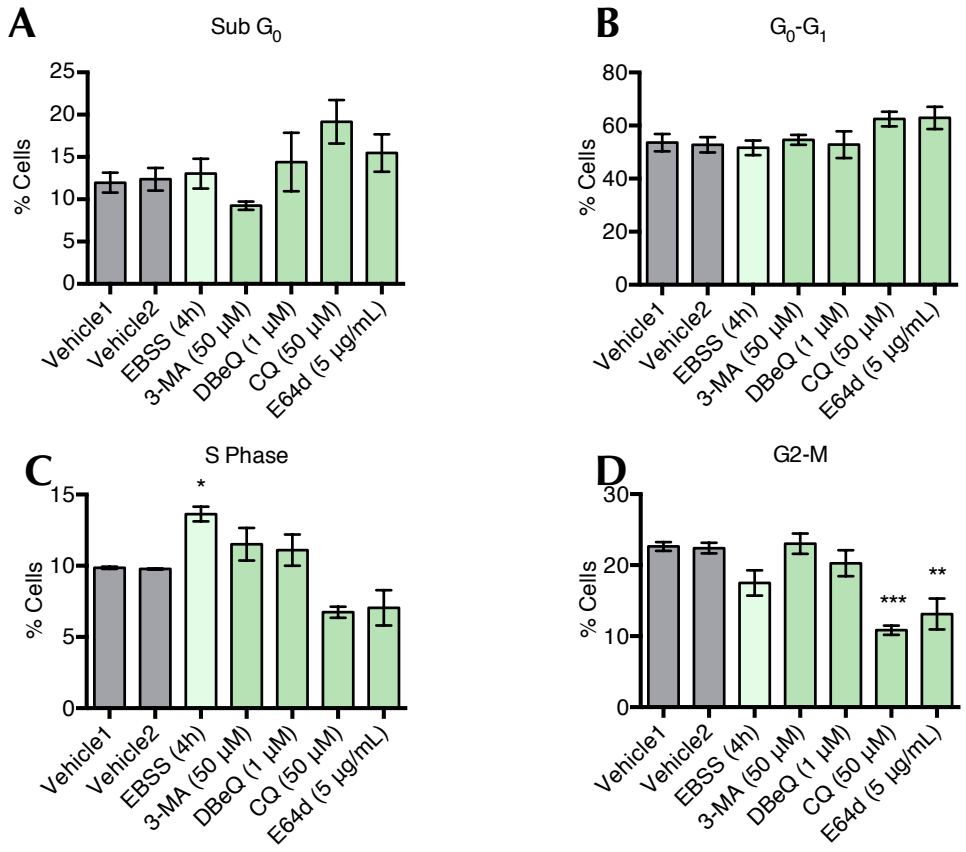

Figure 3.13. Culture of SCC4 cells in EBSS results in an increase in cells in the S phase of the cell cycle while treatment with the late-stage autophagy inhibitors CQ and E64d results in a decrease in the number of cells in the G_2M phase.

SCC4 cells were starved for 24 h in 1% FBS and cultured for a further 24 h in full media (10% FBS), then treated EBSS for 4 h or autophagy inhibitors 3MA (50 μM), DBeq (1 μM), CQ (50 μM) and E64d/pepstatinA (5 μg/mL) for 24 h. Whole cells were then fixed in 100% EtOH and resuspended in PBS containing RNase (500 μg/mL) and PI (150 μg/mL). Graphs show percentage of cells in (A) Sub-G_0, (B) G_0/G_1, (C) S and (D) G_2/M phases of the cell cycle for each population of cells. Vehicle1: SCC4 cells treated for 24h with 1% EtOH (vehicle control for DBeq). Vehicle2: SCC4 cells treated for 24h with 1% DMSO/MeOH mixed at 1:1 ratio (vehicle control for E64d/pepstatinA). Data shown n=3 ± SEM (where experiments were completed in duplicate on three separate treatment occasions). One-way ANOVA followed by Dunnett's multiple comparisons test compared to vehicle control. ***$p<0.001$, **$p<0.01$, *$p<0.05$

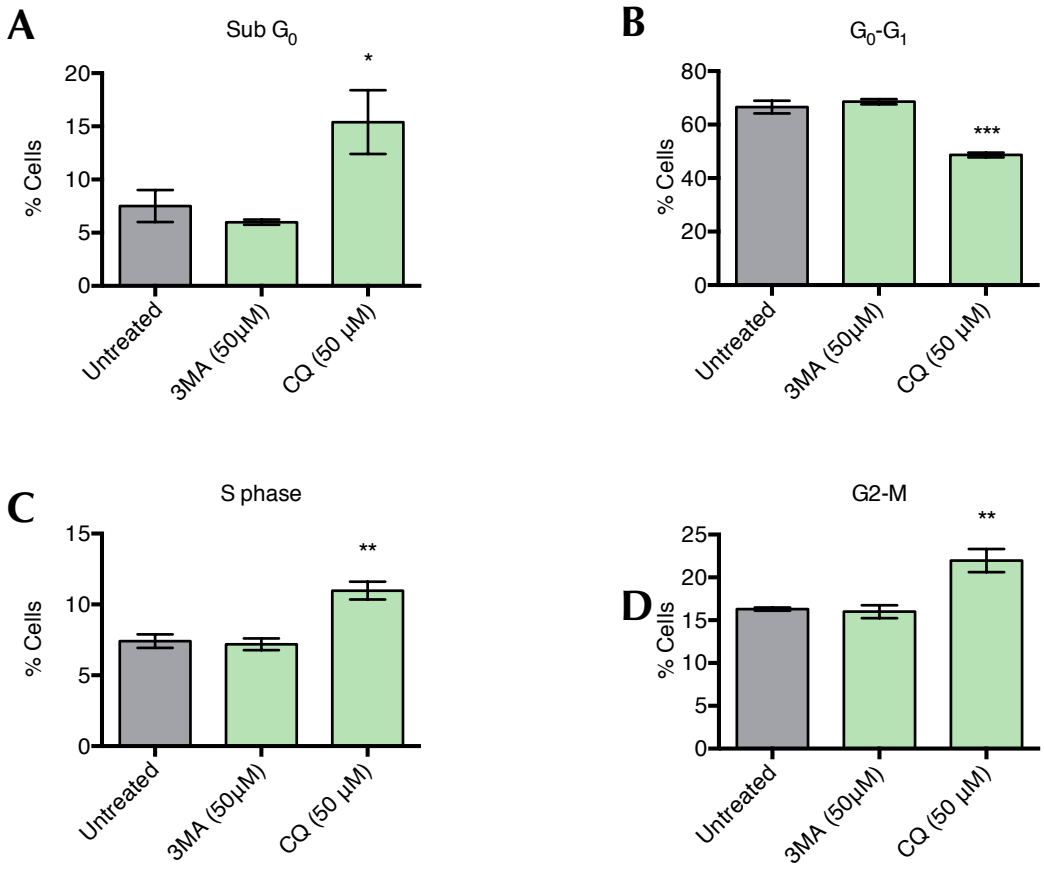

Figure 3.14. Exposure of TR146 cells to the late-stage autophagy inhibitor CQ decreases the quantity cells in the G_1-G_0 phase of the cell cycle with corresponding increase in number of cells in other stages of the cell cycle.

TR146 were starved for 24 h in 1% FBS and cultured for a further 24 h in full media (10% FBS), then treated for 24 h with autophagy inhibitors 3MA (50 μM) or CQ (50 μM). Whole cells were then fixed in 100% EtOH and resuspended in PBS containing RNase (500 μg/mL) and PI (150 μg/mL). Graph show percentage of cells in (A) Sub-G_0, (B) G_0/G_1, (C) S and (D) G_2/M phases of the cell cycle for each population of cells. Data shown n=3 ± SEM (where experiments were performed in duplicate on three separate treatment occasions). One-way ANOVA followed by Dunnett's multiple comparisons test. ***$p<0.001$, **$p<0.01$, *$p<0.05$

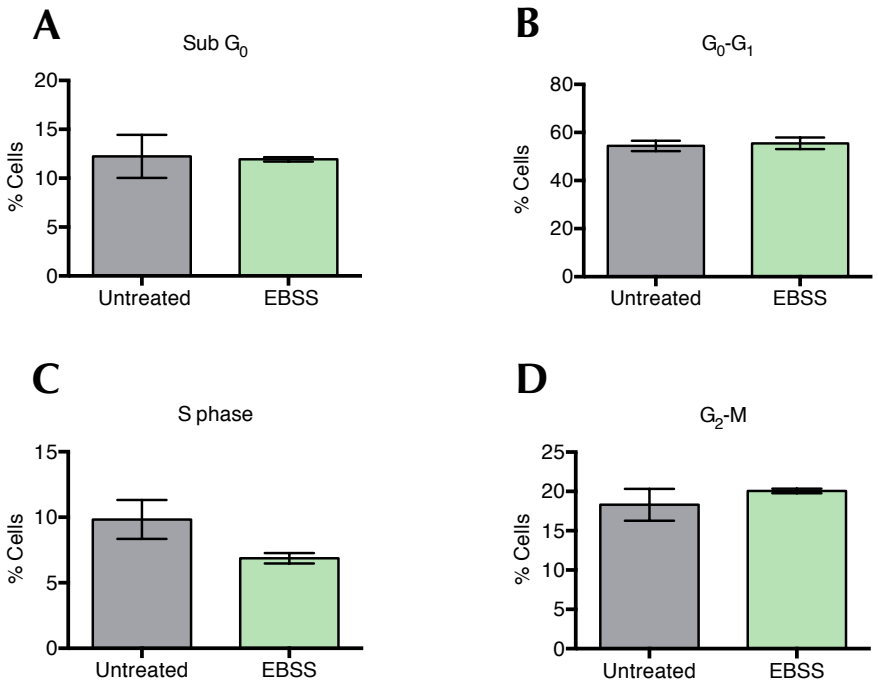

Figure 3.15. Culture of DOK cells in EBSS has no impact on cell cycle.

DOK were starved for 24 h in 1% FBS and cultured for a further 24 h in full media (10% FBS), then treated for 4 h with EBSS. Whole cells were then fixed in 100% EtOH and resuspended in PBS containing RNase (500 μg/mL) and PI (150 μg/mL). Graph show percentage of cells in (A) Sub-G_0, (B) G_0/G_1, (C) S and (D) G_2/M phases of the cell cycle for each population of cells. Data shown n=3 ± SEM (where experiments were performed in duplicate on three separate treatment occasions). Students t-test. P>0.05.

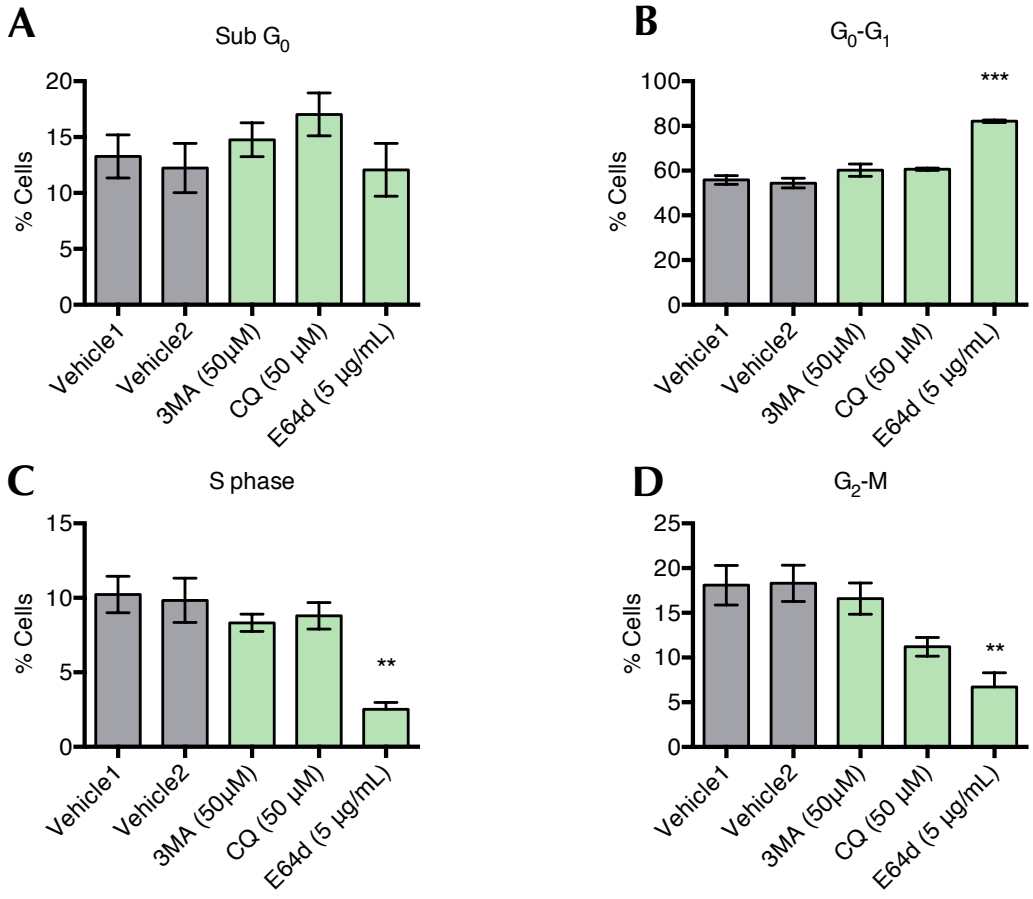

Figure 3.16. E64d induces G_1 arrest in DOK cells.

DOK were starved for 24 h in 1% FBS and cultured for a further 24 h in full media (10% FBS), then treated for 24 h with autophagy inhibitors 3MA (50 μM), CQ (50 μM) and E64d/pepstatinA (5 μg/mL). Whole cells were then fixed in 100% EtOH and resuspended in PBS containing RNase (500 μg/mL) and PI (150 μg/mL). Graph show percentage of cells in (A) Sub-G_0, (B) G_0/G_1, (C) S and (D) G_2/M phases of the cell cycle for each population of cells. Vehicle1: DOK cells treated for 24h with 1% DMSO/MeOH mixed at 1:1 ratio (vehicle control for E64d/pepstatinA). Vehicle2: DOK cells treated with 1% deionised H_2O (vehicle control for 3MA and CQ). Data shown n=3 ± SEM (where experiments were completed in duplicate on three separate treatment occasions). One-way ANOVA followed by Dunnett's multiple comparisons test compared to vehicle control. ***$p<0.001$, **$p<0.01$, *$p<0.05$.

3.4.4 Treatment of OSCC cells with inducers and inhibitors of autophagy can induce cell death.

Autophagy is a survival mechanism and inhibition of this pathway may result in cell death. Similarly, stressors that induce autophagy, such as starvation may result in cell death depending on the severity of the stressor and length of exposure. Using the Alamar Blue viability assay and western blotting of PARP cleavage, cell death response to autophagy modulation was assessed.

Analysis of cell viability by Alamar Blue in all four cell lines (figure 3.17.) shows a common trend of decreased viability in Ca9-22 (figure 3.17. A) SCC4 (figure 3.17. B), TR146 (figure 3.17. C) and DOK (figure 3.17. D) cells after CQ treatment. DBeq also shows a tendency to decrease viability, however this is only statistically significant in TR146 cells. In all four cell lines, 3MA and E64d have no effect on cell viability.

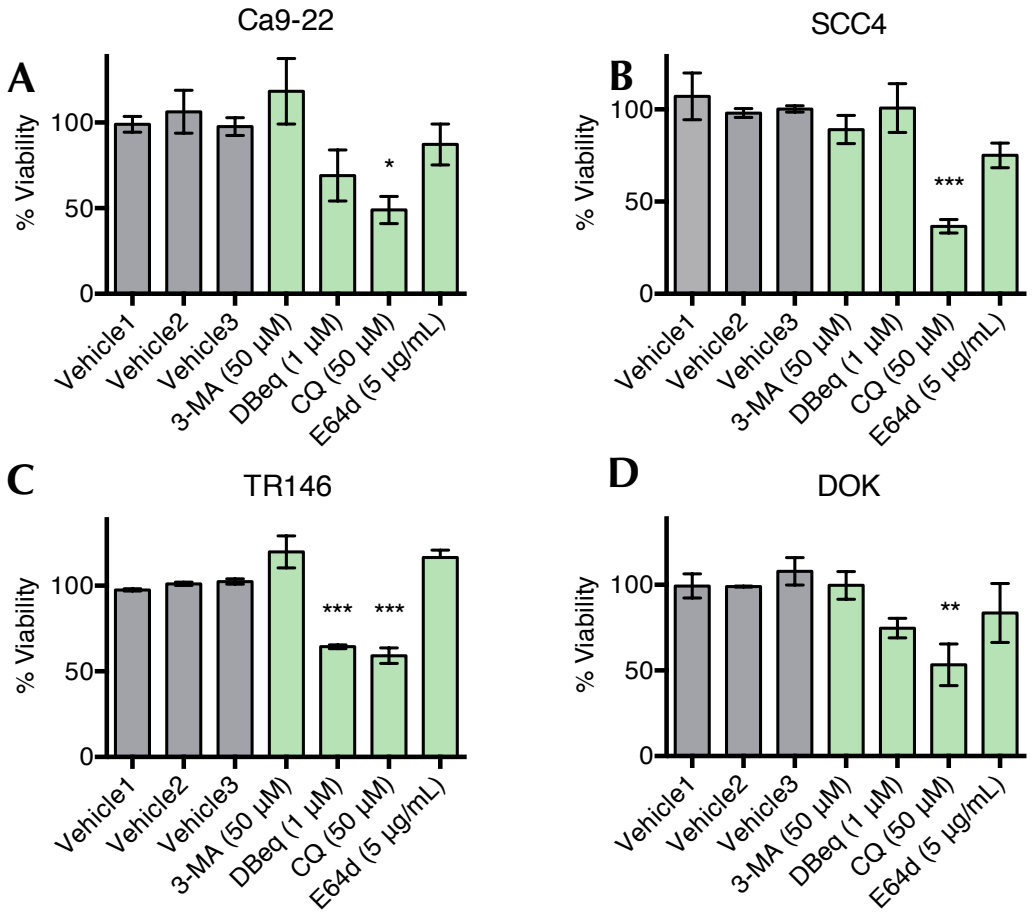

Figure 3.17. Treatment with autophagy inhibitors significantly modulates the viability of discrete OSCC cell lines

(A) Ca9-22, (B) SCC4, (C) TR146, (D) DOK cells were seeded at an appropriate density in a clear 96 well plate in starved medium (1% FBS) for 24 h and allowed to recover in full medium (10%FBS) for a further 24 h before being treated with autophagy inhibitors 3MA (50 μM), DBeq (1 μM), CQ (50 μM) and E64d/pepstatinA (5 μg/mL) for 24 h. Alamar Blue reagent was added 4 h before the end point and absorbance values were read at λ=570 nm and λ=600 nm. Vehicle1: 1% EtOH (vehicle control for DBeq). Vehicle2: 1% DMSO/MeOH mixed at 1:1 ratio (vehicle control for E64d/pepstatinA). Vehicle: 1% deionised H_2O (vehicle control for 3MA and CQ). DBeq and E66d were compared to their vehicle control by students t-test while 3MA and CQ were compared to their vehicle control by one-way ANOVA followed by Dunnet's post-hoc analysis. Data shown n=3 ± SEM. ***p<0.001, ** p<0.01, *p<0.05.

After 4 h incubation in EBSS, in Ca9-22 cells no PARP cleavage can be seen, however PARP cleavage is prominent at 8 h and 12 h treatment (figure 3.18). Treatment of Ca9-22 cells with autophagy inhibitors 3MA, CQ or E64d results in no PARP cleavage (figure 3.19.).

Treatment with EBSS for 4 h in SCC4 cells results in no PARP cleavage (figure 3.20.), similarly treatment with autophagy inhibitors 3MA, CQ and E64d shows no PARP cleavage by western blotting.

TR146 cells treated with the autophagy inhibitors 3MA, CQ and E64d results in no PARP cleavage(figure 3.21.) Similarly, DOK cells undergo no PARP cleavage when treated with either 3MA, CQ or E64d (figure 3.22.).

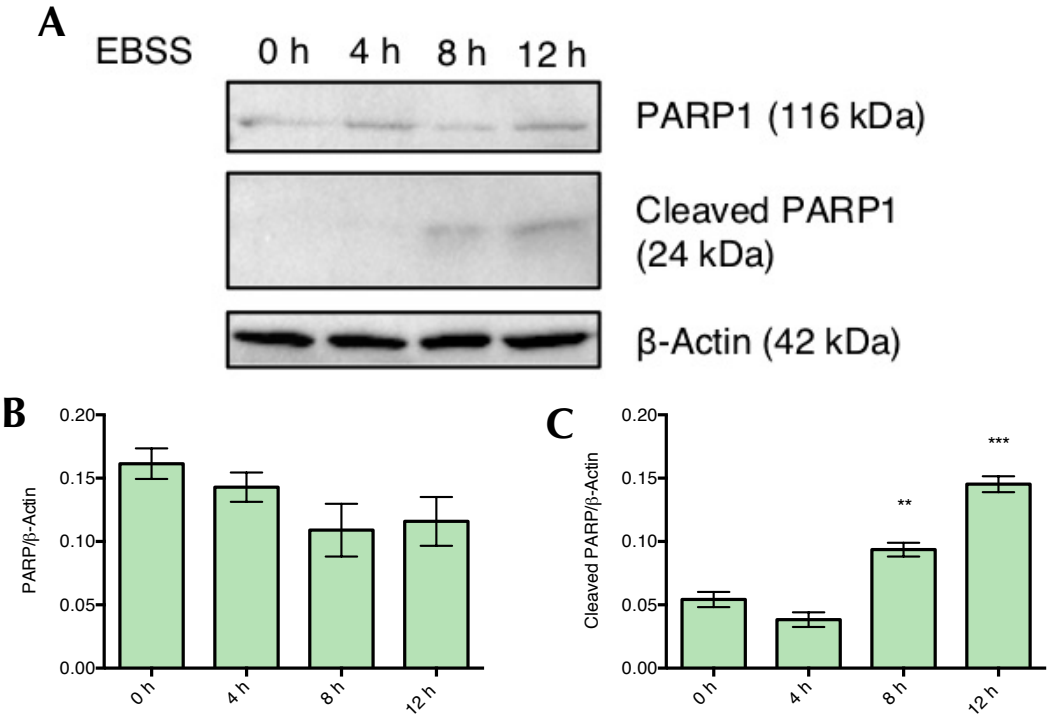

Figure 3.18. Starvation of Ca9-22 cells for more than 4 h results in cell death.

Ca9-22 cells were incubated in EBSS for 0 h, 4 h, 8 h and 12 h at 37°C before being lysed in RIPA buffer. Lysates (20 μg) were resolved by SDS-PAGE on a 10% gel, followed by transfer onto PVDF membrane. The membranes were then probed with anti-PARP1 and ß-actin antibodies and visualised using a gel documentation system (Biorad) and enhanced chemiluminescent HRP substrate (millipore). Blot shown is a representative blot of an experiment performed three times with similar results. Densitometry statistics carried out by one-way ANOVA with Dunnett's post-hoc analysis. Data shown n=3; **$p<0.01$, ***$p<0.001$.

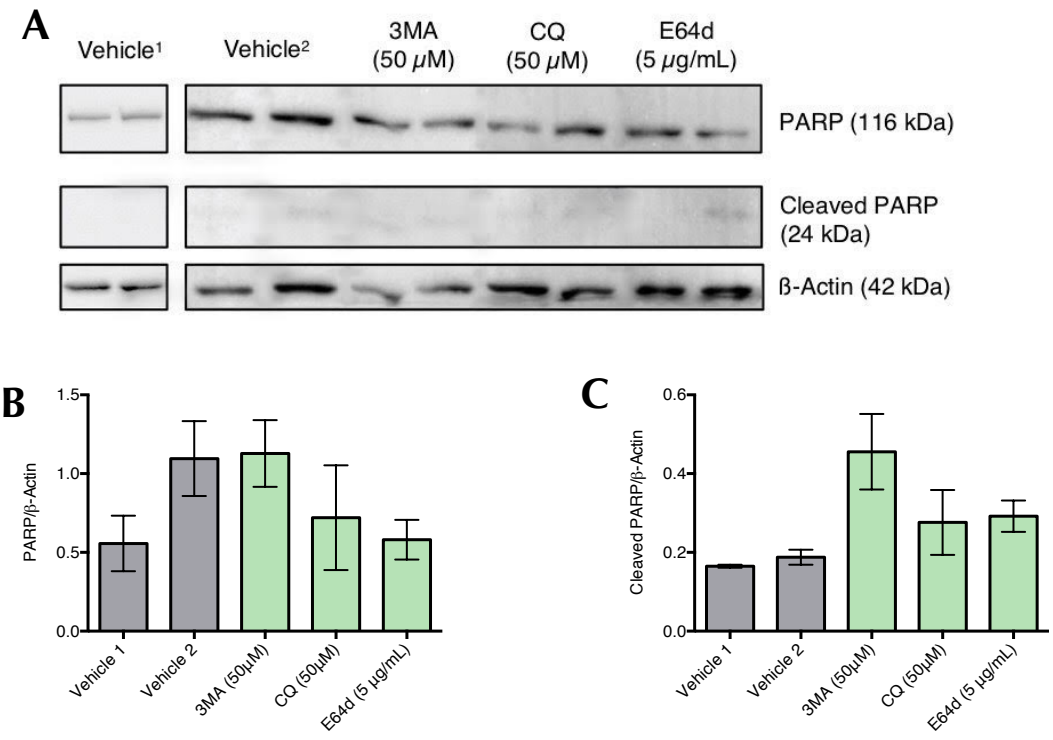

Figure 3.19. Treatment of Ca9-22 cells with autophagy inhibitors results in no PARP cleavage.

Ca9-22 cells were treated with various autophagy inhibitors for 24 h before being lysed in RIPA buffer. Lysates (20 μg) were resolved by SDS-PAGE on a 10% gel, followed by transfer onto PVDF membrane. The membranes were then probed with anti-PARP1 and ß-actin antibodies and visualised using a gel documentation system (Biorad) and enhanced chemiluminescent HRP substrate (millipore). Experiments were repeated on three individual occasions to ensure reproducibility. Vehicle[1]: Ca9-22 cells treated for 24h with 1% DMSO/MeOH mixed at 1:1 ratio (vehicle control for E64d/pepstatinA). Vehicle[2]: Ca9-22 cells treated for 24h with 1% deionised H_2O (vehicle control for 3MA and CQ). All data presented as n=2 where each column represents a separate treatment occasion. Densitometry statistics carried out by one-way ANOVA with Dunnett's post-hoc analysis. Data shown n=3.

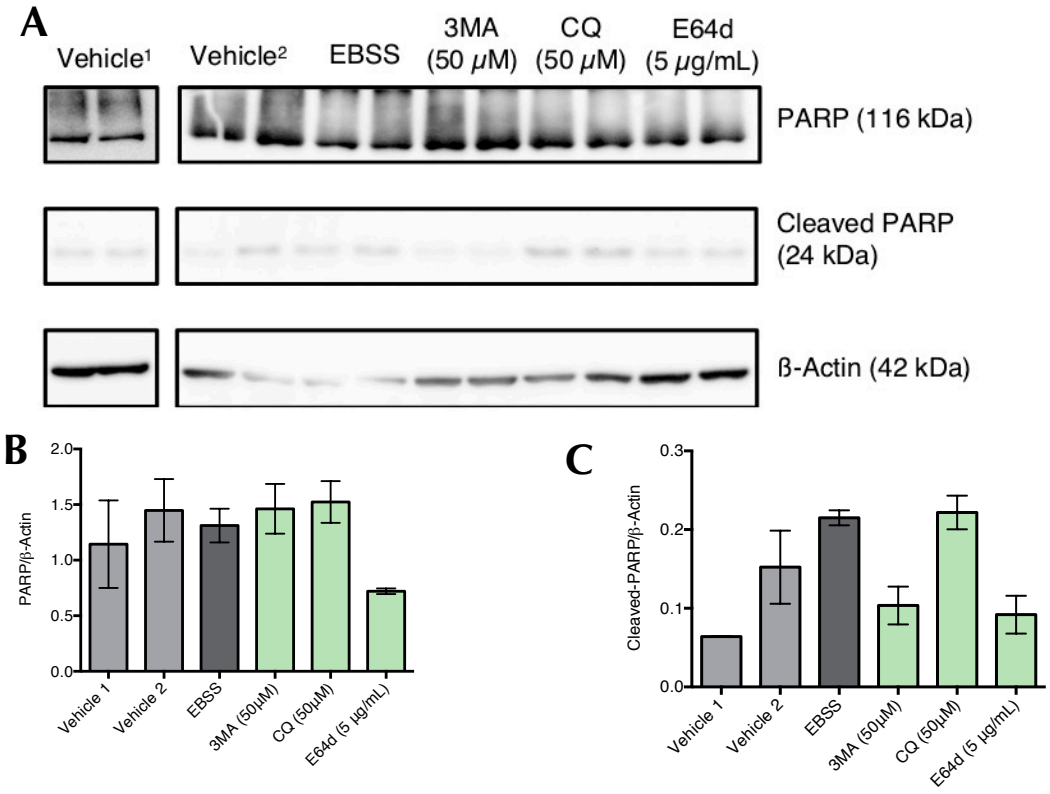

Figure 3.20. Treatment of SCC4 cells with EBSS or autophagy inhibitors results in no PARP cleavage.

SCC4 cells were treated with various autophagy inhibitors for 24 h before being lysed in RIPA buffer. Lysates (20 μg) were resolved by SDS-PAGE on a 10% gel, followed by transfer onto PVDF membrane. The membranes were then probed with anti-PARP1 and ß-actin antibodies and visualised using a gel documentation system (Biorad) and enhanced chemiluminescent HRP substrate (millipore). Experiments were repeated on three individual occasions to ensure reproducibility. Vehicle[1]: SCC4 cells treated for 24h with 1% DMSO/MeOH mixed at 1:1 ratio (vehicle control for E64d/pepstatinA). Vehicle[2]: SCC4 cells treated for 24h with 1% deionised H_2O (vehicle control for 3MA and CQ). All data presented as n=2 where each column represents a separate treatment occasion. Densitometry statistics carried out by one-way ANOVA with Dunnett's post-hoc analysis. Data shown n=3.

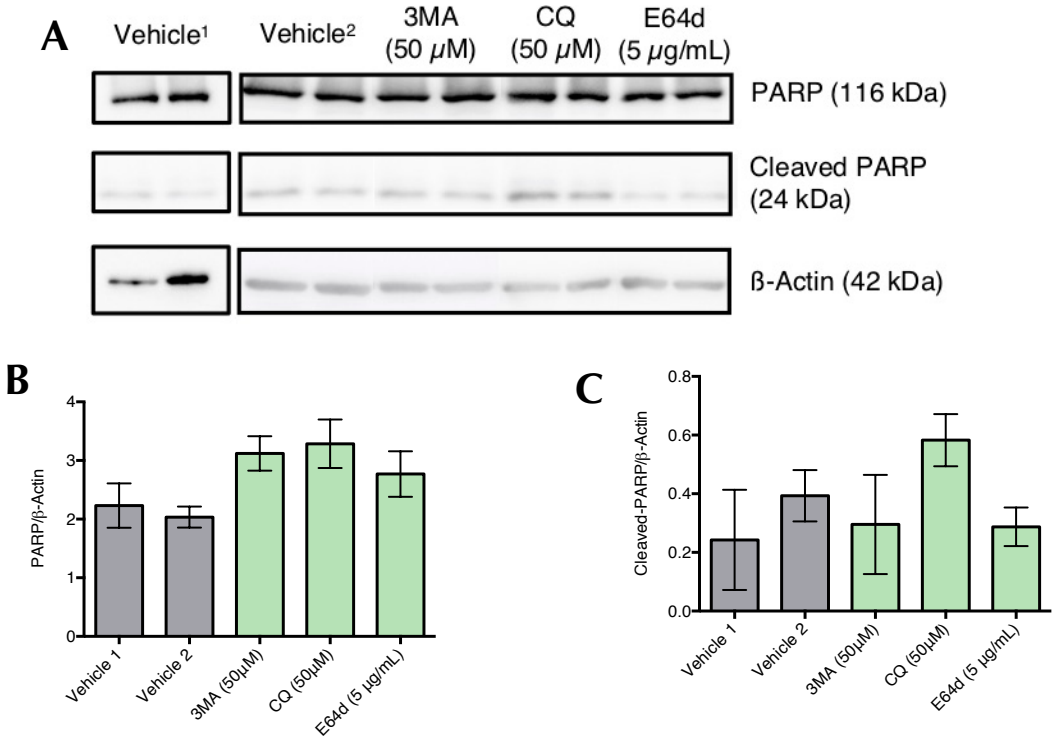

Figure 3.21. Treatment of TR146 cells with autophagy inhibitors results in no PARP cleavage.

TR146 cells were treated with various autophagy inhibitors for 24 h before being lysed in RIPA buffer. Lysates (20 μg) were resolved by SDS-PAGE on a 10% gel, followed by transfer onto PVDF membrane. The membranes were then probed with anti-PARP1 and ß-actin antibodies and visualised using a gel documentation system (Biorad) and enhanced chemiluminescent HRP substrate (millipore). Experiments were repeated on three individual occasions to ensure reproducibility. Vehicle[1]: TR146 cells treated for 24h with 1% DMSO/MeOH mixed at 1:1 ratio (vehicle control for E64d/pepstatinA). Vehicle[2]: TR146 cells treated for 24h with 1% deionised H_2O (vehicle control for 3MA and CQ). All data presented as n=2 where each column represents a separate treatment occasion. Densitometry statistics carried out by one-way ANOVA with Dunnett's post-hoc analysis. Data shown n=3.

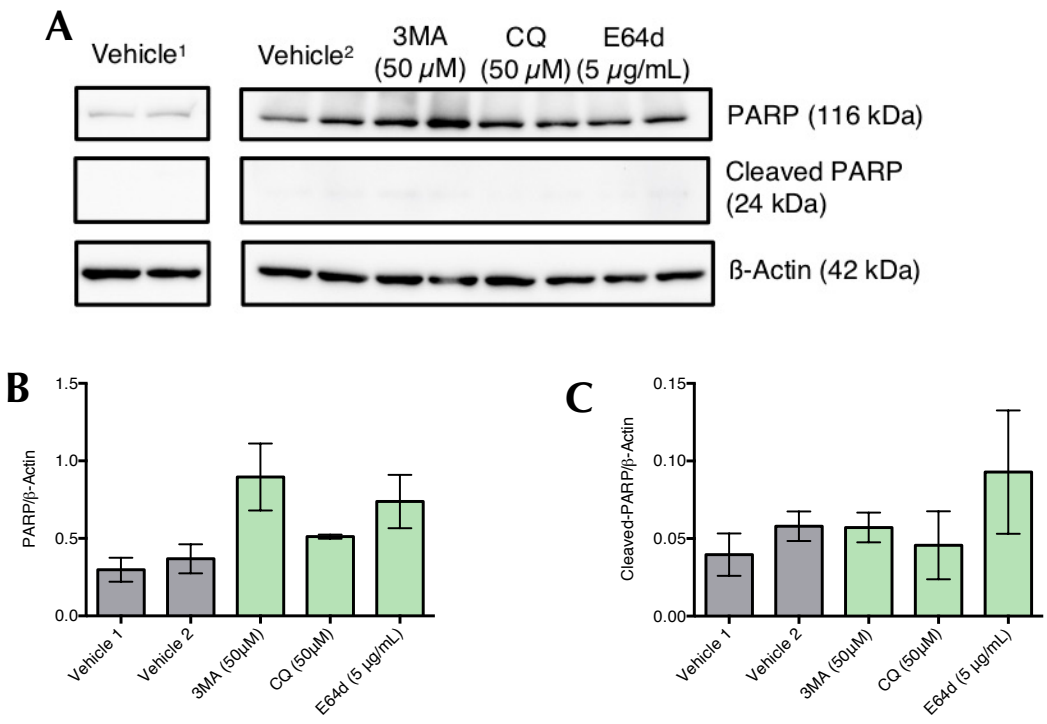

Figure 3.22. Treatment of DOK cells with autophagy inhibitors results in no PARP cleavage in DOK cells.

DOK cells were treated with various autophagy inhibitors for 24 h before being lysed in RIPA buffer. Lysates (20 μg) were resolved by SDS-PAGE on a 10% gel, followed by transfer onto PVDF membrane. The membranes were then probed with anti-PARP1 and ß-actin antibodies and visualised using a gel documentation system (Biorad) and enhanced chemiluminescent HRP substrate (millipore). Experiments were repeated on three individual occasions to ensure reproducibility. Sham[1]: DOK cells treated for 24h with 1% DMSO/MeOH mixed at 1:1 ratio (vehicle control for E64d/pepstatinA). Sham[2]: DOK cells treated for 24h with 1% deionised H_2O (vehicle control for 3MA and CQ). All data presented as n=2 where each column represents a separate treatment occasion. Densitometry statistics carried out by one-way ANOVA with Dunnett's post-hoc analysis. Data shown n=3.

3.4 Discussion

OSCC is one of the most common cancers worldwide. Despite much scientific effort to improve therapies, the prognosis of OSCC patients is still poor and mortality rates have not reduced in recent years. Recent studies suggest that tumour resistance to therapy could be related to cell survival through autophagy[144, 145]. Therefore, heightened autophagy may be a mechanism of resistance for cancer cells faced with metabolic and therapeutic stress. Targeting autophagy has thus been proposed as a new strategy to bypass drug resistance and improve patient outcomes [133, 134]. However, the role of autophagy in OSCC still remains unclear.

In this chapter several methods commonly used to assess autophagy were evaluated in a panel of OSCC cell lines. Furthermore, the ability of a range of reported autophagy inhibitors, both early and late-stage inhibitors, to modulate autophagy in OSCC cells was examined and their effects. As different cell lines have been known to respond differently to treatment with autophagy inducers and inhibitors[139], it was important to determine the response of several oral cancer cell lines to treatment. The response of Ca9-22, SCC4, TR146 and DOK cells to treatment with modulators of autophagy was essential for understanding what autophagy modulation would appear as in different cell lines treated with chemotherapeutics.

It has been shown that using chemical inhibitors of autophagy to highlight disruptions to the flux is very beneficial. Inhibition of later stages of the autophagy pathway by CQ can be used as a tool to identify disruption to earlier stages of the pathway as inhibition of the later stages

of the pathway during autophagy induction results in accumulation of both LC3II and P62 and disruptions to early stages of the pathway under conditions of CQ treatment will result in very little accumulation of LC3II and P62[157]. Western blotting of P62 and LC3II show conflicting results when assessing autophagic flux and inhibition. Although P62 is an adaptor protein that is predominantly degraded in selective autophagy, it is frequently considered to be a good measure autophagic flux[85] due to its ability to bind to LC3II and be degraded alongside it in the autophagosome[85]. It has been shown that the decreased expression of P62 indicates increased degradation of autophagosomes while the increased expression of LC3II suggests increased formation of autophagosomes however, there is a lot of evidence to suggest that large variations exist in these expression levels based on time and cell line[137]. The data captured in this chapter indicate that changes in P62 levels are an unreliable method of monitoring autophagy in these cell lines.

Induction of autophagy should increase autolysosome degradation leading to a decrease in P62 levels during selective autophagy. From the results shown here, 4 h treatment with EBSS shows no change in P62 levels in TR146 cells. In DOK cells, P62 levels increased in response to 4 h treatment with EBSS. P62 induction can occur because of amino acid shortage as is the case during EBSS treatment[158]. Treatment with autophagy inhibitors demonstrated no change to P62 levels in all four cell lines. By monitoring P62, there is an assumption that selective autophagy is occurring however there are several other adaptor proteins associated with selective autophagy, such as NBR1, however these have not been well characterised. Furthermore, it is more likely that bulk

autophagy is taking place where adaptor proteins are not required[79]. As seen in figure 3.18, EBSS induces cell death after only 8h treatment. This is supported by Zhag *et al*. (2017) where EBSS induced cell death is seen after only 6h treatment, coinciding with the induction of autophagy at the same time point[159]. This is a potential bypass mechanism and can go some way to explaining EBSS's inability to induce autophagy in certain cell lines, where a 4h treatment time is insufficient for autophagy induction, but longer treatment time would result in cell death. Although the data is not shown, experiments were completed using the allosteric mTOR inhibitor rapamycin as a means of inducing autophagy. These experiments yielded no significant results, which may be due to incomplete inhibition of mTOR but it is a possibility that these oral cell lines are resistant to its effects[160].

LC3 levels did not respond as predicted in the presence of EBSS. LC3II levels decreased in DOK cells after treatment with EBSS, which backs up the hypothesis that in the case of DOK cells, 4 h treatment with EBSS results in a sufficient level of amino acid depletion to cause both P62 induction and autophagosome degradation. In Ca9-22, SCC4 and TR146 cells, LC3II levels remained unchanged after 4 h treatment with EBSS. Although this may seem counterintuitive, this correlates with a significant increase in autophagic flux, resulting in rapid turnover of LC3[161]. Treatment with autophagy inhibitors demonstrated consistent results across all four cell lines. 3MA had no effect on LC3II levels in any cell line. It would be expected that 3MA treatment would decrease LC3II level due to the prevention of autophagosome formation, however this was not observed. In this incidence it is likely that the concentration of

3MA used (50 μM) was insufficient to effectively inhibit autophagy in these cell lines, however significant cell death was observed at higher concentrations (not shown), limiting the quantity of cells needed to prepare lysates for western blotting. DBeq increased LC3 levels in Ca9-22 cells but not in the other three cell lines. Again, concentration may be a factor here. DBeq inhibits, P97, an essential protein in autophagosome maturation. Complete inhibition of P97 would result in an accumulation of LC3II which is not seen in SCC4, TR146 and DOK cells. For CQ and E64d the results are clear. CQ increases LC3II levels in all four cell lines while E64d significantly increases LC3II levels in all but SCC4 cells where it is elevated in a non-significant manor.

The argument for a rapid turnover of LC3 leading to a static level of LC3II by western blotting is supported in TR146 cells where treatment with EBSS for 4 h increase the quantity of acidic vesicles (figure 3.9, this increase in acidic vesicles is also seen in SCC4 cells (figure 3.8) however it is not seen in Ca9-22 cells.

Acridine orange staining further demonstrated the strong response of the autophagy machinery to treatment with both CQ and E64d where both compounds increased acidic vesicle production in all cell lines examined. As CQ's mechanism of action involves sequestration in acidic vesicles, it is not surprising that CQ has an affinity for endosomes and lysosomes. It has been shown that CQ treatment can interfere with glycosylation and golgi function[162, 163]. Damaged golgi have been shown to recruit LC3 in a PI3K independent manner[164]. It is likely that these off-target effects of CQ in other parts of the cell may have knock-on effects in modulation of

autophagy and cell death. Mauthe *et al.* demonstrated that autophagy inhibition by CQ is mostly due to its impaired autophagosome fusion with the lysosome, however they also discovered that CQ treatment results in severe disorganisation of the golgi and endo-lysosomal systems[165]. Mauthe *et al.* also noted that they did not observe the commonly noted increased lysosomal pH associated with CQ treatment. They suggested that this may be cell/tissue dependant, and this is consistent with this research where increased green fluorescence from acridine orange staining can be seen under CQ treatment in TR146 cells. This green, basic, fluorescence overlapped with the red, acidic, staining associated with lysosomes and autolysosomes indicating a pH that is both acidic and basic (neutral). CQ's mechanism of action is to raise the lysosomal pH which would result in this pH dependant colour change, this may not have been observed in other cell lines due to cell specific changes in time taken for lysosomal pH to change.

3MA and DBeq had no effect on acidic vesicle production which could be linked to the concentrations of the compounds being too low or the mechanism of action preventing an increase in enclosed acidic autophagosomes and thus preventing an increase in acidic vesicles, however the former is the most likely cause here.

Using acridine orange to look at acidic vesicles has similar caveats to western blotting of P62 and LC3, in that it is useful when inhibiting the autophagosome/lysosome fusion stage, but it gives limited and inconsistent information when observing early-stage inhibition or autophagy induction.

When devising a strategy to measure autophagy, the methods used here are relatively simple and inexpensive, however the data produced can leave a lot of room for misinterpretation. The more recent techniques such as tandem mRFP-GFP-LC3 fluorescence microscopy may be a more robust measurement of autophagic flux. This technique takes advantage of the pH-dependant properties of GFP-LC3, which loses fluorescence due to lysosomal acidic conditions and combines this with the pH independent properties of mRFP-LC3, which allows for simultaneous labelling of autophagic compartments before and after fusion with lysosomes[166]. Another novel technique is the staining kit, Cyto-ID which can successfully label accumulated autophagic vacuoles in live cells without the need for transfection. As more novel techniques arise, autophagy research will become streamlined, facilitating easier characterisation of autophagy modulation in a tissue and cell specific manner.

Research on the relationship between autophagy and cell cycle is limited however there are data that link autophagy induction to alterations within specific phases of the cell cycle. Induction of autophagy seems to result in preferential alterations to either the G_1 or S phases of the cell cycle[167]. This can be seen from data shown in this thesis (figure 3.11 and 3.13) where induction of autophagy by EBSS resulted in a small decrease in Ca9-22 cells in the S phase and an increase in SCC4 cells in the S phase. During treatment with inhibitors of autophagy, however, alterations to the cell cycle are more complicated. As autophagy is linked to so many

aspects of cellular function, it is not surprising that inhibition of this pathway interrupts cell cycle progression. It has been shown in the OSCC cell lines SCC25 and Cal27 that CQ treatment leads to cell cycle arrest at the G_0/G_1 phase [147]. In this study, this was not observed in Ca9-22 cells or SCC4 cells and the opposite can be seen in TR146 cells where there are fewer cells in the G_0/G_1 phase and increased cell cycle arrest at the G_2/M phase. An increase in the number of cells at the G_0/G_1 phase can be seen in DOK cells treated with E64d. It has been shown that ubenimex, another protease inhibitor, inhibits autophagy and induces G_2/M arrest in glioma cells[168]. In SCC4 and DOK cells the protease inhibitor E64d shows a decrease in cell passing through the G_2/M phase. 3MA has been shown to increase cell cycle arrest at the G_0/G_1 phase in breast cancer cells[169],this was seen in Ca9-22 cells however the observation was not present in the other three cell lines. An interesting observation was that of CQ in Ca9-22 cells where this treatment had no impact on the sub G_0 phase, research by Zou *et al* demonstrated that CQ had no impact on the sub G_0 phase of the cell cycle in two distinct non-small cell lung cancer cell lines[170] indicating that this may be a cell line specific effect. Once again it would appear that modulation of autophagy has many cell type-specific effects in terms of its impact on cell cycle progression.

After investigating the effects of various autophagy inhibitors on cell viability, it is clear that not all treatments have the same effects. 3MA had no effect on viability in all four cell lines, likely due to its solubility in DMF reducing the ability to reach an effective dose without causing a viability decrease due to the vector itself. The same can be said for E64d/pepstatinA which required a vector cocktail of methanol and

DMSO to achieve a stable solution. DBeq demonstrated a decrease in viability in TR146 cells only, demonstrating a cell-specific effect likely due its mechanism of inhibiting P97 ATPase activity. Inhibition of P97 can lead to P53 activation[171] and likely requires wild-type P53 (found in TR146 cells) for this inhibitor to decrease cell viability. CQ is one of the most widely researched autophagy inhibitors due to its established approval for human use. CQ has been suggested as a potential alternative to chemotherapy[147], as well as being recommended as an adjuvant therapy[151] due to its observed anti-proliferative effect. In the OSCC cell lines studied here, CQ shows no PARP cleavage. The lack of PARP cleavage is surprising given that analysis by Alamar Blue has shown between a 45-65% decrease in cell metabolic activity. As PARP cleavage is a hallmark of apoptosis, this suggests that CQ is either triggering another cell death pathway or is preventing proliferation. Previous research by Nordstrøm *et al.* in both lung and pancreatic cancer cells has shown that CQ has antiproliferative effects in the absence of apoptosis where cells demonstrated a diminishing cell number without any propidium iodide or annexin V positive staining indicating its benefits as an anti-tumour treatment[172]. Due to the lack of alterations to the cell cycle under CQ treatment, it is most likely that another, non-PARP-mediated cell death pathway is at play here.

These data have indicated that CQ is the most promising candidate as an potential anti-cancer treatment within OSCC cells. The combination of the cell death data of CQ with that of the cell cycle analysis, showing no increase in the apoptotic or Sub G_0 phases indicates that CQ may have a substantial role in preventing sufficient metabolic activity therefore

reducing the proliferation of OSCCs, however a decrease in mitotic activity would typically be seen as an increase in the number of cells in the G_2/M peak of the cell cycle. This increase is only seen in TR146 cells, however, an increase at the G_0/G_1 phase in SCC4 and DOK cells may indicate arrest in the cell cycle at an earlier point which would still prevent entry into mitosis. Another possibility is a change in Cdk (cyclin dependant kinase) or cyclin activity in response to CQ treatment. CQ has been shown to upregulate P21[173], a protein induced by P53 and is involved in cellular processes such as apoptosis, senescence, cell growth and cell cycle progression[174]. P21 has been shown to inhibit Cdk2 and CyclinB1 expression, inducing G2/M arrest[175]. This link between CQ and Cdks is extremely novel and it is yet unclear how different cell types respond to CQ-induced P21 upregulation. P21 can have varying effects on the cell depending on localisation, post-translational modifications and P53 status[175], these factors may all have an influence over how OSCC cells respond and may impact cell cycle progression into mitosis differently.

The data shown in this chapter identified cell-specific responses to treatment with autophagy inhibitors and the cellular response to the autophagic proteins P62 and LC3II. Acidic vesicle quantity and LC3II levels were altered by CQ treatment uniformly across all four cell lines tested while 3MA, DBeq and E64d/pepstatinA had a variety of responses to LC3II depending on the cell line and the early-stage inhibitors 3MA and DBeq had no impact on acidic vesicle quantities. Similarly, these inhibitors demonstrated varying effects on cell viability with only DBeq and CQ displaying inhibitory effects on cell viability in OSCC cell lines.

As treatment with CQ demonstrate a consistent elevation in LC3II and acidic vesicle quantity, alongside a consistent induction of reduced cell viability in all four cell lines CQ was selected as a preferred candidate for further studies to investigate its effect as an adjuvant treatment to chemotherapy. It was hypothesised that by combining CQ treatment with known OSCC chemotherapeutics that inhibition of potential chemotherapeutic-induced autophagy could increase their efficacy, this will be explored further in Chapter 4.

Chapter 4

Modulation of cell death pathways in immortalized oral epithelial carcinoma and pre-malignant cell lines using commercially available chemotherapeutics

4.1 Introduction

Oral cancer was identified as the 16th most common cancer worldwide in 2018[176]. Due to its high prevalence, it is imperative that the most effective treatment options are identified to improve the 5-year survival rate from the current estimated 40%. OC is frequently only discovered at a later stage of development, therefore the standard treatment plan for this type of cancer is surgical intervention, often accompanied by radiotherapy or chemotherapy as adjuvant treatments. Chemotherapy is associated with a high rate of resistance but carry's the lowest long-term risks, therefore progress in improving the efficacy of chemotherapeutic treatment while reducing the risk of resistance development will significantly improve the QOL for many patients undergoing invasive surgery and radiation therapy for OC.

4.1.1 Chemotherapy in OSCC

The first use of small-molecule drugs in cancer treatments commenced in the 1900s when mustard gas, used as a weapon with devastating results during the First World War, was discovered to prevent the production of lymphocytes and granulocytes. This led to the use of similar compounds, referred to as 'nitrogen mustards', as therapeutics for malignant lymphomas[177]. Since this discovery, chemotherapeutic agents have been continually developed and improved. From the FDA's approval of Dr Peyron's 'Peyron's salts'[178] (now known as cisplatin (CPt)) in 1978[179] to the relatively recent development of more modern antibody-conjugated therapeutics such as gemtuzimab and ozogamicin at the end of the 21st centry[180]. Currently, the standard treatment in cases of OSCC,

are the platinum-based drugs CPt and carboplatin (CBDCA) (Figures 4.1A and B), the anti-metabolite 5-FU (Figure 4.1C) and the taxane docetaxel (TXT) (Figure 4.1D). These drugs can be administered alone but are regularly used in combination with each other and as adjuvant therapies to surgical resection.

Platinum-based drugs such as CPt and CBDCA are comprised of a doubly charged platinum ion which is surrounded by amine and carboxylate groups. The carboxylates allow for bonds to form with DNA bases[181]. In CPt, these carboxylate groups are in the form of two chloride ligands, however in CBDCA, they take the form of bidentate dicarboxylate which allows for slower DNA binding kinetics. This results in a lower excretion rate and allows for longer retention in the body and prolonged action of the drug.

5-FU is an analogue of uracil containing a fluorine atom in place of one hydrogen. 5-FU undergoes intracellular metabolism and disrupts RNA and DNA synthesis by incorporation of the fluoronucleotides into their helixes and by inhibiting thymidylate synthase[182]. TXT (Docetaxel) disrupts microtubule spindle assembly by binding to ß-tubulin. This causes microtubule polymerisation to occur in the absence of GTP (guanosine triphosphate). Microtubules that are bound by taxanes cannot be depolymerised, which disrupts mitoses and causes cell cycle arrest at the G_2/M phase of the cell cycle, ultimately causing apoptosis[183].

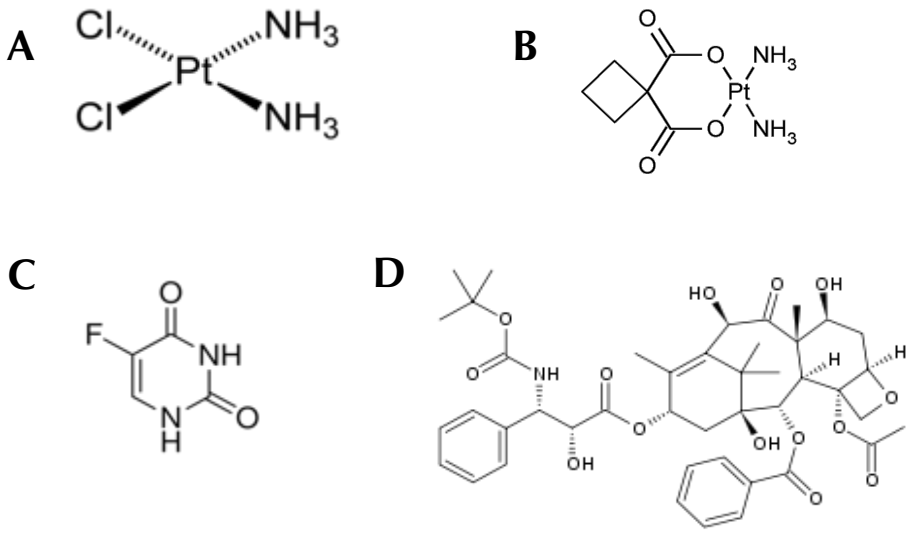

Figure 4.1. Structures of common chemotherapeutics used in OSCC.

Platinum-based drugs Cisplatin (A) and Carboplatin (B) intercalate with DNA molecules while the anti-metabolite 5-fluorouracil (C) inhibits RNA synthesis and the taxane docetaxel (D) interferes with microtubule and spindle assembly through disruption of polymerization and depolymerization equilibrium leading to cell cycle arrest at the G2/M phase.

4.1.2 The relationship between chemotherapy and autophagy

Autophagy can be triggered in response to cellular stress. During chemotherapeutic intervention cells are put under severe stress, therefore it is unsurprising that chemotherapy has been shown to induce autophagy in many cancer types. CPt treatment is known to induce autophagy in renal tubular epithelial cells[184] while both CBDCA and paclitaxel (another taxane based chemotherapeutic) induced autophagy in cervical cancer cells[185]. There are significant levels of research showing that autophagy induction as a result of chemotherapy is linked to the development of resistance. Duan *et al.* demonstrated in both cervical and gastric cancer cell lines that autophagy mediates CPt resistance[186] while it was demonstrated that inhibition of CPt-induced autophagy in human lung cancer cells resulted in increased CPt-induced apoptotic cell death[187]. This increased chemotherapy-induced cell death through the inhibition of autophagy was also observed to occur with CPt treatment in oesophageal SCC [188]and 5-FU in colon cancer[189]. Due to the link between chemoresistance and autophagy, the involvement of P53 (see section 1.4.1) is worthy of investigation. P53's putative role in resistance to chemotherapy drove the selection process for the cell lines utilised throughout this study, the Ca9-22 cells possess a mutated P53 gene, SCC4 cells exhibit upregulated P53 gene expression, TR146 cells have no known mutation and DOK cells have a 12-base pair deletion in the P53 gene. This deletion in the DOK P53 gene has no known impact on gene functionality and these cells are considered to possess a 'normal' P53 gene.

4.2 Aims of Chapter

It is apparent that autophagy has a role in tumour protection during chemotherapy, however, there is a paucity of research on the mechanisms utilised in the autophagy-driven development of chemoresistance in OSCC. To enhance future therapeutic strategies, the impact of chemotherapeutic interference with normal autophagic processes needs to be understood in OSCC cells. This chapter aims to characterise the impact of commercially available chemotherapeutics on OSCC cell lines as per the following specific objectives:

1. **To establish the IC_{50} values of known OSCC chemotherapeutics across four oral cell lines.**

   Despite chemotherapeutic agents being extensively used in OSCC research, there is currently no reference data on associated IC_{50} values in common OSCC cell lines. IC_{50} values will be established through monitoring cellular metabolic activity using Alamar Blue in Ca9-22, SCC4, TR146 and DOK cells treated with titrations of cisplatin, carboplatin, 5-fluorouracil and docetaxel.

2. **To examine the outcome of chemotherapeutic intervention on autophagy in OSCC cell lines.**

   Ca9-22, SCC4, TR146 and DOK cells will be treated with cisplatin, carboplatin, 5-fluorouracil and docetaxel and numbers of acidic vesicles quantified by fluorescent microscopy with acridine orange staining. Further analysis by western blotting will identify modulation of the key autophagy proteins LC3B and P62.

4.3 Results

4.3.1 Platinum based chemotherapeutics show increasing potency in OSCC cell lines in a time dependent manner.

To establish the level of drug potency, the IC_{50} value for each drug was determined through titrating CPt or CBDCA followed by measuring the effect on cellular metabolic activity through the Alamar Blue assay (summary found in table 4.1).

Figure 4.2 A shows the IC_{50} plots of CPt in Ca9-22 cells at 24 h, 48 h, 72 h, 96 h and 120 h as 22.96 ± 2.25 μM, 6.04 ± 0.55 μM, 3.43 ± 1.45 μM, 0.90 ± 0.16 μM and 0.69 ± 0.13 μM respectively. IC_{50} values for SCC4 cells (figure 4.3 B) show an increased potency at 24 h, 48 h, 72 h, 96 h and 120 h with values of 4.4 ± 0.2 μM, 0.7 ± 0.1 μM, 1 ± 0.1 μM, 0.6 ± 0.1 μM and 0.6 ± 0.03 μM respectively. In TR146 cells (figure 4.2 C), the IC_{50} values of CPt are higher than those of both Ca9-22 and SCC4 cells with values for 48 h, 72 h, 96 h and 120 h at 9.75 ± 2.17 μM 6.06 ± 2.1 μM, 5.15 ± 1.48 μM, and 2.89 ± 0.41 μM respectively. IC_{50} values for CPt in DOK cells (figure 4.2 D) were similar to that of TR146, with values for 48 h, 72 h, 96 h an 120 h at 15.46 ± 1.3 μM, 6.7 ± 1.55 μM, 4.43 ± 1.56 μM and 2.71 ± 1.1 μM. Values for 24 h in both TR146 and DOK cells could not be obtained as the higher drug concentrations required to achieve an IC_{50} exceeded the drug's solubility.

A similar trend was observed with the second platinum based chemotherapeutic, CBDCA. In Ca9-22 cells (figure 4.3 A), IC_{50} values for 24 h, 48 h, 72 h, 96 h and 120 h 347 ± 50 μM, 89.2 ± 13.1 μM, 43.2 ± 7.4 μM,

15.6 ± 2 μM and 6.3 ± 1.2 μM respectively. As with CPt, the CBDCA shows an increased potency in SCC4 cells (figure 4.3 B) with IC_{50} values of 359.8 ± 150.5 μM, 21.5 ± 10.2 μM, 14.1 ± 1.4 μM, 5.1 ± 3 μM and 3 ± 1.5 μM. A slight decrease in CBDCA's potency was seen in TR146 cells (figure 4.3 C) with 48 h, 72 h, 96 h and 120 h IC_{50} values given at 227.72 ± 65.1 μM, 81.4 ± 16.18 μM, 20.83 ± 1.04 μM and 8.33 ± 2.64 μM. A decrease in the potency of CBDCA was, again, seen in DOK cells with an increase in IC_{50} values compared to those determined in Ca9-22 cells for 72 h, 96 h and 120 h measured at 114.45 ± 17.43 μM, 60.82 ± 2.36 μM and 45.43 ± 7.61 μM respectively (figure 4.3 D).

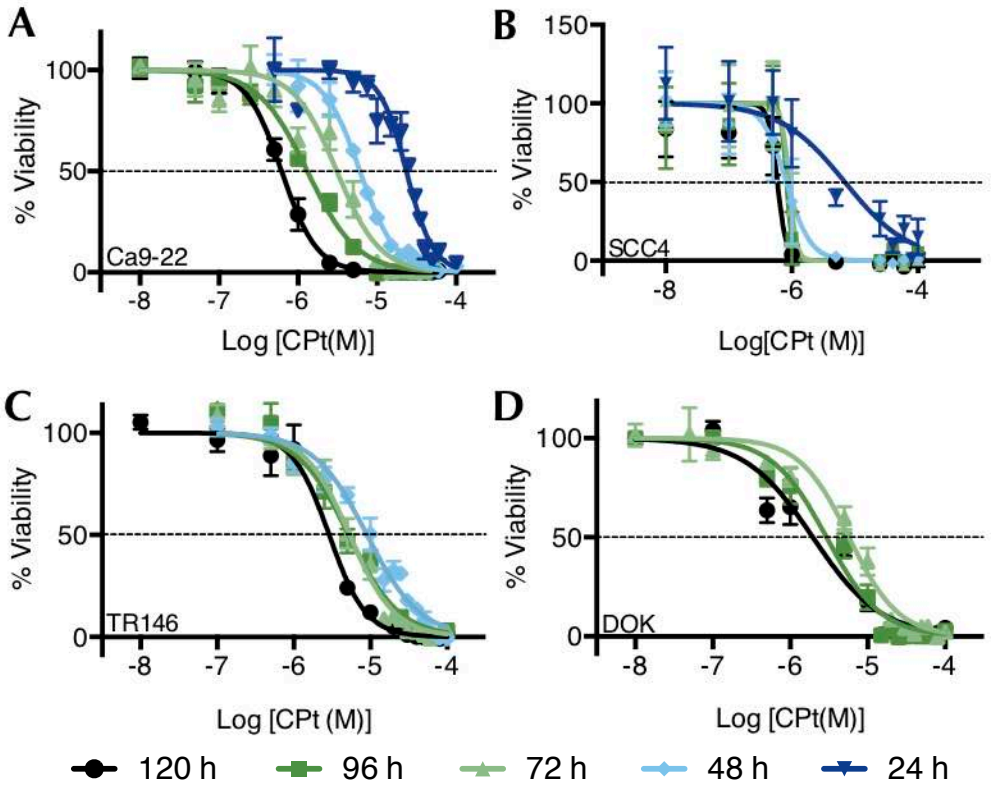

Figure 4.2. The IC_{50} of cisplatin decreases as treatment time increases in distinct OSCC cell lines.

(A) Ca9-22, (B) SCC4, (C) TR146 and (D) DOK Cells were seeded at an appropriate density in a clear 96 well plate in starved medium (1%FBS) for 24 h and allowed to recover in full medium (10% FBS) for a further 24 h before being treated with a range of concentrations of a cisplatin for 24 h, 48 h, 72 h, 96 h and 120 h. Alamar Blue reagent was added 4 h before the end point and absorbance values were read at λ=570 nm and λ=600 nm. Data shown n=9 ± SEM and are a combination of three individual experiments.

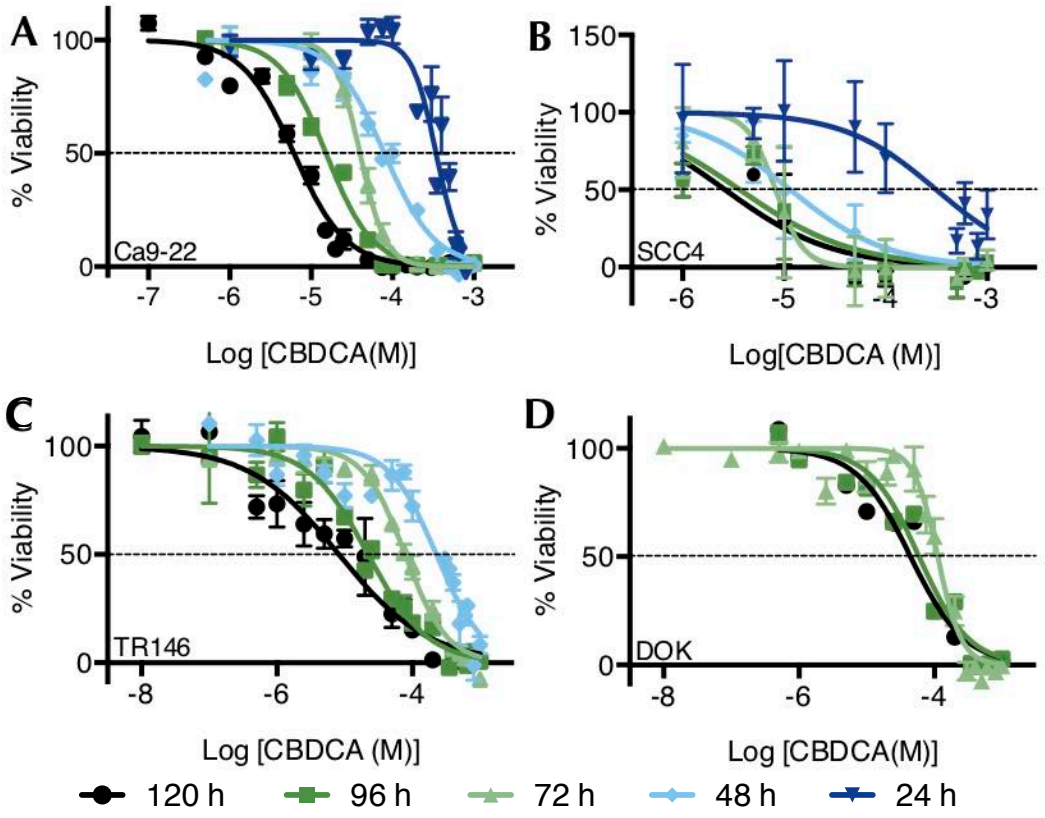

Figure 4.3. The IC_{50} of CBDCA decreases as treatment time increases in distinct OSCC cell lines.

(A) Ca9-22, (B) SCC4, (C) TR146, (D) DOK cells were seeded at an appropriate density in a clear 96 well plate in starved medium (1% FBS) for 24 h and allowed to recover in full medium (10%FBS) for a further 24 h before being treated with a range of concentrations of CBDCA for 24 h, 48 h, 72 h, 96 h and 120 h. Alamar Blue reagent was added 4 h before the end point and absorbance values were read at λ=570 nm and λ=600 nm. Data shown n=9 ± SEM and are a combination of three individual experiments.

4.3.2 The anti-metabolite 5-fluorouracil has a decreased potency in a pre-malignant phenotype cell line compared to three OSCC cell lines.

5-FU showed negligible time-dependent differences in its potency in all cell lines. No IC_{50} value could be obtained at 24 h or 48 h in Ca9-22, TR146 and DOK cells due to limited potency of the compound. Between the four cell lines studied, significant differences were observed (summary found in table 4.1).

5-FU produced IC_{50} values of 7.36 ± 0.37 μM, 5.14 ± 0.68 μM and 4.62 ± 1.08 μM for 72 h, 96 h and 120 h respectively in Ca9-22 cells (figure 4.4 A). SCC4 cells were the only cells it was possible to obtain an IC_{50} curve at 48 h from, yet these cells had the lowest affinity for CBDCA. IC_{50} values of 53.8 ± 48.7 μM, 19.1 ± 1 μM, 26.6 ± 10.1 μM, 15.2 ± 1.7 μM at 48 h, 72 h, 96 h and 120 h respectively. TR146 cells produced IC_{50} values of 2.15 ± 0.36 μM, 1.31 ± 0.41 μM and 3.61 ± 1.18 μM for 72 h, 96 h and 120 h (figure 4.4 C). DOK cells had IC_{50} values similar to those of SCC4 cells with values of 21.25 ± 14.79 μM, 14.44 ± 4.84 μM and 8.14 ± 3.19 μM at 72 h, 96 h and 120 h respectively (figure 4.4 D).

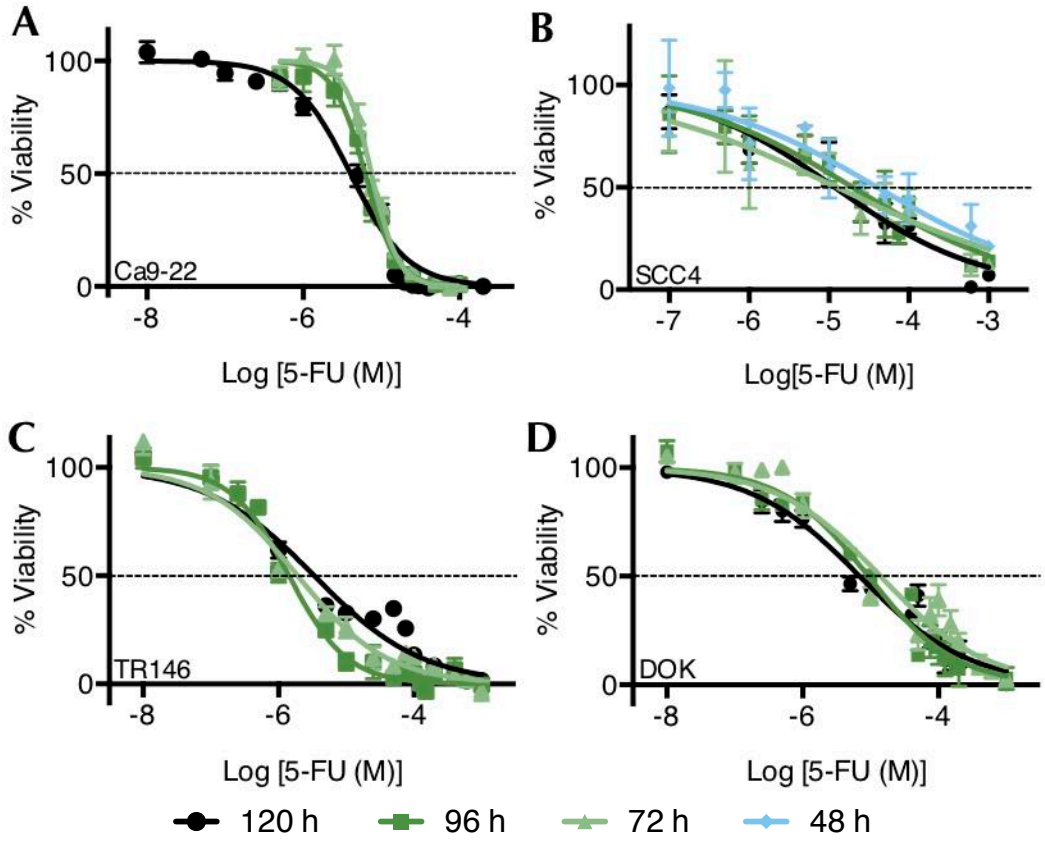

Figure 4.4. The IC_{50} of 5-FU is reduced in the pre-malignant DOK cell line in comparison to OSCC cell lines.

(A) Ca9-22, (B) SCC4, (C) TR146, (D) DOK cells were seeded at an appropriate density in a clear 96 well plate in starved medium (1% FBS) for 24 h and allowed to recover in full medium (10% FBS) for a further 24 h before being treated with a range of concentrations of 5-fluorouracil for 24 h, 48 h 72 h, 96 h and 120 h. Alamar Blue reagent was added 4 h before the end point and absorbance values were read at λ=570 nm and λ=600 nm. Data shown n=9 ± SEM and are a combination of three individual experiments.

4.3.3 Docetaxel displays a time dependant potency in OSCC cell lines but not in pre-malignant cells

Docetaxel (TXT) displayed significant time-dependant differences in IC_{50} values in both Ca9-22 cells and TR146 cells, however both SCC4 and DOK cells showed negligible changes in their IC_{50} values after longer treatment times. No IC_{50} value could be obtained at 24 h or 48 h in Ca9-22, TR146 and DOK cells due to concentrations required being beyond TXT's solubility.

IC_{50} values in Ca9-22 cells at 72 h, 96 h and 120 h were 560 ± 130 pM, 330 ± 70 pM and 170 ± 20 pM respectively (figure 4.5 A). SCC4 cells had a lower affinity for TXT with IC_{50} values of 1293 ± 674 pM, 661 ± 187 pM, 651 ± 158 pM and 500 ± 70 pM at 48 h, 72 h, 96 h and 120 h respectively (figure 4.5 B). TR146 cells had IC_{50} values of 1830 ± 230 pM, 550 ± 65 pM, 200 ± 55 pM and 110 ± 10 pM for 48 h, 72 h, 96 h and 120 h respectively (figure 4.5 C). In DOK cells (figure 4.5 D), TXT showed no significant time dependant differences in IC_{50} values. At 72 h, 96 h and 120 h the respective IC_{50} values were shown to be 410 ± 140 pM, 570 ± 240 pM and 240 ± 45 pM.

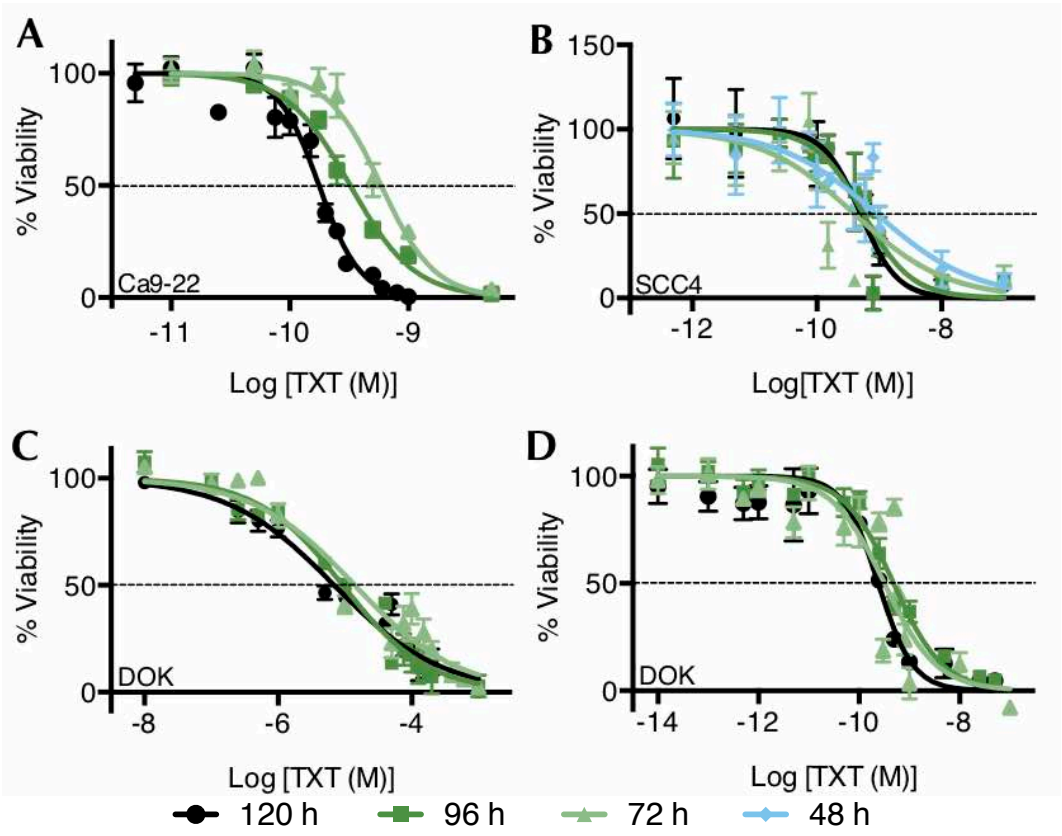

Figure 4.5. IC_{50} values for OSCC cells decrease with increasing treatment time in OSCC cells but not in pre-cancerous DOK cells.

(A) Ca9-22, (B) SCC4, (C) TR146 and (D) DOK cells were seeded at an appropriate density in a clear 96 well plate in starved medium (1% FBS) for 24 h and allowed to recover in full medium (10% FBS) for a further 24 h before being treated with a range of concentrations of docetaxel for 24 h, 48 h, 72 h, 96 h and 120 h. Alamar Blue reagent was added 4 h before the end point and absorbance values were read at λ=570 nm and λ=600 nm. Data shown n=9 ± SEM and are a combination of three individual experiments.

	Drug	24h	48h	72h	96h	120h
Ca9-22	Cisplatin	23 ± 2.3 μM	6 ± 0.6 μM	3.4 ± 1.5 μM	0.9 ± 0.2 μM	0.7 ± 0.1 μM
	Carboplatin	347.7 ± 50 μM	89.2 ± 13.1 μM	43.2 ± 7.4 μM	15.6 ± 2 μM	6.3 ± 1.2 μM
	5-Fluorouracil	-	-	7.4 ± 0.4 μM	5.1 ± 0.7 μM	4.6 ± 1.1 μM
	Docetaxel	-	-	560 ± 130 pM	330 ± 70 pM	170 ± 20 pM
SCC4	Cisplatin	4.4 ± 0.2 μM	0.7 ± 0.1 μM	1 ± 0.1 μM	0.6 ± 0.3 μM	0.6 ± 0.03 μM
	Carboplatin	359.8 ± 150.5 μM	21.5 ± 10.2 μM	14.1 ± 1.4 μM	5.1 ± 3 μM	3 ± 1.5 μM
	5-Fluorouracil	-	53.8 ± 48.7 μM	19.1 ± 1 μM	26.6 ± 10.1 μM	15.2 ± 1.7 μM
	Docetaxel	-	1293 ± 674 pM	661 ± 187 pM	651 ± 158 pM	500 ± 70 pM
TR146	Cisplatin	-	9.8 ± 2.2 μM	6.1 ± 2.1 μM	5.2 ± 1.5 μM	2.9 ± 0.4 μM
	Carboplatin	-	227.7 ± 65.1 μM	81.4 ± 16.2 μM	20.8 ± 1 μM	8.3 ± 2.6 μM
	5-Fluorouracil	-	-	2.2 ± 0.4 μM	1.3 ± 0.4 μM	3.6 ± 1.2 μM
	Docetaxel	-	1830 ± 230 pM*	550 ± 65 pM	200 ± 55 pM	110 ± 10 pM
DOK	Cisplatin	-	15.5 ± 1.3 μM	6.7 ± 1.6 μM	4.4 ± 1.6 μM	2.7 ± 1.1 μM
	Carboplatin	-	-	114.5 ± 17.4 μM	60.8 ± 2.4 μM	45.4 ± 7.6 μM
	5-Fluorouracil	-	-	21.3 ± 14.8 μM	14.4 ± 4.8 μM	8.1 ± 3.2 μM
	Docetaxel	-	-	410 ± 140 pM	570 ± 240 pM	240 ± 45 pM

Table 4.1. IC_{50} values of commonly utilised chemotherapeutics in pre-malignant and OSCC cell lines.

Cells were seeded at an appropriate density in a clear 96 well plate in starved medium (1% FBS) for 24 h and allowed to recover in full medium (10% FBS) for a further 24 h before being treated with a range of concentrations of a given chemotherapeutic. Alamar Blue reagent was added 4 h before the end point and absorbance values were read at λ=570 nm and λ=600 nm Values correct to one significant figure, given as mean ± SEM; n=9. *N=3

4.3.4 Chemotherapeutics induce autophagy in OSCC cell lines

To understand the impact of chemotherapeutic treatment on autophagic processes OSCC cells were treated with the IC_{50} of each chemotherapeutic agent for 24 h or 48 h. For some experiments, where more live cells were required the IC_{25} was used. If an IC_{50} curve could not be obtained for a given time point, the IC_{50} for the lowest calculable time point was used. Acridine orange staining combined with fluorescent microscopy and western blotting for levels of P62 and LC3B were used to assess the modulation of autophagy.

In Ca9-22 cells treated for 24h with CPt, CBDCA or 5-FU, an increase in P62 degradation was observed with no significant decrease in P62 levels observed after treatment with TXT (figure 4.6 A and B). LC3II levels are significantly increased after treatment with CPt and TXT with no change in LC3II observed after treatment with either CBDCA or 5-FU (figure 4.6) A and C. Acridine orange staining after the same treatment time shows an increase in acidic vesicle quantity after treatment with CPt, 5-FU and TXT with higher drug concentrations (figure 4.7).

Western blotting of autophagy proteins in SCC4 cells shows no significant change in the levels of P62 after 24 h treatment (figure 4.8 A and B). LC3II levels of SCC 4 cells are increased after treatment with both CPt and TXT (figure 4.8 A and C). Further analysis by acridine orange staining at slightly increased drug concentrations shows that chemotherapeutic intervention in SCC4 cells does result in increased number of acidic vesicles (figure 4.9).

In TR146 cells 48 h treatment with chemotherapeutics resulted in no change in P62 or LC3II expression (figure 4.10), indicating no effect on autophagy. Staining with acridine orange shows a high basal level of acidic vesicles (figure 4.11) compared to other OSCC cell lines. After 48 h chemotherapeutic intervention, CPt, 5FU and TXT have no impact on the quantity of acidic vesicles, however treatment by CBDCA shows an increase in the quantity of acidic vesicles that occupy much of the cytosol. It is worth noting that treatment by TXT increases the quantity of puncta seen in the cells. These puncta are visible in both the green and red channels indicating a neutral pH, however without further staining, it is impossible to determine what vesicles are being stained.

DOK cells show a time-dependant switch for autophagy induction (figure 4.12). At 24 h all chemotherapeutics decrease both LC3II and P62 levels except for treatment with TXT which demonstrates no significant decrease in P62 levels (figure 4.12 B). These proteins return to normal levels after 48 h of treatment. This was not the case for Ca9-22 cells and TR146 cells (data not shown). Acridine orange staining after 48 h verifies that chemotherapeutic intervention causes no change number of acidic vesicles in DOK cells after 48 h (figure 4.13).

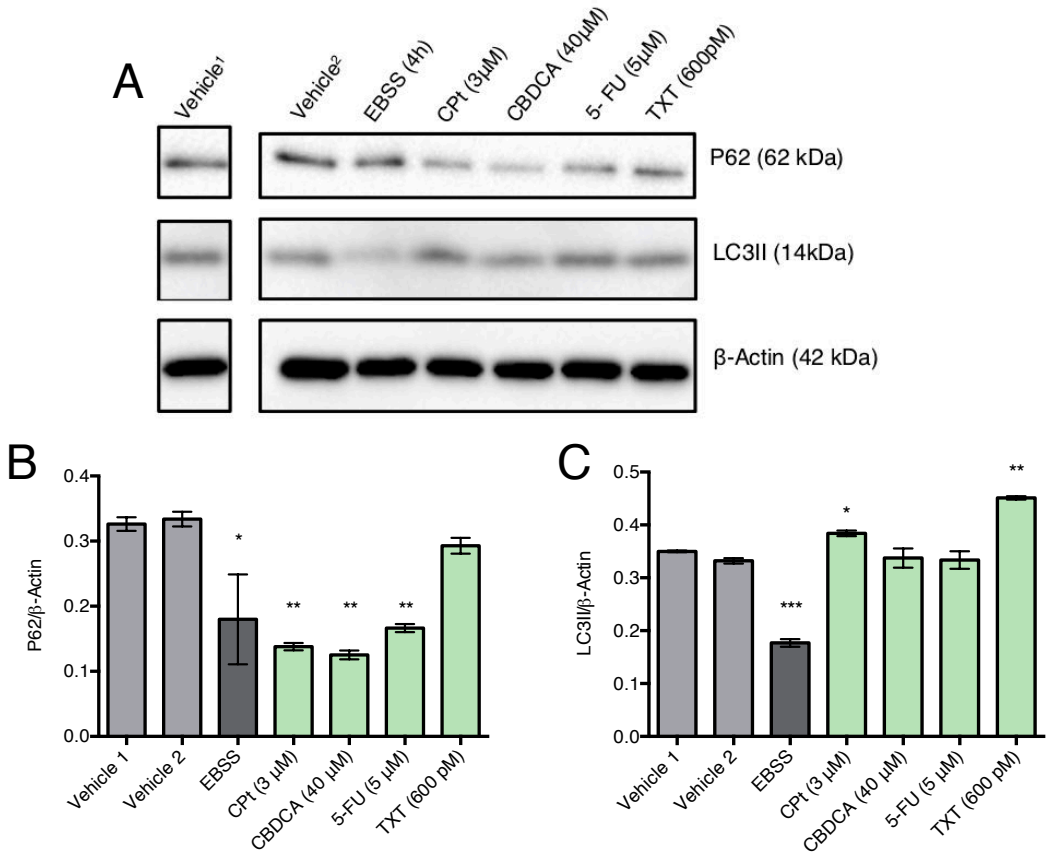

Figure 4.6. Treatment with Cpt, CBDCA or 5FU decrease levels of P62 while CPt and TXT increase LC3II in Ca9-22 cells.

Ca9-22 cells were treated with EBSS for 4 h or CPt (3 μM), CBDCA (40 μM), 5FU (5 μM), or TXT for 24 h before being lysed in RIPA buffer. Lysates (20 μg) were resolved by SDS-PAGE on a 15% gel, followed by transfer onto PVDF membrane. The membranes were then probed with anti-P62, anti-LC3B and anti-ß-actin antibodies and visualised using a gel documentation system (Biorad) and enhanced chemiluminescent HRP substrate (Millipore). Experiments were repeated on three individual occasions to ensure reproducibility. (A) Representative blot of LC3II and P62 expression in Ca9-22 cells. Densitometry was carried out on P62 (B) and L3II (C) by calculating relative intensity to ß-Actin control. Densitometry statistics carried out by one-way ANOVA with Dunnett's post-hoc analysis. Data shown n=3; *$p<0.05$, **$p<0.01$, ***$p<0.001$.
Vehicle[1]: Ca9-22 cells treated for 24h with 1% deionised H_2O (vehicle control for CPt and CBDCA). Vehicle[2]: Ca9-22 cells treated for 24h with 1% EtOH (vehicle control for 5-FU and TXT).

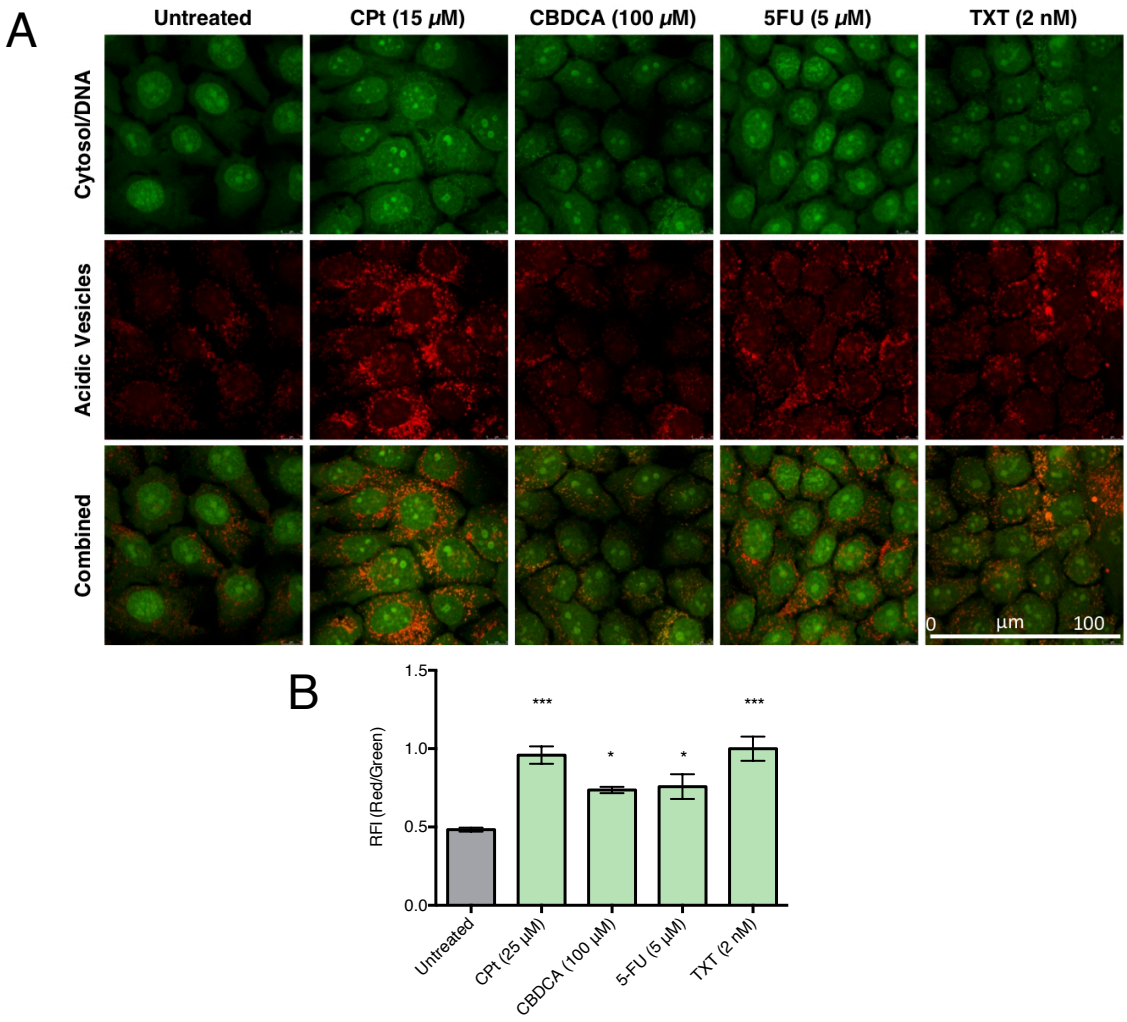

Figure 4.7. CPt, 5-FU and TXT produce an apparent increase in the formation of acidic vesicles in Ca9-22 cells.

Ca9-22 cells were treated 24 h with CPt (15 μM,), CBDCA (100 μM), 5-FU (5 μM) or TXT (2 nM). Acridine orange (1 μg/mL) was added 15 min before experiments. Images were captured using a Leica SP8 scanning confocal microscope and Leica Application Suite X software. An OPSL 488 nm laser provided excitation and emission was set at a range of 500 – 575 nm in the green channel and a range of 625 – 725 nm in the red channel. Cells were viewed at 3x magnification. (A) Representative images of three individual experiments showing acridine orange staining carried out in Ca9-22 cells. (B) Relative fluorescent intensity of red to green staining. Statistical analysis carried about by one-way ANOVA with Dunnett's post-hoc analysis. Data shown as n=3 ± SEM, *$p<0.05$, ***$p<0.001$.

Scale bar 100 μm.

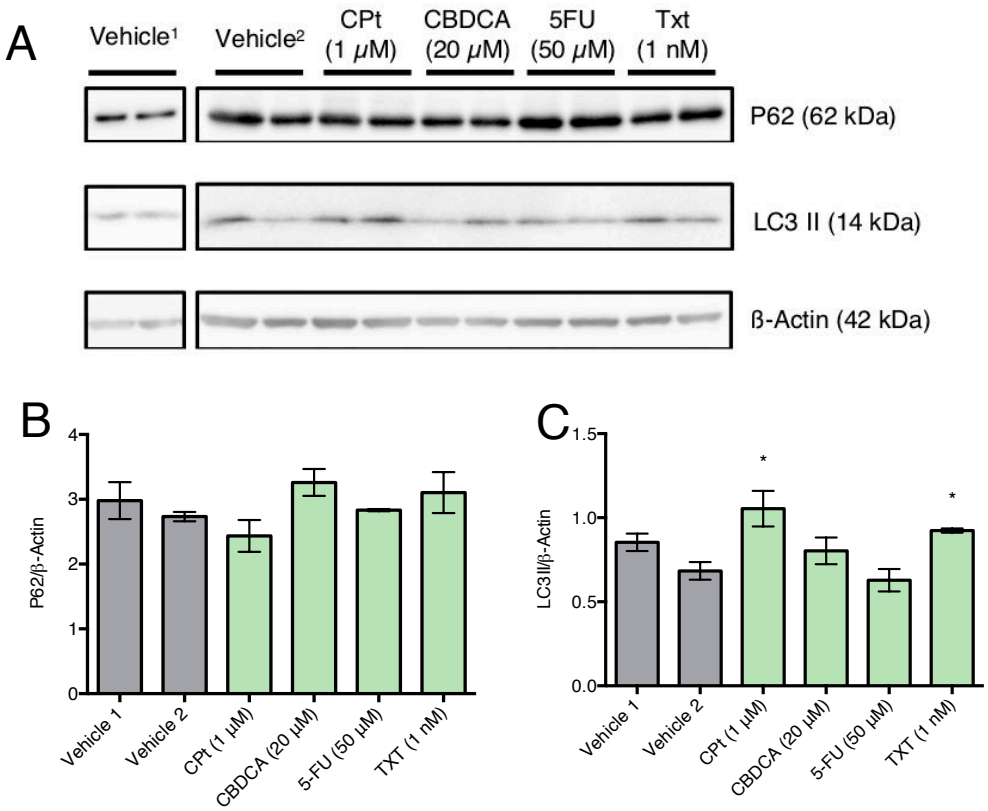

Figure 4.8. CPt and TXT increase levels of LC3II protein in SCC4 cells.

SCC4 cells were treated with CPt (1 μM), CBDCA (20 μM), 5FU (50 μM) or TXT (1 nM) for 24 h before being lysed in RIPA buffer. Lysates (20 μg) were resolved by SDS-PAGE on a 15% gel, followed by transfer onto PVDF membrane. The membranes were then probed with anti-P62, anti-LC3B and anti-ß-actin antibodies and visualised using a gel documentation system (Biorad) and enhanced chemiluminescent HRP substrate (millipore). Experiments were repeated on three individual occasions to ensure reproducibility. Western blot (A) presented as n=2 where each column represents a separate treatment occasion. Densitometry was carried out on P62 (B) and L3II (C) by calculating relative intensity to ß-Actin control. Densitometry statistics carried out by one-way ANOVA with Dunnett's post-hoc analysis. Data shown n=3; *$p<0.05$.

Sham[1]: SCC4 cells treated for 24h with 1% deionised H_2O (vehicle control for CPt and CBDCA). Sham[2]: SCC4 cells treated for 24h with 1% EtOH (vehicle control for 5-FU and TXT).

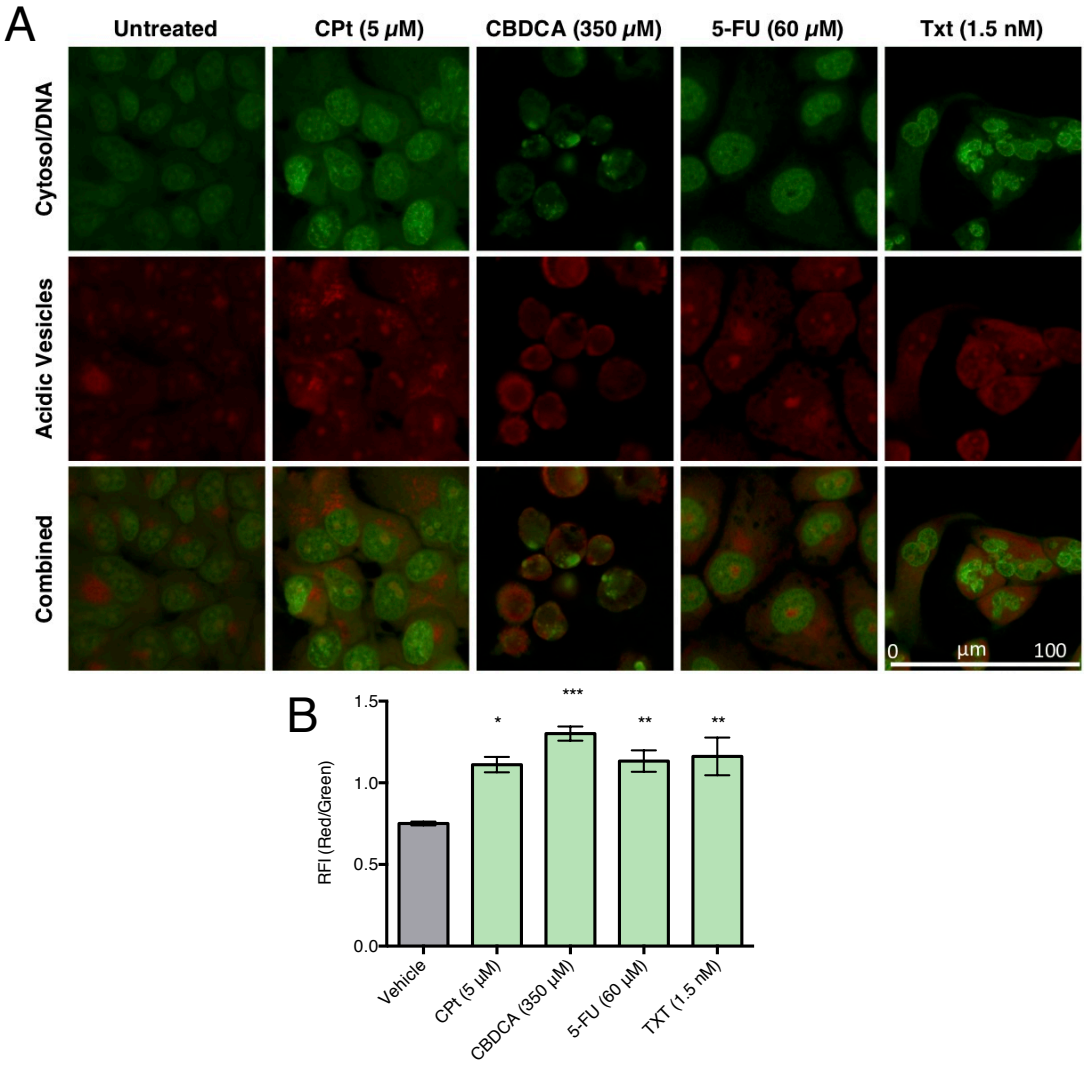

Figure 4.9. Treatment with chemotherapeutics produced an apparent increase in the formation of acidic vesicles in SCC4 cells.

SCC4 cells were treated with Cpt (5 μM), CBDCA (350 μM), 5-FU (60 μM) or Txt (1.5 nM) for 24 h. Acridine orange (1 μg/mL) was added 15 min before experiments. Images were captured using a Leica SP8 scanning confocal microscope and Leica Application Suite X software. An OPSL 488 nm laser provided excitation and emission was set at a range of 500 – 575 nm in the green channel and a range of 625 – 725 nm in the red channel. Cells were viewed at 3x magnification. A – Representative images of three individual experiments showing acridine orange staining carried out in SCC4 cells. B – Relative fluorescent intensity of red to green staining. Statistical analysis carried about by one-way ANOVA with Dunnett's post-hoc analysis. Data shown as n=3 ± SEM, *$p<0.05$, **$p<0.01$, ***$p<0.001$.

Scale bar 100 μm.

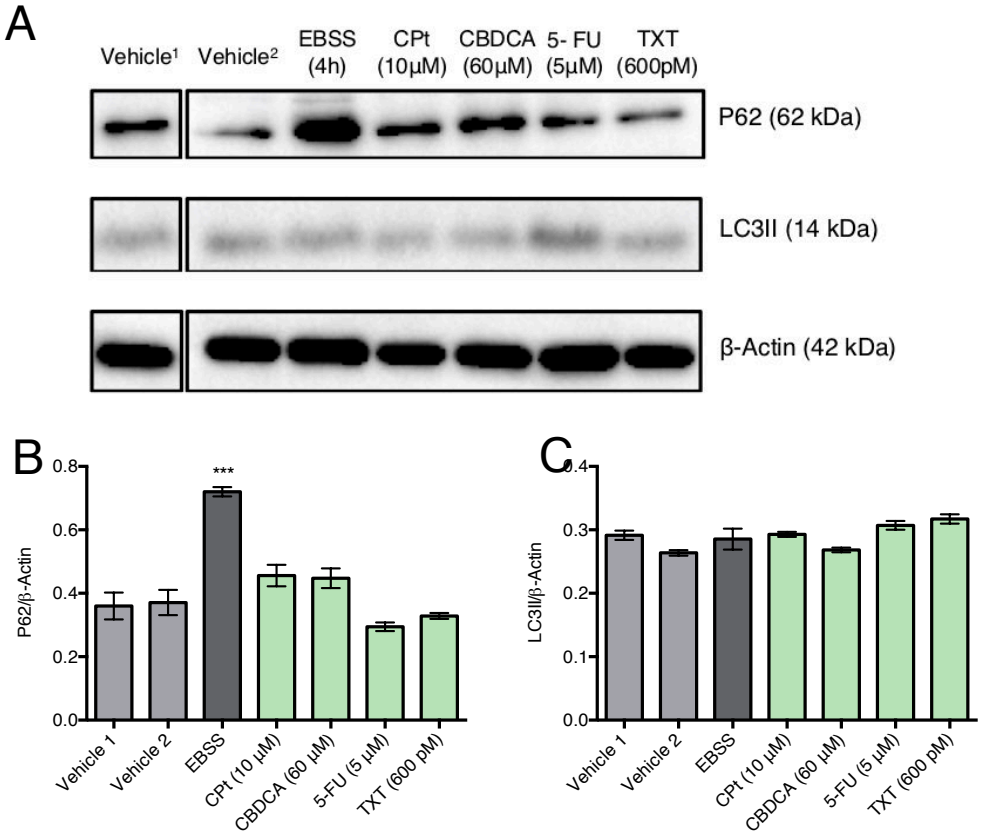

Figure 4.10. Treatment of TR146 cells with chemotherapeutics for 48 h resulted in no significant alteration in LC3II or P62 levels.

TR146 cells were treated with EBSS for 4 h or CPt (10 μM), CBDCA (60 μM), 5FU (5 μM), or TXT (600 pM) for 48 h before being lysed in RIPA buffer. Lysates (10 - 20 μg) were resolved by SDS-PAGE on 15% gels, followed by transfer onto PVDF membrane. The membranes were then probed with anti-P62, anti-LC3B and anti-ß-actin antibodies and visualised using a gel documentation system (Biorad) and enhanced chemiluminescent HRP substrate (millipore). Experiments were repeated on three individual occasions to ensure reproducibility. (A) representative blot showing LC3II and P62 expression in TR146 cells. Densitometry was carried out on P62 (B) and L3II (C) by calculating relative intensity to ß-Actin control. Densitometry statistics carried out by one-way ANOVA with Dunnett's post-hoc analysis. Data shown n=3; ***$p<0.001$.

Vehicle[1]: TR146 cells treated for 24h with 1% deionised H_2O (vehicle control for CPt and CBDCA). Vehicle[2]: TR146 cells treated for 24h with 1% EtOH (vehicle control for 5-FU and TXT).

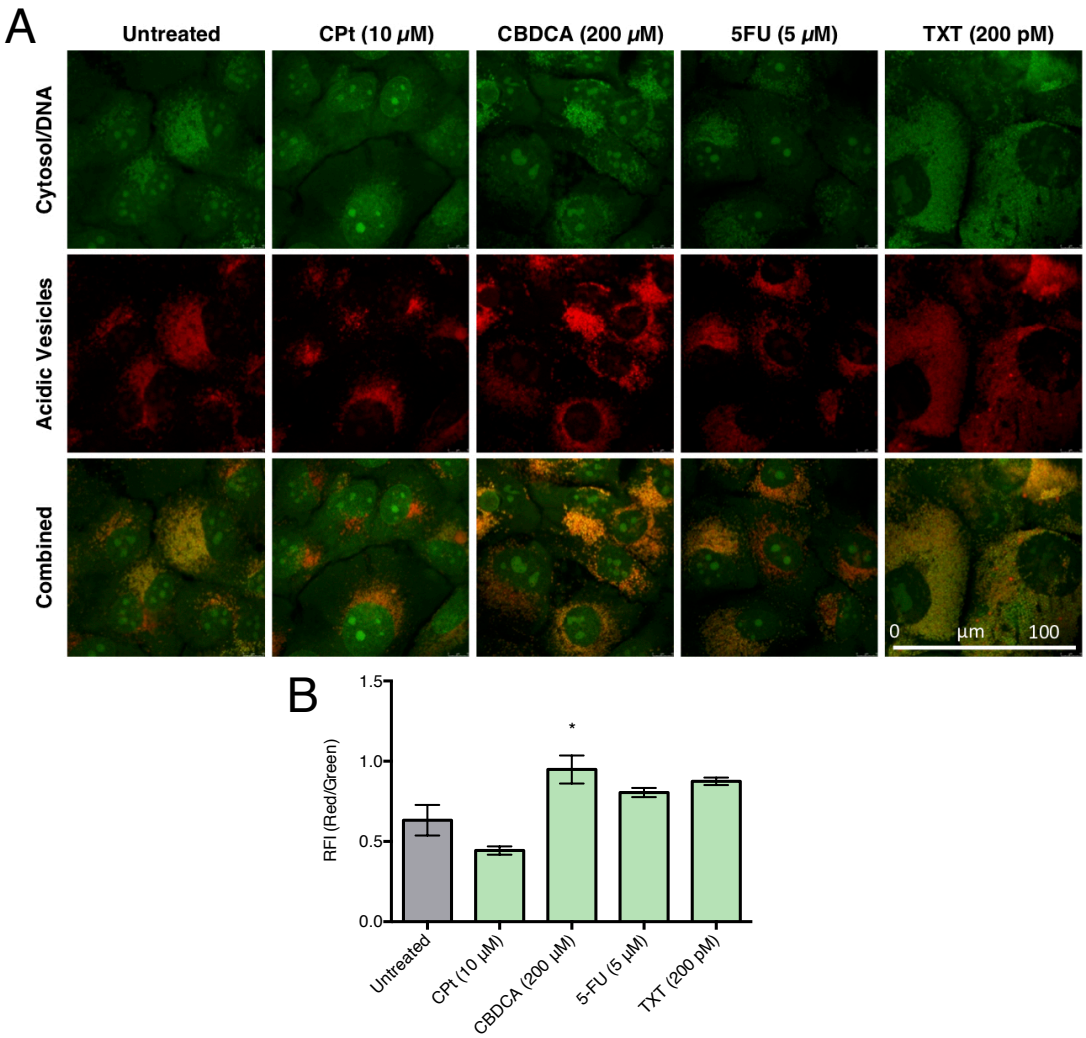

Figure 4.11. Treatment of TR146 cells with CBDCA resulted in a limited increase in the level of acidic vesicles.

TR146 cells were treated with Cpt (10 μM), CBDCA (200 μM), 5-FU (5 μM) or Txt (200 pM) for 48 h. Acridine orange (1 μg/mL) was added 15 min before experiments. Images were captured using a Leica SP8 scanning confocal microscope and Leica Application Suite X software. An OPSL 488 nm laser provided excitation and emission was set at a range of 500 – 575 nm in the green channel and a range of 625 – 725 nm in the red channel. Cells were viewed at 3x magnification. (A) Representative images of three individual experiments showing acridine orange staining carried out in TR146 cells. (B) Relative fluorescent intensity of red to green staining. Statistical analysis carried about by one-way ANOVA with Dunnett's post-hoc analysis. Data shown as n=3 ± SEM, *$p<0.05$.
Scale bar 100 μm.

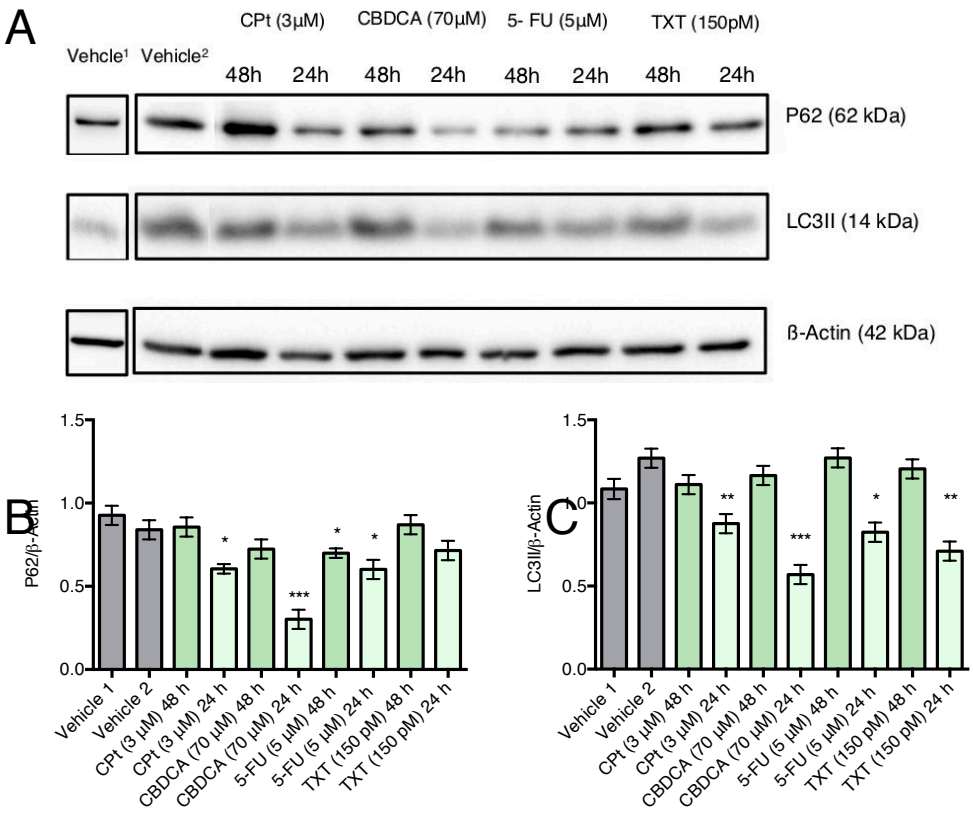

Figure 4.12. Levels of P62 and LC3II decrease after treatment with chemotherapeutics for 24 h in DOK cells.

DOK cells were treated with CPt (3μM), CBDCA (70 μM), 5FU (5 μM) or TXT (150 pM) for 24 h and 48 h before being lysed in RIPA buffer. Lysates (20 μg) were resolved by SDS-PAGE on a 15% gel, followed by transfer onto PVDF membrane. The membranes were then probed with anti-P62, anti-LC3B and anti-ß-actin antibodies and visualised using a gel documentation system (Biorad) and enhanced chemiluminescent HRP substrate (millipore). Experiments were repeated on three individual occasions to ensure reproducibility. (A) Representative blot demonstrating LC3II and P62 expression in DOK cells. Densitometry was carried out on P62 (B) and CL3II (C) by calculating relative intensity to ß-Actin control. Densitometry statistics carried out by one-way ANOVA with Dunnett's post-hoc analysis. Data shown n=3; *$p<0.05$, **$p<0.01$, ***$p<0.001$.

Vehicle[1]: DOK cells treated for 48h with 1% deionised H_2O (vehicle control for CPt and CBDCA). Vehicle[2]: DOK cells treated for 48h with 1% EtOH (vehicle control for 5-FU and TXT).

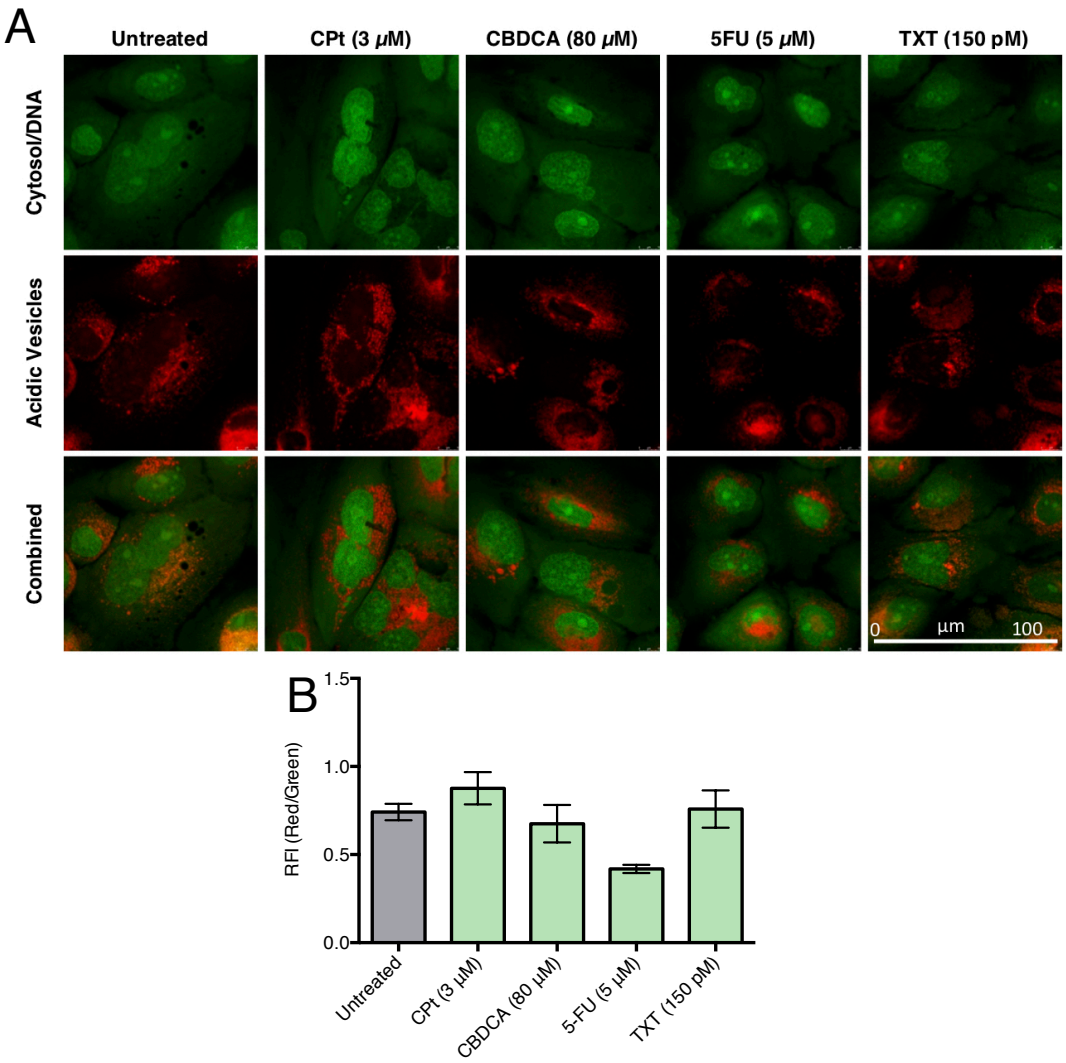

Figure 4.13. Treatment of DOK cells with chemotherapeutics has no effect on the quantity of acidic vesicles after 48 h treatment.

DOK cells were treated with CPt (3 μM), CBDCA (80 μM), 5FU (5 μM) or TXT (150 pM) for 48 h. Acridine orange (1 μg/mL) was added 15 min before experiments. Images were captured using a Leica SP8 scanning confocal microscope and Leica Application Suite X software. An OPSL 488 nm laser provided excitation and emission was set at a range of 500 – 575 nm in the green channel and a range of 625 – 725 nm in the red channel. Cells were viewed at 3x magnification. (A) Representative images of three individual experiments showing acridine orange staining carried out in DOK cells. (B) Relative fluorescent intensity of red to green staining. Statistical analysis carried about by one-way ANOVA with Dunnett's post-hoc analysis. Data shown as n=3 ± SEM.
Scale bar 100 μm.

4.4 Discussion

Treatment for OSCC has remained relatively static for several decades with the use of chemotherapy (most commonly cisplatin, carboplatin, 5-flouroruacil and docetaxel) as an adjuvant therapy to radiotherapy and surgery as the gold standard treatment since the late 1980's[190, 191]. Despite the extensive use of chemotherapeutics as adjuvant treatments in OSCC, there is still relatively little research conducted into the effects of these compounds on other cellular functions and their toxicities in commonly used oral cell lines. Most research into chemotherapeutic treatment has focused on its effect on cellular metabolism allowing insights into CPt treatment in the hypoxic tumour environment where it was shown to have a lower efficacy in HSC-2. This was linked to an upregulation of the glucose transporter protein -1 (GLUT-1) during hypoxia[192]. Over the last three years there has been a huge increase in research examining the effect of chemotherapeutics on autophagy in OSCC. CPt-resistance has been shown to be regulated by mitophagy in hypopharyngeal cancer cells[193]. Conversely it was discovered that overexpression of ceramide synthase 6 increases CPt-induced autophagy in CPt-resistant Cal-27 cells[194] highlighting the already-known double-edged sword of autophagy in cancer. 5-FU resistance has also been linked to autophagy where treatment with the PI3K inhibitor LY294004 increased the efficacy of 5-FU in oesophageal cancer cells[195]. There is currently no reference material on autophagy during treatment with CBDCA or TXT. For this reason, it is essential to understand autophagy modulation in conjunction with chemotherapeutic treatment in OSCC in order to fully

understand the mechanisms behind the efficacy of these compounds and potential role in chemoresistance.

Determining a repertoire of IC_{50} values for CPt, CBDCA, 5-FU and TXT in the pheno/genotypically distinct OSCC cell lines Ca9-22, SCC4 and TR146 along with the dysplastic DOK cell line is a novel beneficial addition to the field of OSCC research and will support future experiments given this is data that is not well documented or available over a range of time points. By analysing the variance in the IC_{50} values over several time points it is possible to get some insight into the potential mechanisms these compounds can elicit and how the cells respond to these insults.

In platinum-based drugs there is a clear time and dose-dependent response to therapy in all cell lines. This clearly demonstrates that prolonged exposure to the drugs results in increased cell death. It is useful to note, however, that chemotherapeutics causing direct DNA damage have a very high propensity for developing resistance through upregulation of DNA damage repair mechanisms[146] such as nucleotide excision repair (commonly damaged during testicular cancer[196]) and mismatch repair (mutations in this pathway are often found in Lynch Syndrome[197]). Variation in toxicity between chemotherapeutics is common and is thought to be driven largely through an individuals' genetic makeup[198, 199]. The platinum-based compounds demonstrate clear variations in toxicity between all four cell lines likely due to the individuality of the genetic profile of the donor the cells were derived from. This is an important factor to for a medical team to consider when treating

a patient and highlights the necessity for further understanding of the toxicity of these compounds across a variety cell lines.

5-FU displayed a decreased potency in both SCC4 and DOK cells compared to the Ca9-22 and TR146 cell lines. Similarly, TXT showed a time dependant decrease in the calculated IC_{50} value in the Ca9-22 and TR146 cell lines that was not observed in the SCC4 or DOK cells. This implies that the SCC4 and DOK cells have an increased defence to damage associated with RNA synthesis and DNA replication or are capable of limiting the intracellular drug concentration or drug-stabilizing effect on microtubules[200]. It is possible that these cells have heightened activity of detoxification enzymes such as glutathione-S-transferase (GST) or aldose reductase (AKR1B1). A successful clinical trial demonstrated that inhibition of GST improved treatment of patients with chronic lymphocytic leukemia[201] implying that heightened GST activity can make treatment more challenging. Similarly, AKR1B1 has been shown to increase chemoresistance to both doxorubicin and cisplatin in HeLa cells[202].

SCC4 cells, with a functional mutation in *P53,* (in this instance the mutation results in its over-expression of the protein) are most susceptible to the platinum-based DNA damaging agents. Ca9-22 cells, possessing *mTP53* (mutant P53, see section 1.4.1) have a high sensitivity to CPt and CBDCA, whereas TR146 (normal *P53*) and DOK (normal *P53*) show the lowest response. This is inconsistent with the literature where wild type *P53* has been shown to increase sensitivity to chemotherapeutic agents[203]. This is still true when looking at 5-FU and

TXT, where TR146 cells have the highest sensitivity to both chemotherapeutics. P53's role as a tumour suppressor acts to regulate the cell cycle by inducing cell cycle arrest at the G_1 checkpoint to allow for repair of double strand breaks and at the G2/M checkpoint to allow for repair of damaged cells prior to mitosis. The interesting aspect of the *P53*-mediated response to the chemotherapeutics used in this study is how the *mTP53*-containing Ca9-22 cells do not display the greatest sensitivity to any of the drugs. It would be expected that the lack of functioning *P53* would lead to increased DNA damage due to the loss of its protective mechanisms, however this is not the case. In fact, mutations to *P53* are associated with a lack of response to chemotherapy in head and neck cancer[204]. It has been documented repeatedly that *P53* status in head and neck cancer patients could be extremely important when it comes to predicting the outcome of both radiotherapy and chemotherapy[205, 206].

In Ca9-22 cells, a decrease in P62 was observed after treatment with CPt, CBDCA and 5-FU (figure 4.6) with elevated LC3II only seen in CPt and TXT. An increase in acidic vesicles is observed for all four chemotherapeutics albeit after treatment with a slightly higher concentration of each compound (figure 4.7). This increase in acidic vesicles mimics the LC3II levels seen at the lower dose where CBDCA and 5-FU have only a 52% and 57% respective increase in acidic vesicles compared to 98% and 107% increases in CPt and TXT respectively. P62 is not unique to autophagy, it is also essential for other processes such adipogenesis[207], NF-κB sigaling[208, 209], tumour necrosis factor receptor-associated factor 6 (TRAF6)[210], response to antioxidative stress[211], apoptotic caspase signalling[212] and nutrient sensing[158]. With all these

functions of P62 in mind, alterations in P62 levels in the absence of LC3 could be considered autophagy independent[213]. SCC4 cells demonstrated no P62 changes in response to treatment with any of the four chemotherapeutics (figure 4.8), however LC3II levels were increased under treatment with CPt and TXT similarly to Ca9-22 cell. In a similar manner to Ca9-22 cells, SCC4 cells in the presence of acridine orange demonstrated an increase in the quantity of acidic produced (figure 4.9) with CPt. CBDCA, 5-FU and TXT showed an increase of 48%, 73%, 51% and 55% respectively when compared to untreated cells. TR146 cells demonstrated no changes to P62 or LC3II levels under treatment with any of the four chemotherapeutics, however treatment with an increased concentration (200 μM rather than 60 μM) of CBDCA demonstrated a 50% increase in the quantity of acidic vesicles. The higher concentration in this instance was chosen intentionally in the hopes of driving autophagy despite knowing this concentration would result in a lower cell density. Some studies have identified that bulk-autophagy can be LC3-independent[214, 215]. In the event that chemotherapeutic treatment of these cells is causing widespread damage to cellular organelles bulk autophagy is likely, which may explain the lack of LC3 elevation with increased acidic vesicle production under specific treatments within these cell lines.

The switch noted in P62 and LC3II expression in DOK cells at 24 h and 48 h is a novel and interesting observation. This switch is not observed in experiments utilising Ca9-22, SCC4 or TR146 cells, suggesting this may be due to variations in the genetic or phenotypic make-up of these cells resulting in differing interactions with the therapeutics. Studies have

shown that cleavage of Atg5, a protein required for autophagosome formation, induces apoptosis[216]. Similarly, caspase 3, which activates apoptosis, is involved in the cleavage of multiple Atg proteins required for autophagic vesicle formation[217]. It is likely that induction of apoptosis is causing autophagy to be downregulated, facilitating the occurrence of autophagy and apoptosis to take place simultaneously for a limited duration as previously shown in colorectal carcinoma cells in association with ROS production[218] and also in breast cancer cells[219].

Qualitative observations from acridine orange staining, shows the variations in key vesicle formation rates between the different cell lines which may be interpreted as modulation in autophagy when taken in context with the observed fluctuations in LC3II. Both the TR146 and DOK cell lines show increased acidic vesicle staining compared to Ca9-22 or SCC4 cells. There is evidence that *P53* can activate the transcription of autophagy genes such as *Ulk1* and *Atg7*[220]. Similarly, one of *P53*'s targets is damage related autophagy modulator or *DRAM*, expression of which induces autophagy[221]. There is significant data to suggest that the wild-type status of *P53* in TR146 and DOK cells may indeed be contributing to the higher level of basal autophagy compared to Ca9-22 cells with mTP53, however SCC4 cells, with *P53* overexpression, would be expected to have a higher level of basal autophagy which is not observed. Another potential explanation is that DOK cells, with a pre-malignant phenotype, demonstrate a different autophagic response due to the lack of metabolic changes associated with tumour cells. A knockdown of *P53* in TR146 cells would be required to confirm this hypothesis.

These data indicate that chemotherapeutics may be having some impact on autophagic flux, however the extent of the effect is not clear. CPt treatment is the standard chemotherapeutic used in OSCC treatment and for this reason, its performance across the four cell lines was of particular interest. CPt demonstrated an apparent increase in autophagy in Ca9-22, SCC4 and DOK cells however it demonstrated no impact on autophagic proteins or acidic vesicle production in TR146 cells. The difference between Ca9-22 cells and TR146 cells in terms of response to CPt is worthy of further investigation due to the stark differences in P53 expression between the two cell lines .It was hypothesised that inhibition of autophagy may increase the efficacy of chemotherapeutics by preventing the autophagy-mediated cell survival mechanisms frequently employed by cancer cells[65]. Due to the increased acidic vesicle formation, increased LC3II and decreased P62 levels observed after CPt treatment in Ca9-22 cells, this hypothesis was tested in chapter 5 by focusing on CPt treatment under conditions of autophagy inhibition in Ca9-22 cells compared to TR146 cells (normal P53) and DOK cells (pre-cancerous with normal P53).

The data in this chapter highlights the stark differences in response to chemotherapeutic intervention in several OSCC cell lines and the pre-malignant DOK cell line. This data has not previously been characterised over a vast range of time points which is essential pharmacological data for future research in OSCC treatments. The data shown here indicate that CPt may not be as potent in cells containing LOF mutations in the *P53* gene while taxanes such as docetaxel have a higher potency in OSCC and pre-malignant cells. The cell lines chosen display distinct

genealogical differences in P53 expression highlighting the importance of considering mutations in the *P53* gene when choosing chemotherapy treatments in patients.

Chapter 5

Treatment of OSCC cells with chloroquine can increase the potency of cisplatin

5.1 Introduction

Autophagy is frequently induced by chemotherapeutic intervention in human cancer[137], however there is limited research into the impact of chemotherapy on autophagy in head and neck cancer or OSCC. Increasing evidence shows that inhibition of autophagy can improve the efficacy of chemotherapeutic intervention[187-189]. This increase in chemotherapeutic efficacy is often, but not always, linked to apoptotic cell death. The autophagic inhibition-linked increase in chemotherapeutic efficacy has been linked to ROS-mediated cell death[222], however, in most studies, the increased cell death is not linked to any particular PCD pathway or mechanism.

5.1.1 Links between autophagy and other types of programmed cell death

PCD is classified into three different categories: type I, apoptosis; type II, autophagy; and type III, necrosis. These pathways are characterised by easily recognisable phenotypes. Apoptosis is associated with membrane blebbing, membrane-bound apoptotic bodies, chromatic condensation and nuclear fragmentation. Autophagy (described in detail in Chapter 1 section 1.5) is characterised by the formation of the double-membraned autophagosomes and necrosis is identified by cellular and organelle swelling and rupture of the plasma membrane. These PCD pathways are often regulated by the same pathways and share many effector and initiator molecules[223].

Induction of apoptosis is commonly associated with caspase activation. Caspase 3 can cleave the cysteine protease Atg4D, which in turn cleaves LC3. It has been shown that overexpression of Atg4D can induce apoptosis. Atg4D-mediated cleavage of LC3 would prevent autophagic flux, indicating that inhibition of autophagy can induce apoptosis[224]. Caspases cleave Beclin1 and PI3K, both of which are involved in autophagy induction. BAX (a pro-apoptotic member of the Bcl-2 family) reduces autophagy levels by enhancing the caspase mediated cleavage of Beclin1[225]. Beclin1 can also drive apoptosis through its interaction with Bcl-2 resulting in the inhibition of Beclin1-mediated autophagy[226]. Bcl-2 expression can be decreased by P53 induction. P53 also induces the transcription of BAX implicating P53's role in both autophagy and apoptosis[227]. Another downstream action of P53 is to inhibit mTOR. This can occur through the activation of AMP kinase (AMPK)[228] or DRAM[221]. Inhibition of mTOR (a known method of autophagy induction) can both induce and inhibit apoptosis given its downstream targets such as P53 and Bcl-2 depending on the cellular conditions[229]. An additional protein associated with both apoptosis and autophagy is the death associated protein kinase, DAPK. DAPK is a calcium/calmodulin regulated serine/threonine kinase that mediates cell death via caspase activation and autophagy induction[230].

The crosstalk between autophagy and necrosis is more complicated and autophagy has been demonstrated to both promote and inhibit necrosis[231, 232]. Treatment of breast cancer cells with the small peptide caspase inhibitor, zVAD, was shown to induce necrosis[232]. A secondary function of zVAD is the inhibition of lysosomal cathepsin, which results

in the inhibition of autophagy. Additionally, autophagy inhibition via mTOR enhanced necrosis but during this process the induction of starvation was able to protect cells against zVAD-induced cell death[233]. Autophagy can also be initiated through AMPK signalling in response to ATP depletion via mTOR[234] or the Ulk1 complex[235]. During DNA damage, over activation of PARP1 (a nuclear enzyme involved in DNA repair and transcriptional regulation) can cause ATP depletion and induce necrosis while preventing energy-dependant apoptosis[236, 237]. Under these conditions, ATP depletion, followed by AMPK activation can lead to both induction of autophagy through mTOR inhibition and induction of necrosis allowing for simultaneous activation of both pathways.

5.1.2 The influence of autophagy on glycolysis.

Activation of autophagy results in an increase in glucose consumption and lactate production in hepatocellular carcinoma cells[176]. The opposite was also determined (by the same researchers) where inhibition of autophagy lead to a decrease in glucose consumption and decreased lactate production. The link between autophagy and glycolysis may seem obvious given that autophagy's main role is to provide nutrients and ATP in times of nutrient and energy deprivation, however, the exact mechanism through which autophagy influences glycolysis is not completely understood. The mTOR pathway has become the central focus of research when considering links between autophagy and glycolysis due to its role in regulating cellular functions including metabolism. In oesophageal SCC, the mTOR pathway has been shown to

regulate pyruvate kinase M2 (PKM2), the enzyme responsible for the conversion of phosphoenolpyruvate to pyruvate during glycolysis[238]. Findings showed that inhibition of mTOR led to a decrease in PKM2, which lead to an increase in glucose levels. This research implies a potential link between autophagy induction and glycolysis suppression. Watson *et al.* also showed in ovarian cancer cells that inhibition of glycolysis was regulated by suppression of mTORC1[239]. They confirmed that autophagy reduced proliferation and glycolytic metabolism in acute myeloid leukaemia. Hexokinase (HKII; the enzyme that catalyses glucose to glucose-6-phosphate) and LDH (involved in the maintenance of glycolysis by the regeneration of NADH from NAD^+) are key enzymes in glucose metabolism. Activation of mTOR can stimulate HIF1α and induce expression of both HKII and LDH[240]. HKII is degraded in an autophagy-dependant manner in liver cancer cells[241], once again tying autophagy induction to glycolysis suppression.

5.1.3 Interplay between autophagy and oxidative stress

Oxidative stress is closely linked to autophagy. ROS production from oxidative stress can induce autophagy under conditions of nutrient deprivation as demonstrated on numerous occasions[242]. Although mitophagy is a particular type of autophagy, concerned with the selective removal of damaged mitochondria[243], there are still links between oxidative stress and autophagy. ROS-mediated autophagy induction is driven predominantly by mitochondrial ROS production[244], with superoxide (O^-) as the major contributor[245].

ROS accumulation can result in cellular damage that activates necrosis, apoptosis and autophagy via the protein kinase d (PKD)/DAPK pathway. PKD is a serine/threonine kinase that is involved in cell motility, cell death and cell proliferation[246]. In conditions of oxidative stress, PKD phosphorylates VSP34, which promotes autophagosomal formation[247]. DAPK is also activated by oxidative stress and can induce autophagy by both releasing Beclin1 from Bcl-X_L[248] and the phosphorylation of PDK[249]. As PDK is located downstream of DAPK, activation of both is necessary for induction of autophagy under an oxidative stress environment. Mitochondrial-bound HKII was shown to decrease ROS production in rat brain cortical neurons[250]. HKII is positively regulated by both Akt[251] and MDPK (myotonic dystrophy protein kinase)[252], which are both negative regulators of autophagy.

5.2 Aims of Chapter

This chapter examines the potential for autophagy to be used as a therapeutic target in OSCC with a secondary goal to understand the mechanism behind the relationship between chemotherapeutic efficacy and autophagy inhibitors whilst gaining a clearer insight into the link between autophagy and cellular metabolism. This was achieved through the following objectives:

1. **Determining the effect of chloroquine treatment on the efficacy of the chemotherapeutic drug, CPt, in OSCC cells.**

   Changes in the IC_{50} value of CPt will be observed through monitoring the cellular metabolic state utilising the Alamar Blue assay in several phenotypically distinct oral cell lines, Ca9-22, TR146 and DOK in the presence or absence of chloroquine.

2. **Identification of the cell death pathways perturbed due to the increased efficacy of CPt following treatment with chloroquine.**

   Western blotting of PARP cleavage alongside flow cytometric analysis of PI/AnnexinV will be used to determine changes in apoptotic activation alongside flow cytometric analysis of PI to examine modulations in the cell cycle. These techniques will be completed using Ca9-22, TR146 and DOK cells treated with CPt in the presence or absence of chloroquine.

3. **Investigation of the relationship between glycolysis, autophagy and CPt-mediated cell toxicity**

Seahorse analysis will be used to determine any variation in basal glycolysis, and glycolytic reserve in Ca9-22, TR146 and DOK cells treated with CPt in the presence or absence of chloroquine.

4. **Investigation into the relationship between mitochondrial function, autophagy and CPt-mediated cell toxicity**

   Seahorse metabolic analysis will be used to determine any variation in basal, maximum and spare respiratory capacity alongside flow cytometric analysis using TMRM and MTG to determine changes in mitochondrial polarisation in Ca9-22, TR146 and DOK cells treated with CPt in the presence or absence of chloroquine.

5.3 Results

5.3.1 Chloroquine can increase the potency of Cisplatin in OSCC cell lines

As CPt altered LC3II levels in both CPt and DOK cells, it was important to explore the potential benefit of combining CPt with CQ, a known inhibitor of autophagy with potential anti-tumour effects. Ca9-22, TR146 and DOK cells were treated with a titration of CPt combined with CQ at 50 μM after which proliferation measurements, as determined by the Alamar Blue assay would establish if co-treatment results in a change of the IC_{50} of CPt.

In Ca9-22 cells, CQ treatment had no significant impact on the IC_{50} of CPt after 24h treatment (figure 5.1). TR146 cells treated with CQ resulted in a highly significant reduction of the IC_{50} of CPt from 7.80 $\pm$ 0.62 μM to 0.07 $\pm$ 0.02 μM (figure 5.2). DOK cells displayed a significant reduction in the IC_{50} value of CPt after treatment with CQ with a 5-fold reduction from 13 $\pm$ 1.35 μM to 2.35 $\pm$ 0.97 μM.

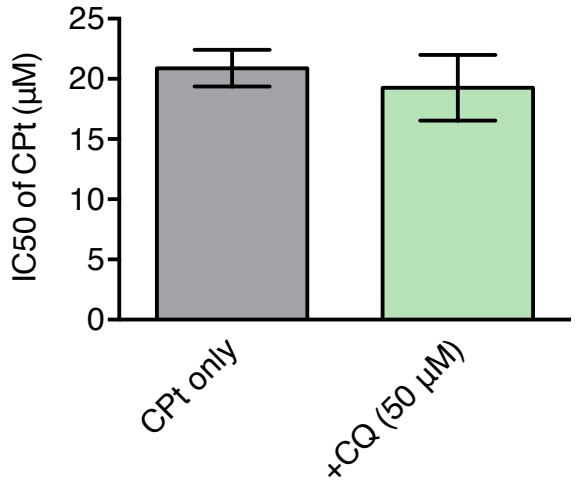

Figure 5.1. Treatment with CQ has no impact on the IC_{50} value of CPt in Ca9-22 cells

Ca9-22 cells were seeded at an appropriate density in a clear 96 well plate in starvation media (1%FBS) for 24 h and allowed to recover in full media (10% FBS) for a further 24 h prior to treatment with a range of concentrations of CPt for 24 h In the presence of CQ (50 μM). Alamar Blue reagent was added 4 h before the end point and absorbance values were read at λ=570 nm and λ=600 nm. Statistical analysis was carried out by students t-test using GraphPad Prism® v6. Data shown n=9 ± SEM. P>0.05.

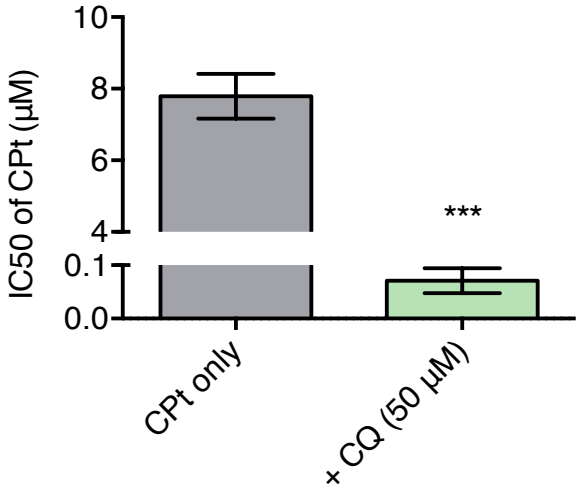

Figure 5.2. CQ lowers the IC_{50} value of CPt in TR146 cells

TR146 cells were seeded at an appropriate density in a clear 96 well plate in starvation media (1%FBS) for 24 h and allowed to recover in full media (10% FBS) for a further 24 h prior to being treated with a range of concentrations of CPt for 48 h in the presence or absence of CQ (50 μM). Alamar Blue reagent was added 4 h before the end point and absorbance values were read at λ=570 nm and λ=600 nm. Statistical analysis was carried out by students t-test using GraphPad Prism® v6. Data shown n=9 ± SEM. ***$p<0.001$.

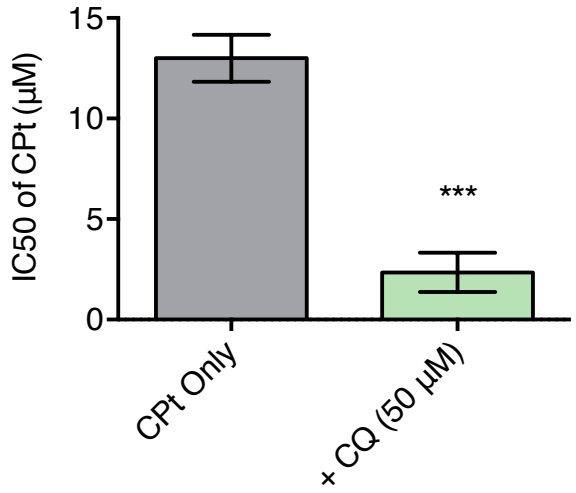

Figure 5.3. Treatment with CQ decreases the IC_{50} value of CPt of DOK cells.

DOK cells were seeded at an appropriate density in a clear 96 well plate in starvation media (1%FBS) for 24 h and allowed to recover in full media (10% FBS) for a further 24 h prior to being treated with a range of concentrations of CPt for 48 h in the presence or absence of CQ (50 μM). Alamar Blue reagent was added 4 h before the end point and absorbance values were read at λ=570 nm and λ=600 nm. Statistical analysis was carried out by students t-test using GraphPad Prism® v6. Data shown n=9 ± SEM. ***p<0.001.

5.3.2 Co-treatment with CPt and CQ increases the level of LC3II in OSCC cells.

To investigate the role of autophagy in CPt-mediated cell death during CQ treatment in Ca9-22, TR146 and DOK cells, western blotting was performed and changes in the levels of the autophagy marker proteins, P62 and LC3B, in cells treated with CPt in the presence or absence of CQ were determined.

Chapter 4 (section 4.3.4) demonstrated that CPt treatment with a concentration as low as 3 μM increases the levels of LC3II in Ca9-22 cells while decreasing levels of P62. CPt was also shown to have no effect on LC3II or P62 in TR146 cells while DOK cells displayed a decrease of LC3II alongside a decrease in P62.

Treatment of Ca9-22 cells with CPt (25 μM) showed an increase in the ratio of LC3II:LC3I. This increase can also be seen during co-treatment with CPt and CQ (50 μM) (Figure 5.4) however this increase in LC3II:LC3I was lower in co-treated cells compared to cells treated with CPt alone. Ca9-22 cells showed no variation in P62 levels after any of the treatments.

CQ (50 μM) treatment in TR146 cells after 48 h resulted in an increase in both the LC3II:LC3I ratio and P62 (Figure 5.5), however, when these cells were treated with both CPt (10 μM) and CQ, there was no significant difference in LC3II or P62 levels compared to treatment with CQ alone while treatment with CPt alone resulted in no change in autophagy protein levels compared to the vehicle control.

In DOK cells, the opposite response to P62 was observed to that of TR146 cells where although both CQ (50 μM) and co-treatment with CPt (15 μM) increase LC3II, P62 is only decreased under dual treatment after 48 h (Figure 5.6).

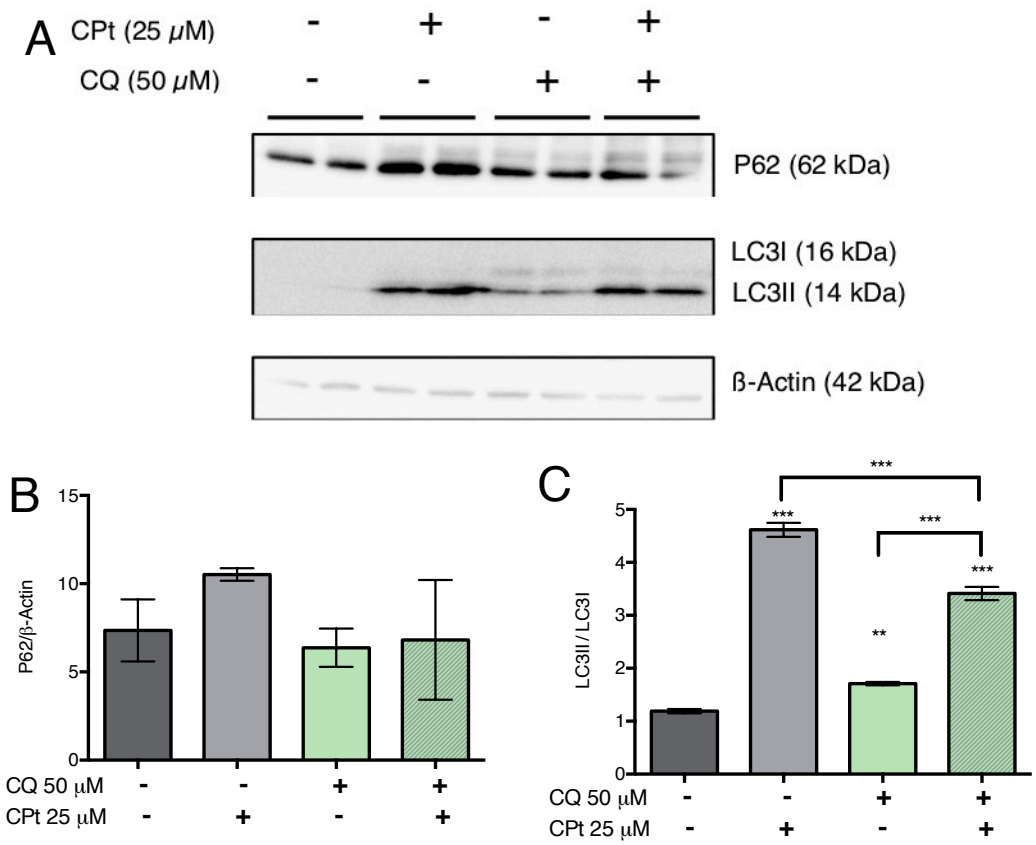

Figure 5.4. Co-treatment with CQ and CPt lowers the ratio of LC3I:LC3II in Ca9-22 cells compared to treatment with CPt alone.

Ca9-22 cells were treated with CPt (25 μM) for 24 h in the presence or absence of CQ (50 μM) or with a vehicle control (H_2O) before being lysed in RIPA buffer. Protein lysates (20 μg) were resolved by SDS-PAGE on a 15% gel, followed by transfer onto PVDF membrane. The membranes were then probed with anti-P62 and anti-LC3B antibodies and visualised using a gel documentation system (Biorad) and enhanced chemiluminescent HRP substrate (millipore). Experiments were repeated on three individual occasions to ensure reproducibility. (A) Western blot analysis with each column representing a separate treatment (n=2). Densitometry was carried out on P62 (B) and L3II (C) by normalising relative intensity to a ß-Actin control. Densitometry statistics carried out by one-way ANOVA with Dunnett's post-hoc analysis using GraphPad Prism® v6. Data shown n=3; **p<0.01, ***p<0.001.

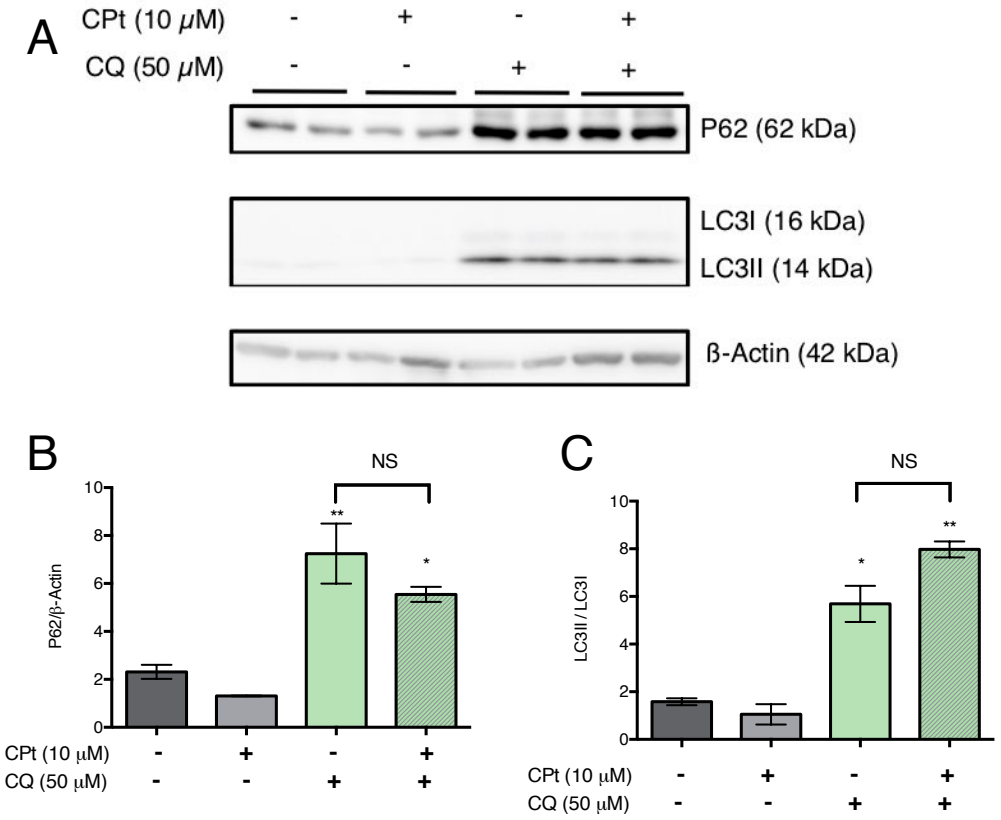

Figure 5.5. Treatment with CQ increases both P62 and LC3II levels in TR146 cells.

TR146 cells were treated with the IC_{50} of CPt for 48 h in the presence or absence of CQ (50 μM) or with a vehicle control (H_2O) before being lysed in RIPA buffer. Lysates (20 μg) were resolved by SDS-PAGE on a 15% gel, followed by transfer onto PVDF membrane. The membranes were then probed with anti-P62 and anti-LC3B antibodies and visualised using a gel documentation system (Biorad) and enhanced chemiluminescent HRP substrate (millipore). Experiments were repeated on three individual occasions to ensure reproducibility. A) Western blot analysis with each column representing a separate treatment (n=2). Densitometry was carried out on P62 (B) and L3II (C) by calculating relative intensity to ß-Actin control. Densitometry statistics carried out by one-way ANOVA with Dunnett's post-hoc analysis using GraphPad Prism® v6. Data shown n=3; **p<0.01, *p<0.05, NS = Not Significant.

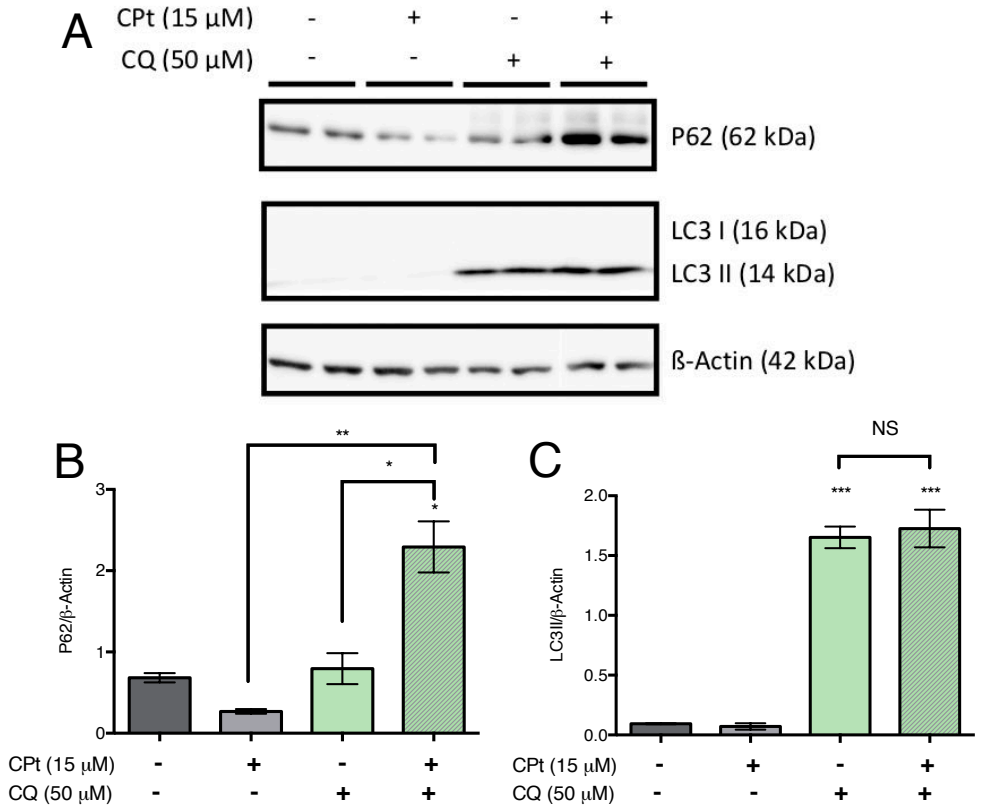

Figure 5.6. Co-treatment of DOK cells with CQ and Cpt increases both P62 and the LC3II:LC3I ratio, however treatment with CQ alone has no impact on P62 levels.

DOK cells were treated with the IC_{50} of CPt for 48 h in the presence or absence of CQ (50 μM) or with a vehicle control (H_2O) before being lysed in RIPA buffer. Lysates (20 μg) were resolved by SDS-PAGE on a 15% gel, followed by transfer onto PVDF membrane. The membranes were then probed with anti-P62 and anti-LC3B antibodies and visualised using a gel documentation system (Biorad) and enhanced chemiluminescent HRP substrate (millipore). Experiments were repeated on three individual occasions to ensure reproducibility. A) Western blot analysis with each column representing a separate treatment (n=2). Densitometry was carried out on P62 (B) and L3II (C) by calculating relative intensity to ß-Actin control. Densitometry statistics carried out by one-way ANOVA with Dunnett's post-hoc analysis using GraphPad Prism® v6. Data shown n=3; *p<0.05, **p<0.01, ***p<0.001.

5.3.3 Increased CPt-induced cell death by autophagy inhibition is PARP independent.

PARP cleavage is an apoptotic event that occurs down-stream of caspase activity. The intensity of PARP cleavage was determined by western blotting analysis of full-length PARP and the 28 kDa cleavage fragment. Ca9-22, TR146 and DOK cells were treated with CPt in the presence or absence of CQ (50 μM) to ascertain if the increase in CPt-mediated cell death by autophagy inhibition was apoptotic.

Ca9-22 cells co-treated with CQ (50 μM) and CPt (25 μM) show no change in PARP cleavage when compared to cells treated with CPt alone after 24 h treatment (figure 5.7). The increase in cleaved PARP in co-treated cells compared to the vehicle control was not accompanied by the expected decrease in the full-length PARP.

TR146 cells do not undergo PARP cleavage in response to CPt (10 μM) exposure up to 48 h. Similarly, treatment with CQ (50 μM) results in no PARP cleavage in these cells (figure 5.8).

DOK cells display no difference in PARP cleavage when treated with both CPt (15 μM) and CQ (50 μM) (figure 5.9) when compared to cells treated with CPt alone. Similar to Ca9-22 cells, this was not accompanied by a corresponding decrease in full length PARP.

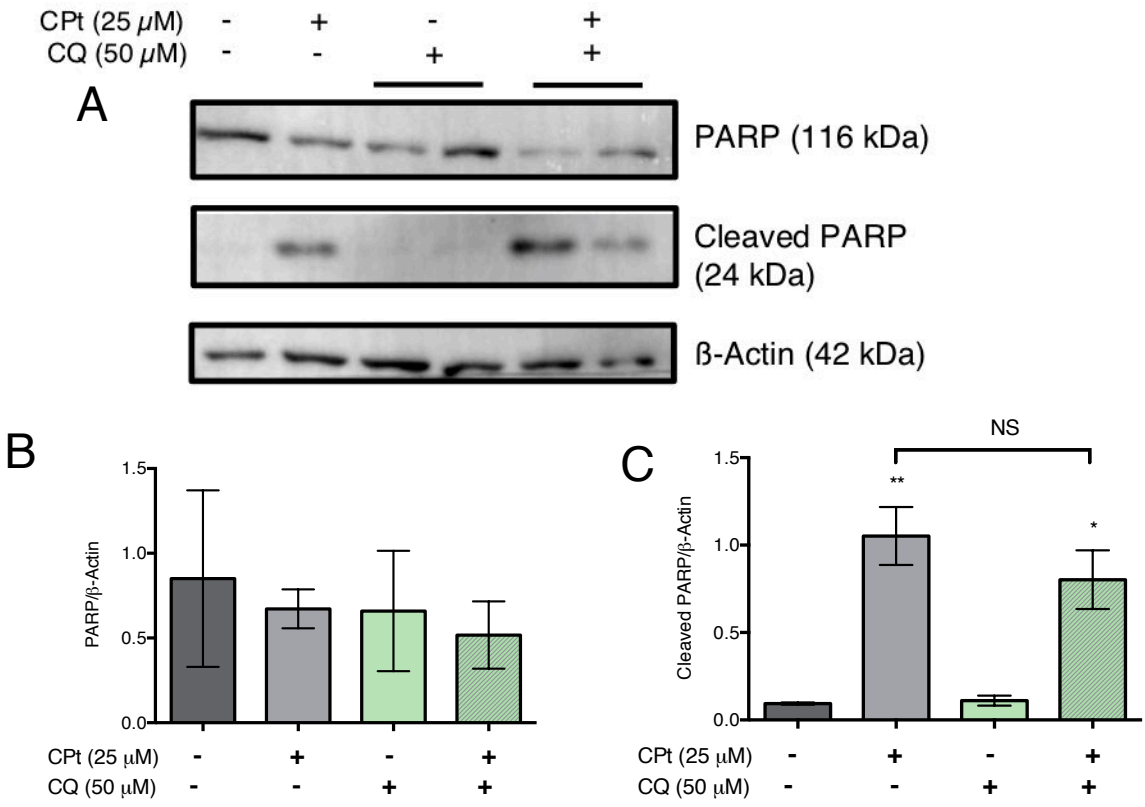

Figure 5.7. Dual treatment of Ca9-22 cells with CPt and autophagy inhibitors shows no increase in PARP cleavage compared to treatment with CPt alone.

Ca9-22 cells were treated with the IC_{50} of CPt for 24 h in the presence or absence of CQ (50 μM) or with a vehicle control (H_2O) before being lysed in RIPA buffer. Lysates (20 μg) were resolved by SDS-PAGE on a 10% gel, followed by transfer onto PVDF membrane. Membranes were then probed with anti-PARP and anti-ß-actin antibodies and visualised using a gel documentation system (Biorad) and enhanced chemiluminescent HRP substrate (millipore). Experiments were repeated on three individual occasions to confirm reproducibility. A) Western blot analysis with each column representing a separate treatment (n=2). Densitometry was carried out on PARP (B) and cleaved-PARP (C) by calculating relative intensity to ß-Actin control. Densitometry statistics carried out by one-way ANOVA with Dunnett's post-hoc analysis using GraphPad Prism® v6. Data shown n=3; *$p<0.05$, **$p<0.01$.

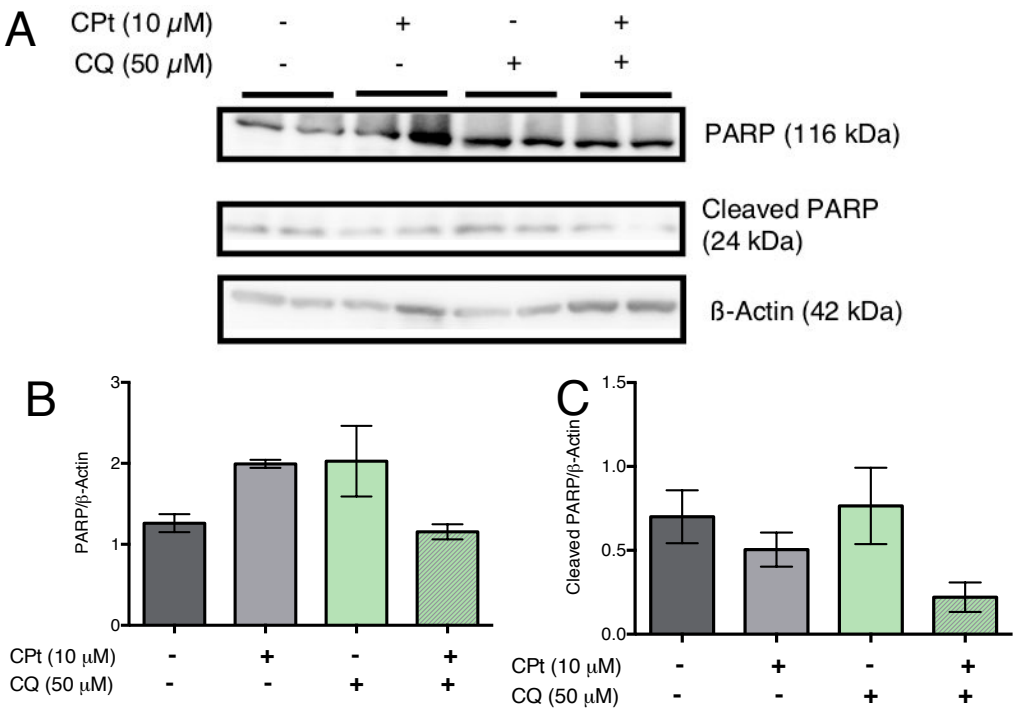

Figure 5.8. Dual treatment of TR146 cells with CPt and autophagy inhibitors shows no increase in PARP cleavage compared to treatment with CPt alone.

TR146 cells were treated with the IC_{50} of CPt for 48 h in the presence or absence of CQ (50 μM) or with a vehicle control (H_2O) before being lysed in RIPA buffer. Lysates (20 μg) were resolved by SDS-PAGE on a 10% gel, followed by transfer onto PVDF membrane. Membranes were then probed with anti-PARP and anti-ß-actin antibodies then visualised using a gel documentation system (Biorad) and enhanced chemiluminescent HRP substrate (millipore). Experiments were repeated on three individual occasions to confirm reproducibility. A) Western blot analysis with each column representing a separate treatment (n=2). Densitometry was carried out on PARP (B) and cleaved-PARP (C) by calculating relative intensity to ß-Actin control. Densitometry statistics carried out by one-way ANOVA with Dunnett's post-hoc analysis using GraphPad Prism® v6. Data shown n=3; *$p<0.05$, **$p<0.01$.

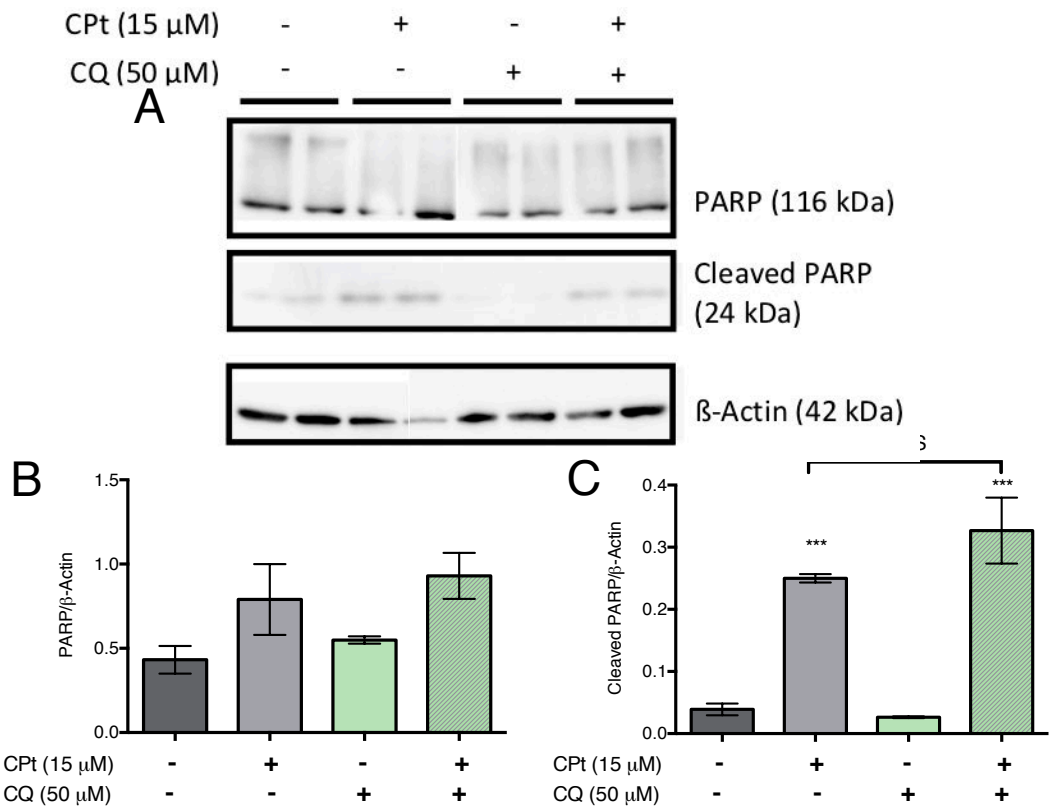

Figure 5.9. Co-treatment of DOK cells with CPt and autophagy inhibitors shows no increase in PARP cleavage compared to treatment with CPt alone.

DOK cells were treated with the IC_{50} of CPt for 48 h in the presence or absence of CQ (50 μM) or with a vehicle control (H_2O) before being lysed in RIPA buffer. Lysates (20 μg) were resolved by SDS-PAGE on a 10% gel, followed by transfer onto PVDF membrane. The membranes were then probed with anti-PARP and anti-ß-actin antibodies and visualised using a gel documentation system (Biorad) and enhanced chemiluminescent HRP substrate (millipore). Experiments were repeated on three individual occasions to ensure reproducibility. Data shown in western blot (A) is shown as n=2 where each column represents a separate treatment occasion. Densitometry was carried out on PARP (B) and cleaved-PARP (C) by calculating relative intensity to ß-Actin control. Densitometry statistics carried out by one-way ANOVA with Dunnett's post-hoc analysis. Data shown n=3; *$p<0.05$, **$p<0.01$.

5.3.4 Co-treatment with CPt and CQ targets different stages of apoptosis in a cell-line dependant manner.

Using flow cytometry, Annexin V and PI can be used to identify populations of cells in early apoptosis (stained with Annexin V only), late apoptosis (stained with both Annexin V and PI), and necrosis (stained with PI only). Ca9-22, TR146 and DOK cells were treated with CPt in the presence or absence of autophagy inhibitors to assess the effect of autophagy inhibition on CPt-mediated apoptosis and necrosis.

Annexin V/PI analysis of Ca9-22 cells treated with CPt (25 μM) for 24 h resulted in a decrease in the percentage of live cells (figure 5.10 A) and an increase in both early apoptotic (figure 5.10 B) and late apoptotic/necrotic cells (figure 5.10 C). Co-treatment with CPt and CQ (50 μM) resulted in significantly less live cells compared to treatment with CPt alone and this corresponds to a significant increase in cells undergoing late apoptosis/necrosis.

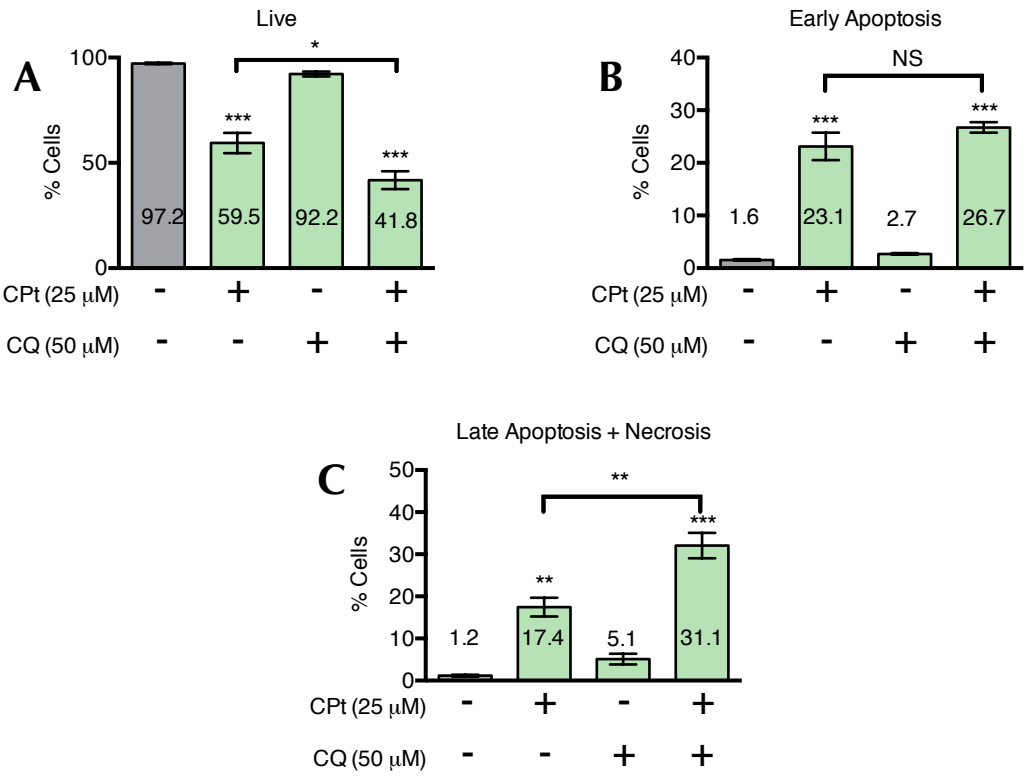

Figure 5.10. Dual treatment with CQ and CPt results in an increase in late apoptosis and necrosis compared to treatment with CPt alone in Ca9-22 cells.

Ca9-22 were serum starved for 24 h in 1% FBS and cultured for a further 24 h in full medium (10% FBS) prior to treatment with CPt (25 μM) in the presence or absence of CQ (50 μM) or with a vehicle control (H_2O) for 24 h. Whole cells were centrifuged at 600 g for 5 min at 4°C and resuspended in 100 µL Annexin V binding buffer, 5 µL PI (75 µM) and 5 µL FITCAnnexin V (BD Pharmingen). The Annexin V-FITC and PI were excited using a 488 nm laser in a BD Accuri C6 flow cytometer. Graphs shown as percentage of cells (A) live, (B) early apoptosis, (C) late apoptosis and necrosis for each population of cells. Data shown n=3 ± SEM. One-way ANOVA followed by Tukey's multiple comparisons test. ***p<0.001, **p<0.01, *p<0.05, NS=not significant.

Annexin V/PI analysis showed that CPt (10 μM) treatment for 48 h in TR146 cells had no effect on the levels of live cells (figure 5.11 A), early apoptotic cells (figures 5.12 B) or late apoptotic/necrotic cells (figure 5.11 C) after 48 h treatment.

Flow cytometric analysis of Annexin V/PI in TR146 cells treated with CQ (50 μM) demonstrates a decrease in the levels of live cells (figure 5.11 A) and a decrease in the levels of both early (figure 5.11 B) and late apoptosis/necrosis (figure 5.11 C). Co-treatment with CQ and CPt resulted in a further decrease in the live cell population (figure 5.11A) and a further increase in cells undergoing both early and late apoptosis (figure 5.11 B-C).

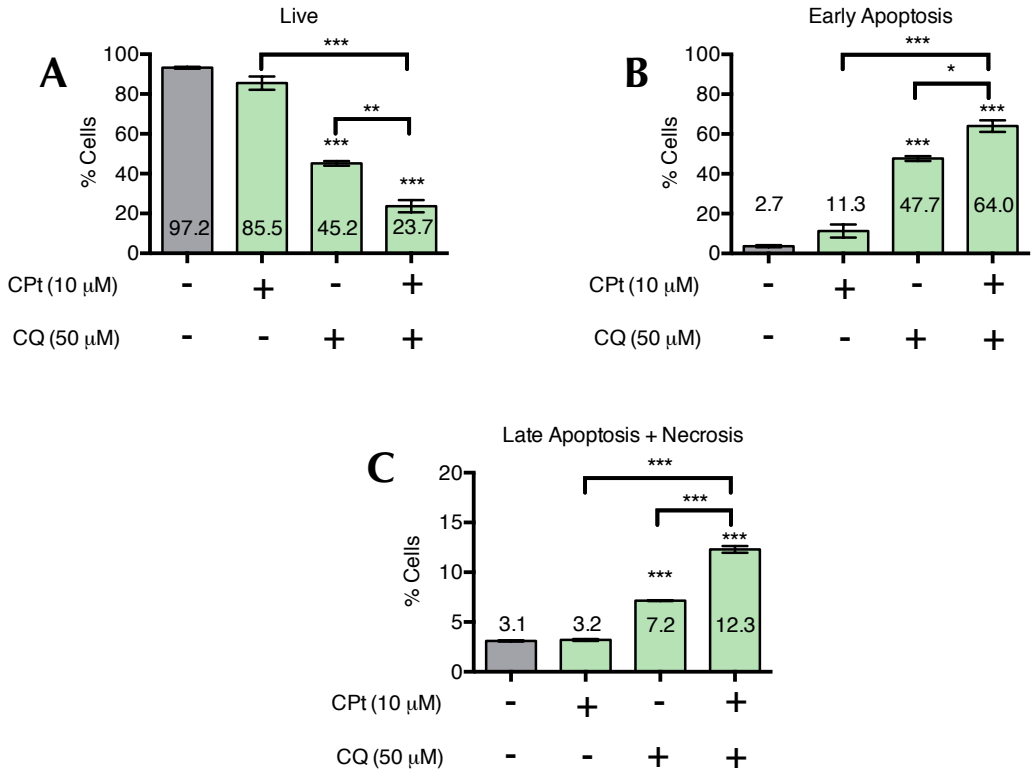

Figure 5.11. Co-treatment with CQ and CPt results in an increase in early and late apoptosis compared to treatment with CPt alone in TR146 cells.

TR146 were serum starved for 24 h in 1% FBS and cultured for a further 24 h in full medium (10% FBS) prior to treatment with CPt (10 μM) in the presence or absence of CQ (50 μM) or with a vehicle control (H_2O) for 48 h. Whole cells were centrifuged at 600 g for 5 min at 4°C and resuspended in 100 µL Annexin V binding buffer, 5 µL PI (75 µM) and 5 µL FITCAnnexin V (BD Pharmingen). The Annexin V-FITC and PI were excited using a 488 nm laser in a BD Accuri C6 flow cytometer. Graphs shown as percentage of cells (A) live, (B) early apoptosis, (C) late apoptosis and necrosis for each population of cells. Data shown n=3 ± SEM. One-way ANOVA followed by Tukey's multiple comparisons test. ***p<0.001, **p<0.01, *p<0.05.

In DOK cells, Annexin V/PI analysis shows no significant difference between cells treated with CPt (15 μM) and the vehicle control in the levels of live cells (figure 5.12 A), early apoptotic cells (figures 5.12 B) or late apoptotic/necrotic cells (figures 5.12 C) after 48 h treatment.

Annexin V/PI analysis of dual treatment in DOK cells shows no significant difference between cells treated with both CPt and CQ (figure 5.12) when compared to cells treated with either CPt or CQ alone.

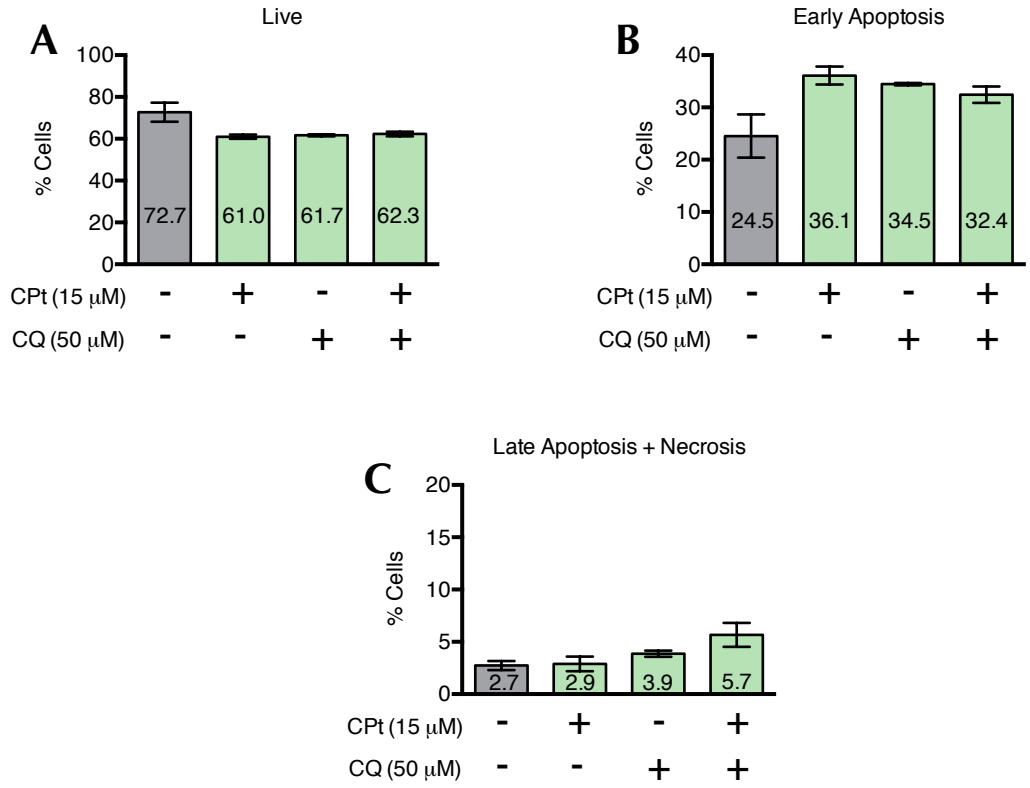

Figure 5.12. Co-treatment with CQ and/or CPt results in no increase in apoptosis after 48 h in DOK cells.

DOK were serum starved for 24 h in 1% FBS and cultured for a further 24 h in full media (10% FBS prior to treatment with CPt (15 μM) in the presence or absence of CQ (50 μM) or with a vehicle control (H_2O) for 48 h. Whole cells were centrifuged at 600 g for 5 min at 4^{o}C and resuspended in 100 µL Annexin V binding buffer, 5 µL PI (75 µM) and 5 µL FITCAnnexin V (BD Pharmingen). The Annexin V-FITC and PI were excited using a 488 nm laser in a BD Accuri C6 flow cytometer. Graphs shown as percentage of cells (A) live, (B) early apoptosis, (C) late apoptosis and necrosis for each population of cells. Data shown n=3 ± SEM. One-way ANOVA followed by Tukey's multiple comparisons test.

5.3.5 Inhibition of autophagy in combination with CPt treatment can increase the number of cells in the Sub G_0 phase of the cell cycle

As many chemotherapeutic agents disrupt the cell cycle, the role of autophagy was investigated as a potential mechanism through which this disruption results. Cell cycle alterations were measured through flow cytometric analysis of propidium iodide-stained DNA fragments in Ca9-22 and TR146 cells in the presence or absence of CQ (50 μM).

In Ca9-22 cells exposed to CPt (25 μM) treatment for 24 h, an insignificant increase in cells in the Sub G_0 phase of the cell cycle of 3.37 ± 0.26% compared to the vehicle control of 1.67 ± 0.26% (figure 5.13 A) was observed. CPt treatment alone displayed a decrease within the G_2/M phase of 13.73 ± 0.95% compared to the vehicle control of 27.10 ± 1.13% (figure 5.13 D). CPt can also induce cell cycle arrest at the G_0 and G_1 phase (figures 5.13 D). Autophagy inhibition by the late-stage inhibitor CQ alongside CPt treatment significantly increases cells in the Sub G_0 phase to 8.29 ± 1.00% (figure 5.13 A) compared to treatment with CPt alone with a corresponding decrease of cells at the G_2/M point of 13.63 ± 0.27% (figure 5.13D). This decrease at G_2/M is not significantly different to that of treatment with CPt alone.

In TR146 cells 48 h treatment with CPt (10 μM) significantly increased the percentage of cells in the Sub G_0 phase with 51.10 ± 2.14% compared to 7.51 ± 1.50% in the vehicle control (figure 5.14 A). CPt treatment also resulted in an increase of cells in the S phase with 12.43 ± 0.42 compared to 7.41 ±0.48% in the vehicle control (figure 5.14 C). These increases in the Sub G_0 and S phase correspond to decreases in cell numbers in at both

the G_0 and the G_1 phase (figure 5.14 B) and G_2/M (figure 5.14 D) points. CPt treatment results in 22.70 ± 0.41% cells at the G_0/G_1 peak compared to 66.75 ± 2.34% in cells treated with a vehicle control (figure 5.14 B). Cells treated with CPt also decreased the percentage of cells going through the G_2/M phases of the cell cycle to 10.07 ± 0.42% compared to 16.30 ± 0.17% in the vehicle control (figure 5.14 D). Co-treatment with CQ shows a similar pattern to treatment with CPt alone, however cells treated with both CPt and CQ have a much higher percentage of cells in the Sub G_0 phase at 64.97 ± 4.02% (figure 5.14 A). Co-treatment with CQ also results in a no change to cells in the S-phase unlike cells treated with CPt only (figure 5.14 C).

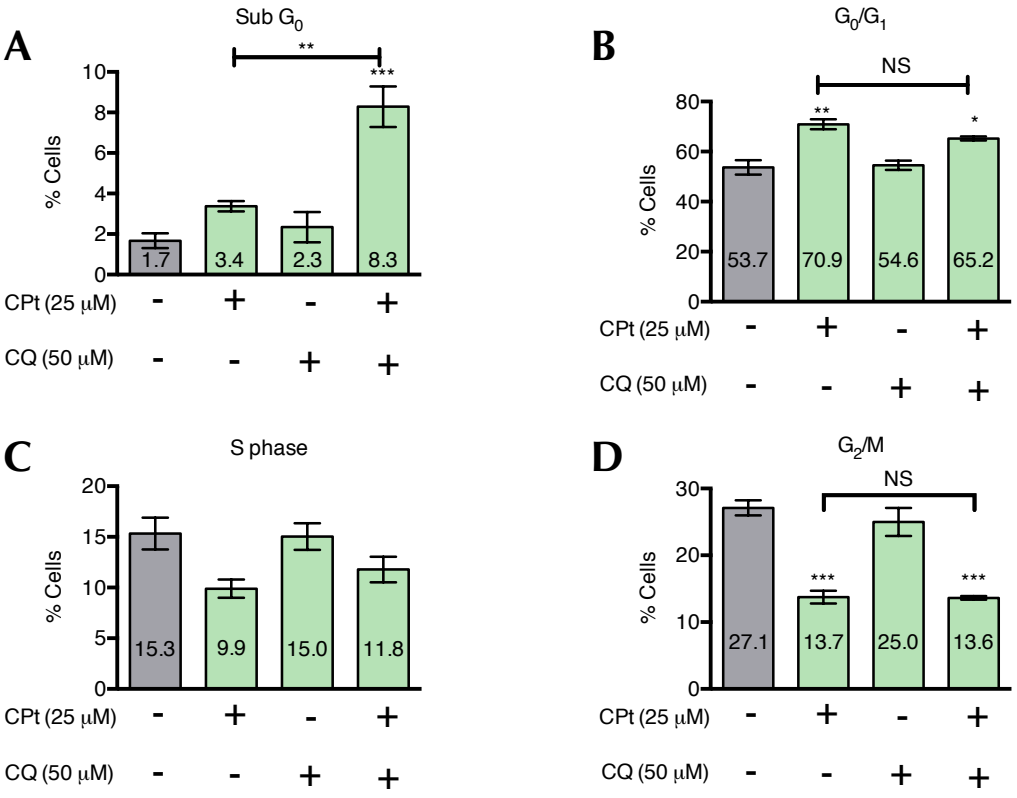

Figure 5.13. Co-treatment with CQ and CPt results in an increase in cells in the Sub G_0 phase of the cell cycle compared to treatment with CPt alone in Ca9-22 cells.

Ca9-22 were serum starved for 24 h in 1% FBS and cultured for a further 24 h in full medium (10% FBS) prior to treatment with CPt (25 μM) in the presence or absence of CQ (50 μM) or with a vehicle control (H_2O) for 24 h. Whole cells were then fixed in 100% EtOH and resuspended in PBS containing RNase (500 μg/mL) and PI (150 μg/mL). Graphs shown as percentage of cells in (A) Sub-G_0, (B) G_0/G_1, (C) S and (D) G_2/M phases of the cell cycle for each population of cells. Data shown n=3 ± SEM. One-way ANOVA followed by Dunnett's multiple comparisons test. ***p<0.001, **p<0.01, *p<0.05, NS=Not significant.

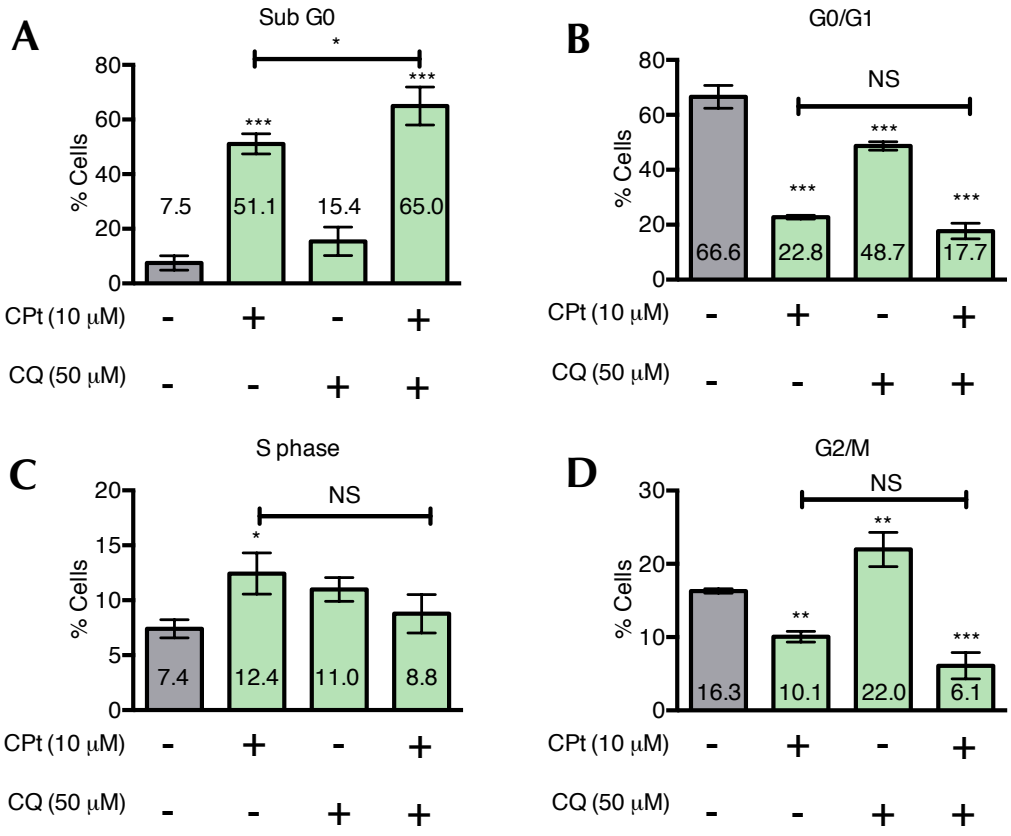

Figure 5.14. Co-treatment with CQ and CPt results in an increase in cells in the Sub G_0 phase of the cell cycle compared to treatment with CPt alone in TR146 cells.

TR146 were starved for 24 h in 1% FBS and grown for a further 24 h in full media (10% FBS) prior to treatment with CPt (10 μM) in the presence or absence of CQ (50 μM) or with a vehicle control (H_2O) for 48 h. Whole cells were then fixed in 100% EtOH and resuspended in PBS containing RNase (500 μg/mL) and PI (150 μg/mL). Graphs shown as percentage of cells in (A) Sub-G_0, (B) G_0/G_1, (C) S and (D) G_2/M phases of the cell cycle for each population of cells. Data shown n=3 ± SEM. One-way ANOVA followed by Dunnett's multiple comparisons test. ***p<0.001, **p<0.01, *p<0.05, NS=Not significant.

5.3.6 Treatment with CPt or CQ has no impact on basal glycolysis in OSCC cells.

To investigate if dual treatment with CPt and CQ can cause alterations to glycolytic metabolism, analysis of extracellular acidification rate (ECAR) by seahorse was carried out on Ca9-22, TR146 and DOK cells treated with CPt in the presence or absence CQ.

Treatment with either CPt (25 μM) or CQ (50 μM) after 8 h treatment in Ca9-22 cells has no impact on either basal glycolysis (figure 5.15 A) or glycolytic reserve (figure 5.15 B). A similar response was noted in TR146 cells where treatment with CPt (10 μM) or CQ (50 μM) had no effect on the basal levels of glycolysis (figure 5.16 A) or glycolytic reserve after 8 h treatment (figure 5.16 B).

DOK cells treated with either CPt (15 μM) or CQ (50 μM) showed no changed in basal levels of glycolysis after 8h treatment (figure 5.17 A), however treatment with either CPt, CQ or in combination decreased the glycolytic reserve (figure 5.17 B). Treatment with CPt decreased the glycolytic reserve to 64.30 $\pm$ 1.35 mpH/min compared to the vehicle control of 87.75 $\pm$ 1.95 mpH/min. CQ treatment reduced the glycolytic reserve to 76.25 $\pm$ 1.53 mpH/min while dual treatment reduced the glycolytic reserve to 66.79 $\pm$ 2.22 mpH/min, however there was no significant difference between dual treated cells and treatment with CPt alone.

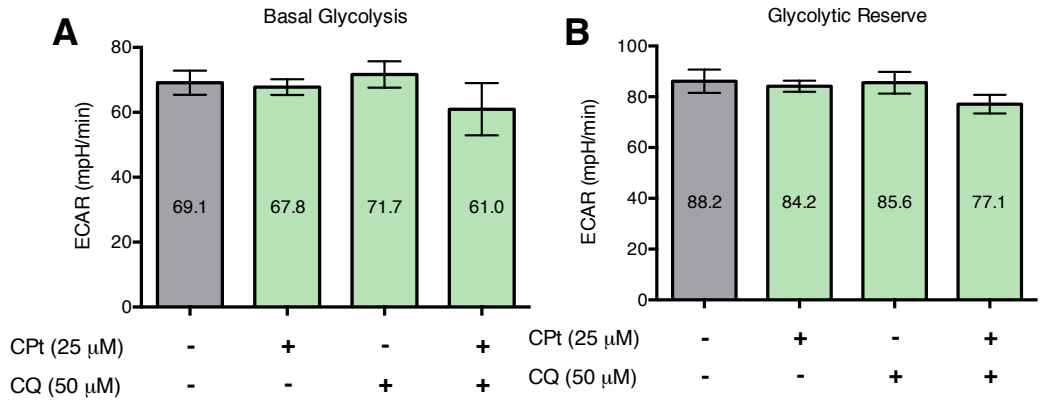

Figure 5.15. CPt and CQ have no impact on ECAR in Ca9-22 cells after 8 h treatment.

Ca9-22 cells were seeded in a 96 well seahorse plate at 20,000 cells per well and allowed to adhere before being treated with CPt (25 μM) in the presence or absence of CQ (50 μM) or with a vehicle control (H_2O) for 8 h. One hour before analysis, media was replaced by supplemented seahorse media and the plate was placed in a non-CO_2 incubator. The pre-hydrated inhibitor cartridge was loaded with the appropriate volume of various glycolytic and respiratory inhibitors and was calibrated in the Seahorse XF-96 extracellular flux analyser before the cell plate was analysed. (A) changes in basal glycolysis. (B) changes in glycolytic reserve with/without treatment. Data shown n=3 ± SEM, one-way ANOVA. P>0.05.

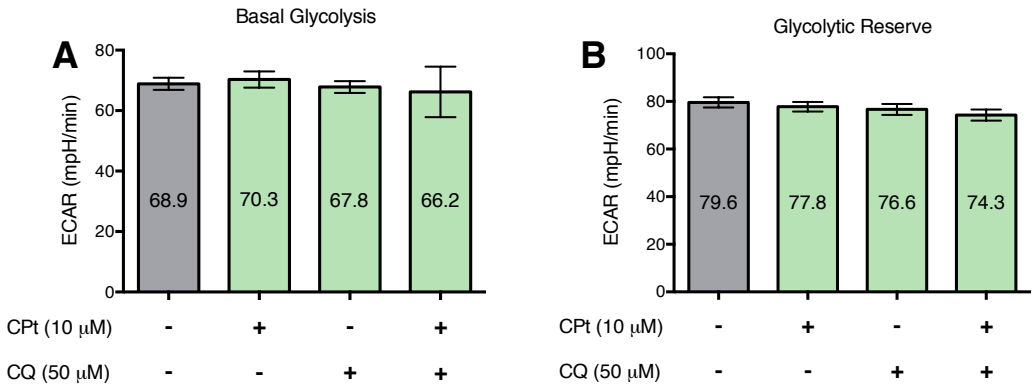

Figure 5.16. CPt and CQ have no effect on basal glycolysis or glycolytic reserve in TR146 cells after 8 h treatment

TR146 cells were seeded in a 96 well seahorse plate at 20,000 cells per well and allowed to adhere before being treated with CPt (10 μM) in the presence or absence of CQ (50 μM) or with a vehicle control (H_2O) for 8 h. One hour before analysis, media was replaced by supplemented seahorse media and the plate was placed in a non-CO_2 incubator. The pre-hydrated inhibitor cartridge was loaded with the appropriate volume of various glycolytic and respiratory inhibitors and was calibrated in the Seahorse XF-96 extracellular flux analyser before the cell plate was analysed. Figure A shows changes in basal glycolysis while figure B shows changes in glycolytic reserve with/without treatment. Data shown n=3 ± SEM, one-way ANOVA.

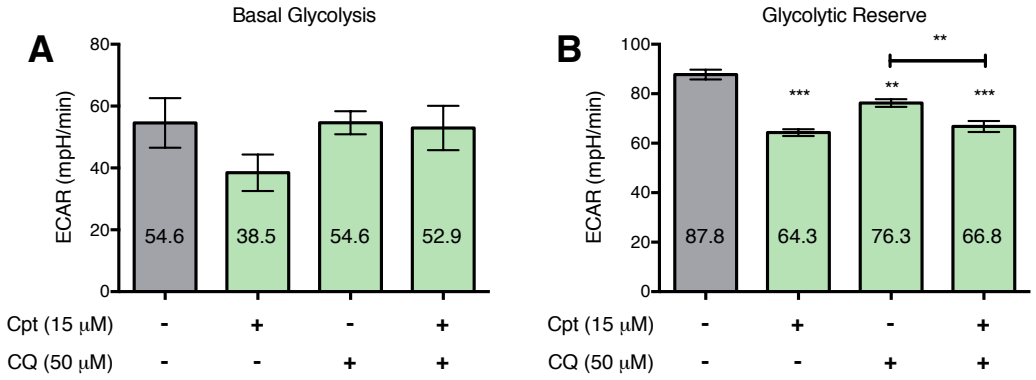

Figure 5.17. Glycolytic reserve is decreased in DOK cells after treatment with either CPt or CQ for 8 h.

DOK cells were seeded in a 96 well seahorse plate at 20,000 cells per well and allowed to adhere before being treated with CPt (15 μM) in the presence or absence of CQ (50 μM) or with a vehicle control (H_2O) for 8 h. One hour before analysis, media was replaced by supplemented seahorse media and the plate was placed in a non-CO_2 incubator. The pre-hydrated inhibitor cartridge was loaded with the appropriate volume of various glycolytic and respiratory inhibitors and was calibrated in the Seahorse XF-96 extracellular flux analyser before the cell plate was analysed. (A) changes in basal glycolysis. (B) changes in glycolytic reserve with/without treatment. Data shown n=3 ± SEM, one-way ANOVA, followed by Tukey's multiple comparisons test. ***$p<0.001$, **$p<0.01$.

5.3.7 Mitochondrial polarisation state and oxygen consumption rate are affected by autophagy inhibition during CPt treatment

Alterations in oxidative phosphorylation due to co-treatment with CPt and autophagy inhibition were examined by seahorse analysis of oxygen consumption rate (OCR). Mitochondrial polarisation was analysed using flow cytometric analysis of tetramethylrhodamine methyl ester (TMRM) normalised to mitotracker green (MTG) levels to account for variations in mitochondrial numbers. Experiments were completed on Ca9-22, TR146 and DOK cells treated with CPt in the presence or absence of CQ (50 μM).

Ca9-22 cells treated with CPt (25 μM) for 8 h show no alterations to the OCR (figure 5.18 A). Analysis of TMRM shows no change in mitochondrial polarisation after 1 h CPt treatment (figure 5.19).

Although CQ treatment alone in Ca9-22 cells has no impact on the OCR, basal respiration decreases with co-treatment of CPt and CQ with a rate of 37.13 ± 6.39 pmol/min compared to CPt alone (54.18 ±3.48 pmol/min) or CQ alone (52.13 ± 4.34 pmol/min) after 8 h (figure 5.18 A). Investigation of the mitochondrial membrane polarisation by TMRM shows that after 1 h treatment, CQ reduces the membrane polarisation to 0.87 MFI relative to the vehicle control (figure 5.19).

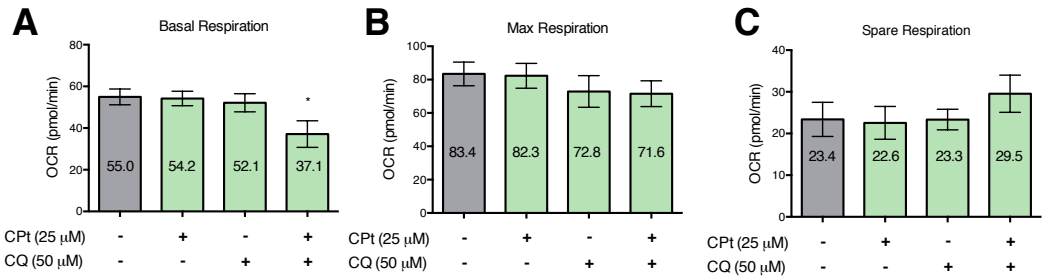

Figure 5.18. Dual treatment with CPt and CQ reduces basal respiration in Ca9-22 cells.

Ca9-22 cells were seeded in a 96 well seahorse plate at 20,000 cells per well and allowed to adhere before being treated with CPt (25 μM) in the presence or absence of CQ (50 μM) or with a vehicle control (H_2O) for 8 h. One hour before analysis, media was replaced by supplemented seahorse media and the plate was placed in a non-CO_2 incubator. The pre-hydrated inhibitor cartridge was loaded with the appropriate volume of various glycolytic and respiratory inhibitors and was calibrated in the Seahorse XF-96 extracellular flux analyser before the cell plate was analysed. (A)_ changes in basal respiration. (B) changes in maximum respiratory capacity. (C) shows changes in spare respiration with/without treatment. Data shown n=3 ± SEM, one-way ANOVA, followed by Tukey's multiple comparisons test. *p<0.5.

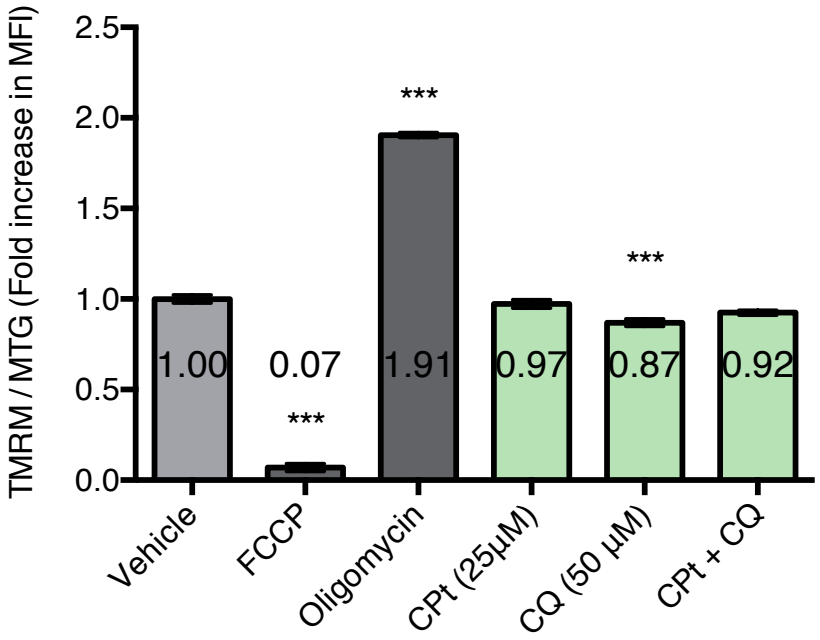

Figure 5.19. CQ decreases the polarisation of the mitochondrial membrane in Ca9-22 cells after 1h treatment.

Ca9-22 were seeded at an appropriate density for 24 h in full media (10% FBS), then treated for 1 h with CPt (25 μM) in the presence or absence of CQ (50 μM) or with a vehicle control (H_2O). Cells were trypsinised, washed in PBS and resuspended in 100μL flow cytometry buffer containing MTG (100 μM) and TMRM (100 μM). Cells were incubated at 37^{o}C for 30 min before washing off the stain and resuspending the cells in flow cytometry buffer. Cells were analysed using a BD LSRFortessa cytometer. The MTG and TMRM were excited using lasers at 488nm and 561nm respectively. Data shown n=3 ± SEM. One-way ANOVA followed by Tukey's multiple comparisons test. ***$p<0.001$, *$p<0.05$.

CPt (25 μM) treatment for 8 h in TR146 cells has no effect on OCR (figure 5.20) or on mitochondrial polarisation after 1 h CPt treatment (figure 5.21). Treatment with CQ (50 μM), however, results in a reduction of both the maximum respiration and spare respiratory capacity (figures 5.20 B and C respectively). Under CQ treatment, the max respiration was reduced to 66.45 ± 3.55 pmol/min from 94.55 ± 4.85 in the vehicle control. Co-treatment reduces the max respiration to 65.57 ± 4.53 pmol/min, however there is no significant distinction between the co-treated cells and those treated with CQ alone. Spare respiration was reduced to 20.21 ± 4.88 pmol/min in cells treated with CQ alone and to 17.51 ± 2.75 pmol/min in dual treated cells compared to 39.27 ± 4.35 pmol/min in the vehicle control. CQ treatment for 1 h has no impact on the mitochondrial membrane potential (figure 5.21).

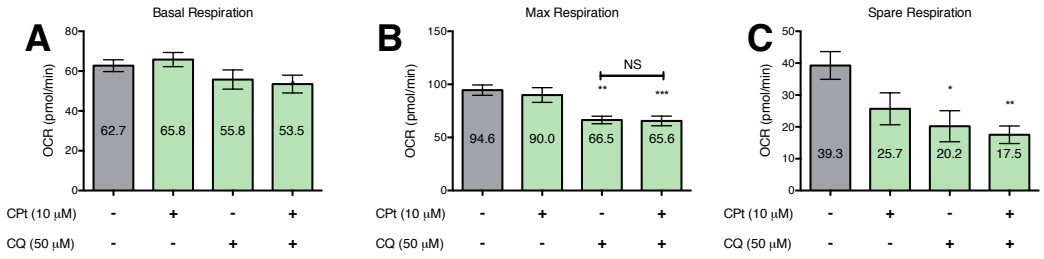

Figure 5.20. CQ decreases both the maximum and spare respiratory capacity of TR146 cells after 8h treatment.

TR146 cells were seeded in a 96 well seahorse plate at 20,000 cells per well and allowed to adhere before being treated with CPt (10 μM) in the presence or absence of CQ (50 μM) or with a vehicle control (H_2O) for 8 h. One hour before analysis, media was replaced by supplemented seahorse media and the plate was placed in a non-CO_2 incubator. The pre-hydrated inhibitor cartridge was loaded with the appropriate volume of various glycolytic and respiratory inhibitors and was calibrated in the Seahorse XF-96 extracellular flux analyser before the cell plate was analysed. (A) changes in basal respiration. (B) changes in maximum respiratory capacity. (C) changes in spare respiration with/without treatment. Data shown n=3 ± SEM, one-way ANOVA, followed by Tukey's multiple comparisons test. *p<0.05, **p<0.01, ***p<0.001, NS=Not significant.

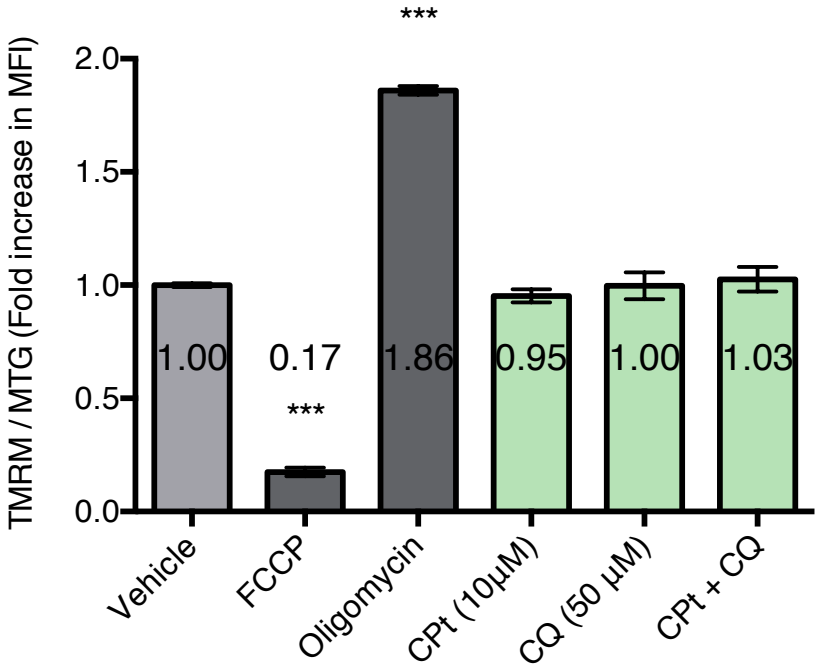

Figure 5.21. Treatment of TR146 cells with CPt or CQ has no impact on the mitochondrial membrane potential after 1 h treatment.

TR146 were seeded at an appropriate density for 24 h in full media (10% FBS), then treated for 1 h with CPt (10 μM) in the presence or absence of CQ (50 μM) or with a vehicle control (H_2O). Cells were trypsinised, washed in PBS and resuspended in 100μL flow cytometry buffer containing MTG (100 μM) and TMRM (100 μM). Cells were incubated at 37^{o}C for 30 min before washing off the stain and resuspending the cells in flow cytometry buffer. Cells were analysed using a BD LSRFortessa cytometer. The MTG and TMRM were excited using lasers at 488nm and 561nm respectively. Data shown n=3 ± SEM. One-way ANOVA followed by Tukey's multiple comparisons test. ***$p<0.001$.

Treatment with CPt (15 μM) for 8 h increases the basal OCR in DOK cells (figure 5.22 A) from 88.49 ± 5.75 pmol/min in the vehicle control to 114.50 ± 4.14 pmol/min. Co-treatment with CQ also increases the basal respiration to 114.30 ± 5.28 pmol/min, however this is not significantly different to treatment with CPt alone. The max respiration in DOK cells is increased under dual treated cells to 144.8 ± 11.32 pmol/min from 112.5 ± 5.18 pmol/min in the vehicle control (figure 5.22 B). The spare respiratory capacity also demonstrated and increase with co treatment at 62.03 ± 4.81 pmol/min compared to the vehicle control of 35.-5 ± 4.94 pmol/min in the vehicle control (figure 5.22 C), an increase in spare respiration was also seen under treatment with CQ alone at 55.94 ± 0.68 pmol/min, this was not significantly different to that of the dual treated DOK cells. Investigation of mitochondrial polarisation by TMRM demonstrated an increase in polarisation of the mitochondrial membrane in DOK cells treated with CQ and both CQ and CPt by a factor of 1.10 ± 0.03 and 1.16 ± 0.02 respectively with no statistical significance between the two (figure 5.23).

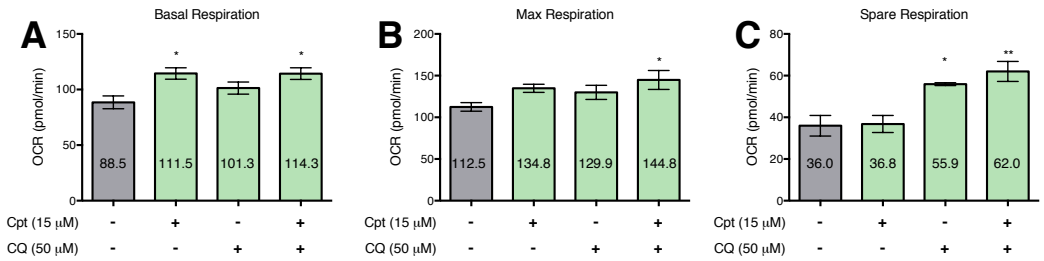

Figure 5.22. CPt increases basal respiration in DOK cells after 8h treatment while CQ increases spare respiration whereas co-treatment increases basal, maximum, and spare respiration.

DOK cells were seeded in a 96 well seahorse plate at 20,000 cells per well and allowed to adhere before being treated with CPt (15 μM) in the presence or absence of CQ (50 μM) or with a vehicle control (H_2O) for 8 h. One hour before analysis, media was replaced by supplemented seahorse media and the plate was placed in a non-CO_2 incubator. The pre-hydrated inhibitor cartridge was loaded with the appropriate volume of various glycolytic and respiratory inhibitors and was calibrated in the Seahorse XF-96 extracellular flux analyser before the cell plate was analysed. (A) changes in basal respiration. (B) changes in maximum respiratory capacity. (C) changes in spare respiration with/without treatment. Data shown n=3 ± SEM, one-way ANOVA, followed by Tukey's multiple comparisons test. **p<0.01, *p<0.05.

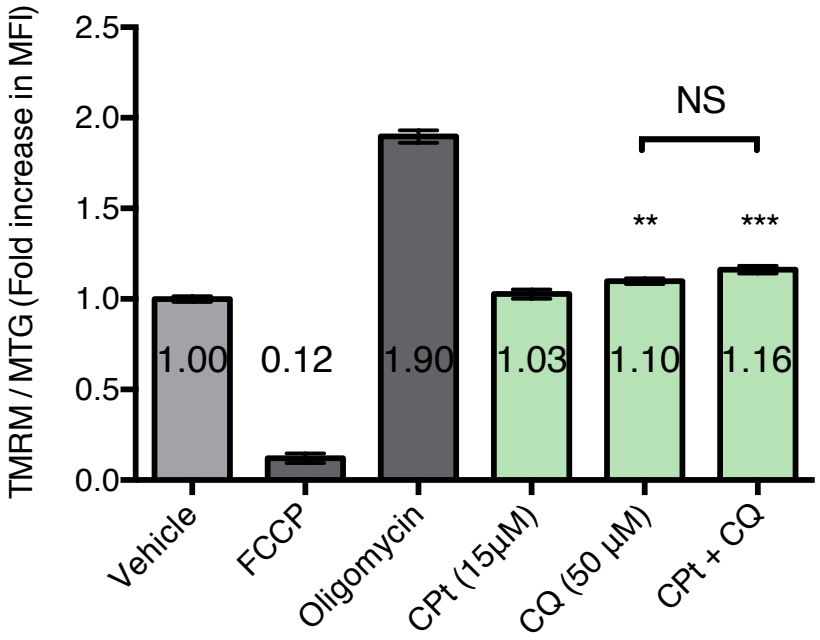

Figure 5.23. Treatment with CPt has no effect on mitochondrial polarisation in DOK cells however, CQ treatment increases the membrane polarisation.

DOK were seeded at an appropriate density for 24 h in full media (10% FBS), then treated for 1 h with CPt (15 μM) in the presence or absence of CQ (50 μM) or with a vehicle control (H_2O). Cells were trypsinised, washed in PBS and resuspended in 100μL flow cytometry buffer containing MTG (100 μM) and TMRM (100 μM). Cells were incubated at 37^{o}C for 30 min before washing off the stain and resuspending the cells in flow cytometry buffer. Cells were analysed using a BD LSRFortessa cytometer. The MTG and TMRM were excited using lasers at 488nm and 561nm respectively. Data shown n=3 ± SEM. One-way ANOVA followed by Tukey's multiple comparisons test. ***p<0.001, **p<0.01, NS=Not significant.

5.4 Discussion

The use of autophagy inhibitors to increase the efficacy of chemotherapeutic treatment is becoming a focal point for cancer therapy with CQ and HCQ (hydroxychloroquine) already being used as part of many clinical and pre-clinical trials as part of a cancer therapy regime[253]. Although autophagy inhibitors such as CQ and HCQ are already approved for human use, it is important to explore the potential of other autophagy inhibitors and to understand the mechanism behind their chemotherapy-enhancing abilities. This chapter has focused on the potential benefits of co-treatment of CQ with CPt to enhance the efficacy of chemotherapy in OSCC. The use of CQ to enhance chemotherapy has been explored for other cancers such as multiple myeloma, melanoma, pancreatic adenocarcinoma and non-small cell lung cancer[254]. Additionally, there have been some positive clinical trial results being shown for glioblastoma multiforme under co-treatment with CQ and carmustine [255] and for solid tumours treated with low-doses of chemotherapeutics combined with HCQ[256]. Due to the high rate of chemoresistance in OSCC, the ability to enhance therapy and prevent resistance would be extremely beneficial in a clinical setting.

The data presented in this chapter outlines the differential responses to CQ treatment in concert with CPt in several OSCC cell lines. TR146 and DOK cells demonstrated an increased CPt efficacy during co-treatment with CQ (figures 5.2 and 5.3 respectively). This is consistent with research by Zhu *et al.*[257] and Qin *et al.*[258] who showed that inhibiting autophagy by CQ could increase the efficacy of CPt in ovarian cancer

cells and adrenocortical carcinoma cells respectively. Interestingly Ca9-22 cells demonstrated no decrease in the IC_{50} of CPt (figure 5.1). CQ had previously been shown to decrease cell viability for all three cell lines (chapter 3, figure 3.17), indicating that the increase in cell death may be due to the combination of both treatments in TR146 and DOK cells. CQ has been shown to activate the P53 pathway to induce apoptosis in glioblastoma cells[259]. This CQ-induced, P53-mediated cell death may explain why Ca9-22 cells have no decrease in cell viability during co-treatment given this cell line's LOF mutation in the *P53* gene.

A further hypothesis underlying this observed increase in CPt's efficacy may result from the loss of autophagy's protective mechanism allowing CPt to carry out more DNA damage, leading to increased cell death. CPt was shown in chapter 4 to increase LC3 levels in Ca9-22 cells (figure 4.6), and DOK cells (figure 4.12) after 24 h treatment, however in TR146 cells (4.10) and DOK cells treated with CPt for 48 h, no changes in autophagic protein levels were observed. Co-treatment of TR146 cells and DOK cells with CPt and CQ had no impact on LC3 levels compared to treatment with CQ alone (figures 5.5 and 5.6 respectively), however, in Ca9-22 cells the LC3I:LC3II ratio was lower in co-treated cells when compared to cells treated with CPt alone, due to the increase in cytosolic LC3I during co-treatment (figure 5.4).

A further analysis of the changes in viability under co-treatment demonstrated that treatment with CPt only resulted in PARP cleavage in Ca9-22 and DOK cells (figures 5.7 and 5.9 respectively). TR146 cells demonstrated no PARP cleavage after 48 h treatment (figure 5.8) despite

the clear reduction in metabolic activity as shown using the Alamar Blue. CPt reduced the number of cells undergoing cell cycle arrest at the G_2/M phase of the cell cycle for both TR146 cells (figure 5.14) and Ca9-22 cells (figure 5.13), however TR146 cells also demonstrated a decreased G_0/G_1 peak indicating a lower level of cell cycle arrest at the G_0 point. It is likely that CPt is inducing cell death in TR146 cells along with a prolonged quiescent phase in Ca9-22 cells. It is unlikely that these Ca9-22 cells are undergoing senescence as senescence requires activation of the p53 gene. Treatment with CQ resulted in no PARP cleavage for any of the three investigated cell lines.

Increasing evidence is highlighting links between autophagy inhibition and metabolic alterations that could result in the enhanced action of CPt[260-263]. Examination of the extracellular acidification rate (ECAR) allows for analysis of changes in the glycolytic pathway. OSCC cells Ca9-22 and TR146 cells demonstrated no changes to ECAR under treatment with either CPt or CQ for 8 h (figures 5.15 and 5.16 respectively), however the pre-malignant DOK cells underwent a decrease in glycolytic reserve after CPt treatment and to a lesser extent with CQ (figure 5.17). The glycolytic reserve is a measure of the cell's ability to respond to energetic demand. Alterations in cellular metabolism have been suspected of playing a causal role in the development in chemoresistance where drug resistant cells have been shown to possess defective ATP production[264]. DOK cells undergoing chemotherapeutic treatment are likely to be functioning at a maximum ATP capacity to attempt to combat the DNA damage caused by CPt, thus reducing their reserve. In OSCC cells this reserve is likely not impacted as these cells may have developed

mechanisms to evade the extent of DNA damage induced in dysplastic cells. When comparing the basal glycolysis between cell lines, TR146 cells and Ca9-22 cells have a higher rate of basal glycolysis than DOK cells. DOK would be expected to have a lower level of glycolysis due to their decreased requirement for glycolysis without the Warburg effect in place.

Inhibition of autophagy by CQ has been shown to cause mitochondrial damage in breast cancer stem cells[265]. The OSCC cells, Ca9-22 and TR146, showed no changes to OCR upon treatment with CPt for 8 h (figures 5.18 and 5.20 respectively), however, DOK cells underwent an increase in basal respiration in response to CPt treatment (figure 5.22). CQ treatment had no impact on Ca9-22 cell respiration, however TR146 cells displayed a decrease in both maximum and spare respiration while DOK cells demonstrated an increase in spare respiration after CQ treatment. Despite the stark differences in cellular respiration between these distinct cell lines, the most interesting response was to that of co-treatment with both CPt and CQ. CQ has been shown to sensitise cells to CPt treatment in both hepatocellular carcinoma cells and cholangiocarcinoma cells and this sensitisation has been associated with mitochondrial dysfunction and reactive oxygen species (ROS) production prespectively[222, 266], highlighting the links between co-treatment and respiratory alterations. Ca9-22 cells demonstrated a decrease of basal respiration in response to co-treatment (figure 5.18) while TR146 cells had no change in cellular respiration in response to co-treatment compared to treatment with CQ alone (figure 5.20). DOK cells, on the other hand demonstrated an increase in maximum respiration in response to co-treatment (figure

5.22). Ca9-22 and TR146 cells have a decreased reliance on oxidative phosphorylation as cancer cells rely primarily on glycolysis for energy production, it is not surprising, therefore, that DOK cells are more sensitive to changes in respiration in response to chemical intervention. The polarisation of the mitochondrial membrane (ΔΨm) was also examined as a potential root cause of alterations in oxidative phosphorylation in response to either CPt or CQ. None of the three cell lines underwent changes to ΔΨm in response to CPt treatment, however CQ decreased ΔΨm in Ca9-22 cells (figure 5.19) and increased ΔΨm in DOK cells (figure 5.21). DOK cells also showed an increase in ΔΨm in response to co-treatment however this was likely due to the CQ as there was no significant difference between co-treated cells and those treated with CQ alone. These contrasting results are likely characteristics of the phenotypic and genotypic differences of these cells. CQ has been shown in glioma cells to dissipate the mitochondrial membrane potential without causing oxidative stress[267] which may explain the decrease in ΔΨm in the absence of alterations to basal respiration in Ca9-22 cells. While the degrees of fluctuations in ΔΨm may not be excessive in either Ca9-22 or DOK cells, a prolonged period of depolarisation or hyperpolarisation can lead to a complete loss of mitochondrial functionality. As stated previously, CQ activates the P53 gene, with this gene product shown to regulate ΔΨm[268] therefore, TR146 cells with a functional P53 gene may be more equipped to regulate the ΔΨm in response to CQ treatment than the P53 deficient Ca9-22 cells.

The data presented here demonstrates the direct effects P53 functionality may have on OSCC cells. While the differential metabolic responses

between DOK and OSCC cells may be expected due to cancer cell's reliance on glycolysis, the P53 status of OSCC cells is a much more important factor to take into account when considering treatment choices. CQ's differential effects in $P53^{+}$ and $P53^{-}$ cells is discerned from the impacts observed in Ca9-22 and TR146 cells and their apoptotic and metabolic responses to exposure to this drug. The following chapter will explore this further through the silencing of P53 in TR146 cells with targeted siRNA and to compare these $P53^{-}$ cells to Ca9-22 cells to further understand the effects of P53 status on CQ co-treatment with CPt in OSCC cells.

Chapter 6

Is there a P53 mediated response to cisplatin in OSCC cell lines?

6.1 Introduction

P53 is a tumour supressing gene encoding a nuclear transcription factor. *P53* transactivates a wide range of genes associated with apoptosis and cell cycle arrest[269]. In healthy cells, P53 is present at low levels, however, in conditions of DNA damage P53 accumulates within the nucleus due to a reduction in its association with MDM2, a nuclear export protein[270], where it is converted to its active form by post-translational modifications which initiates the transcription of the gene p21 (the cyclin dependent kinase (Cdk) inhibitory protein).Increased levels of p32 inhibit the cyclinA/cdk2 and cyclinE/cdk2 kinases which prevents these kinases from promoting cell cycle progression at the G_1 phase of the cell cycle[271]. Once the DNA damage has been repaired, cells are able to resume their position in the cell cycle. In cells with sufficient DNA damage, P53 can engage a pro-apoptotic mechanism to prevent passing mutations on to daughter cells. Human cancers show frequent mutations in this gene with more than 50% showing loss of function (LOF) mutations[272]. Within OSCC, *P53* mutations have been found in up to 70% of patients[273]. It was determined that these mutations or deletions of *P53* had no correlation with smoking status[274] and in one study group, *P53* mutations were shown to be associated with reduced survival[275]. There are distinct differences in *P53* expression within the cell lines used in the following experiments, a carry-over from the initial isolation of the cells themselves. Ca9-22 cells carry a LOF mutant *P53* gene, while TR146 cells carry an upregulated *P53* gene.

P53 is a known regulator of cellular metabolism and can act to decrease glycolytic flux and promote oxidative phosphorylation[56, 57]. As a result of this capability, tumour cells with *mTP53* experience elevated glycolysis and decreased mitochondrial respiration, as described by the Warburg effect. The presence of *mTP53* can also contribute to the resistance to apoptotic signalling by diminishing signalling though BAX, PUMA and NOXA[62].For this reason, *mTP53* is often associated with an increased resistance to chemotherapeutics[63]. Activation of *P53* can downregulate Bcl-2 through negative regulation of endogenous bcl-2 mRNA and ultimately the protein[276], leading to the release of the Beclin-1 complex, inducing Beclin1-mediated autophagy[226, 277]. *P53* induction can also result in the inhibition of mTOR via AMPK or DRAM activation[221, 228], implicating a role for *P53* as a mediator of cellular metabolism and cell death pathways.

6.2 Aims of Chapter

This chapter will examine the involvement of P53 in OSCC cell's response to CPt exposure. The functional P53 gene in theTR146 cells, was knocked down using targeted siRNA to create a genotypic mimic of Ca9-22 cells. The functional response of these knockdown cells was then compared to wild-type TR146 cells in order to complete the following objectives:

1. **Determine a role for *P53*'s in cell viability in response to CPt treatment**

   Viability of $P53^{+}$ and $P53^{-}$ TR146 cells will be examined through monitoring cellular viability using the Alamar Blue assay to determine

   the IC_{50}s of both TR146 cells in comparison with Ca9-22 cells.

2. **Elucidating the role of *P53*'s in glycolytic flux of OSCC cell lines undergoing therapeutic exposure**

   $P53^{+}$ and $P53^{-}$ TR146 cells will be treated with the appropriate IC_{50} as determined previously in TR146 and Ca9-22 cells in the presence or absence of CQ and ECAR will be captured by Seahorse Real-Time cell metabolic analysis.

3. **Investigation of the relationship between *P53* and mitochondrial respiration**

P53^{+} and *P53*$^{-}$ TR146 cells will be treated with the appropriate IC_{50} for both Ca9-22 and TR146 cells in the presence or absence of CQ. The OCR will be captured by Seahorse Real-Time analysis while mitochondrial membrane potential will be determined by TMRM and flow cytometry.

6.3 Results

6.3.1 *P53* expression influences CPt-mediated effects on cell viability under conditions of autophagy inhibition.

TR146 cells overexpress *P53*. By selectively knocking down the *P53* gene with targeted siRNA, TR146 cell responses to CPt treatment can be examined and compared in $P53^+$ and $P53^-$ cells to explore whether *P53* is mediating the CPt sensitivities observed in these OSCC cells. CPt sensitivity was assessed through monitoring cellular viability using the Alamar Blue assay after incubating the $P53^+$ and $P53^-$ TR146 cells with CPt in the presence or absence of CQ for 48h.

Knockdown of *P53* was verified 48 h after incubation with siRNA by western blotting of P53 protein expression where an almost complete knockdown of *P53* was observed compared to transfection with a negative control of scrambled siRNA (figure 6.1).

The Alamar Blue assay showed no differential response in cell viability CPt in $P53^+$ and $P53^-$ TR146 cells treated with the IC_{50} of Ca9-22 cells (5 μM) or IC_{50} of TR146 cells (10 μM) (figure 6.2).

$P53^-$ cells demonstrated no significant change in response to co-treatment with CPt and CQ compared to $P53^+$ cells (figure 6.3).

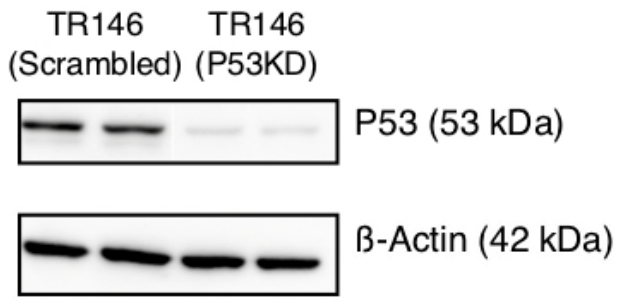

Figure 6.1. P53 expression in TR146 cells was significantly reduced after the introduction of targeted siRNA

TR146 cells were seeded at a concentration of 2.5 x10^5 cells per well in a 6-well plate with serum starved medium (1% FBS). Following incubation overnight, targeting siRNA (20 nm IBONI p53-siRNA pool or scrambled negative control) was transfected using RIBOXX-FECT transfection reagent (1% v/v) (MSC) in full media (10% FBS). Following 48 h incubation cells were lysed in RIPA buffer. Lysates (20 µg) were resolved by SDS-PAGE on a 10% gel, followed by transfer to a PVDF membrane. The membranes were then probed with an anti-P53 antibody (Abcam, mouse-anti-human) and visualised using a gel documentation system (Biorad) and enhanced chemiluminescent HRP substrate (millipore). Data shown is a representative blot of routine blots performed to verify successful knock down after each siRNA transfection was completed.

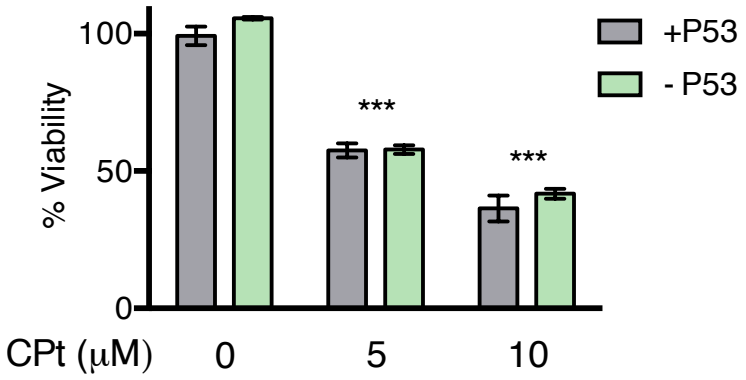

Figure 6.2. P53 status of TR146 cells has no impact on viability in response to CPt treatment

TR146 cells were seeded at a concentration of 2.5 x10^4 cells per well in a 96-well plate with serum starved medium (1% FBS). Following incubation overnight, targeting siRNA (20 nm IBONI p53-siRNA pool or scrambled negative control) was transfected using RIBOXX-FECT transfection reagent (1% v/v) (MSC) in full media (10% FBS). Following 24 h incubation cells were treated various concentrations of CPt for 48 h. Alamar Blue reagent was added 4 h before the end point and absorbance values were read at λ=570 nm and λ=600 nm. $P53^+$ cells have been transfected with a scrambled negative control. Data shown n=3 ± SEM. Two-way ANOVA followed by Sidak's multiple comparisons test. ***$p<0.001$

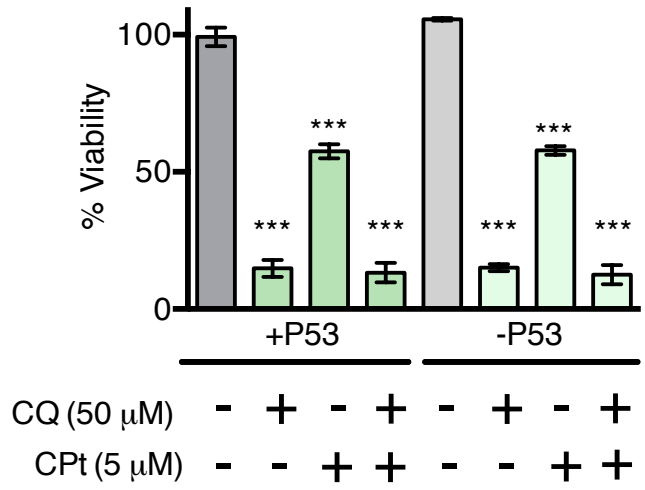

Figure 6.3. The effect of co-treatment with CPt and CQ on TR146 cell viability is independent of the P53 status of the cell.

TR146 cells were seeded at 2.5 x10^4 cells per well in a 96-well plate with serum starved medium (1% FBS). Following incubation overnight, targeting siRNA (20 nm IBONI p53-siRNA pool or a scrambled negative control) was transfected using RIBOXX-FECT transfection reagent (1% v/v) (MSC) in full media (10% FBS). Following 24 h incubation cells were treated with CPt (5 μM) in the presence or absence of CQ (50 μM) for 48 h. Alamar Blue reagent was added 4 h before the end point and absorbance values were read at λ=570 nm and λ=600 nm. $P53^+$ cells have been transfected with a negative control. Data shown n=3 ± SEM. One-way ANOVA followed by Tukey's multiple comparisons test. ***$p<0.001$.

6.3.2 Glycolytic flux is not affected by changes in *P53* expression.

As *P53* status has been linked to alterations in glycolytic flux, therefore fluctuations in cellular metabolism in TR146 cells were determined. ECAR was measured using Seahorse Real-Time cell metabolic analysis in both $P53^{+}$ and $P53^{-}$ TR146 cells in the presence or absence of CPt to assess the CPt-mediated glycolytic response to *P53* status.

Knockdown of *P53* had no effect on ECAR of TR146 cells either in the presence or absence of CPt (figure 6.4).

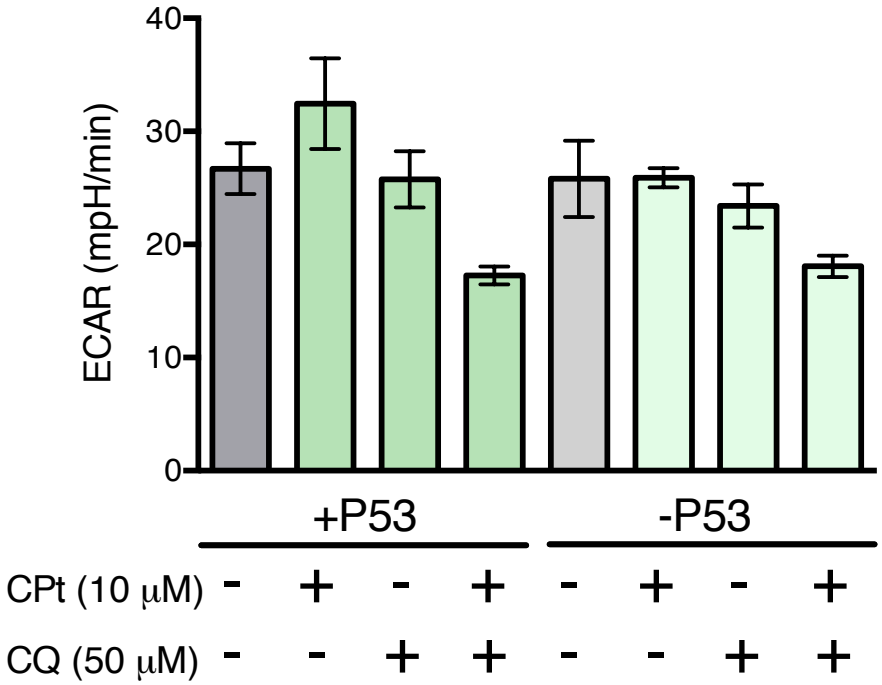

Figure 6.4. CPt and CQ have no impact on basal glycolysis in TR146 cells with no variation arising from the P53 status.

TR146 cells were seeded at 2.5 x10^4 cells per well in a 96-well seahorse plate with serum starved medium (1% FBS). Following incubation overnight, targeting siRNA (20 nm IBONI p53-siRNA pool) was transfected using RIBOXX-FECT transfection reagent (1% v/v) (MSC) in full media (10% FBS). Following 24 h incubation cells were treated in the presence or absence of CPt (10 μM) and/or CQ (50 μM) for 8 h. One hour before analysis, media was replaced by supplemented seahorse media and the plate was placed in a non-CO_2 incubator. The pre-hydrated inhibitor cartridge was loaded with the appropriate volume of glycolytic and respiratory inhibitors and was calibrated in the Seahorse XF-96 extracellular flux analyser before the cell plate was analysed. $P53^+$ cells have been transfected with a negative control. Data shown n=3 ± SEM, one-way ANOVA, followed by Tukey's multiple comparisons test.

6.3.3 Silencing of P53 in OSCC cells increases susceptibility to CPt-mediated changes in OCR

Due to an apparent contrast in OCR between Ca9-22 and TR146 cells (section 5.3.8), it was hypothesised that the *P53* status of these cell lines was mediating the differential response. OCR was measured using Seahorse Real-Time cell metabolic analysis in $P53^{+}$ and $P53^{-}$ TR146 cells in the presence or absence of CPt to assess the CPt-mediated respiratory response to *P53* status.

Silencing of P53 in TR146 cells resulted in an overall decrease in basal respiration compared to $P53^{+}$ cells (figure 6.5). Treatment of these cells with either CPt or CQ had no further impact on OCR. It is important to note that there was no significant increase in basal glycolysis of CPt treated $P53^{-}$ cells compared to untreated $P53^{-}$ cells.

Further investigation of the impacts of knocking down P53 on the oxidative pathway were undertaken by examining the effects of P53 status on mitochondrial membrane potential. It was noted that after 1 h treatment, P53 status has no impact on mitochondrial membrane potential using TMRM and flow cytometry (figure 6.6).

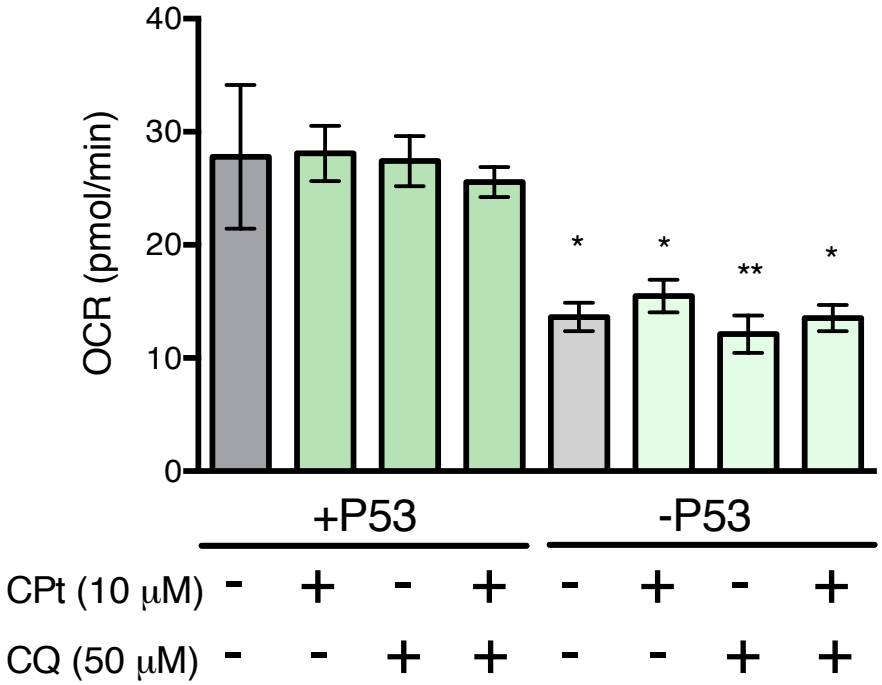

Figure 6.5. Basal respiration in TR146 cells is decreased when P53 is silenced compared to those with wildtype P53

TR146 cells were seeded at 2.5 x10^4 cells per well in a 96-well seahorse plate with serum starved medium (1% FBS). Following incubation overnight, targeting siRNA (20 nm IBONI p53-siRNA pool) was transfected using RIBOXX-FECT transfection reagent (1% v/v) (MSC) in full media (10% FBS). Following 24 h incubation cells were treated in the presence or absence of CPt (10 μM) and CQ (50 μM) for 8h. One hour before analysis, media was replaced by supplemented seahorse media and the plate was placed in a non-CO_2 incubator. The pre-hydrated inhibitor cartridge was loaded with the appropriate volume of glycolytic and respiratory inhibitors and was calibrated in the Seahorse XF-96 extracellular flux analyser before the cell plate was analysed. $P53^+$ cells have been transfected with a negative control. Data shown n=3 ± SEM, one-way ANOVA, followed by Tukey's multiple comparisons test. *$p<0.05$, **$p<0.01$, compared to $P53^+$ cells with the same treatment.

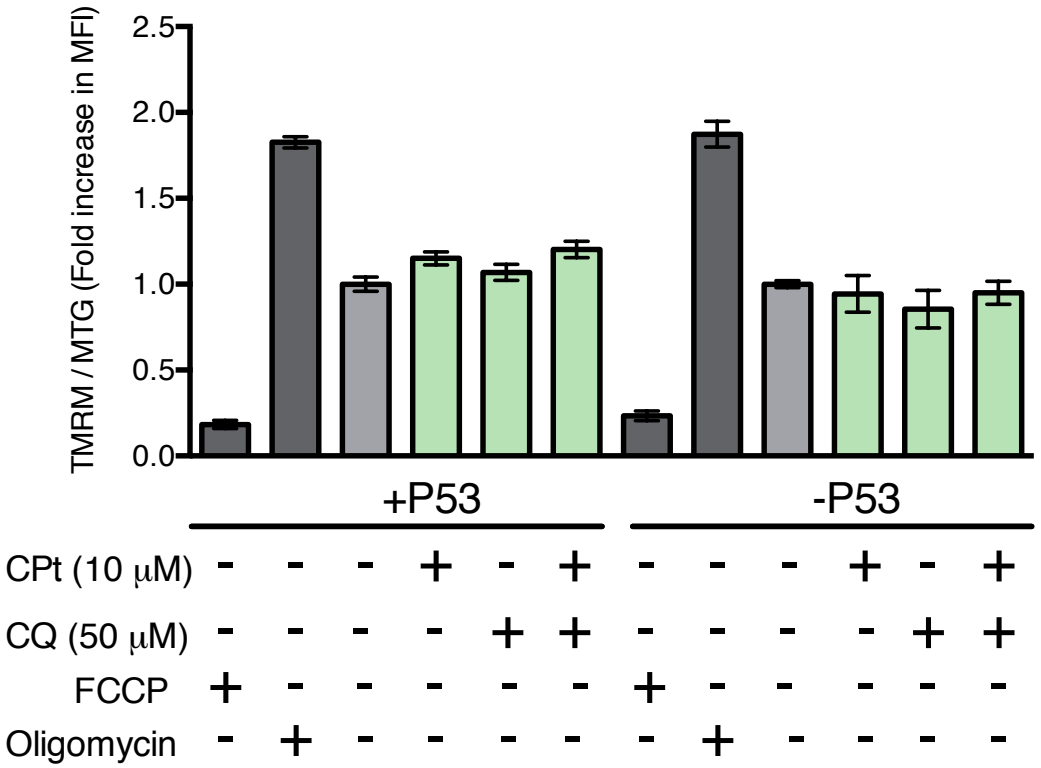

Figure 6.6. Silencing P53 in TR146 cells, followed by exposure to CPt and/or CQ has no impact on the mitochondrial membrane potential after 1 h treatment.

TR146 were seeded at an appropriate density for 24 h in full media (10% FBS). Following incubation overnight, targeting siRNA (20 nm IBONI p53-siRNA pool) was transfected using RIBOXX-FECT transfection reagent (1% v/v) (MSC) in full media (10% FBS). Following 24 h incubation cells were then treated for 1 h with CPt (10 μM) in the presence or absence of CQ (50 μM) or with a vehicle control of H_2O. Cells were trypsinised, washed in PBS and resuspended in 100μL flow cytometry buffer containing MTG (100 μM) and TMRM (100 μM). Cells were incubated at 37^{o}C for 30 min before washing off the stain and resuspending the cells in flow cytometry buffer. Cells were analysed using a BD LSRFortessa cytometer. The MTG and TMRM were excited using lasers at 488nm and 561nm respectively. $P53^{+}$ cells have been transfected with a negative control. Data shown n=3 ± SEM. One-way ANOVA followed by Tukey's multiple comparisons test.

6.5 Discussion

Tumour Protein 53 (P53) is a commonly mutated gene which has been found to be mutated in up to 70% of OSCC patients[273]. P53 is an essential tumour suppressor protein and is involved in activating cell cycle arrest and apoptosis. Many links between autophagy and *P53* have been identified. *P53* has been shown to inhibit a subunit of PI3K, thus blocking the PI3K/Akt pro-survival pathway[278-280]. P53 can induce autophagy by upregulating tuberous sclerosis complex 2 (TSC2) and AMP-activated protein kinase (AMPK) thereby supressing mTOR[277]. Conversely, P53 can also negatively regulate autophagy whereby cytosolic p53 can inhibit autophagy via its inhibition of AMP-dependent kinase which, in turn, activates mTOR[111]. Following on from Chapter 5 where Ca9-22 cells (with a LOF mutation in P53) demonstrated no increase in cell death when undergoing co-treatment with CPt and CQ compared to TR146 cells (wt-P53) which showed a very significant increase in cell death under co-treatment, this chapter focused on the comparison between TR146 cells and a genotypic mimic of Ca9-22 cells by silencing the P53 gene in TR146 cells with targeted siRNA.

A comparative study of $P53^{+}$ and $P53^{-}$ TR146 cells demonstrated that the P53 status of TR146 cells has no impact on cell metabolic activity in response to CPt treatment or in response to co-treatment with CQ (figure 6.2). Chapter 5 hypothesised that Ca9-22 cells' lack of susceptibility to cell death was due to its mP53 status, however this is clearly not the case. There has been some research indicating that RAS promotes CQ toxicity[281], however in autophagy deficient tumour cells, this does not

occur. As seen in Chapter 3, Ca9-22 cells appear to have a lower rate of basal autophagy compared to TR146 cells based on acidic vesicle production (figures 3.7 and 3.9). It is likely that there are other, undocumented mutations within these cell lines that are contributing to their individual susceptibility to CQ other than P53.

Although there is no change in metabolic activity of P53 positive and negative there is metabolic connection to *P53* status when you consider the nature of the metabolic activity. While no change could be seen in the glycolytic flux between TR146 cells with a silenced *P53* and their $P53^{+}$ control (figure 6.4), TR146 cells with a silenced P53 gene displayed a decreased basal respiration in response to CPt, CQ and co-treatment compared to the scrambled siRNA control (figure 6.5). *P53* is known to promote oxidative phosphorylation, as such, a deletion of *P53* or a loss of function mutation should be less dependent on mitochondrial respiration as a source of ATP. CPt has been shown to lower ATP levels by inducing mitochondrial damage in kidney cells[282].It is possible that CPt-mediated mitochondrial damage is forcing $P53^{-}$ cells to use even less oxidative phosphorylation, resulting in decrease in OCR, however this does not explain the lack of a corresponding increase in glycolytic flux.

The mitochondrial response of P53 knockdown cells was not the same as Ca9-22 cell response. OCR measurements in Ca9-22 cells did show a decrease in basal respiration but only in response to co-treatment (figure 5.18). Although the alterations in mitochondrial respiration are clear in wild-type TR146 cells compared to their $P53^{-}$ counterpart, this cannot be seen in Ca9-22 cells possessing *mTP53*. The links between oxidative

phosphorylation and *P53*-mediated signalling are complicated and there are many other genes and proteins that could be differently affected in these two cell types. Cruz-Bermúdez *et al*. described an early metabolic reprogramming event in non-small cell lung cancer in response to CPt treatment that increases oxidative phosphorylation[283]. As response to CPt was seen to be slower in TR146 cells, compared to Ca9-22 cells (see Chapter 4), it is feasible that Ca9-22 cells may be experiencing an upregulation of oxidative phosphorylation after 24 h treatment that is not seen in TR146 cells until a later time point, independent of *P53* status.

These data demonstrate that the P53 status of OSCC does have an impact on cellular metabolism, however it alone does not have the ability to alter response to treatment with CQ and CPt either alone or in combination. There are many other genetic variations possible within OSCC cells that may contribute to treatment sensitivities, and it is still a topic of major importance for research and clinicians. P53's role in alteration of basal respiration should not be overlooked. In a tumour environment, where glycolysis drives tumour growth, a reduction in basal respiration may indicate a stronger reliance on glycolysis and may indicate a more aggressive tumour that has developed to survive in the absence of oxygen.

Chapter 7

General Discussion

7.1 General Discussion

Oral cancer is often diagnosed at later stages, due to late presentation of distinctive symptoms. Treatment for oral cancer, therefore, is often particularly invasive as surgical intervention is usually required by the time of diagnosis. Surgical intervention can result in the removal of large amounts of facial tissue and lymph nodes which may result in severe scarring, facial disfigurement, speech difficulties and difficulty eating or drinking. The treatment protocol for oral cancer usually combines chemotherapy, radiotherapy, and surgery. Overall, this treatment regime is extremely invasive and can severely impact the patient's QOL even if they are in remission. Chemotherapy, although associated with fewer long-term complications is rarely used alone as development of resistance to CPt, the most frequently used chemotherapeutic in OSCC, is a high probability when treating OSCC[284]. The involvement of autophagy with resistance to chemotherapy has been a hot topic in recent years, leading to numerous clinical trials employing autophagy inhibitors such as CQ and HCQ in combination with chemo or radiotherapy[253]. Despite the increased interest in the autophagy during chemotherapeutic intervention, there is a lot yet to understand about its mechanism regarding improving cancer therapy. More importantly, there is still no consensus as to which are the best experimental methods to use when assessing modulations in the autophagic flux, this has led to inconsistencies in reporting the observed effects of autophagy on chemotherapy.

Two methods of autophagy measurements were compared in this study, acridine orange (staining of acidic vesicles) and western blotting of LC3B and P62. Acridine orange is known to be unspecific method of autophagy measurement due to its affinity for other acidic organelles such as lysosomes[285], however when compared to the more commonly used western blot technique, it can provide equally reliable data in the context of autophagic induction or inhibition. Klionsky *et al.* have repeatedly tried to compile up-to-date methods of measuring autophagy [137, 286]. Despite multiple publications and attempts to find a consensus amongst autophagy researchers, there remain a lot of disputes as to the most reliable method. The data provided in Chapter 3 indicates that the combination of both acridine orange staining supported by western blotting can provide enough information to identify modulations in autophagic flux, however these methods could clearly be more robust. Acridine orange staining has the potential for type I errors due to lysosomal staining, P62 levels do not always decrease in response to autophagy and LC3B analysis can be challenging as LC3I does not always appear in western blots due to a much higher affinity of available antibodies for LC3II. Another caveat of LC3 immunoblotting is the difficulty in interpreting the cause of an increase or decrease in LC3II levels. Increased autophagic flux can result in more autophagosomes and therefore more LC3II, however an increase in flux will also result in a more rapid breakdown of autolysosomes leading to a decrease in LC3II. For this reason, it is incredibly difficult to monitor autophagic flux in response to a single treatment alone. LC3II is frequently monitored in the presence of CQ to prevent the formation (and, therefore, breakdown) of

autolysosomes, allowing the capture of changes in LC3II levels in response to specific interventions. This can be seen in Chapter 5 where treatment of Ca9-22 cells with both CQ and CPt increased the level of LC3II expression compared to treatment with CQ alone (figure 5.4) this was not seen in TR146 cells (figure 5.5) or DOK cells (figure 5.6) indicating that CPt is inducing autophagy in Ca9-22 cell sand not TR146 or DOK cells.

The chemotherapeutic induction of autophagy has been well documented in cancer[287], however, there is very limited research into autophagy in response to chemotherapy in OSCC. Studies have demonstrated that anticancer drugs induce different effects of autophagy on cell survival in different cancer types[146]. Studies examining LC3 and P62 expression in OSCC patients, concluded that patients with an increased expression of LC3 on the peripheral site of the tumour had more unfavourable clinicopathological parameters[288]. It was also noted that expression of both Beclin-1 and Atg5 is an indicator of poor prognosis in OSCC[289]. What is still unclear is if inducing or inhibiting autophagy alongside chemotherapeutic intervention will decrease the likelihood of chemoresistance forming in these OSCC cells given that currently available data supports both theories where autophagy in OSCC can act as a tumour suppressor[290] and can promote tumour survival[291].

The data presented in this thesis demonstrate that autophagy induction is occurring in response to distinct chemotherapeutic treatments in OSCC cell lines. In a clinical setting, the induction of autophagy in

response to chemotherapy can lead to the protection of cancer cells and the development of chemoresistance, as a possible mechanism of recurring chemo-resistant tumours in OSCC patients[292]. Inhibition of CPt-induced autophagy resulted in a decrease in OSCC cell viability in a cell-type specific manner with the *P53*$^{-}$ cell line, Ca9-22 did not correlate to increased cell death response in combination with CQ treatment. The TR146 cell line, with an over expressed *P53* gene, however, demonstrated a large decrease in cell viability in response to co-treatment without any indication that CPt is inducing autophagy in this cell line. Furthermore, this decrease in cell viability was not linked to an increase in necrosis or apoptosis. Cell cycle analysis of TR146 cells demonstrated a decreased G_0/G_1 peak in response to CPt treatment corresponding to an increase in cells at the sub G0 phase. This is a clear indication of cell death, however in the absence of necrosis or apoptosis it is unclear what cell death mechanism is being utilised here. Studies have shown that high concentrations of chemotherapeutic agents can cause cell death in a caspase independent manner[293]. It has also been suggested that there may be many undiscovered forms of non-apoptotic cell death, any of which could be involved in P53-mediated cell death in response to CPt treatment. Ca9-22 cells, on the other hand, demonstrated PARP cleavage in response to CPt treatment, indicating a distinctly different cell death response to that of TR146 cells.

Chemotherapy is a known inducer of oxidative stress[294]and reactive oxygen species (ROS), which have been shown to induce autophagy[242]. OSCC cells displayed mitochondrial alterations during the co-treatment with CPt and CQ. Autophagy inhibition by CQ resulted in a

depolarisation of $\Delta\Psi m$ in the presence or absence of CPt in Ca9-22 cells while co-treatment resulted in a decrease in basal respiration. TR146 cells demonstrated a decrease in the maximum and spare respiration in response to CQ treatment while DOK cells underwent an increase of $\Delta\Psi m$ in response to CQ treatment with a corresponding increase in spare respiration. These data could indicate that modulation of autophagy is taking place. It has previously been shown that induction of autophagy can induce hyperpolarisation of $\Delta\Psi m$[295], however, autophagy induction can also result from the depolarisation of mitochondria[296]. There is an abundance of research to support a role for the mitochondrial membrane potential in the regulation of autophagy[297] and this response can be seen in the work presented in this thesis whereby OSCC cell lines displayed a differential response of the mitochondrial membrane potential in order to regulate modulations in autophagy.

The presence of different genetic expressions of *P53* in cancer cells has long been associated with cancer and response to chemotherapeutics with overexpression of the mutated form of *P53* leading to increased drug resistance[298]. *P53* mutations are seen in almost 50% of cancer patients[272] and are associated with reduced survival[275]. In OSCC, mTP53 is associated with a lower response to CPt-based therapies[132]. In the cell lines investigated for this study, TR146 cells with an upregulated *P53* gene show the lowest sensitivity to platinum-based chemotherapeutic drugs (Chapter 4). These cells also display a naturally high level of basal autophagic flux, which indicates a potential link between *P53* mediated resistance and autophagy's survival response.

The data, shown in Chapter 6, indicates that the P53 status of OSCC cells is not as integral to CPt sensitivity as has previously been seen in other cancer cell types. P53 status was shown to have no impact on cell death in response to treatment with either CPt alone or when co-treated with CQ. P53 status also had no impact on basal glycolysis in response to treatment. What was intriguing was the stark contrast between the basal respiratory capacity of $P53^{+}$ and $P53^{-}$ cells where $P53^{-}$ cells demonstrated dramatically reduced basal respiration. A reduction in basal respiration can be also seen in in Ca9-22 cells under co-treatment with CPt and CQ (chapter 5). This reduction was not present in TR146 cells under the same treatment conditions, indicating the P53 status of OSCC cells influences oxidative phosphorylation in response to chemical intervention. Research has shown that p53 promotes the use of oxidative phosphorylation with ATP levels being higher in $P53^{+}$ colon cancer cells than their P53 knockdown counterpart[299].

The inhibition of autophagy by CQ during chemotherapeutic intervention has great potential. As CQ is already licensed, available and safe to use in humans, it is an economic choice for health care professionals. Clinical trials have already demonstrated that the combined use of up to 150 mg CQ a day, in combination with chemotherapy and radiation therapy can prolong the survival of glioblastoma patients[300]. The availability of this treatment in OSCC could reduce the high level of chemo-resistance and result in a reduced use of radiotherapy and surgery, lowering the risk of long-term complications associate with OSCC treatment.

Autophagy's ability to act as a cell's defence mechanism pinpoints this pathway as an obvious target when undergoing chemotherapeutic cell death. It is discernible from the data presented in this thesis that inhibiting autophagy has significant advantages in increasing the efficacy of CPt treatment in OSCC cells and continuation of this work in combination with other OSCC chemotherapeutics and the development of robust OSCC animal models will help to verify this proposition as a potential therapeutic strategy.

7.2 Future Work

7.2.1 Visualisation of autophagy induction in OSSC cells using tandem GFP-RFP-LC3

The development of a robust method for measuring autophagic flux is an essential tool for the future of autophagy research. The tandem mRFP-GFP-LC3 fluorescence microscopy technique has shown a lot of promise and provides more reliable evidence of alterations to autophagic flux, however, analysis of microscopy images leaves a lot of room for observation bias. By combining the use of mRFP-GFP-LC3 fluorescence with flow cytometry could eliminate this bias and provide quantitative data on autophagic flux.

7.2.2 Further understanding of the metabolic reprogramming during CPt treatment in OSCC

Building on the observed CPt-induced alterations in mitochondrial $\Delta\Psi$m and basal respiration in OSCC cells with differential *P53* status, it was hypothesised that metabolic reprogramming may be occurring in response to CPt treatment. In order to investigate this further, analysis of alterations to the mETC complex enzymatic activity should be completed[301]. Furthermore, to identify evidence of an earlier metabolic response to CPt in Ca9-22 cells, a time-dependant OCR response should be conducted using seahorse analysis to verify this. In addition to seahorse analysis of OCR the complimentary use of a system such as the

Oroboros oxygraphy can provide a much higher resolution analysis of the respiratory activity of cells. The role of mitophagy cannot be ignored when identifying alterations to mitochondrial metabolism. Understanding the role of mitophagy in this process will be essential to understanding the full mechanism behind the autophagy inhibition-mediated increase in CPt's potency. Comparing metabolic alterations in OSCC cells to the DOK cell line and the non-cancerous, Normal Oral Keratinocyte (NOK) cell line would provide more information on how CPt intervention and autophagy inhibition differs between tumour cells and healthy cells.

7.2.3 Development of chemoresistant models in OSCC cell lines of varying genotype and phenotypes.

Development of CPt-resistant cell lines from OSCC cell lines with a broad range of genetic and phenotypic variance (such as ATG and oncogene mutations) would allow for the verification of the hypothesis that inhibition of autophagy can re-sensitise resistant cells to CPt treatment. This has been shown in CPt-resistant urothelial cancer under CQ treatment[302]. Interestingly, it has been shown in breast cancer cells that CQ has an ability to sensitise cells to CPt independent of autophagy. CPt-resistant OSCC cell lines could provide a significant amount of information as to the cellular changes that occur as resistance forms and therefore, could provide information on how to prevent it.

7.2.4 Modulation of autophagy related genes in OSSC cell lines

By performing targeted silencing of distinct autophagy related genes such as LC3B or ATG8, a clear relationship between CPt treatment and autophagy could be identified in OSCC cells. This relationship could confirm if sensitisation to CPt can be achieved by autophagy inhibition. A genetic knockdown would also remove the off-target effects associated with CQ such as damage to the golgi apparatus and altered endosomal trafficking[165].

7.3 Conclusion of the Thesis

This study has provided novel data on the IC_{50} values of common chemotherapeutics in three OSCC cell lines and DOK cells. It has been shown that treatment of OSCC cells with CPt, CBDCA, and TXT induces autophagy to varying degrees in distinct OSCC cell lines and co-treatment with CPt and CQ can decrease cell viability in OSCC cell lines. Data presented has also shown that inhibition of autophagy increases CPt-mediated cell death by mitochondrial damage and that the *P53* status of cells may not be as integral to chemotherapeutic resistance was previously believed. Although a considerable amount of further study is required into the delicate relationship between chemotherapeutic intervention and autophagy, the research shown in this thesis has clearly shown that distinct OSCC cell lines have vastly different autophagic responses to chemotherapy and that these responses have unique impacts on oxidative phosphorylation. Further investigation into this relationship has the potential to reduce the risk of therapeutic compilations for OSCC patients and could significantly improve their

QOL after treatment is complete. By further exploring the genetic variations associated with OSCC and how these variations impact autophagy it is highly likely that it will be possible to prevent or reduce the abundance of recurring resistant tumours associated with OSCC. The research presented within this thesis forms a strong foundation for the continual investigation of the complex and dynamic relationship between oxidative phosphorylation and autophagy in oral squamous cell carcinoma.

Appendix I

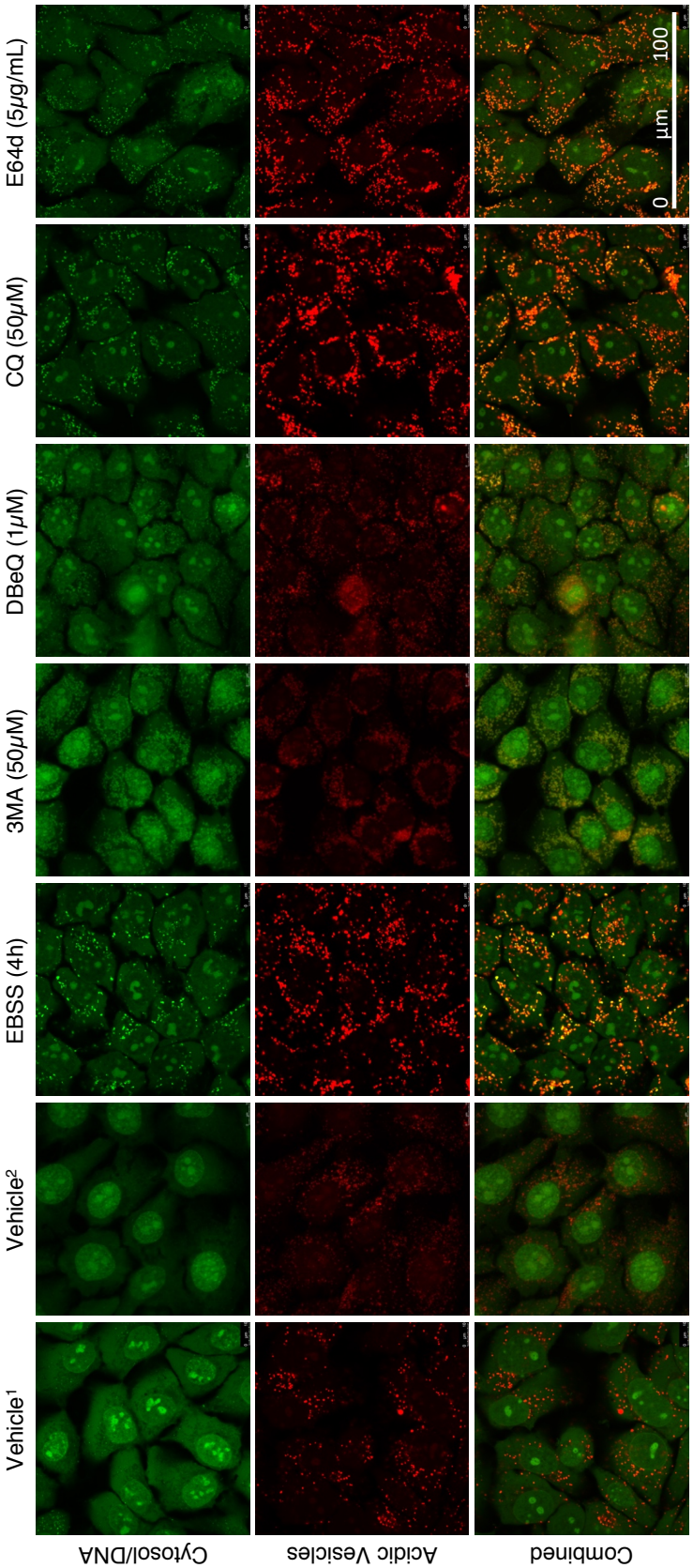

Figure 3.7 enlarged (for figure legend main text)

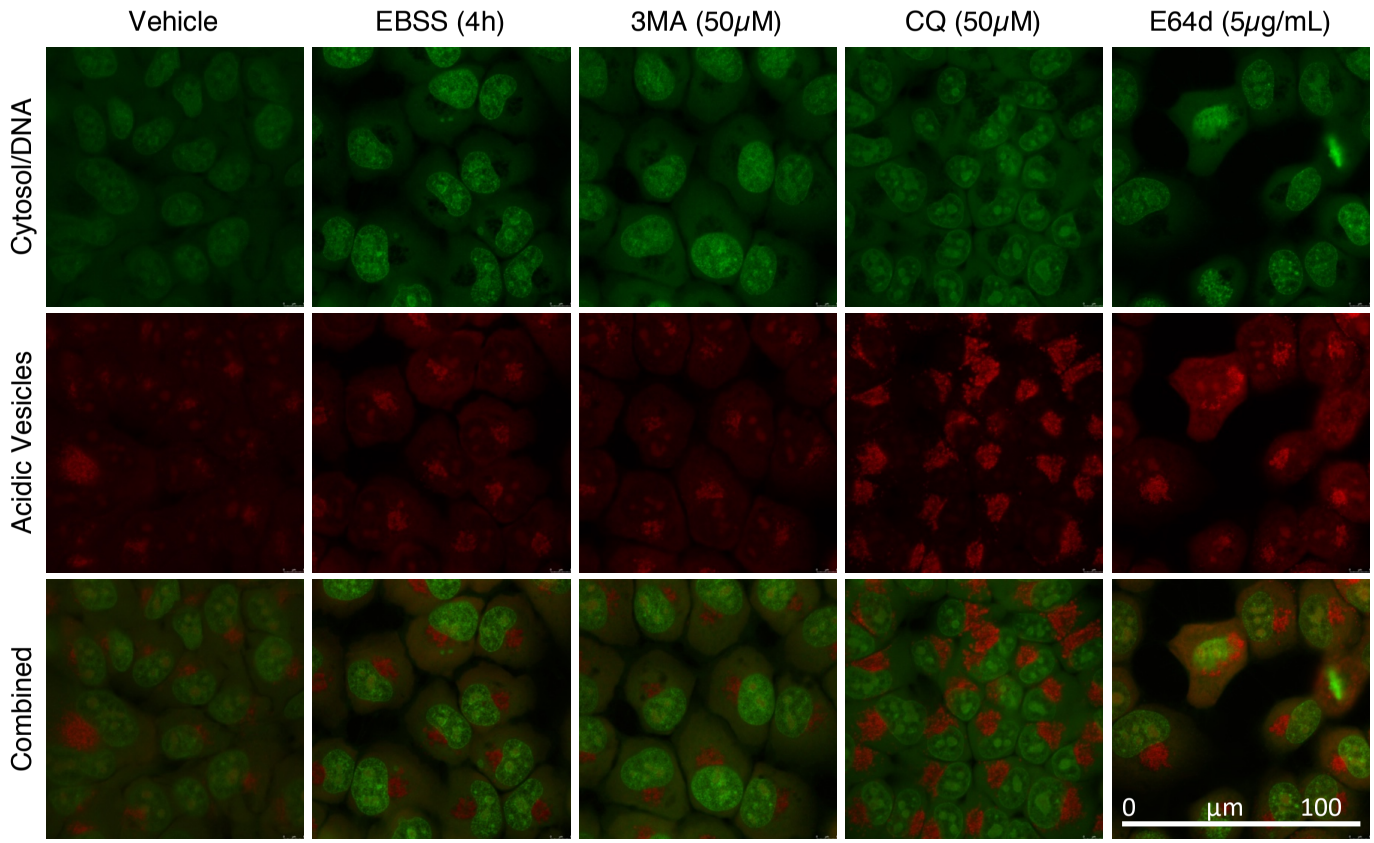

Figure 3.8 enlarged (for figure legend main text)

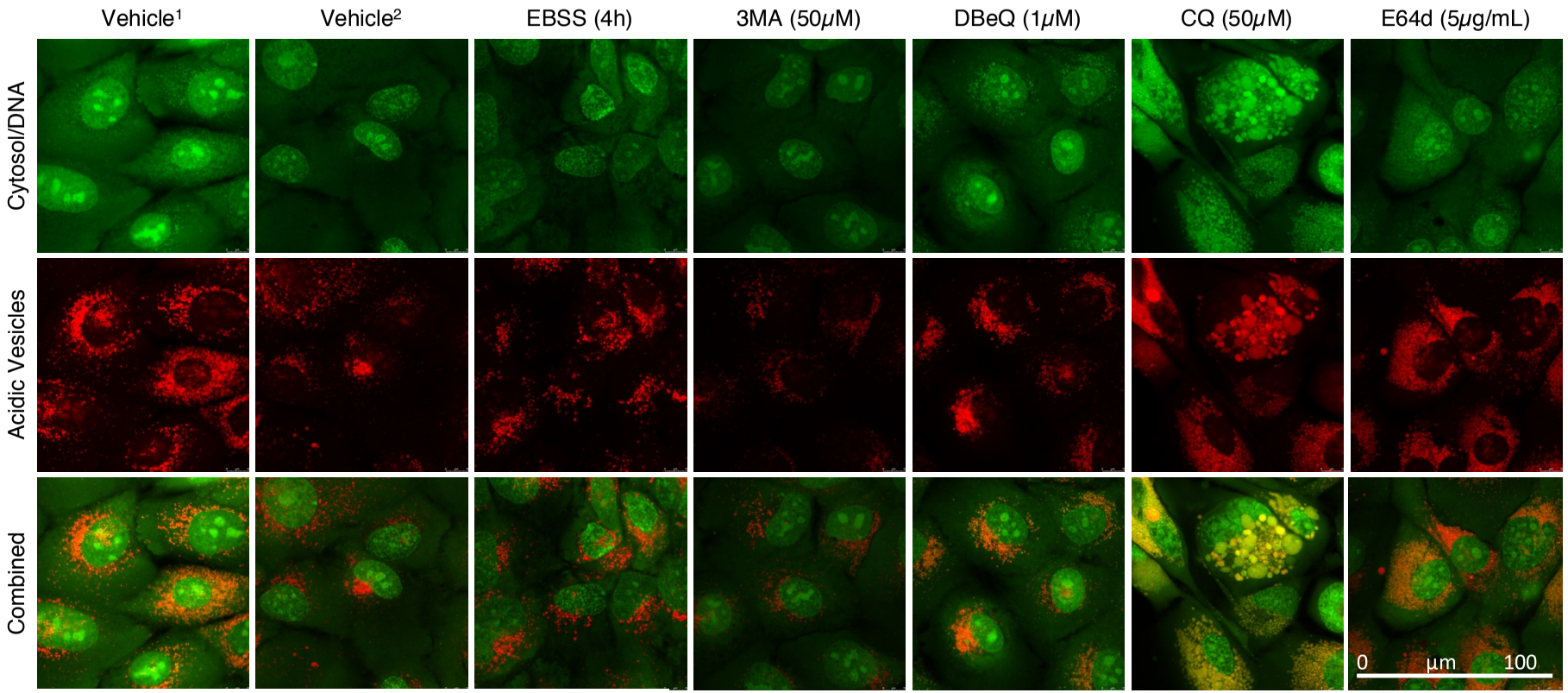

Figure 3.9 enlarged (for figure legend main text)

Figure 3.10 enlarged (for figure legend main text)

Bibliography

1. Jiang, P. & Mizushima, N. Autophagy and human diseases. *Cell Res* **24**, 69-79 (2014).

2. White, E. & DiPaola, R.S. The double-edged sword of autophagy modulation in cancer. *Clin Cancer Res* **15**, 5308-5316 (2009).

3. , Vol. 2019 https://www.wcrf.org/dietandcancer/cancer-trends/worldwide-cancer-data (World Cancer Research Fund, 2019).

4. Massano, J., Regateiro, F.S., Januário, G. & Ferreira, A. Oral squamous cell carcinoma: review of prognostic and predictive factors. *Oral Surg Oral Med Oral Pathol Oral Radiol Endod* **102**, 67-76 (2006).

5. Curado, M.P. & Hashibe, M. Recent changes in the epidemiology of head and neck cancer. *Current opinion in oncology* **21**, 194-200 (2009).

6. Jerjes, W. *et al.* Clinicopathological parameters, recurrence, locoregional and distant metastasis in 115 T1-T2 oral squamous cell carcinoma patients. *Head Neck Oncol* **2**, 9 (2010).

7. Gupta, S. Role of human papillomavirus in oral squamous cell carcinoma and oral potentially malignant disorders: A review of the literature. *Indian J Dent* **6**, 91-98 (2015).

8. Tezal, M. Interaction between Chronic Inflammation and Oral HPV Infection in the Etiology of Head and Neck Cancers. *Int J Otolaryngol* **2012** (2012).

9. Subapriya, R., Thangavelu, A., Mathavan, B., Ramachandran, C.R. & Nagini, S. Assessment of risk factors for oral squamous cell carcinoma in Chidambaram, Southern India: a case-control study. *European journal of cancer prevention : the official journal of the European Cancer Prevention Organisation (ECP)* **16**, 251-256 (2007).

10. Bouquot, J.E., Speight, P.M. & Farthing, P.M. Epithelial dysplasia of the oral mucosa—Diagnostic problems and prognostic features. *Current Diagnostic Pathology* **12**, 11-21 (2006).

11. Guneri, P. & Epstein, J.B. Late stage diagnosis of oral cancer: components and possible solutions, in *Oral Oncol*, Vol. 50 1131-1136 (2014 Elsevier Ltd, England; 2014).

12. Shukla, A. Potentially malignant disorders of the oral cavity: a clinical study. *Indian J Otolaryngol Head Neck Surg* **66**, 79-85 (2014).

13. van der Waal, I. Oral potentially malignant disorders: is malignant transformation predictable and preventable? *Med Oral Patol Oral Cir Bucal* **19**, e386-390 (2014).

14. Huber, M.A. & Tantiwongkosi, B. Oral and oropharyngeal cancer. *Med Clin North Am* **98**, 1299-1321 (2014).

15. Bessell, A. *et al.* Interventions for the treatment of oral and oropharyngeal cancers: surgical treatment. *Cochrane Database of Systematic Reviews* (2011).

16. Glenny, A. *et al.* Interventions for the treatment of oral cavity and oropharyngeal cancer: radiotherapy. *Cochrane Database of Systematic Reviews* (2010).

17. Furness, S. *et al.* Interventions for the treatment of oral cavity and oropharyngeal cancer: chemotherapy. *Cochrane Database of Systematic Reviews* (2010).

18. da Silva, S.D., Hier, M., Mlynarek, A., Kowalski, L.P. & Alaoui-Jamali, M.A. Recurrent oral cancer: current and emerging therapeutic approaches. *Front Pharmacol* **3**, 149 (2012).

19. Hanahan, D. & Weinberg, R.A. The hallmarks of cancer. *Cell* **100**, 57-70 (2000).

20. Hanahan, D. & Weinberg, R.A. Hallmarks of cancer: the next generation. *Cell* **144**, 646-674 (2011).

21. Moses, C., Garcia-Bloj, B., Harvey, A.R. & Blancafort, P. Hallmarks of cancer: The CRISPR generation, in *Eur J Cancer*, Vol. 93 10-18 (2018 The Author(s). Published by Elsevier Ltd., England; 2018).

22. WARBURG, O. On the origin of cancer cells. *Science* **123**, 309-314 (1956).

23. Vander Heiden, M.G., Cantley, L.C. & Thompson, C.B. Understanding the Warburg effect: the metabolic requirements of cell proliferation. *Science* **324**, 1029-1033 (2009).

24. Epstein, T., Xu, L., Gillies, R.J. & Gatenby, R.A. Separation of metabolic supply and demand: aerobic glycolysis as a normal physiological response to fluctuating energetic demands in the membrane. *Cancer Metab* **2**, 7 (2014).

25. Locasale, J.W. & Cantley, L.C. Metabolic flux and the regulation of mammalian cell growth. *Cell metabolism* **14**, 443-451 (2011).

26. Shestov, A.A. *et al.* Quantitative determinants of aerobic glycolysis identify flux through the enzyme GAPDH as a limiting step. *Elife* **3** (2014).

27. Boroughs, L.K. & DeBerardinis, R.J. Metabolic pathways promoting cancer cell survival and growth. *Nat Cell Biol* **17**, 351-359 (2015).

28. Ward, P.S. & Thompson, C.B. Metabolic reprogramming: a cancer hallmark even warburg did not anticipate. *Cancer Cell* **21**, 297-308 (2012).

29. Cascone, T. *et al.* Increased Tumor Glycolysis Characterizes Immune Resistance to Adoptive T Cell Therapy. *Cell metabolism* **27**, 977-987.e974 (2018).

30. Brand, A. *et al.* LDHA-Associated Lactic Acid Production Blunts Tumor Immunosurveillance by T and NK Cells. *Cell metabolism* **24**, 657-671 (2016).

31. Peng, W. *et al.* Loss of PTEN Promotes Resistance to T Cell-Mediated Immunotherapy. *Cancer Discov* **6**, 202-216 (2016).

32. Jiang, B. Aerobic glycolysis and high level of lactate in cancer metabolism and microenvironment. *Genes Dis* **4**, 25-27 (2017).

33. Gottfried, E. *et al.* Tumor-derived lactic acid modulates dendritic cell activation and antigen expression. *Blood* **107**, 2013-2021 (2006).

34. Todenhöfer, T. *et al.* Selective Inhibition of the Lactate Transporter MCT4 Reduces Growth of Invasive Bladder Cancer. *Mol Cancer Ther* **17**, 2746-2755 (2018).

35. Sonveaux, P. *et al.* Targeting the lactate transporter MCT1 in endothelial cells inhibits lactate-induced HIF-1 activation and tumor angiogenesis. *PLoS One* **7**, e33418 (2012).

36. Wellen, K.E. *et al.* ATP-citrate lyase links cellular metabolism to histone acetylation. *Science* **324**, 1076-1080 (2009).

37. Lee, M. & Yoon, J.H. Metabolic interplay between glycolysis and mitochondrial oxidation: The reverse Warburg effect and its therapeutic implication. *World J Biol Chem* **6**, 148-161 (2015).

38. D'Autréaux, B. & Toledano, M.B. ROS as signalling molecules: mechanisms that generate specificity in ROS homeostasis. *Nat Rev Mol Cell Biol* **8**, 813-824 (2007).

39. Tan, A.S. *et al.* Mitochondrial genome acquisition restores respiratory function and tumorigenic potential of cancer cells without mitochondrial DNA. *Cell metabolism* **21**, 81-94 (2015).

40. Distelmaier, F. *et al.* Trolox-sensitive reactive oxygen species regulate mitochondrial morphology, oxidative phosphorylation and cytosolic calcium handling in healthy cells. *Antioxidants & redox signaling* **17**, 1657-1669 (2012).

41. Koopman, W.J., Willems, P.H. & Smeitink, J.A. Monogenic mitochondrial disorders. *N Engl J Med* **366**, 1132-1141 (2012).

42. Pathak, R.U. & Davey, G.P. Complex I and energy thresholds in the brain. *Biochimica et Biophysica Acta (BBA) - Bioenergetics* **1777**, 777-782 (2008).

43. Webster, K.A. Mitochondrial membrane permeabilization and cell death during myocardial infarction: roles of calcium and reactive oxygen species. *Future Cardiol* **8**, 863-884 (2012).

44. Zhang, R. *et al.* Hirsutine induces mPTP-dependent apoptosis through ROCK1/PTEN/PI3K/GSK3β pathway in human lung cancer cells. *Cell Death Dis* **9**, 598 (2018).

45. Solaini, G., Sgarbi, G. & Baracca, A. Oxidative phosphorylation in cancer cells. *Biochim Biophys Acta* **1807**, 534-542 (2011).

46. Mathupala, S.P., Ko, Y.H. & Pedersen, P.L. The pivotal roles of mitochondria in cancer: Warburg and beyond and encouraging prospects for effective therapies. *Biochim Biophys Acta* **1797**, 1225-1230 (2010).

47. Reitzer, L.J., Wice, B.M. & Kennell, D. Evidence that glutamine, not sugar, is the major energy source for cultured HeLa cells. *J Biol Chem* **254**, 2669-2676 (1979).

48. Rossignol, R. *et al.* Energy substrate modulates mitochondrial structure and oxidative capacity in cancer cells. *Cancer Res* **64**, 985-993 (2004).

49. Mitri, Z., Constantine, T. & O'Regan, R. The HER2 Receptor in Breast Cancer: Pathophysiology, Clinical Use, and New Advances in Therapy. *Chemother Res Pract* **2012**, 743193 (2012).

50. Xu, J. & Lin, D.I. Oncogenic c-terminal cyclin D1 (CCND1) mutations are enriched in endometrioid endometrial adenocarcinomas. *PLoS One* **13**, e0199688 (2018).

51. Benzeno, S. *et al.* Identification of mutations that disrupt phosphorylation-dependent nuclear export of cyclin D1. *Oncogene* **25**, 6291-6303 (2006).

52. Sinevici, N. & O'sullivan, J. Oral cancer: Deregulated molecular events and their use as biomarkers. *Oral Oncol* **61**, 12-18 (2016).

53. Hobbs, G.A., Der, C.J. & Rossman, K.L. RAS isoforms and mutations in cancer at a glance. *J Cell Sci* **129**, 1287-1292 (2016).

54. Vélez-Cruz, R. & Johnson, D.G. The Retinoblastoma (RB) Tumor Suppressor: Pushing Back against Genome Instability on Multiple Fronts. *Int J Mol Sci* **18** (2017).

55. Sherr, C.J. & McCormick, F. The RB and p53 pathways in cancer. *Cancer Cell* **2**, 103-112 (2002).

56. Bensaad, K. *et al.* TIGAR, a p53-inducible regulator of glycolysis and apoptosis. *Cell* **126**, 107-120 (2006).

57. Kawauchi, K., Araki, K., Tobiume, K. & Tanaka, N. p53 regulates glucose metabolism through an IKK-NF-kappaB pathway and inhibits cell transformation. *Nat Cell Biol* **10**, 611-618 (2008).

58. Lane, D. & Levine, A. p53 Research: the past thirty years and the next thirty years. *Cold Spring Harb Perspect Biol* **2**, a000893 (2010).

59. Gnanapradeepan, K. *et al.* The p53 Tumor Suppressor in the Control of Metabolism and Ferroptosis. *Front Endocrinol (Lausanne)* **9**, 124 (2018).

60. Gualberto, A., Aldape, K., Kozakiewicz, K. & Tlsty, T.D. An oncogenic form of p53 confers a dominant, gain-of-function phenotype that disrupts spindle checkpoint control. *Proc Natl Acad Sci U S A* **95**, 5166-5171 (1998).

61. Muller, P.A., Vousden, K.H. & Norman, J.C. p53 and its mutants in tumor cell migration and invasion. *J Cell Biol* **192**, 209-218 (2011).

62. Fernald, K. & Kurokawa, M. Evading apoptosis in cancer. *Trends Cell Biol* **23**, 620-633 (2013).

63. Muller, P.A. & Vousden, K.H. p53 mutations in cancer. *Nat Cell Biol* **15**, 2-8 (2013).

64. Glick, D., Barth, S. & Macleod, K.F. Autophagy: cellular and molecular mechanisms. *J Pathol* **221**, 3-12 (2010).

65. Wu, W.K. *et al.* The autophagic paradox in cancer therapy. *Oncogene* **31**, 939-953 (2012).

66. Gupta, A. *et al.* Autophagy inhibition and antimalarials promote cell death in gastrointestinal stromal tumor (GIST). *Proc Natl Acad Sci U S A* **107**, 14333-14338 (2010).

67. Yu, L. *et al.* Termination of autophagy and reformation of lysosomes regulated by mTOR. *Nature* **465**, 942-946 (2010).

68. Wilkinson, S. & Ryan, K.M. Autophagy: an adaptable modifier of tumourigenesis. *Curr Opin Genet Dev* **20**, 57-64 (2010).

69. Shen, H.M. & Codogno, P. Autophagic cell death: Loch Ness monster or endangered species? *Autophagy* **7**, 457-465 (2011).

70. Jung, C.H. *et al.* ULK-Atg13-FIP200 complexes mediate mTOR signaling to the autophagy machinery. *Molecular biology of the cell* **20**, 1992-2003 (2009).

71. Yla-Anttila, P., Vihinen, H., Jokitalo, E. & Eskelinen, E.L. 3D tomography reveals connections between the phagophore and endoplasmic reticulum. *Autophagy* **5**, 1180-1185 (2009).

72. Funderburk, S.F., Wang, Q.J. & Yue, Z. The Beclin 1-VPS34 complex--at the crossroads of autophagy and beyond. *Trends Cell Biol* **20**, 355-362 (2010).

73. Romanov, J. *et al.* Mechanism and functions of membrane binding by the Atg5-Atg12/Atg16 complex during autophagosome formation. *EMBO J* **31**, 4304-4317 (2012).

74. Harrison, R.E., Bucci, C., Vieira, O.V., Schroer, T.A. & Grinstein, S. Phagosomes fuse with late endosomes and/or lysosomes by extension of membrane protrusions along microtubules: role of Rab7 and RILP. *Mol Cell Biol* **23**, 6494-6506 (2003).

75. Fader, C.M., Sánchez, D.G., Mestre, M.B. & Colombo, M.I. TI-VAMP/VAMP7 and VAMP3/cellubrevin: two v-SNARE proteins involved in specific steps of the autophagy/multivesicular body pathways. *Biochim Biophys Acta* **1793**, 1901-1916 (2009).

76. Nishida, Y. *et al.* Discovery of Atg5/Atg7-independent alternative macroautophagy. *Nature* **461**, 654-658 (2009).

77. Laplante, M. & Sabatini, D.M. mTOR signaling in growth control and disease. *Cell* **149**, 274-293 (2012).

78. Pattingre, S., Bauvy, C. & Codogno, P. Amino acids interfere with the ERK1/2-dependent control of macroautophagy by controlling the activation of Raf-1 in human colon cancer HT-29 cells. *J Biol Chem* **278**, 16667-16674 (2003).

79. Johansen, T. & Lamark, T. Selective autophagy mediated by autophagic adapter proteins. *Autophagy* **7**, 279-296 (2011).

80. Reggiori, F., Komatsu, M., Finley, K. & Simonsen, A. Selective types of autophagy. *Int J Cell Biol* **2012**, 156272 (2012).

81. Sánchez-Martín, P. & Komatsu, M. p62/SQSTM1 - steering the cell through health and disease. *J Cell Sci* **131** (2018).

82. Pankiv, S. *et al.* p62/SQSTM1 binds directly to Atg8/LC3 to facilitate degradation of ubiquitinated protein aggregates by autophagy. *J Biol Chem* **282**, 24131-24145 (2007).

83. Aichem, A. *et al.* The proteomic analysis of endogenous FAT10 substrates identifies p62/SQSTM1 as a substrate of FAT10ylation. *J Cell Sci* **125**, 4576-4585 (2012).

84. Mejlvang, J. *et al.* Starvation induces rapid degradation of selective autophagy receptors by endosomal microautophagy. *J Cell Biol* **217**, 3640-3655 (2018).

85. Yoshii, S.R. & Mizushima, N. Monitoring and Measuring Autophagy. *Int J Mol Sci* **18** (2017).

86. Lange, S. *et al.* The kinase domain of titin controls muscle gene expression and protein turnover. *Science* **308**, 1599-1603 (2005).

87. Mardakheh, F.K., Yekezare, M., Machesky, L.M. & Heath, J.K. Spred2 interaction with the late endosomal protein NBR1 down-regulates fibroblast growth factor receptor signaling. *J Cell Biol* **187**, 265-277 (2009).

88. Whitehouse, C.A. *et al.* Neighbor of Brca1 gene (Nbr1) functions as a negative regulator of postnatal osteoblastic bone formation and p38 MAPK activity. *Proc Natl Acad Sci U S A* **107**, 12913-12918 (2010).

89. Yang, J.Q., Liu, H., Diaz-Meco, M.T. & Moscat, J. NBR1 is a new PB1 signalling adapter in Th2 differentiation and allergic airway inflammation in vivo. *EMBO J* **29**, 3421-3433 (2010).

90. Aita, V.M. *et al.* Cloning and genomic organization of beclin 1, a candidate tumor suppressor gene on chromosome 17q21. *Genomics* **59**, 59-65 (1999).

91. Karantza-Wadsworth, V. *et al.* Autophagy mitigates metabolic stress and genome damage in mammary tumorigenesis. *Genes Dev* **21**, 1621-1635 (2007).

92. Mathew, R. *et al.* Autophagy suppresses tumorigenesis through elimination of p62. *Cell* **137**, 1062-1075 (2009).

93. Mathew, R. *et al.* Autophagy suppresses tumor progression by limiting chromosomal instability. *Genes Dev* **21**, 1367-1381 (2007).

94. Degenhardt, K. *et al.* Autophagy promotes tumor cell survival and restricts necrosis, inflammation, and tumorigenesis. *Cancer Cell* **10**, 51-64 (2006).

95. Sun, B. & Karin, M. NF-kappaB signaling, liver disease and hepatoprotective agents. *Oncogene* **27**, 6228-6244 (2008).

96. Liang, X.H. *et al.* Induction of autophagy and inhibition of tumorigenesis by beclin 1. *Nature* **402**, 672-676 (1999).

97. Park, S. *et al.* PI-103, a dual inhibitor of Class IA phosphatidylinositide 3-kinase and mTOR, has antileukemic activity in AML. *Leukemia* **22**, 1698-1706 (2008).

98. de Lima, T.B. *et al.* Autophagy analysis in oral carcinogenesis. *Pathol Res Pract* **213**, 1072-1077 (2017).

99. Lai, K. *et al.* Differences in LC3B expression and prognostic implications in oropharyngeal and oral cavity squamous cell carcinoma patients. *BMC Cancer* **18**, 624 (2018).

100. Terabe, T. *et al.* Expression of autophagy-related markers at the surgical margin of oral squamous cell carcinoma correlates with poor prognosis and tumor recurrence. *Hum Pathol* **73**, 156-163 (2018).

101. Marchand, B., Arsenault, D., Raymond-Fleury, A., Boisvert, F.M. & Boucher, M.J. Glycogen synthase kinase-3 (GSK3) inhibition induces prosurvival autophagic signals in human pancreatic cancer cells. *J Biol Chem* **290**, 5592-5605 (2015).

102. Mishra, R. Glycogen synthase kinase 3 beta: can it be a target for oral cancer. *Mol Cancer* **9**, 144 (2010).

103. Kühn, K. & Römer, W. Considering autophagy, β -Catenin and E-Cadherin as innovative therapy aspects in AML. *Cell Death Dis* **6**, e1950 (2015).

104. Chen, G. *et al.* Deregulation of Hexokinase II Is Associated with Glycolysis, Autophagy, and the Epithelial-Mesenchymal Transition in Tongue Squamous Cell Carcinoma under Hypoxia. *Biomed Res Int* **2018**, 8480762 (2018).

105. Chen, G. *et al.* Silencing PFKP inhibits starvation-induced autophagy, glycolysis, and epithelial mesenchymal transition in oral squamous cell carcinoma. *Exp Cell Res* (2018).

106. Nomura, H. *et al.* Overexpression and altered subcellular localization of autophagy-related 16-like 1 in human oral squamous-cell carcinoma: correlation with lymphovascular invasion and lymph-node metastasis. *Hum Pathol* **40**, 83-91 (2009).

107. Song, X. *et al.* ATG12 expression quantitative trait loci associated with head and neck squamous cell carcinoma risk in a Chinese Han population. *Mol Carcinog* (2018).

108. Wei, H. *et al.* Suppression of autophagy by FIP200 deletion inhibits mammary tumorigenesis. *Genes Dev* **25**, 1510-1527 (2011).

109. Takamura, A. *et al.* Autophagy-deficient mice develop multiple liver tumors. *Genes Dev* **25**, 795-800 (2011).

110. Fan, T.F. *et al.* Dihydromyricetin promotes autophagy and apoptosis through ROS-STAT3 signaling in head and neck squamous cell carcinoma. *Oncotarget* **7**, 59691-59703 (2016).

111. Tasdemir, E. *et al.* Regulation of autophagy by cytoplasmic p53. *Nat Cell Biol* **10**, 676-687 (2008).

112. Vera-Ramirez, L. & Hunter, K.W. Tumor cell dormancy as an adaptive cell stress response mechanism. *F1000Res* **6**, 2134 (2017).

113. Chaisuparat, R., Limpiwatana, S., Kongpanitkul, S., Yodsanga, S. & Jham, B.C. The Akt/mTOR pathway is activated in verrucous carcinoma of the oral cavity. *J Oral Pathol Med* **45**, 581-585 (2016).

114. Hong, K.O. *et al.* Inhibition of Akt activity induces the mesenchymal-to-epithelial reverting transition with restoring E-cadherin expression in KB and KOSCC-25B oral squamous cell carcinoma cells. *J Exp Clin Cancer Res* **28**, 28 (2009).

115. Pópulo, H., Lopes, J.M. & Soares, P. The mTOR signalling pathway in human cancer. *Int J Mol Sci* **13**, 1886-1918 (2012).

116. Sato, T., Nakashima, A., Guo, L., Coffman, K. & Tamanoi, F. Single amino-acid changes that confer constitutive activation of mTOR are discovered in human cancer. *Oncogene* **29**, 2746-2752 (2010).

117. Ilagan, E. & Manning, B.D. Emerging role of mTOR in the response to cancer therapeutics. *Trends Cancer* **2**, 241-251 (2016).

118. Arico, S. *et al.* The tumor suppressor PTEN positively regulates macroautophagy by inhibiting the phosphatidylinositol 3-

kinase/protein kinase B pathway. *J Biol Chem* **276**, 35243-35246 (2001).

119. Ueno, T. *et al.* Loss of Pten, a tumor suppressor, causes the strong inhibition of autophagy without affecting LC3 lipidation. *Autophagy* **4**, 692-700 (2008).

120. Dillon, L.M. & Miller, T.W. Therapeutic targeting of cancers with loss of PTEN function. *Current drug targets* **15**, 65-79 (2014).

121. Inoki, K., Li, Y., Zhu, T., Wu, J. & Guan, K.L. TSC2 is phosphorylated and inhibited by Akt and suppresses mTOR signalling. *Nat Cell Biol* **4**, 648-657 (2002).

122. Engelman, J.A., Luo, J. & Cantley, L.C. The evolution of phosphatidylinositol 3-kinases as regulators of growth and metabolism. *Nature reviews. Genetics* **7**, 606-619 (2006).

123. Samuels, Y. *et al.* High frequency of mutations of the PIK3CA gene in human cancers. *Science* **304**, 554 (2004).

124. Cage, T.A. *et al.* Downregulation of MYCN through PI3K Inhibition in Mouse Models of Pediatric Neural Cancer. *Front Oncol* **5**, 111 (2015).

125. Wang, L., Mosel, A.J., Oakley, G.G. & Peng, A. Deficient DNA damage signaling leads to chemoresistance to cisplatin in oral cancer. *Mol Cancer Ther* **11**, 2401-2409 (2012).

126. Bonneau, C. *et al.* Predictive markers of chemoresistance in advanced stages epithelial ovarian carcinoma. *Gynecologic oncology* **136**, 112-120 (2015).

127. López-Verdín, S. *et al.* Molecular Markers of Anticancer Drug Resistance in Head and Neck Squamous Cell Carcinoma: A Literature Review. *Cancers (Basel)* **10** (2018).

128. Gómez-Ruiz, S., Maksimović-Ivanić, D., Mijatović, S. & Kaluđerović, G.N. On the discovery, biological effects, and use of Cisplatin and metallocenes in anticancer chemotherapy. *Bioinorg Chem Appl* **2012**, 140284 (2012).

129. Dasari, S. & Tchounwou, P.B. Cisplatin in cancer therapy: molecular mechanisms of action. *Eur J Pharmacol* **740**, 364-378 (2014).

130. Tung, M.C. *et al.* Mutant p53 confers chemoresistance in non-small cell lung cancer by upregulating Nrf2. *Oncotarget* **6**, 41692-41705 (2015).

131. Lin, X. & Howell, S.B. DNA mismatch repair and p53 function are major determinants of the rate of development of cisplatin resistance. *Mol Cancer Ther* **5**, 1239-1247 (2006).

132. Perrone, F. *et al.* TP53 mutations and pathologic complete response to neoadjuvant cisplatin and fluorouracil chemotherapy in resected oral cavity squamous cell carcinoma. *J Clin Oncol* **28**, 761-766 (2010).

133. Cai, Y. *et al.* Inhibition of PI3K/Akt/mTOR signaling pathway enhances the sensitivity of the SKOV3/DDP ovarian cancer cell line to cisplatin in vitro. *Chin J Cancer Res* **26**, 564-572 (2014).

134. Chen, Y.S. *et al.* Autophagy inhibition contributes to radiation sensitization of esophageal squamous carcinoma cells. *Diseases of the esophagus : official journal of the International Society for Diseases of the Esophagus / I.S.D.E* **24**, 437-443 (2011).

135. Ma, C., Wang, J., Fan, L. & Guo, Y. Inhibition of CD147 expression promotes chemosensitivity in HNSCC cells by deactivating MAPK/ERK signaling pathway, in *Exp Mol Pathol*, Vol. 102 59-64 (2017. Published by Elsevier Inc., Netherlands; 2017).

136. Huang, Z. *et al.* Overexpression of CD147 contributes to the chemoresistance of head and neck squamous cell carcinoma cells. *J Oral Pathol Med* **42**, 541-546 (2013).

137. Klionsky, D.J. *et al.* Guidelines for the use and interpretation of assays for monitoring autophagy in higher eukaryotes. *Autophagy* **4**, 151-175 (2008).

138. Thomé, M.P. *et al.* Ratiometric analysis of Acridine Orange staining in the study of acidic organelles and autophagy. *J Cell Sci* **129**, 4622-4632 (2016).

139. Bhat, P. *et al.* Modulating autophagy in cancer therapy: Advancements and challenges for cancer cell death sensitization. *Biochem Pharmacol* **147**, 170-182 (2018).

140. Liu, W.J. *et al.* p62 links the autophagy pathway and the ubiqutin-proteasome system upon ubiquitinated protein degradation. *Cell Mol Biol Lett* **21**, 29 (2016).

141. Pircs, K. *et al.* Advantages and limitations of different p62-based assays for estimating autophagic activity in Drosophila. *PLoS One* **7**, e44214 (2012).

142. Sahani, M.H., Itakura, E. & Mizushima, N. Expression of the autophagy substrate SQSTM1/p62 is restored during prolonged

starvation depending on transcriptional upregulation and autophagy-derived amino acids. *Autophagy* **10**, 431-441 (2014).

143. Gubas, A. & Dikic, I. A guide to the regulation of selective autophagy receptors. *FEBS J* (2021).

144. Boya, P. *et al.* Inhibition of macroautophagy triggers apoptosis. *Mol Cell Biol* **25**, 1025-1040 (2005).

145. Li, D.D. *et al.* The inhibition of autophagy sensitises colon cancer cells with wild-type p53 but not mutant p53 to topotecan treatment. *PLoS One* **7**, e45058 (2012).

146. Sui, X. *et al.* Autophagy and chemotherapy resistance: a promising therapeutic target for cancer treatment. *Cell Death Dis* **4**, e838 (2013).

147. Jia, L. *et al.* In vitro and in vivo antitumor effects of chloroquine on oral squamous cell carcinoma. *Mol Med Rep* **16**, 5779-5786 (2017).

148. Circu, M. *et al.* Correction: Modulating lysosomal function through lysosome membrane permeabilization or autophagy suppression restores sensitivity to cisplatin in refractory non-small-cell lung cancer cells. *PLoS One* **13**, e0197016 (2018).

149. Quan, H.Y., Zhou, L.J., Li, A.D. & Zhang, Z.B. [Mechanism of chloroquine in promoting sensitivity of chemotherapeutics in oral squamous cell carcinoma CAL-27 cell line to cisplatin]. *Shanghai Kou Qiang Yi Xue* **24**, 30-36 (2015).

150. Zhao, X.G. *et al.* Chloroquine-enhanced efficacy of cisplatin in the treatment of hypopharyngeal carcinoma in xenograft mice. *PLoS One* **10**, e0126147 (2015).

151. Molenaar, R.J. *et al.* Study protocol of a phase IB/II clinical trial of metformin and chloroquine in patients with. *BMJ Open* **7**, e014961 (2017).

152. Chiu, Y.H. *et al.* Human non-small cell lung cancer cells can be sensitized to camptothecin by modulating autophagy. *Int J Oncol* **53**, 1967-1979 (2018).

153. Chen, Y. *et al.* Combining radiation with autophagy inhibition enhances suppression of tumor growth and angiogenesis in esophageal cancer. *Mol Med Rep* **12**, 1645-1652 (2015).

154. Zhang, R., Wang, R., Chen, Q. & Chang, H. Inhibition of autophagy using 3-methyladenine increases cisplatin-induced apoptosis by increasing endoplasmic reticulum stress in U251 human glioma cells. *Mol Med Rep* **12**, 1727-1732 (2015).

155. Shin, S.W., Kim, S.Y. & Park, J.W. Autophagy inhibition enhances ursolic acid-induced apoptosis in PC3 cells. *Biochim Biophys Acta* **1823**, 451-457 (2012).

156. Paglin, S. *et al.* A novel response of cancer cells to radiation involves autophagy and formation of acidic vesicles. *Cancer Res* **61**, 439-444 (2001).

157. Gottlieb, R.A., Andres, A.M., Sin, J. & Taylor, D.P. Untangling autophagy measurements: all fluxed up. *Circ Res* **116**, 504-514 (2015).

158. Duran, A. *et al.* p62 is a key regulator of nutrient sensing in the mTORC1 pathway. *Mol Cell* **44**, 134-146 (2011).

159. Zhang, Y. *et al.* Inhibition of Starvation-Triggered Endoplasmic Reticulum Stress, Autophagy, and Apoptosis in ARPE-19 Cells by Taurine through Modulating the Expression of Calpain-1 and Calpain-2. *Int J Mol Sci* **18** (2017).

160. Gruppuso, P.A., Boylan, J.M. & Sanders, J.A. The physiology and pathophysiology of rapamycin resistance: implications for cancer. *Cell Cycle* **10**, 1050-1058 (2011).

161. Ju, J.S., Varadhachary, A.S., Miller, S.E. & Weihl, C.C. Quantitation of "autophagic flux" in mature skeletal muscle. *Autophagy* **6**, 929-935 (2010).

162. Maeda, Y. & Kinoshita, T. The acidic environment of the Golgi is critical for glycosylation and transport. *Methods Enzymol* **480**, 495-510 (2010).

163. Thorens, B. & Vassalli, P. Chloroquine and ammonium chloride prevent terminal glycosylation of immunoglobulins in plasma cells without affecting secretion. *Nature* **321**, 618-620 (1986).

164. Gomes-da-Silva, L.C. *et al.* Recruitment of LC3 to damaged Golgi apparatus. *Cell Death Differ* **26**, 1467-1484 (2019).

165. Mauthe, M. *et al.* Chloroquine inhibits autophagic flux by decreasing autophagosome-lysosome fusion. *Autophagy* **14**, 1435-1455 (2018).

166. Kimura, S., Noda, T. & Yoshimori, T. Dissection of the autophagosome maturation process by a novel reporter protein, tandem fluorescent-tagged LC3. *Autophagy* **3**, 452-460 (2007).

167. Tasdemir, E. *et al.* Cell cycle-dependent induction of autophagy, mitophagy and reticulophagy. *Cell Cycle* **6**, 2263-2267 (2007).

168. Han, L. *et al.* Autophagy flux inhibition, G2/M cell cycle arrest and apoptosis induction by ubenimex in glioma cell lines. *Oncotarget* **8**, 107730-107743 (2017).

169. Liu, Q. *et al.* Effect of autophagy inhibition on cell viability and cell cycle progression in MDA-MB-231 human breast cancer cells. *Mol Med Rep* **10**, 625-630 (2014).

170. Zou, Y. *et al.* The autophagy inhibitor chloroquine overcomes the innate resistance of wild-type EGFR non-small-cell lung cancer cells to erlotinib. *J Thorac Oncol* **8**, 693-702 (2013).

171. Sherman, M.Y., Sherman, M., Gabai, V., O'Callaghan, C. & Yaglom, J. Molecular chaperones regulate p53 and suppress senescence programs. *FEBS Lett* **581**, 3711-3715 (2007).

172. Nordstrøm, L.U. *et al.* Discovery of autophagy inhibitors with antiproliferative activity in lung and pancreatic cancer cells. *ACS Med Chem Lett* **6**, 134-139 (2015).

173. Hwang, J.R. *et al.* Chloroquine reverses chemoresistance via upregulation of p21. *Cell Death Dis* **11**, 1034 (2020).

174. Li, R., Waga, S., Hannon, G.J., Beach, D. & Stillman, B. Differential effects by the p21 CDK inhibitor on PCNA-dependent DNA replication and repair. *Nature* **371**, 534-537 (1994).

175. Abbas, T. & Dutta, A. p21 in cancer: intricate networks and multiple activities. *Nat Rev Cancer* **9**, 400-414 (2009).

176. Bray, F. *et al.* Global cancer statistics 2018: GLOBOCAN estimates of incidence and mortality worldwide for 36 cancers in 185 countries. *CA Cancer J Clin* **68**, 394-424 (2018).

177. Fenn, J.E. & Udelsman, R. First use of intravenous chemotherapy cancer treatment: rectifying the record. *J Am Coll Surg* **212**, 413-417 (2011).

178. Peyrone, M. Ueber die Einwirkung des Ammoniaks auf Platinchlorür. *Justus Liebigs Annalen der Chemie* **51**, 1-29 (1844).

179. Raja, W., Mir, M.H., Dar, I., Banday, M.A. & Ahmad, I. Cisplatin induced paroxysmal supraventricular tachycardia. *Indian J Med Paediatr Oncol* **34**, 330-332 (2013).

180. Niculescu-Duvaz, I. Technology evaluation: gemtuzumab ozogamicin, Celltech Group. *Curr Opin Mol Ther* **2**, 691-696 (2000).

181. Goodsell, D.S. The molecular perspective: Cisplatin. *Stem Cells* **24**, 514-515 (2006).

182. Longley, D.B., Harkin, D.P. & Johnston, P.G. 5-fluorouracil: mechanisms of action and clinical strategies. *Nat Rev Cancer* **3**, 330-338 (2003).

183. Pienta, K.J. Preclinical mechanisms of action of docetaxel and docetaxel combinations in prostate cancer. *Semin Oncol* **28**, 3-7 (2001).

184. Yang, C., Kaushal, V., Shah, S.V. & Kaushal, G.P. Autophagy is associated with apoptosis in cisplatin injury to renal tubular epithelial cells. *Am J Physiol Renal Physiol* **294**, F777-787 (2008).

185. Wahba, J. *et al.* Chemotherapy-induced apoptosis, autophagy and cell cycle arrest are key drivers of synergy in chemo-immunotherapy of epithelial ovarian cancer. *Cancer Immunol Immunother* **67**, 1753-1765 (2018).

186. Duan, G. *et al.* Increased Autophagy Levels Mediate Cisplatin Resistance in Cisplatin-Resistant Cells While Also Rendering Them Vulnerable to Autophagy Induction. *Biomed Res Int* **2018**, 1736738 (2018).

187. Chen, J. *et al.* Inhibition of autophagy promotes cisplatin-induced apoptotic cell death through Atg5 and Beclin 1 in A549 human lung cancer cells. *Mol Med Rep* **17**, 6859-6865 (2018).

188. Liu, D., Yang, Y., Liu, Q. & Wang, J. Inhibition of autophagy by 3-MA potentiates cisplatin-induced apoptosis in esophageal squamous cell carcinoma cells. *Med Oncol* **28**, 105-111 (2011).

189. Sasaki, K. *et al.* Chloroquine potentiates the anti-cancer effect of 5-fluorouracil on colon cancer cells. *BMC Cancer* **10**, 370 (2010).

190. Holoye, P.Y. *et al.* Randomized study of adjuvant chemotherapy for head and neck cancer. *Otolaryngol Head Neck Surg* **93**, 712-717 (1985).

191. Ervin, T.J. *et al.* An analysis of induction and adjuvant chemotherapy in the multidisciplinary treatment of squamous-cell carcinoma of the head and neck. *J Clin Oncol* **5**, 10-20 (1987).

192. Shimanishi, M. *et al.* Silencing of GLUT-1 inhibits sensitization of oral cancer cells to cisplatin during hypoxia. *J Oral Pathol Med* **42**, 382-388 (2013).

193. Naik, P.P. *et al.* Autophagy regulates cisplatin-induced stemness and chemoresistance via the upregulation of CD44, ABCB1 and ADAM17 in oral squamous cell carcinoma. *Cell Prolif* **51** (2018).

194. Li, S., Wu, Y., Ding, Y., Yu, M. & Ai, Z. CerS6 regulates cisplatin resistance in oral squamous cell carcinoma by altering mitochondrial fission and autophagy. *J Cell Physiol* **233**, 9416-9425 (2018).

195. Feng, Y. *et al.* Autophagy Inhibitor (LY294002) and 5-fluorouracil (5-FU) Combination-Based Nanoliposome for Enhanced Efficacy Against Esophageal Squamous Cell Carcinoma. *Nanoscale Res Lett* **13**, 325 (2018).

196. Köberle, B. *et al.* DNA repair capacity and cisplatin sensitivity of human testis tumour cells. *Int J Cancer* **70**, 551-555 (1997).

197. Lynch, H.T., Lynch, J.F., Lynch, P.M. & Attard, T. Hereditary colorectal cancer syndromes: molecular genetics, genetic counseling, diagnosis and management. *Fam Cancer* **7**, 27-39 (2008).

198. Kislukhin, G., Murphy, M.L., Jafari, M. & Long, A.D. Chemotherapy-induced toxicity is highly heritable in Drosophila melanogaster. *Pharmacogenet Genomics* **22**, 285-289 (2012).

199. Moen, E.L., Godley, L.A., Zhang, W. & Dolan, M.E. Pharmacogenomics of chemotherapeutic susceptibility and toxicity. *Genome Med* **4**, 90 (2012).

200. Galletti, E., Magnani, M., Renzulli, M.L. & Botta, M. Paclitaxel and docetaxel resistance: molecular mechanisms and development of new generation taxanes. *ChemMedChem* **2**, 920-942 (2007).

201. Petrini, M. *et al.* Reversing of chlorambucil resistance by ethacrynic acid in a B-CLL patient. *Br J Haematol* **85**, 409-410 (1993).

202. Lee, E.K., Regenold, W.T. & Shapiro, P. Inhibition of aldose reductase enhances HeLa cell sensitivity to chemotherapeutic drugs and involves activation of extracellular signal-regulated kinases. *Anticancer Drugs* **13**, 859-868 (2002).

203. Sax, J.K. *et al.* BID regulation by p53 contributes to chemosensitivity. *Nat Cell Biol* **4**, 842-849 (2002).

204. Cabelguenne, A. *et al.* p53 alterations predict tumor response to neoadjuvant chemotherapy in head and neck squamous cell carcinoma: a prospective series. *J Clin Oncol* **18**, 1465-1473 (2000).

205. Bradford, C.R. *et al.* P53 mutation correlates with cisplatin sensitivity in head and neck squamous cell carcinoma lines. *Head Neck* **25**, 654-661 (2003).

206. Koch, W.M. *et al.* p53 mutation and locoregional treatment failure in head and neck squamous cell carcinoma. *J Natl Cancer Inst* **88**, 1580-1586 (1996).

207. Lee, S.J. *et al.* A functional role for the p62-ERK1 axis in the control of energy homeostasis and adipogenesis. *EMBO Rep* **11**, 226-232 (2010).

208. Puls, A., Schmidt, S., Grawe, F. & Stabel, S. Interaction of protein kinase C zeta with ZIP, a novel protein kinase C-binding protein. *Proc Natl Acad Sci U S A* **94**, 6191-6196 (1997).

209. Sanchez, P., De Carcer, G., Sandoval, I.V., Moscat, J. & Diaz-Meco, M.T. Localization of atypical protein kinase C isoforms into lysosome-targeted endosomes through interaction with p62. *Mol Cell Biol* **18**, 3069-3080 (1998).

210. Sanz, L., Diaz-Meco, M.T., Nakano, H. & Moscat, J. The atypical PKC-interacting protein p62 channels NF-kappaB activation by the IL-1-TRAF6 pathway. *EMBO J* **19**, 1576-1586 (2000).

211. Komatsu, M. *et al.* The selective autophagy substrate p62 activates the stress responsive transcription factor Nrf2 through inactivation of Keap1. *Nat Cell Biol* **12**, 213-223 (2010).

212. Jin, Z. *et al.* Cullin3-based polyubiquitination and p62-dependent aggregation of caspase-8 mediate extrinsic apoptosis signaling. *Cell* **137**, 721-735 (2009).

213. Alegre, F. *et al.* Role of p62/SQSTM1 beyond autophagy: a lesson learned from drug-induced toxicity in vitro. *Br J Pharmacol* **175**, 440-455 (2018).

214. Engedal, N. & Seglen, P.O. Autophagy of cytoplasmic bulk cargo does not require LC3. *Autophagy* **12**, 439-441 (2016).

215. Szalai, P. *et al.* Autophagic bulk sequestration of cytosolic cargo is independent of LC3, but requires GABARAPs. *Exp Cell Res* **333**, 21-38 (2015).

216. Yousefi, S. *et al.* Calpain-mediated cleavage of Atg5 switches autophagy to apoptosis. *Nat Cell Biol* **8**, 1124-1132 (2006).

217. Norman, J.M., Cohen, G.M. & Bampton, E.T. The in vitro cleavage of the hAtg proteins by cell death proteases. *Autophagy* **6**, 1042-1056 (2010).

218. Wong, C.H. *et al.* Simultaneous induction of non-canonical autophagy and apoptosis in cancer cells by ROS-dependent ERK and JNK activation. *PLoS One* **5**, e9996 (2010).

219. Antonietti, P. *et al.* AT-101 simultaneously triggers apoptosis and a cytoprotective type of autophagy irrespective of expression levels and the subcellular localization of Bcl-xL and Bcl-2 in MCF7 cells. *Biochim Biophys Acta* **1863**, 499-509 (2016).

220. Kenzelmann Broz, D. *et al.* Global genomic profiling reveals an extensive p53-regulated autophagy program contributing to key p53 responses. *Genes Dev* **27**, 1016-1031 (2013).

221. Crighton, D. *et al.* DRAM, a p53-induced modulator of autophagy, is critical for apoptosis. *Cell* **126**, 121-134 (2006).

222. Qu, X. *et al.* Autophagy inhibitor chloroquine increases sensitivity to cisplatin in QBC939 cholangiocarcinoma cells by mitochondrial ROS. *PLoS One* **12**, e0173712 (2017).

223. Nikoletopoulou, V., Markaki, M., Palikaras, K. & Tavernarakis, N. Crosstalk between apoptosis, necrosis and autophagy. *Biochim Biophys Acta* **1833**, 3448-3459 (2013).

224. Betin, V.M. & Lane, J.D. Caspase cleavage of Atg4D stimulates GABARAP-L1 processing and triggers mitochondrial targeting and apoptosis. *J Cell Sci* **122**, 2554-2566 (2009).

225. Luo, S. & Rubinsztein, D.C. Apoptosis blocks Beclin 1-dependent autophagosome synthesis: an effect rescued by Bcl-xL. *Cell Death Differ* **17**, 268-277 (2010).

226. Pattingre, S. *et al.* Bcl-2 antiapoptotic proteins inhibit Beclin 1-dependent autophagy. *Cell* **122**, 927-939 (2005).

227. Fridman, J.S. & Lowe, S.W. Control of apoptosis by p53. *Oncogene* **22**, 9030-9040 (2003).

228. Feng, Z., Zhang, H., Levine, A.J. & Jin, S. The coordinate regulation of the p53 and mTOR pathways in cells. *Proc Natl Acad Sci U S A* **102**, 8204-8209 (2005).

229. Castedo, M., Ferri, K.F. & Kroemer, G. Mammalian target of rapamycin (mTOR): pro- and anti-apoptotic. *Cell Death Differ* **9**, 99-100 (2002).

230. Gozuacik, D. *et al.* DAP-kinase is a mediator of endoplasmic reticulum stress-induced caspase activation and autophagic cell death. *Cell Death Differ* **15**, 1875-1886 (2008).

231. Bonapace, L. *et al.* Induction of autophagy-dependent necroptosis is required for childhood acute lymphoblastic leukemia cells to overcome glucocorticoid resistance. *J Clin Invest* **120**, 1310-1323 (2010).

232. Farkas, T., Daugaard, M. & Jäättelä, M. Identification of small molecule inhibitors of phosphatidylinositol 3-kinase and autophagy. *J Biol Chem* **286**, 38904-38912 (2011).

233. Wu, Y.T. *et al.* Autophagy plays a protective role during zVAD-induced necrotic cell death. *Autophagy* **4**, 457-466 (2008).

234. Gwinn, D.M. *et al.* AMPK phosphorylation of raptor mediates a metabolic checkpoint. *Mol Cell* **30**, 214-226 (2008).

235. Kim, J., Kundu, M., Viollet, B. & Guan, K.L. AMPK and mTOR regulate autophagy through direct phosphorylation of Ulk1. *Nat Cell Biol* **13**, 132-141 (2011).

236. Los, M. *et al.* Activation and caspase-mediated inhibition of PARP: a molecular switch between fibroblast necrosis and apoptosis in death receptor signaling. *Molecular biology of the cell* **13**, 978-988 (2002).

237. Zong, W.X., Ditsworth, D., Bauer, D.E., Wang, Z.Q. & Thompson, C.B. Alkylating DNA damage stimulates a regulated form of necrotic cell death. *Genes Dev* **18**, 1272-1282 (2004).

238. Xiaoyu, H. *et al.* The mTOR Pathway Regulates PKM2 to Affect Glycolysis in Esophageal Squamous Cell Carcinoma. *Technol Cancer Res Treat* **17**, 1533033818780063 (2018).

239. Watson, A.S. *et al.* Autophagy limits proliferation and glycolytic metabolism in acute myeloid leukemia. *Cell Death Discov* **1** (2015).

240. Mi, C. *et al.* 4′,6-dihydroxy-4-methoxyisoaurone inhibits the HIF-1α pathway through inhibition of Akt/mTOR/p70S6K/4E-BP1 phosphorylation. *J Pharmacol Sci* **125**, 193-201 (2014).

241. Jiao, L. *et al.* Regulation of glycolytic metabolism by autophagy in liver cancer involves selective autophagic degradation of HK2 (hexokinase 2). *Autophagy* **14**, 671-684 (2018).

242. Filomeni, G., Desideri, E., Cardaci, S., Rotilio, G. & Ciriolo, M.R. Under the ROS…thiol network is the principal suspect for autophagy commitment. *Autophagy* **6**, 999-1005 (2010).

243. Ding, W.X. & Yin, X.M. Mitophagy: mechanisms, pathophysiological roles, and analysis. *Biol Chem* **393**, 547-564 (2012).

244. Scherz-Shouval, R. & Elazar, Z. ROS, mitochondria and the regulation of autophagy. *Trends Cell Biol* **17**, 422-427 (2007).

245. Chen, Y., Azad, M.B. & Gibson, S.B. Superoxide is the major reactive oxygen species regulating autophagy. *Cell Death Differ* **16**, 1040-1052 (2009).

246. Jaggi, M., Du, C., Zhang, W. & Balaji, K.C. Protein kinase D1: a protein of emerging translational interest. *Front Biosci* **12**, 3757-3767 (2007).

247. Eisenberg-Lerner, A. & Kimchi, A. PKD is a kinase of Vps34 that mediates ROS-induced autophagy downstream of DAPk. *Cell Death Differ* **19**, 788-797 (2012).

248. Zalckvar, E. *et al.* DAP-kinase-mediated phosphorylation on the BH3 domain of beclin 1 promotes dissociation of beclin 1 from Bcl-XL and induction of autophagy. *EMBO Rep* **10**, 285-292 (2009).

249. Eisenberg-Lerner, A. & Kimchi, A. DAP kinase regulates JNK signaling by binding and activating protein kinase D under oxidative stress. *Cell Death Differ* **14**, 1908-1915 (2007).

250. da-Silva, W.S. *et al.* Mitochondrial bound hexokinase activity as a preventive antioxidant defense: steady-state ADP formation as a regulatory mechanism of membrane potential and reactive oxygen species generation in mitochondria. *J Biol Chem* **279**, 39846-39855 (2004).

251. Wang, R.C. *et al.* Akt-mediated regulation of autophagy and tumorigenesis through Beclin 1 phosphorylation. *Science* **338**, 956-959 (2012).

252. Oude Ophuis, R.J. *et al.* A tail-anchored myotonic dystrophy protein kinase isoform induces perinuclear clustering of mitochondria, autophagy, and apoptosis. *PLoS One* **4**, e8024 (2009).

253. Chude, C.I. & Amaravadi, R.K. Targeting Autophagy in Cancer: Update on Clinical Trials and Novel Inhibitors. *Int J Mol Sci* **18** (2017).

254. Verbaanderd, C. *et al.* Repurposing Drugs in Oncology (ReDO)-chloroquine and hydroxychloroquine as anti-cancer agents. *Ecancermedicalscience* **11**, 781 (2017).

255. Briceño, E., Calderon, A. & Sotelo, J. Institutional experience with chloroquine as an adjuvant to the therapy for glioblastoma multiforme. *Surg Neurol* **67**, 388-391 (2007).

256. Chi, K.H. *et al.* Addition of rapamycin and hydroxychloroquine to metronomic chemotherapy as a second line treatment results in high salvage rates for refractory metastatic solid tumors: a pilot

safety and effectiveness analysis in a small patient cohort. *Oncotarget* **6**, 16735-16745 (2015).

257. Zhu, J., Zheng, Y., Zhang, H. & Sun, H. Low concentration of chloroquine enhanced efficacy of cisplatin in the treatment of human ovarian cancer dependent on autophagy. *Am J Transl Res* **9**, 4046-4058 (2017).

258. Qin, L. *et al.* Chloroquine enhances the efficacy of cisplatin by suppressing autophagy in human adrenocortical carcinoma treatment. *Drug Des Devel Ther* **10**, 1035-1045 (2016).

259. Kim, E.L. *et al.* Chloroquine activates the p53 pathway and induces apoptosis in human glioma cells. *Neuro Oncol* **12**, 389-400 (2010).

260. Lock, R. *et al.* Autophagy facilitates glycolysis during Ras-mediated oncogenic transformation. *Molecular biology of the cell* **22**, 165-178 (2011).

261. Strohecker, A.M. *et al.* Autophagy sustains mitochondrial glutamine metabolism and growth of BrafV600E-driven lung tumors. *Cancer Discov* **3**, 1272-1285 (2013).

262. Guo, J.Y. *et al.* Activated Ras requires autophagy to maintain oxidative metabolism and tumorigenesis. *Genes Dev* **25**, 460-470 (2011).

263. Galluzzi, L., Pietrocola, F., Levine, B. & Kroemer, G. Metabolic control of autophagy. *Cell* **159**, 1263-1276 (2014).

264. Zhou, Y. *et al.* Intracellular ATP levels are a pivotal determinant of chemoresistance in colon cancer cells. *Cancer Res* **72**, 304-314 (2012).

265. Liang, D.H. *et al.* The autophagy inhibitor chloroquine targets cancer stem cells in triple negative breast cancer by inducing mitochondrial damage and impairing DNA break repair. *Cancer Lett* **376**, 249-258 (2016).

266. Zhang, N. *et al.* Chloroquine sensitizes hepatocellular carcinoma cells to chemotherapy via blocking autophagy and promoting mitochondrial dysfunction. *Int J Clin Exp Pathol* **10**, 10056-10065 (2017).

267. Vessoni, A.T. *et al.* Chloroquine-induced glioma cells death is associated with mitochondrial membrane potential loss, but not oxidative stress. *Free Radic Biol Med* **90**, 91-100 (2016).

268. Li, P.F., Dietz, R. & von Harsdorf, R. p53 regulates mitochondrial membrane potential through reactive oxygen species and induces cytochrome c-independent apoptosis blocked by Bcl-2. *EMBO J* **18**, 6027-6036 (1999).

269. Sionov, R.V. & Haupt, Y. The cellular response to p53: the decision between life and death. *Oncogene* **18**, 6145-6157 (1999).

270. O'Hagan, H.M. & Ljungman, M. Nuclear accumulation of p53 following inhibition of transcription is not due to diminished levels of MDM2. *Oncogene* **23**, 5505-5512 (2004).

271. Lakin, N.D. & Jackson, S.P. Regulation of p53 in response to DNA damage. *Oncogene* **18**, 7644-7655 (1999).

272. Ozaki, T. & Nakagawara, A. Role of p53 in Cell Death and Human Cancers. *Cancers (Basel)* **3**, 994-1013 (2011).

273. Singh, R.D., Patel, K.R. & Patel, P.S. "p53 mutation spectrum and its role in prognosis of oral cancer patients: A study from Gujarat, West India". *Mutat Res* **783**, 15-26 (2016).

274. Faden, D.L. *et al.* Targeted next-generation sequencing of TP53 in oral tongue carcinoma from non-smokers. *J Otolaryngol Head Neck Surg* **45**, 47 (2016).

275. Lapke, N. *et al.* Missense mutations in the TP53 DNA-binding domain predict outcomes in patients with advanced oral cavity squamous cell carcinoma. *Oncotarget* **7**, 44194-44210 (2016).

276. Wu , Y., Mehew, J.W., Heckman, C.A., Arcinas, M. & Boxer, L.M. Negative regulation of bcl-2 expression by p53 in hematopoietic cells. *Oncogene* **20**, 240-251 (2001).

277. Mrakovcic, M. & Fröhlich, L.F. p53-Mediated Molecular Control of Autophagy in Tumor Cells. *Biomolecules* **8** (2018).

278. Feng, Z. p53 regulation of the IGF-1/AKT/mTOR pathways and the endosomal compartment. *Cold Spring Harb Perspect Biol* **2**, a001057 (2010).

279. Levine, A.J., Feng, Z., Mak, T.W., You, H. & Jin, S. Coordination and communication between the p53 and IGF-1-AKT-TOR signal transduction pathways. *Genes Dev* **20**, 267-275 (2006).

280. Singh, B. *et al.* p53 regulates cell survival by inhibiting PIK3CA in squamous cell carcinomas. *Genes Dev* **16**, 984-993 (2002).

281. Morgan, M.J. *et al.* Regulation of autophagy and chloroquine sensitivity by oncogenic RAS in vitro is context-dependent. *Autophagy* **10**, 1814-1826 (2014).

282. Choi, Y.M. *et al.* Mechanism of Cisplatin-Induced Cytotoxicity Is Correlated to Impaired Metabolism Due to Mitochondrial ROS Generation. *PLoS One* **10**, e0135083 (2015).

283. Cruz-Bermúdez, A. *et al.* Cisplatin resistance involves a metabolic reprogramming through ROS and PGC-1 α in NSCLC which can be overcome by OXPHOS inhibition. *Free Radic Biol Med* **135**, 167-181 (2019).

284. Higuchi, E. *et al.* Differentially expressed genes associated with CIS-diamminedichloroplatinum (II) resistance in head and neck cancer using differential display and CDNA microarray. *Head Neck* **25**, 187-193 (2003).

285. Zhang, X. & Liu, Q. Autophagy Assays (LC3B immunofluorescence, LC3B western blot, acridine orange assay). *Bio-protocol* **3**, e1012

C1011 - Bio-protocol 2013;1013:e1012 (2013).

286. Klionsky, D.J. *et al.* Guidelines for the use and interpretation of assays for monitoring autophagy (3rd edition). *Autophagy* **12**, 1-222 (2016).

287. Yun, C.W. & Lee, S.H. The Roles of Autophagy in Cancer. *Int J Mol Sci* **19** (2018).

288. Sakakura, K. *et al.* Immunological significance of the accumulation of autophagy components in oral squamous cell carcinoma. *Cancer Sci* **106**, 1-8 (2015).

289. Tang, J.Y. *et al.* Immunopositivity of Beclin-1 and ATG5 as indicators of survival and disease recurrence in oral squamous cell carcinoma. *Anticancer Res* **33**, 5611-5616 (2013).

290. Zhang, L. *et al.* Dual induction of apoptotic and autophagic cell death by targeting survivin in head neck squamous cell carcinoma. *Cell Death Dis* **6**, e1771 (2015).

291. Yen, C.Y. *et al.* Long-term stimulation of areca nut components results in increased chemoresistance through elevated autophagic activity. *J Oral Pathol Med* **43**, 91-96 (2014).

292. Lin, F. *et al.* Knockdown of KPNA2 inhibits autophagy in oral squamous cell carcinoma cell lines by blocking p53 nuclear translocation. *Oncol Rep* **40**, 179-194 (2018).

293. Tsujimoto, Y. Multiple ways to die: non-apoptotic forms of cell death. *Acta Oncol* **51**, 293-300 (2012).

294. Conklin, K.A. Chemotherapy-associated oxidative stress: impact on chemotherapeutic effectiveness. *Integr Cancer Ther* **3**, 294-300 (2004).

295. Paglin, S. *et al.* Rapamycin-sensitive pathway regulates mitochondrial membrane potential, autophagy, and survival in irradiated MCF-7 cells. *Cancer Res* **65**, 11061-11070 (2005).

296. Lyamzaev, K.G. *et al.* Induction of autophagy by depolarization of mitochondria. *Autophagy* **14**, 921-924 (2018).

297. Roca-Agujetas, V. *et al.* Recent Insights into the Mitochondrial Role in Autophagy and Its Regulation by Oxidative Stress. *Oxid Med Cell Longev* **2019**, 3809308 (2019).

298. Hientz, K., Mohr, A., Bhakta-Guha, D. & Efferth, T. The role of p53 in cancer drug resistance and targeted chemotherapy. *Oncotarget* **8**, 8921-8946 (2017).

299. Ma, W., Sung, H.J., Park, J.Y., Matoba, S. & Hwang, P.M. A pivotal role for p53: balancing aerobic respiration and glycolysis. *J Bioenerg Biomembr* **39**, 243-246 (2007).

300. Sotelo, J., Briceno, E. & Lopez-Gonzalez, M.A. Adding chloroquine to conventional treatment for glioblastoma multiforme: a randomized, double-blind, placebo-controlled trial. *Annals of internal medicine* **144**, 337-343 (2006).

301. Spinazzi, M., Casarin, A., Pertegato, V., Salviati, L. & Angelini, C. Assessment of mitochondrial respiratory chain enzymatic activities on tissues and cultured cells. *Nat Protoc* **7**, 1235-1246 (2012).

302. Hsin, I.L. *et al.* Immunomodulatory proteins FIP-gts and chloroquine induce caspase-independent cell death via autophagy for resensitizing cisplatin-resistant urothelial cancer cells. *Phytomedicine* **23**, 1566-1573 (2016).